MATHEMATICAL MODELING AND CONTROL OF THE DRY DEPOSITION FLUX OF NITROGEN-CONTAINING AIR POLLUTANTS

Final Report
Contract No. A6-188-32

Prepared for:

Research Division
California Air Resources Board
2020 L Street
Sacramento, CA 95814

Submitted by
and
Prepared by:

Armistead G. Russell
Department of Mechanical Engineering
Carnegie-Mellon University
Pittsburgh, PA

and

Darrell A. Winner, Kenneth F. McCue, and Glen R. Cass
Environmental Quality Laboratory
California Institute of Technology
Pasadena, CA 91125

MARCH 1990

Disclaimer

The statements and conclusions in this report are those of the Contractor and not necessarily those of the State Air Resources Board. The mention of commerical products, their source or their use in connection with material reported herein is not to be construed as either an actual or an implied endorsement of such products.

Executive Summary

The largest fluxes of acidic air pollutants to the vegetation, materials and soils of the South Coast Air Basin are believed to be from the nitrogen-containing acid gases, including NO, NO_2 and nitric acid, along with the aerosol nitrates. The goal of this research project is to determine the effects that alternative emission control strategies would have on the dry flux of NO, NO_2, PAN, HNO_3, aerosol nitrate and NH_3.

An Eulerian grid-based air quality model, constructed to predict the atmospheric concentration of those pollutants, has been modified to include a resistance-based dry deposition code in order to permit the calculation of the magnitude and spatial distribution of the dry flux of nitrogen-containing pollutants to different surfaces. The resistance to deposition includes atmospheric transport processes that convey the pollutants to the vicinity of the earth's surface plus the resistance to dry deposition due to chemical interaction at the surface. Surface resistances are specified as a function of land cover type (e.g., cropland, forests, suburban residential), season of the year, and solar radiation intensity.

The dry deposition model has been applied using existing aerometric and emissions data from August, 1982, to calculate the dry flux of nitrogen-containing air pollutants to the surface of the central portion of the South Coast Air Basin. The land cover for the air basin was described spatially using 31 different land use categories, each with its own surface resistance and surface roughness characteristics.

The dry deposition flux of nitrogen-containing pollutants to the surface of the modeling region was calculated for 1982 base case conditions (in metric tons N/day) as follows: NO (4.8); NO_2 (49.1); HNO_3 (101.4); PAN (7.2); NH_3 (58.7); and ammonium nitrate (25.9). NO_x emissions accounted for 175.5 tons/day of the total 247.1 tons/day of deposited nitrogen, while the remainder originated from ammonia emissions. That 175.5 tons/day of nitrogen is equivalent to 577 metric tons/day of NO_x emissions if stated at the molecular weight of NO_2, which corresponds to more than half of the NO_x daily emissions to the local atmosphere. Gas phase species delivered 90% of the deposited nitrogen.

Model verification studies show that atmospheric ozone and inorganic nitrate concentrations are over-predicted when the new dry deposition code is used in place

of the former Caltech airshed model dry deposition code. The new dry deposition code requires data on the surface resistance to dry deposition as a function of land use type for a very large number of surface types. For pollutants other than SO_2, the experimental data simply do not exist that accurately specify the surface resistance values needed to perform such detailed calculations with high precision. In particular, the scientific literature contains nothing more than educated estimates of the surface resistance values for large urban areas. This is a critical matter when evaluating the South Coast Air Basin, where most of the surface of the center of the air basin consists of a giant urban area. A program of experiments is needed to measure the surface resistance parameters required by the present model. An experimental determination of the effect of the surface area of buildings and other roughness elements on the effective surface area for removal of pollutants also is needed.

The revised dry deposition model was employed to examine the nature of the effects that would occur if emission controls were applied to the NO_x and hydrocarbon sources in the South Coast Air Basin as they existed in 1982. At the highest level of control studied (37% reactive hydrocarbon reduction, 61% NO_x reduction), the nitrogen dry flux would be reduced from 247 tons per day N in the pre-control Base Case to 174 tons/day N after control. Of that 174 tons/day N, 87 tons/day N would be derived from deposition of acid gases plus PAN, while 75 tons/day N would be deposited as NH_3. The remaining 12 tons/day N would be deposited as ammonium nitrate. In general, as emission controls are applied to reactive hydrocarbons and NO_x, the dry flux of acid gases declines while the dry flux of NH_3 increases (due to greater NH_3 emissions and due to higher NH_3 concentrations that result from lowered aerosol nitrate formation).

TABLE OF CONTENTS

TABLE OF CONTENTS

LIST OF FIGURES

LIST OF TABLES

Chapter 1

Introduction

On a daily basis, approximately 1000 tons of nitrogen oxides are emitted to the atmosphere of the South Coast Air Basin (Russell and Cass, 1986). These direct emissions to the atmosphere consist principally of nitric oxide (NO). Atmospheric photochemical reactions subsequently convert this original NO burden into an entire family of nitrogen-containing pollutants, including NO_2, HNO_3, PAN and aerosol nitrates. Eventually, these pollutants are removed by wet or dry deposition at the earth's surface. In the Los Angeles area, the dry flux of nitrogen-containing pollutants has been estimated to be the largest contributor to the local acid deposition flux (Liljestrand, 1979).

The delivery of acids to surfaces has the potential to corrode materials, and to damage economically valuable forest areas and crops. The actual magnitude of this potential threat is not well defined at present. For that reason, the legislature of the State of California has adopted the Kapiloff Act, a comprehensive research program designed to quantify the character of acid deposition phenomena in California. Two crucial parts of that research program involve (1) determination of the magnitude of the dry acid deposition flux as a function of geographic location (and thus ground cover type), and (2) determination of the technological effectiveness of emission control technologies and strategies that might result in altered dry deposition flux patterns in California.

For the past several years, research has been underway on how to control the atmospheric concentrations of nitrogen-containing air pollutants in the South Coast Air Basin. As an important step in that research effort, computer-based mathematical models have been developed that compute the atmospheric concentrations of NO, HNO_3, PAN, NH_3, aerosol nitrate and O_3 from input data on reactive hydrocarbons, NO_x and NH_3 emission patterns (Russell and Cass, 1986; Russell et. al., 1983; 1988a). Both trajectory models that follow the fate of individual air parcels over time and

grid-based airshed models that view all points in the air basin simultaneously have been created.

These air quality models incorporate detailed calculations of the air pollutant dry deposition rate at the ground. Accurate treatment of this pollutant removal route is a prerequisite to the accurate prediction of atmospheric pollutant levels. However, in most past air quality modeling studies, ground level pollutant deposition has been viewed solely from the perspective of its effect on reducing atmospheric pollutant concentration predictions: the dry flux results are not accumulated or otherwise tracked by the model and are therefore "thrown away" (just as the pollutant fluxes to the outside boundaries of the modeling region often are not saved). The air quality models, however, can be reprogrammed to record and store information on the spatial distribution and temporal characteristics of the pollutant dry flux to surfaces. This has been done in one brief test case using the trajectory version of the photochemical modeling system, and the results along a single trajectory across the South Coast Air Basin during a day in June 1974 are shown in Figure 1.1.

In the present study, the grid-based version of the Caltech airshed model has been modified to compute the spatial distribution of the pollutant fluxes for NO, NO_2, PAN, aerosol nitrate, NH_3, and HNO_3 for conditions that prevailed in the 1980's. In pursuit of that objective, important technical modifications to the dry deposition module within the airshed model have been made. First, the treatment of the surface chemical resistance to dry deposition has been modified such that the deposition flux to particular types of ground cover (e.g., urban areas, grassland, forests) can be computed based on the latest information on the affinity of various pollutant species for each type of ground cover. The model has been modified to read gridded land use data from input data files, and the new land use data have been used to improve both the deposition flux calculations and to calculate the surface roughness parameter values used within the model. The model computes the spatial distribution of the deposition velocity for each pollutant at each hour and the spatial distribution of pollutant dry flux values at each hour.

A detailed data set on land uses within the South Coast Air Basin has been assembled, based on the most recent United States Geological Survey land use maps. Historical emissions, meteorological, and air quality data available in the South Coast

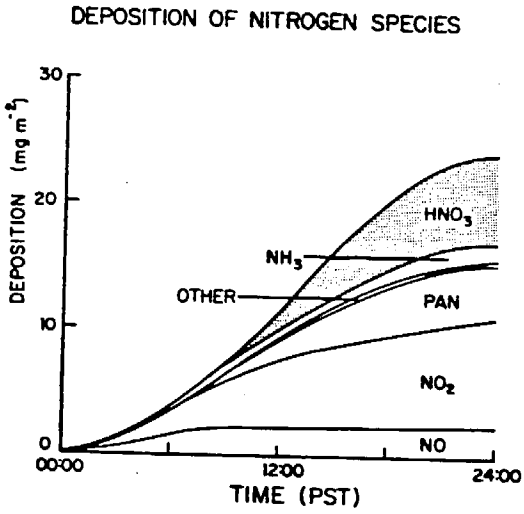

Cumulative dry deposition flux of nitrogen-containing air pollutants along a 24-hour trajectory starting over the ocean at midnight, then passing over Upland at 1600 hours PST, 27 June 1974.

Figure 1.1

Air Basin for the period August 30-31, 1982, have been used along with the new land use data, to test the characteristics of the modified airshed model against field observations. The spatial distributions of the deposition velocity and of dry deposition flux to the surface of the South Coast Air Basin have been computed and displayed.

The air quality model discussed here derives its predictions directly from information on the emissions from each air pollution source in the air basin. The model, therefore, can be used to predict the effect of candidate emission control measures in advance of their adoption. Following the determination of the historically observed dry flux of nitrogen-containing pollutants to surfaces, a study of the effect of a wide variety of emission control measures on achieving altered levels of pollutant dry flux was undertaken. Mobile source controls considered include the effects of a vehicle inspection and maintenance plan, recent USEPA proposals for future NO_x reductions from heavy duty vehicles, plus the possible conversion of the light-duty vehicle fleet to reflect attainment of either a 0.7 g/mi or 0.4 g/mi NO_x emission rate. Stationary source controls examined include future hydrocarbon and NO_x controls expected as part of the Air Quality Management Plan (AQMP) for the South Coast Air Basin that was in force at the start of this research project, plus the possible addition of catalytic or non-catalytic NH_3 injection technology for NO_x control at large stationary sources. Attention was paid to noting any side effects on ambient pollutant concentrations of NO_2, HNO_3, aerosol nitrate, NH_3, PAN and O_3 that may accompany the changes in dry deposition flux studied here.

Chapter 2

Formulation of an Improved Dry Deposition Module for Use in the Airshed Model

2.1 OVERVIEW OF THE ORIGINAL DRY DEPOSITION MODULE USED IN THE CALTECH AIRSHED MODEL

Before describing the formulation of a new dry deposition module for use in the airshed model, a brief review of the preexisting dry deposition calculation scheme is in order. The local flux, F, of acid gases to the surface of an air basin is defined by $F=v_g \cdot c(z_r)$, where v_g is the deposition velocity and $c(z_r)$ is the local ambient pollutant concentration at a chosen reference height, z_r (typically z_r equals about 10 m). The deposition velocity is a parameter that incorporates at least two effects: (1) turbulent transport of pollutants to the vicinity of the surfaces and (2) the chemical interaction of the pollutants with surfaces that ultimately must occur if pollutant attachment to the surface is to occur. The dry deposition velocity as calculated in the original Caltech airshed model is described by Russell et. al. (1984). "Within the layer $0 \leq z \leq z_r$, deposition is assumed to be a one-dimensional, steady state, constant flux process occurring without reentrainment. With these assumptions the deposition flux of gaseous materials is described by $F = [K_{zz} + D]\ \delta c/\delta z$ where K_{zz} is the pollutant eddy diffusion coefficient in the vertical dimension and D the molecular diffusion coefficient of the material in the air. By equating fluxes and assuming that u_* is constant in the surface layer, then it is possible to show using Monin-Obukov similarity theory, that

$$v_g = \frac{k\left[1 - \frac{c(z_d)}{c(z_r)}\right]}{\int_{z_d}^{z_r} \frac{1}{zu_*}\phi_p(\frac{z}{L})dz} = \frac{k^2 u(z_r)\left[1 - \frac{c(z_d)}{c(z_r)}\right]}{\left[\int_{z_o}^{z_r} \phi_m(\frac{z}{L})\frac{dz}{z}\right]\left[\ln(\frac{z_o}{z_d}) + \int_{z_o}^{z_r} \phi_p(\frac{z}{L})\frac{dz}{z}\right]} \qquad (2.1)$$

where k is von Karman's constant, $u(z_r)$ is the wind velocity at reference elevation z_r, u_* is the friction velocity, and L is the Monin-Obukov length. The expressions ϕ_m and ϕ_p used in the above equation are experimentally derived functions that account for the influence of atmospheric stability on turbulent transport (Businger et. al., 1971). The lower limits of integration, z_d, and $c(z_d)$, refer to the elevation and concentration

of material at the effective pollutant sink height, and z_o is the momentum sink height. If the ratio $c(z_d)/c(z_r)$ is zero then the surface is considered to be a perfect sink. Then v_g is simply the reciprocal of the aerodynamic resistance, and dry deposition is said to be atmospheric transport limited. The effect of a significant chemical or biological resistance to dry deposition is captured by values of the term $\left[1 - \frac{c(z_d)}{c(z_r)}\right]$ that are less than unity. Values of $\left[1 - \frac{c(z_d)}{c(z_r)}\right]$ for various pollutants and surface types are extracted from field experiments on dry deposition rates. Evaluation of the term $\ln(z_0/z_d)$ in the denominator of the above equation requires a knowledge of z_d and of the transfer processes at the surface. Based on a survey of the heat transfer literature and in particular the work of Brutsaert (1975), and Wesely and Hicks (1977), it is assumed that

$$\ln\left(\frac{z_o}{z_d}\right) = 2\left(\frac{Sc}{Pr}\right)^{2/3} \tag{2.2}$$

where Sc and Pr are the Schmidt and Prandtl numbers associated with the pollutant material in air. The complete expression is then

$$v_g = \frac{k^2 u(z_r)\left[1 - \frac{c(z_d)}{c(z_r)}\right]}{\left[\int_{z_o}^{z_r} \phi_m(\frac{z}{L})\frac{dz}{z}\right]\left[2(\frac{Sc}{Pr})^{2/3} + \int_{z_o}^{z_r} \phi_p(\frac{z}{L})\frac{dz}{z}\right]} \tag{2.3}$$

The integrals required to evaluate v_g are given in McRae et. al. (1982ab)."

The final form for v_g is dependent on local wind velocity, atmospheric stability and the surface chemical or biological resistance to dry deposition. Over the range of atmospheric meteorological conditions that can be expected, v_g can vary by almost a factor of 5 for each pollutant of interest. The approach given above which is based on local meteorological conditions is expected to yield more accurate results than use of a single constant dry deposition velocity for each pollutant.

Once the deposition velocity has been calculated for each pollutant, the ground level concentration for each pollutant is multiplied by its deposition velocity (adjusted to reflect model cell height) to obtain the pollutant flux, F, to the surface in units, for example, of mg/m^2 sec. This calculation is repeated at each time step, in each ground level grid cell for each chemical species. Over the course of the day, a time history of the spatial distribution of pollutant flux to the surface could be accumulated

if the model were reprogrammed to store the deposition flux calculations. A very detailed description of the dry deposition calculation procedure is given by McRae et. al. (1982ab) and by Russell et. al. (1984).

2.2 FORMULATION OF AN IMPROVED DRY DEPOSITION MODULE

Dry deposition processes often are represented in the form of an electrical resistance analog. The total resistance to pollutant deposition, r_t, is taken as the inverse of the deposition velocity:

$$r_t = \frac{1}{v_g} \tag{2.4}$$

That total resistance to deposition is then composed of several parts:

$$r_t = r_a + r_b + r_s \tag{2.5}$$

where r_a is the resistance to deposition due to turbulent transport through the atmosphere from reference height z_r down to a thin fluid layer very near the surface, r_b is the resistance due to molecular scale diffusive transport through the thin atmospheric sublayer near the surface, and r_s is the resistance due to the chemical interaction between the surface and the pollutant of interest once the gas molecules have reached the surface. The derivation of equation (2.3) adequately captures the fluid mechanical aspects of pollutant transport through the atmosphere to the surface. In the case of a pollutant for which the surface is a perfect sink (i.e.., $r_s = 0$ and $c\ (z_d) = 0$)) then equation (2.3) becomes

$$v_{g\ max} = \frac{k^2 u(z_r)}{\left[\int_{z_o}^{z_r} \phi_m(\frac{z}{L})\frac{dz}{z}\right]\left[2(\frac{Sc}{Pr})^{2/3} + \int_{z_o}^{z_r} \phi_p(\frac{z}{L})\frac{dz}{z}\right]} \tag{2.6}$$

and

$$r_a + r_b = \frac{1}{v_{g\ max}} \tag{2.7}$$

The treatment of the chemical reaction resistance to dry deposition in equation (2.3) is captured in the term $\left[1 - \frac{c(z_d)}{c(z_r)}\right]$, which will be called the surface "affinity" for

each pollutant. As implemented in the original version of the Caltech airshed model, $\left[1 - \frac{c(z_d)}{c(z_r)}\right]$ is read as a single constant value for each pollutant species, ranging from 1.0 for pollutants that show no appreciable surface resistance to deposition, like HNO_3, to essentially zero for pollutants like CO that do not readily react with surfaces. For many of the most important acid gases (e.g., SO_2, NO_2) and oxidants (e.g., O_3), the recommended values of the parameter $\left[1 - \frac{c(z_d)}{c(z_r)}\right]$ lie between zero and one. These values should depend on the chemical nature of the surface as well as the pollutant, but in the original formulation of the airshed model, only the relative reactivity of the pollutant of interest is considered in setting these surface affinity values.

A more flexible approach to capturing the effect of varying surface type on pollutant dry flux calculations is possible and has been adopted for use in the present study. Gridded land use data are introduced into the model, and a table look-up procedure is adopted to specify the surface resistance, r_s, in equation (2.5) directly as a function of the surface type, the season of the year (which is important for vegetative surfaces) and the pollutant of interest. The completed dry deposition model then becomes:

$$v_g = (r_a + r_b + r_s)^{-1} \tag{2.8}$$

where the value of $r_a + r_b$ is calculated from equations (2.6) and (2.7) and where the value of r_s is obtained from the table look-up. The deposition flux to each of the various land uses that occur within a particular grid cell within the model is computed separately and then summed to obtain the total flux from the atmosphere to the surface of that grid cell at each time step. Flux calculations are corrected for the dimensions of the ground level cell in the model as described by McRae et. al. (1982ab).

2.3 LAND USE AND SURFACE RESISTANCE DATA

The procedure used for specifying surface characteristics within the model has been geared to a readily available source of land use data. The United States Geological Survey (USGS) has produced extremely detailed maps in which the surface characteristics of large areas of the United States have been specified according to the categories listed in Table 2.1. Also shown in Table 2.1 are land use-specific values for the surface roughness height parameter, z_o, that appears in equation (2.6). The Caltech airshed

Table 2.1
Land Use Categories and Surface Roughness Values

Land Use		Roughness Height $z_o(m)$	References
URBAN OR BUILT-UP LAND			
11	Residential	2	(a)
12	Commerical and Services	3	(a)
13	Industrial	3	(a)
14	Transportation, Communications and Utilities	0.3	(b)
15	Industrial and Commercial Complexes	3	(a)
16	Mixed Urban or Built-Up Land	2.5	(c)
17	Other Urban or Built-Up Land	2.5	(c)
AGRICULTURAL LAND			
21	Cropland and Pasture	0.1	(d)
22	Orchards, Groves, Vineyards, Nurseries and Ornamental Horticultural Areas	0.45	(e)
23	Confined Feeding Operations	0.3	(f)
24	Other Agricultural Land	0.1	(g)
RANGELAND			
31	Herbaceous Rangeland	0.1	(h)
32	Shrub and Brush Rangeland	0.25	(i)
33	Mixed Rangeland	0.25	(i)
FOREST LAND			
41	Deciduous Forest Land	1.0	(j)
42	Evergreen Forest Land	1.0	(j)
43	Mixed Forest Land	1.0	(j)

Table 2.1 (cont.)
Land Use Categories and Surface Roughness Values

Land Use	Roughness Height $z_o(m)$	References
WATER		
50 Ocean	0.0001	(k)
51 Streams and Canals	0.002	(l)
52 Lakes	0.0001	(m)
53 Reservoirs	0.0001	(m)
54 Bays and Estuaries	0.0001	(m)
WETLAND		
61 Forested Wetland	1.0	(n)
62 Non-Forested Wetland	0.15	(o)
BARREN LAND		
71 Dry Salt Flats	0.00004	(p)
72 Beaches	0.0004	(q)
73 Sandy Areas Other than Beaches	0.0004	(q)
74 Bare Exposed Rock	0.10	(r)
75 Strip Mines, Quarries and Gravel Pits	0.10	(s)
76 Transitional Areas	0.002	(t)
77 Mixed Barren Land	0.002	(u)

Footnotes

(a) McRae et al. (1982b), Figure 4.3.

(b) Estimated as open land with nursery plants or cars and fences. Roughness element height $\approx$ 2 m. $z_o = 0.15\text{x}2 \cong 0.3$.

(c) Estimated to be a mixture of commercial and residential areas.

(d) Value for mixed agricultural and rangeland from Sheih et al. (1986).

(e) Orchard roughness elements estimated to be 4 m high; nursery roughness elements estimated to be 2 m high; average of roughness elements is thus about 3 m high. $z_o \approx 0.15 \text{ x } 3 \cong 0.45$.

(f) Roughness elements are cows (1.5 m), fences (1.5 m) and a few buildings (4 m). Use $h_c = 2$ m. $z_o = 0.15 \text{ x } 2 \approx 0.30$.

(g) Estimated to be the same as land use 21 above.

(h) Sheih et al. (1986). Mid-summer rangeland given $z_o = 0.05$ m, but higher value used here because most of herbaceous rangeland left in Southern California is located in hilly areas.

(i) McRae et al. (1982b). Figure 4.3; value at the high end of the range given is used because most such land in Southern California is in hilly areas.

(j) Sheih et al. (1986); $z_o = 1$ m. McRae et al. (1982); $z_o = 1$ m.

(k) McRae et al. (1982b); p 144; $z_o = 0.0001$ m.

(l) Streams in this area treated as being dry in the summer, z_o estimated as same as mixed barren land.

(m) Sheih et al. (1986); computed to be about $z_o = 0.0001$ m.

(n) Sheih et al. (1986).

(o) Sheih et al. (1986).

(p) McRae et al. (1982b); Figure 4.3.

(q) McRae et al. (1982b); Figure 4.3; bare sand.

(r) Sheih et al. (1986); rocky land.

(s) Highly variable topography: some deep pits, some rocky and sandy land with shrubs, range; sand with $z_o = 0.0004$, depth of pits $\cong$ 30 m, with $z_o \approx 4.5$.

(t) Estimated to be similar to mixed barren land.

(u) Sheih et al. (1986); barren land $z_o = 0.002$ m.

model has been reprogrammed to compute surface roughness values from the new land use data file, thereby automating the calculation of surface roughness fields.

Walcek et. al. (1986), Sheih et. al. (1986), and Chang et. al. (1987) reviewed the technical literature and recommended values for the surface resistance for SO_2 deposition to urban, agricultural, range, deciduous forest, coniferous forest, forested swamp, water, swamp, and mixed agricultural-range land covers. These recommended values for the SO_2 surface resistance taken from Sheih et. al. (1986) are used in the revised Caltech deposition module. The complete table of SO_2 surface resistance values, as a function of land use type and solar insolation level are shown in Table 2.2, for the summer season. Values for other seasons of the year are available in the references cited. In Table 2.2, the small number of generic land use categories used in these prior studies has been extrapolated to match the 31 land use types that are available from USGS maps for Southern California by assigning their single recommended urban surface resistance value to all urban land uses, by assigning their single agricultural value to all agricultural uses, and so forth.

Relatively few field experiments have been conducted from which surface resistance values can be calculated for pollutants other than SO_2. Huebert and Robert (1985) have shown that the HNO_3 flux to pasture land proceeds at a diffusion-limited rate, indicating that r_s for HNO_3 is essentially zero. Wesely et. al. (1982) have measured the flux of O_3 and NO_2 to vegetation with sufficient detail to infer surface resistance values as shown in Table 2.3. The surface resistances for NO_2 are generally higher than for O_3, indicating that in their experiments, NO_2 was removed more slowly than ozone. Garland (1976) has reported surface resistance values for SO_2 to grass in the range 0.56-0.41 sec cm^{-1} compared to O_3 surface resistances in the range 1.11–0.72 sec cm^{-1}. Garland and Penkett (1976) place the surface resistance for PAN at about 4.5 sec cm^{-1} to surfaces other than water; the rate of loss of PAN to water is very low.

The relative ordering of surface resistance values between pollutants also can be inferred from studies in which the deposition velocity to the same surface is reported during a single experiment. Dolski and Gatz (1985) compared the deposition flux of HNO_3, SO_2 and O_3 to a rural grassy area and showed that the relative rates of removal of these pollutants proceed in the order $HNO_3 > SO_2 > O_3$, indicating that surface resistances are ordered as $O_3 > SO_2 > HNO_3$. Hill and Chamberlain (1976) measured

Table 2.2
Summertime SO_2 Surface Resistances (sec cm^{-1})
from Sheih et. al. (1986)

Land Use	Insolation (Watts m^{-2})				
	>400	200-400	0-200	Night	Wetted
URBAN OR BUILT-UP LAND					
11 Residential	5.0	5.0	5.0	5.0	0.1
12 Commerical and Services	5.0	5.0	5.0	5.0	0.1
13 Industrial	5.0	5.0	5.0	5.0	0.1
14 Transportation, Communications and Utilities	5.0	5.0	5.0	5.0	0.1
15 Industrial and Commercial Complexes	5.0	5.0	5.0	5.0	0.1
16 Mixed Urban or Built-Up Land	5.0	5.0	5.0	5.0	0.1
17 Other Urban or Built-Up Land	5.0	5.0	5.0	5.0	0.1
AGRICULTURAL LAND					
21 Cropland and Pasture	0.7	1.2	2.0	4.0	0.1
22 Orchards, Groves, Vineyards, Nurseries and Ornamental Horticultural Areas	0.7	1.2	2.0	4.0	0.1
23 Confined Feeding Operations	0.7	1.2	2.0	4.0	0.1
24 Other Agricultural Land	0.7	1.2	2.0	4.0	0.1
RANGELAND					
31 Herbaceous Rangeland	1.0	1.4	2.0	4.0	0.1
32 Shrub and Brush Rangeland	1.0	1.4	2.0	4.0	0.1
33 Mixed Rangeland	1.0	1.4	2.0	4.0	0.1
FOREST LAND					
41 Deciduous Forest Land	0.9	1.5	3.0	12.0	0.5
42 Evergreen Forest Land	1.5	2.4	4.0	12.0	0.5
43 Mixed Forest Land	0.7	1.4	3.0	10.5	0.0

Table 2.2 (cont.)
Summertime SO_2 Surface Resistances (sec cm^{-1})

Land Use	Insolation (Watts m^{-2})				
	>400	200-400	0-200	Night	Wetted
WATER					
50 Ocean	0.0	0.0	0.0	0.0	0.0
51 Streams and Canals	0.0	0.0	0.0	0.0	0.0
52 Lakes	0.0	0.0	0.0	0.0	0.0
53 Reservoirs	0.0	0.0	0.0	0.0	0.0
54 Bays and Estuaries	0.0	0.0	0.0	0.0	0.0
WETLAND					
61 Forested Wetland	0.7	1.4	3.0	10.0	0.5
62 Non-Forested Wetland	0.5	0.6	0.8	1.0	0.1
BARREN LAND					
71 Dry Salt Flats	10.0	10.0	10.0	10.0	5.0
72 Beaches	10.0	10.0	10.0	10.0	5.0
73 Sandy Areas Other than Beaches	10.0	10.0	10.0	10.0	5.0
74 Bare Exposed Rock	1.5	3.0	4.0	5.0	0.2
75 Strip Mines, Quarries and Gravel Pits	10.0	10.0	10.0	10.0	5.0
76 Transitional Areas	10.0	10.0	10.0	10.0	5.0
77 Mixed Barren Land	10.0	10.0	10.0	10.0	5.0

Table 2.3

Surface Resistance Values for NO_2 and O_3 Flux to Vegetation (from Wesely et al. 1982)

Measurement Period	Stability	Surface Resistance, r_s	
		O_3	NO_x[(a)]
		sec cm^{-1}	sec cm^{-1}
daytime	unstable	0.84±0.04	1.6±0.2
late afternoon	near neutral	2.4±0.5	2.8±1.6
night	slightly stable	1.8±0.4	15±2

Notes

(a) Nearly all of the NO_x during this experiment was present as NO_2.

(b) There was an indication that some of the deposited NO_2 was re-released from the surface as NO.

the deposition velocity of a large number of gaseous pollutants to alfalfa in a chamber study. For equivalent fluid flow conditions their data show that deposition velocities to alfalfa lie in the following order (deposition velocities in cm/sec from Table 1 of their study are given in parentheses): HF (3.77) > SO_2 (2.83) > NO_2 (1.90) > O_3 (1.67) > PAN (0.63) > NO (0.1) > CO (0.0). Their study thus implies that surface resistance values, r_s, over alfalfa proceed in the order CO > NO > PAN > O_3 > NO_2 > SO_2 > HF.

Finally, several authors have reviewed the technical literature and provide summaries of deposition velocity data. In some cases, these reviews were intended simply to show the full range of values over which experimental results have been obtained, while in other cases, the purpose of the study was to select typical values for use in an air quality modeling study. The rank ordering of deposition velocity values between pollutant species based on several such studies is summarized in Table 2.4. There is general agreement that HNO_3 is removed at the highest observed rates, consistent with inferences from the work of Huebert and Robert (1985) suggesting that the surface resistance for HNO_3 is essentially zero. Most of these surveys are roughly consistent with the relative deposition velocity ordering seen in the experiments of Hill and Chamberlain (1976): diffusion-limited acids > SO_2 >NO_2 $\approx$ O_3 > PAN > NO > CO. This suggests that surface resistance values, r_s, should be ordered approximately as: CO > NO > PAN > O_3 $\approx$ NO_2 > SO_2 > HNO_3 = 0.0. The notable exception to this summary is provided by the treatment of Chang et. al. (1987) which has been used with the RADM model that has been assembled for the National Acid Precipitation Assessment Program. They place the surface resistance values for both NO and NO_2 at a level equal to that of SO_2, and do not calculate depositional losses for PAN. Based on personal experience gained with the modeling of indoor NO concentrations (Nazaroff and Cass, 1986), we believe that the NO dry deposition velocity is likely to be quite low, and find it unlikely that NO_2 and NO are removed at the same rate. Therefore, the surface resistance for NO should probably be set at a higher value than for NO_2, in a manner consistent with Hill and Chamberlain's (1976) experiments.

Surface resistance values used in the present model for pollutants other than SO_2 must be set in large part based on engineering judgment. The values chosen should be consistent with the existing experimental values for vegetative surfaces, and

Table 2.4

The Relative Ordering of Pollutant Deposition Velocity Values

(Numbers in parentheses are deposition velocity values, v_g, in cm/sec)

1. Finlayson-Pitts and Pitts (1986) citing McRae and Russell (1984)

   HNO_3 (1.0–4.7) > SO_2 (0.1–4.5) > NO_2 (0.3–0.8; 1.9) $\approx$ O_3 (0.10–2.10, 0.47–0.55, 0.20–0.84) > PAN (0.14–0.30; 0.63) > NO (0.10–0.20)

2. Derwent and Hov (1988)

   HNO_3 (2.0) > SO_2 (0.8) = O_3 (0.8) > NO_2 (0.6) > PAN (0.3)

3. McRae et al. (1982b); Table 6.7

   O_3 (0.025–6.3) > NO_2 (0.5–2.0) > PAN (0.14–0.63) > NO (0.0–0.1) > CO (0.0–0.03)

4. Chang et al. (1987)

   HNO_3 > H_2O_2 > NH_3 > HCHO > O_3 = SO_2 = NO_2 = NO > RCHO

5. Sehmel (1980)

   SO_2 (0.04–7.5) > O_3 (0.002–2.0); NO_2 (1.9) > PAN (0.8) > NO (negative to 0.9)

should preserve the apparent rank ordering between the pollutant species that was just discussed. In the case of O_3, surface resistance values as a function of land use type have been recommended by Sheih et. al. (1986), and their recommendations will be used in the present study. Values for O_3 surface resistances for the summer season are presented in Table 2.5, and estimates for other seasons of the year are available in the work by Sheih et. al. (1986). For the pollutants NO, NO_2, NH_3, H_2O_2, HCHO and higher aldehydes (RCHO), the approach of Chang et. al. (1987) will be followed in which the surface resistances will be set for each land use in fixed proportion to the values for SO_2. These surface resistance values are shown in Table 2.6, and are the same as recommended by Chang et. al. for NO_2, NH_3, H_2O_2, HCHO and RCHO. Following the rationale explained in the previous paragraph, the surface resistance for NO is set to a value much higher than that for SO_2.

For the remaining pollutant species, there is no basis for trying to distinguish between the surface resistance values for different land use types. There are simply insufficient experimental data on the subject, and there are no systematic expert recommendations for drawing distinctions between land use types. For HNO_3 and for the highly reactive species NO_3 and N_2O_5, it is assumed that removal at surfaces occurs at a diffusion-limited rate. Values of r_s for these pollutants are set to zero over all land uses. For PAN, the surface resistance value is set to 4.5 sec cm^{-1}, except that deposition of PAN over the ocean is suppressed, based on the findings of Garland and Penkett (1976). The surface resistance for CO is set to a high enough value (r_s = 50 sec cm^{-1}) to prevent substantial CO loss to surfaces. For the remaining gaseous pollutant species, no deposition data exist, and values of r_s are set by analogy to related pollutants for which some data are available. All hydrocarbon species (alkanes, olefins, aromatics, ethene) are treated by analogy to CO; it is assumed that they are removed by dry deposition at a negligible rate. RONO and RNO_4 are assumed to behave like PAN and are assigned a surface resistance of 4.5 sec cm^{-1}. Nitrous acid (HONO) is assigned a low surface resistance of 0.4 sec cm^{-1} on the expectation that it will be removed by dry deposition at a fairly rapid rate. The surface resistance values are summarized in Table 2.6.

In addition to these gaseous pollutants, aerosol nitrate concentrations also are predicted by the Caltech photochemical airshed model. Aerosol nitrate predictions are

Table 2.5
Summertime O_3 Surface Resistances (sec cm^{-1})
from Sheih et. al. (1986)

Land Use	Insolation (Watts m^{-2})				
	>400	200-400	0-200	Night	Wetted
URBAN OR BUILT-UP LAND					
11 Residential	3.0	3.0	4.0	4.0	4.0
12 Commerical and Services	3.0	3.0	4.0	4.0	4.0
13 Industrial	3.0	3.0	4.0	4.0	4.0
14 Transportation, Communications and Utilities	3.0	3.0	4.0	4.0	4.0
15 Industrial and Commercial Complexes	3.0	3.0	4.0	4.0	4.0
16 Mixed Urban or Built-Up Land	3.0	3.0	4.0	4.0	4.0
17 Other Urban or Built-Up Land	3.0	3.0	4.0	4.0	4.0
AGRICULTURAL LAND					
21 Cropland and Pasture	0.6	1.0	1.5	2.5	4.0
22 Orchards, Groves, Vineyards, Nurseries and Ornamental Horticultural Areas	0.6	1.0	1.5	2.5	4.0
23 Confined Feeding Operations	0.6	1.0	1.5	2.5	4.0
24 Other Agricultural Land	0.6	1.0	1.5	2.5	4.0
RANGELAND					
31 Herbaceous Rangeland	0.9	1.2	1.5	3.0	4.0
32 Shrub and Brush Rangeland	0.9	1.2	1.5	3.0	4.0
33 Mixed Rangeland	0.8	1.1	1.5	3.0	4.0
FOREST LAND					
41 Deciduous Forest Land	0.8	1.3	1.7	12.0	15.0
42 Evergreen Forest Land	1.3	2.0	3.5	12.0	15.0
43 Mixed Forest Land	1.0	2.0	4.0	11.0	15.0

Table 2.5 (cont.)
Summertime O_3 Surface Resistances (sec cm^{-1})

Land Use	Insolation (Watts m^{-2})				
	>400	200-400	0-200	Night	Wetted
WATER					
50 Ocean	20.0	20.0	20.0	20.0	20.0
51 Streams and Canals	20.0	20.0	20.0	20.0	20.0
52 Lakes	20.0	20.0	20.0	20.0	20.0
53 Reservoirs	20.0	20.0	20.0	20.0	20.0
54 Bays and Estuaries	20.0	20.0	20.0	20.0	20.0
WETLAND					
61 Forested Wetland	1.0	2.0	4.0	11.0	15.0
62 Non-Forested Wetland	1.5	2.0	3.0	10.0	12.0
BARREN LAND					
71 Dry Salt Flats	3.0	3.0	4.0	4.0	4.0
72 Beaches	3.0	3.0	4.0	4.0	4.0
73 Sandy Areas Other than Beaches	3.0	3.0	4.0	4.0	4.0
74 Bare Exposed Rock	1.2	2.0	3.0	3.0	4.0
75 Strip Mines, Quarries and Gravel Pits	3.0	3.0	4.0	4.0	4.0
76 Transitional Areas	3.0	3.0	4.0	4.0	4.0
77 Mixed Barren Land	3.0	3.0	4.0	4.0	4.0

Table 2.6 Surface Resistance As a Function of Pollutant Species

Species	r (sec/cm)
NO	13.9 x r_{so_2}
NO_2	1.0 x r_{so_2}
NH_3	0.2 x r_{so_2}
H_2O_2	0.1 x r_{so_2}
HCHO	0.5 x r_{so_2}
RCHO	2.0 x r_{so_2}
HNO_3	0.01
NO_3	0.01
N_2O_5	0.01
PAN	4.5
HONO	0.4
RNO_4	4.5
RONO	4.5
OTHER	50
AEROSOL NITRATE	v=0.182 x v_{HNO_3}

based on the upper limit to the gas phase product of NH_3 times HNO_3 concentrations that can be sustained in equilibrium with pure aerosol NH_4NO_3. If coarse particle nitrates are present, then the deposition velocity that results from sedimentation and impaction could be as high as that for a gas such as HNO_3 that is removed at a diffusion-limited rate, while if all aerosol nitrates are in the fine particle mode, then the deposition velocity could be very low indeed. As aerosol nitrate size distribution predictions are not produced by the model, it is not possible to calculate aerosol nitrate dry deposition fluxes from first principles based on aerosol mechanics considerations. Instead, the following empirical approach is taken, based on experimental data from Southern California. During the 1985 Claremont Nitrogen Species Methods Comparison Study, the deposition velocities of nitric acid vapor and aerosol nitrate to surrogate surfaces were measured simultaneously by Pierson et. al. (1988). The average of the ratio of the deposition velocity for aerosol nitrate to the deposition velocity for HNO_3 can be computed, and is found to be 0.182. Nitric acid vapor is assumed to be removed at a diffusion-limited rate that can be calculated accurately by the present model. Therefore, in the present model, aerosol nitrate will be removed from the atmosphere with a deposition velocity that is 18.2% of that calculated for HNO_3 at the same time and place.

The revised model is now completely specified.

Chapter 3

Model Application: Determination of Base Case 1982 Dry Deposition Fluxes

3.1 SELECTION OF THE CASE STUDY

Nitric acid, aerosol nitrate, PAN and ammonia are unregulated pollutants. As a result, their concentrations have not been measured routinely by governmental air monitoring networks. Comprehensive data sets on these pollutants that can be used for checking air quality model predictions are *very* rare. However, during the period August 30-31, 1982, a field experiment was conducted to measure the concentrations of HNO_3, NH_3, and aerosol nitrates over consecutive 2-hr. periods at ten monitoring sites in the South Coast Air Basin (Hildemann et. al. 1984; Russell and Cass 1984). SCAQMD air monitoring stations provided concurrent data on NO, NO_2, and O_3 concentrations, while PAN concentrations were measured at Pasadena (Caltech) and at U.C. Riverside. This data set provided the only opportunity available during the term of this research effort for assessing model performance for the entire family of nitrogen-containing air pollutants. Therefore, model applications will focus on calculations for the South Coast Air Basin over the period August 30-31, 1982.

3.2 REVIEW OF PREVIOUS MODELING STUDIES OF THE AUGUST 30-31, 1982, DATA SET

The August 30-31, 1982, field experimental data set has been used previously to evaluate the ability of the Caltech photochemical trajectory model and photochemical airshed model to accurately predict NO_2, total inorganic nitrate, HNO_3, NH_3, PAN, aerosol nitrate and O_3 concentrations in the South Coast Air Basin (Russell and Cass 1986; Russell et. al. 1988a). To apply these modeling procedures, a grid system is laid down over the South Coast Air Basin, as seen in Figure 3.1. An inventory of pollutant emissions for hydrocarbons, NO_x and NH_3 is developed for each of the many source types in the air basin, as shown in Tables 3.1 and 3.2 and Figure 3.2. Then, given the meteorological conditions for the time period of interest, a simulation of pollutant transport with the prevailing winds, combined with a detailed description of atmospheric photochemical and thermochemical reactions proceeds to compute the

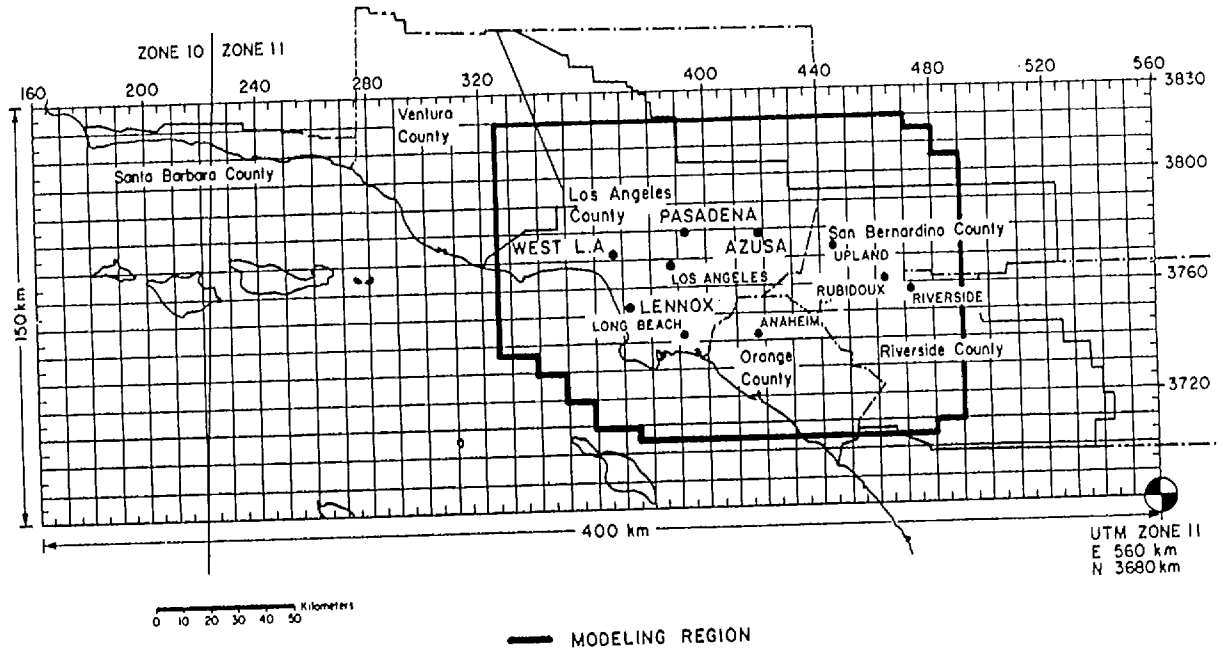

Fig. 3.1 South Coast Air Basin of California, plus Ventura and coastal Santa Barbara Counties. Emissions and meteorological data fields are developed over the 150 km × 400 km gridded area. Air monitoring sites at which HNO_3, NH_3, and aerosol nitrate data are available from ref 2 are shown by (●). Air quality modeling calculations are performed within the region bounded by the heavy solid line in the center of the map.

Table 3.1

1982 estimated emissions within the modeling region

Source type	Emission rate THC tons/day	NO_x tons/day	CO tons/day
Stationary sources			
Fuel combustion			
External combustion boilers			
Utilities	6.7	97.7	8.2
Industrial	3.0	41.0	7.1
Commercial and institutional	0.1	3.6	0.03
Internal combustion engines			
Utilities	4.5	8.4	3.0
Industrial	25.1	58.1	19.2
Petroleum refining and production	2.8	35.3	1.1
Other manufacturing	3.1	39.5	181.3
Residential, agricultural and other	16.9	53.3	127.1
Subtotal fuel combustion	62.2	336.9	347.0
Waste burning and incineration	0.09	0.4	0.3
Landfill	777.9	0.0	0.0
Solvent use			
Surface coating	195.4	1.9	0.4
Other	161.8	0.2	0.03
Petroleum processes, storage and transfer	99.9	11.3	13.6
Industrial processes	26.1	2.6	18.1
Miscellaneous	440.0	3.8	118.6
Subtotal stationary sources	1763.4	357.1	498.0
Motor vehicle emissions			
On-road vehicles	581.4	662.5	5001.9
Off-road vehicles	26.8	67.1	172.6
Railroads	3.8	15.3	5.8
Ships	22.2	16.0	88.6
Aircraft	18.1	16.3	84.5
Subtotal motor vehicle emissions	652.3	777.2	5353.4
Total	2415.7	1134.3	5851.4

Table 3.2

Summary of ammonia emissions by source category within the modeling region

Source category	Total emissions (tons day^{-1})	
Stationary fuel combustion		
Electric utility	1.2	
Natural gas	0.38	
Residual oil	0.00	
Digester gas		
Refinery fuel burning	0.12	
Natural gas	0.015	
Residual oil	0.39	
Refinery gas		
Industrial fuel burning	0.47	
Natural gas	0.008	
Liquified petroleum gas (LPG)	0.022	
Residual oil	0.12	
Distillate oil	0.026	
Digester gas	0.015	
Coke oven gas		
Residential/commercial fuel burning	0.21	
Natural gas	0.004	
Liquid petroleum gas (LPG)	0.085	
Residual oil	0.079	
Distillate oil	0.023	
Coal		
Subtotals	3.2	(1.9%)
Mobile source fuel combustion		
Automobiles	2.4	
Catalyst autos and light trucks	0.48	
Non-catalyst autos and light trucks	0.004	
Diesel autos and light trucks	0.23	
Catalyst medium vehicles	0.14	
Non-catalyst medium and heavy trucks	0.023	
Diesel trucks	0.007	
LPG for carburetion		
Civilian aircraft	0.007	
Jet	0.002	
Piston		
Shipping	0.068	
Residual oil boilers	0.002	
Diesel ships	0.004	
Railroad-diesel oil		
Military	0.005	
Gasoline	0.002	
Diesel	0.002	
Jet fuel	0.001	
Residual oil	0.006	
Off-highway vehicles		
Subtotals	3.4	(2.0%)
	2.4	(1.5%)
Industrial point sources	14.6	(8.9%)
Sewage treatment plants	23.8	(14.5%)
Soil surface		
Fertilizer	2.0	
Farm crop	1.6	
Orchards	0.4	
Handling	4.8	
Non-farm		
Subtotals	8.8	(5.4%)

Table 3.2 (continued)

Summary of Ammonia Emissions by Source Category Within the Modeling Region

Source category	Total emissions (tons day^{-1})	
Livestock		
Cattle		
Dairy	29.8	
Feedlot	7.2	
Range	13.6	
Horses	16.2	
Sheep	0.86	
Hogs	0.26	
Chickens	16.4	
Turkeys	0.49	
Subtotals	84.8	(51.6%)
Domestic		
Dogs	11.6	
Cats	3.5	
Human respiration	0.046	
Human perspiration	7.6	
Household ammonia use	0.57	
Subtotals	23.3	(14.2%)
Total	164.3	(100%)

Figure 3.2

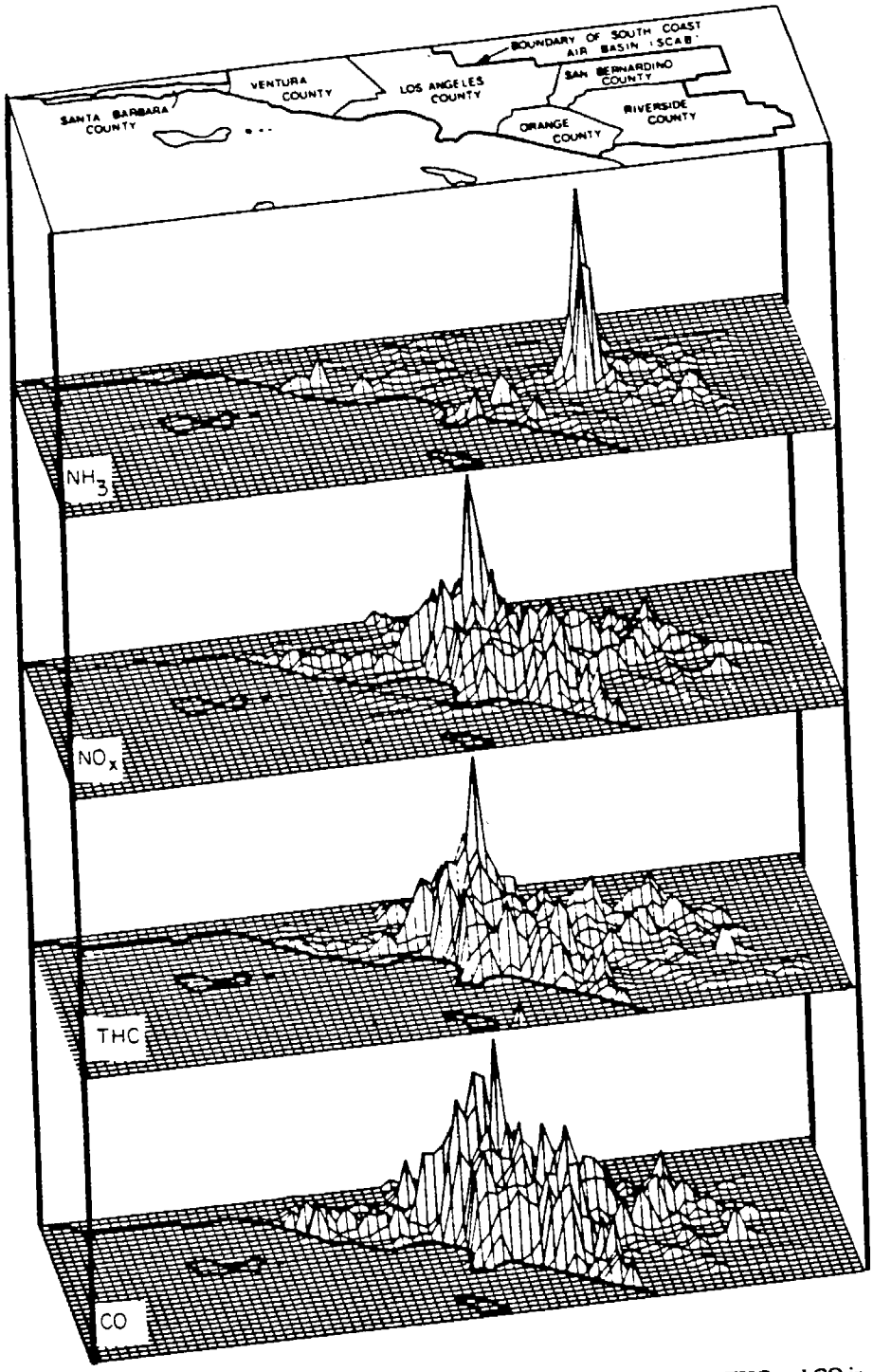

Spatial distribution of the 1982 estimated daily emissions of NH_3, NO_x, THC and CO in the South Coast Air Basin.

spatial distribution and temporal pattern of the concentrations of the atmospheric pollutants of interest.

Comparison of trajectory model predictions to observations is shown in Figure 3.3. The spatial distribution of basin-wide pollutant concentrations predicted by the grid model is shown in Figure 3.4. The dashed line shows the location of the coast. Grid model predictions at individual monitoring sites have been compared to observations as shown by the example in Figure 3.5. A complete description of these model verification tests is given in Appendices A and B to the present report. In general, air quality model predictions for O_3, NO_2, PAN and total inorganic nitrate were shown to be quite close to the observations— both in absolute value and in a relative sense over time. Predicted HNO_3 and aerosol nitrate levels were within the equivalent of a few ppb NO_x of the observed values.

3.3 PREPARATION OF LAND-USE DATA REQUIRED FOR THE REVISED DEPOSITION MODULE

In order to use the revised deposition model, land-use data organized according to the grid system shown in Figure 3.1 were prepared. That grid system first was drawn over USGS land-use maps. Then each 5 km x 5 km grid cell was subdivided into 100 smaller squares, each 0.5 km x 0.5 km on a side. Each of the 0.5 km x 0.5 km cells was assigned to the appropriate land-use type, chosen from the 31 land-use categories given in Table 2.1. The results for these small 0.5 km x 0.5 km cells then were used to assign the percentage of each 5 km x 5 km grid cell that falls into each land-use category.

Gridded land-use maps that result from this process are shown in Figures 3.6-3.36. The grid system shown is the same as that in Figure 3.1, and the percentage of each grid square devoted to a particular land-use is indicated by the density of the dot pattern in each cell. If a cell is entirely devoted to a particular use, the cell is shaded black on the relevant land-use map. If the cell is not at all devoted to a given use, then it appears to be white on that particular land-use map. A cell that was 50% covered by residential uses in Figure 3.6 would be shown with a pattern covering 50%of its surface area with black dots.

Residential land uses shown for land-use type 11 are distributed in a pattern similar to that seen for vehicular-derived pollutants (e.g., CO) shown in Figure 3.2.

Figure 3.3 Observed and predicted pollutant concentrations at Rubidoux, 31 August 1982. Results are from the trajectory modeling study of Russell and Cass (1986).

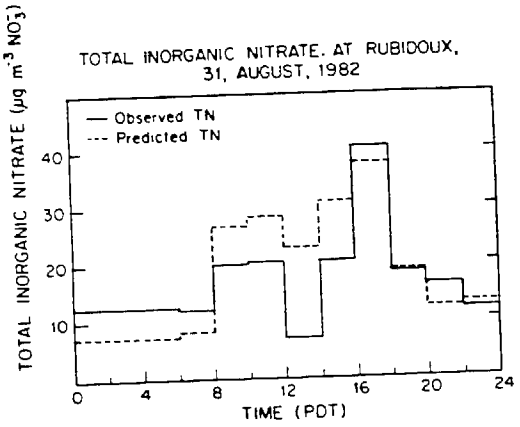

Observed and predicted total nitrate (TN = AN + HNO_3) at Rubidoux, CA, 31 August 1982.

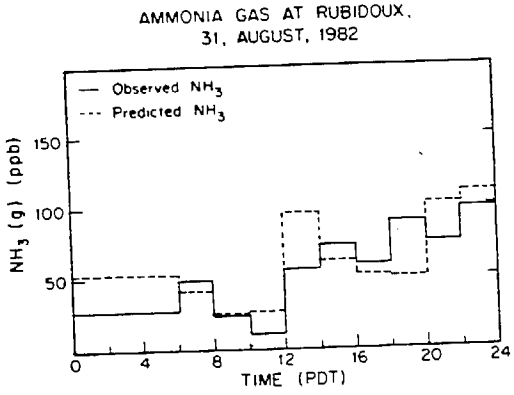

Observed and predicted NH_3 at Rubidoux, CA, 31 August 1982.

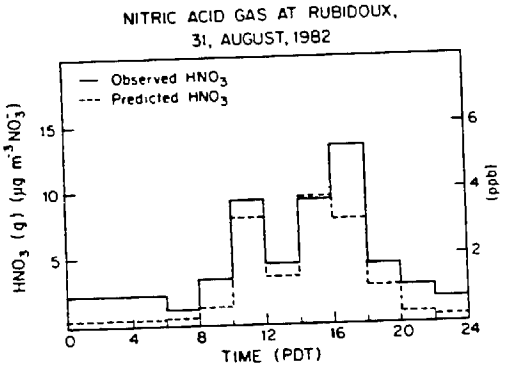

Observed and predicted HNO_3 (g) at Rubidoux, CA, 31 August 1982.

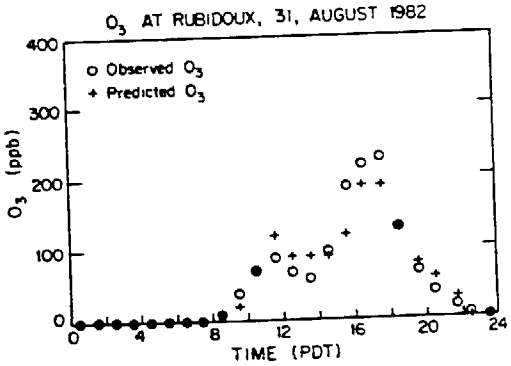

Observed and predicted O_3 at Rubidoux, CA, 31 August 1982.

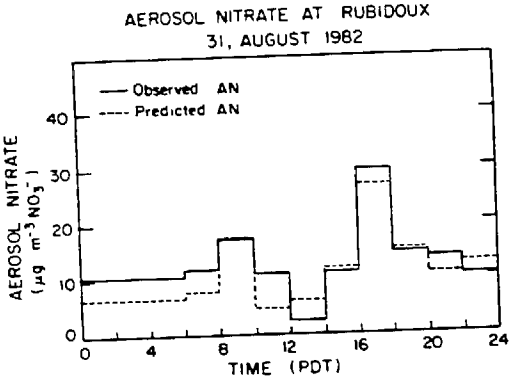

Observed and predicted NO_3^- at Rubidoux, CA, 31 August 1982.

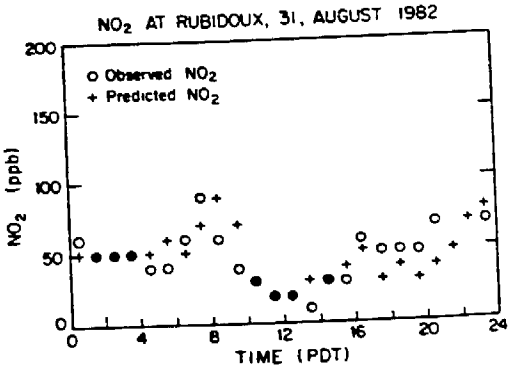

Observed and predicted NO_2 at Rubidoux, CA, 31 August 1982.

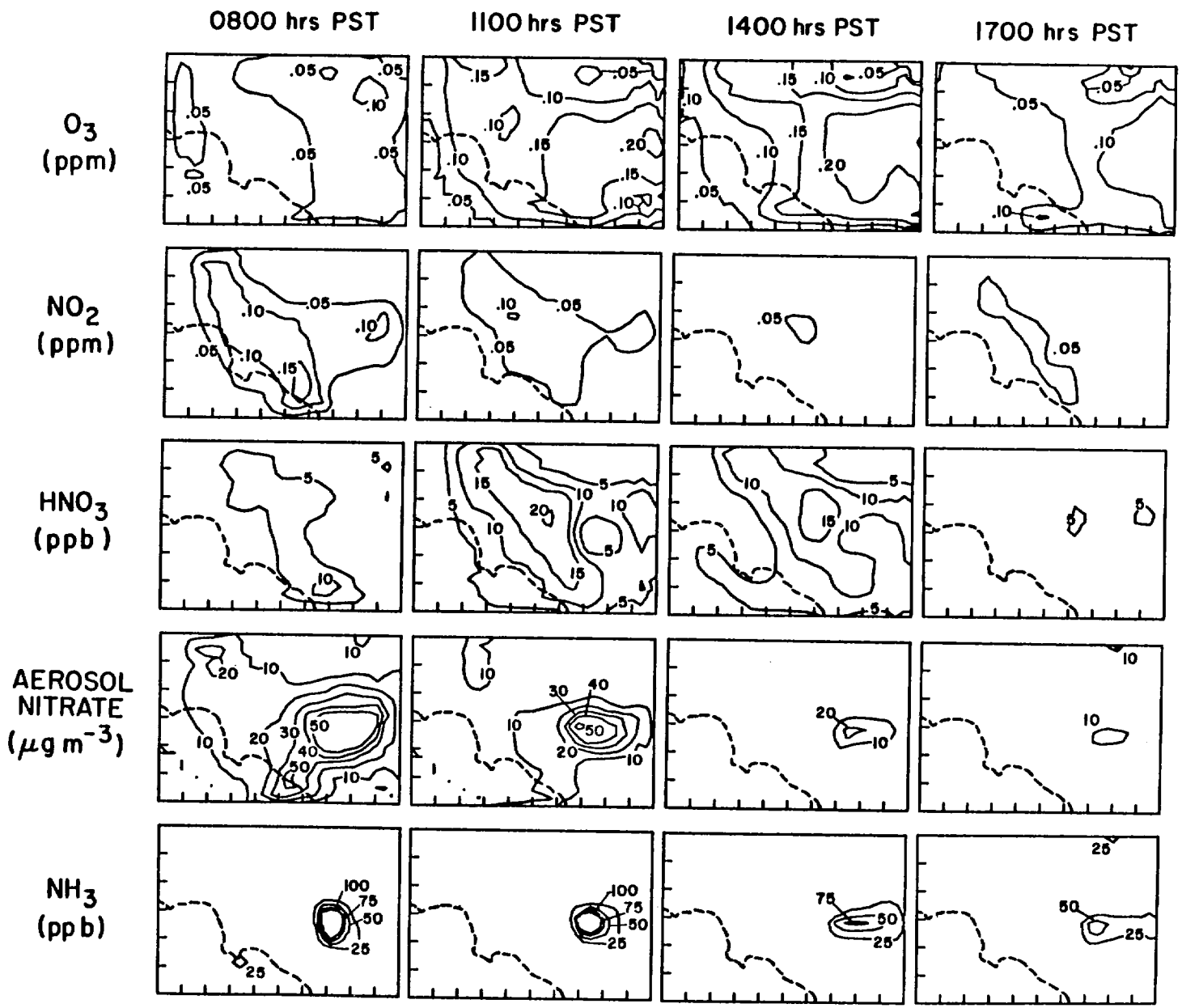

Figure 3.4 Spatial distribution of pollutant concentration predictions in the South Coast Air Basin produced by the photochemical grid model, August 31, 1982. Dashed line shows the location of the coast.

Figure 3.5 Comparison of observed pollutant concentrations to concentration predictions made by the grid model at Anaheim, August 30-31, 1982.

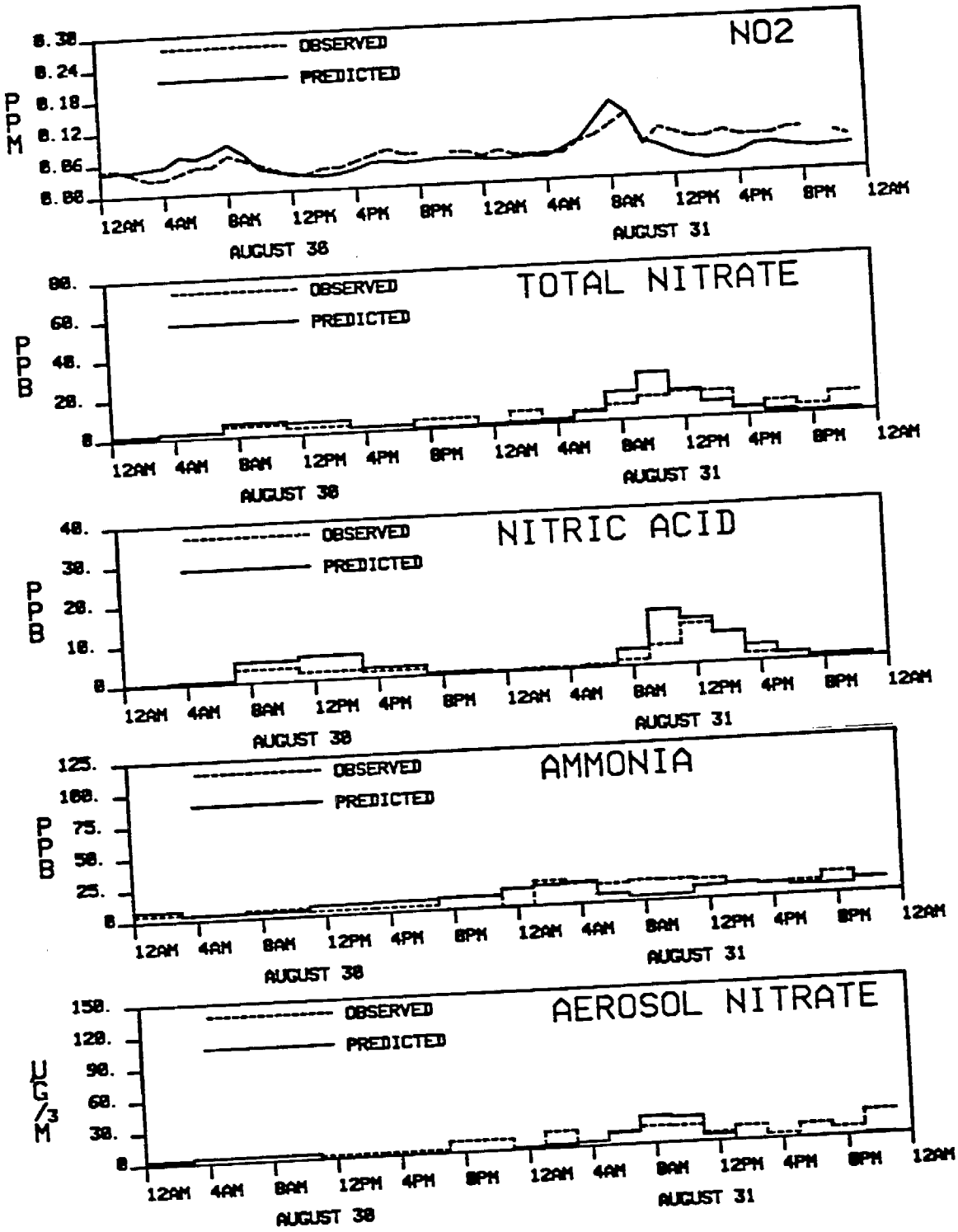

Figure 3.6

LANDUSE 11 (RESIDENTIAL)

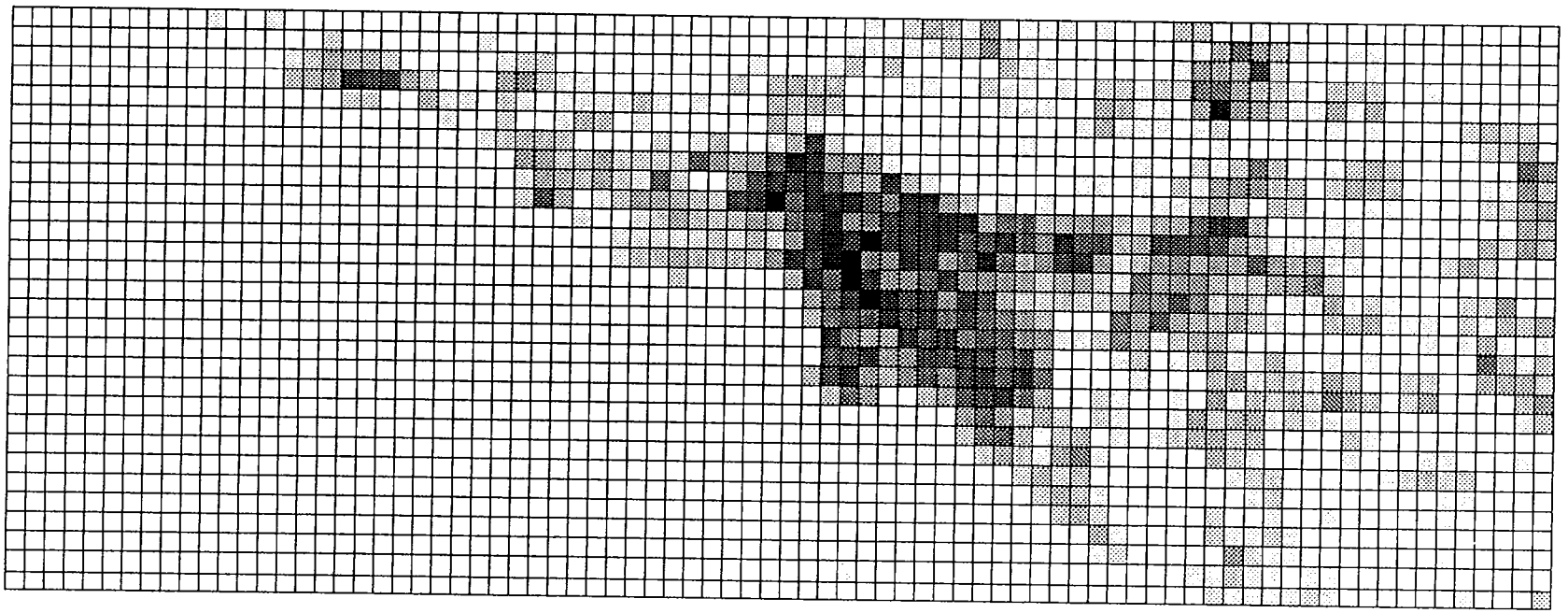

Figure 3.7

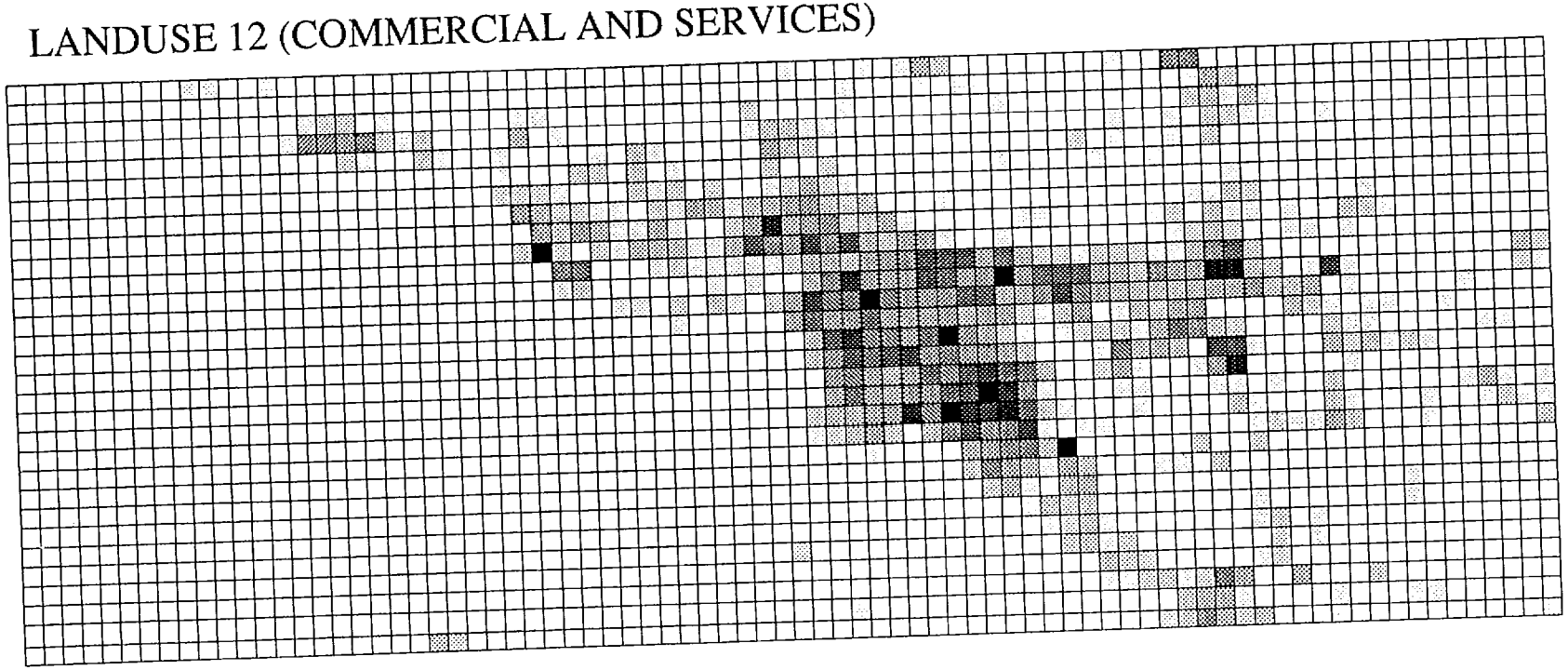

Figure 3.8

LANDUSE 13 (INDUSTRIAL)

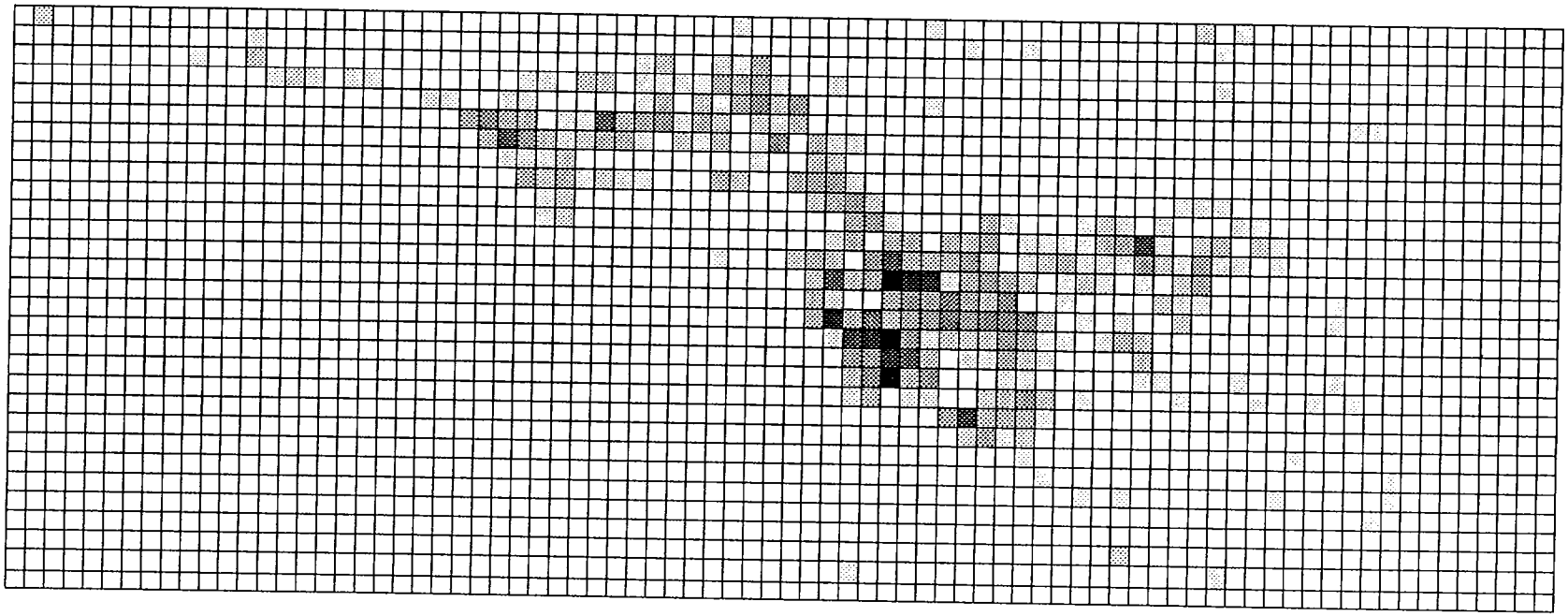

Figure 3.9

LANDUSE 14 (TRANSPORTATION, COMMUNICATIONS AND UTILITIES)

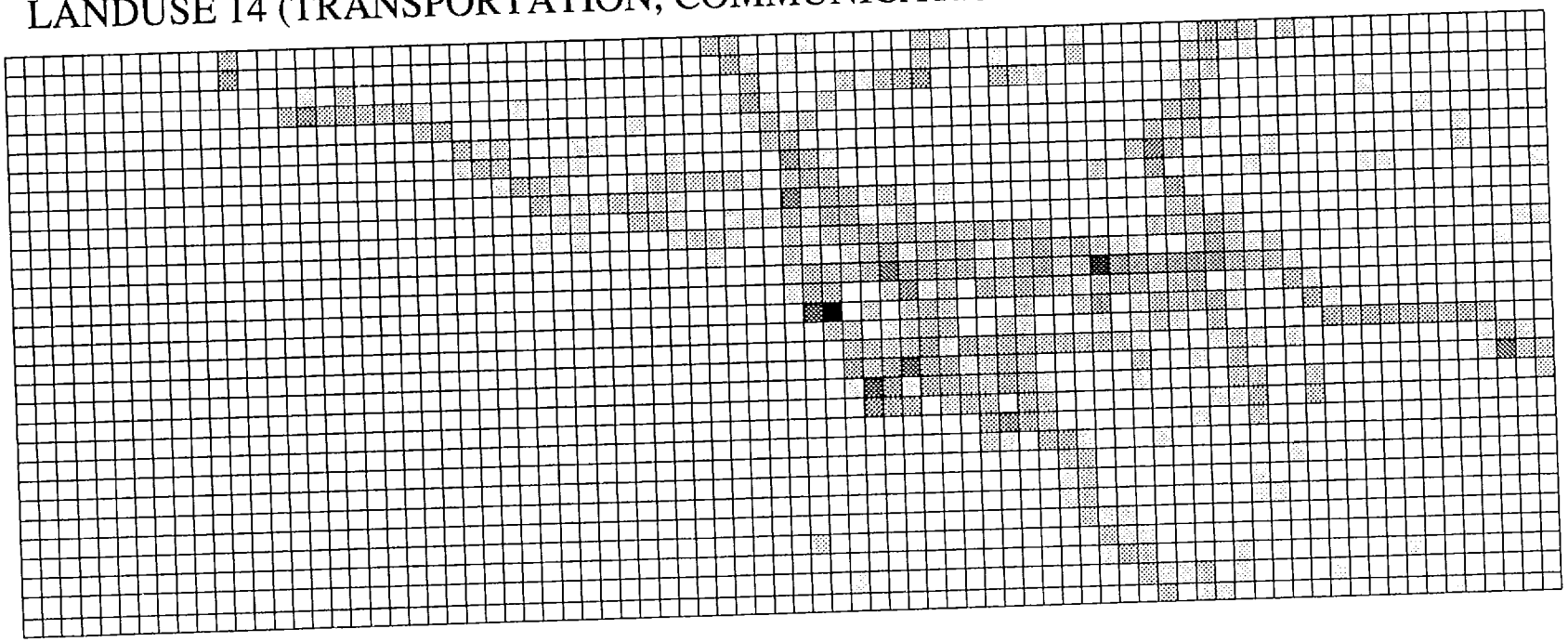

Figure 3.10

LANDUSE 15 (INDUSTRIAL AND COMMERCIAL COMPLEXES)

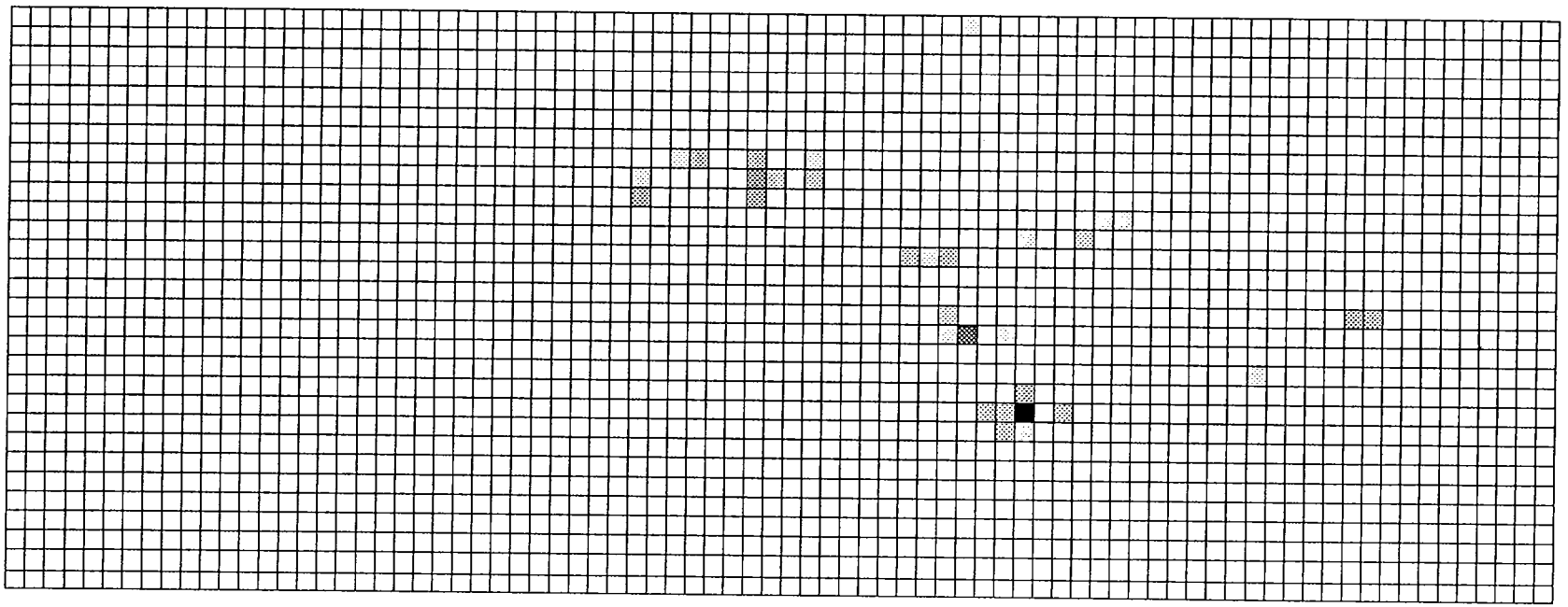

Figure 3.11

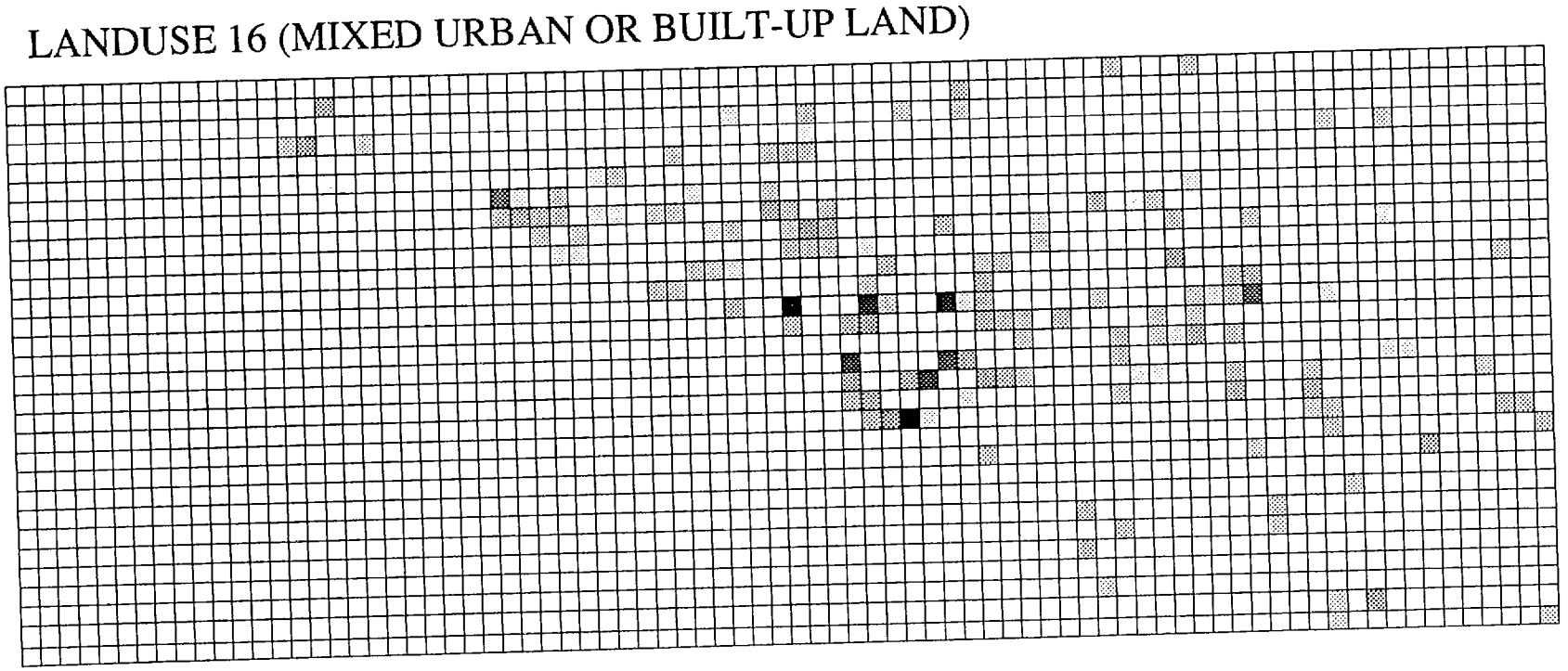

Figure 3.12

LANDUSE 17 (OTHER URBAN OR BUILT-UP LAND)

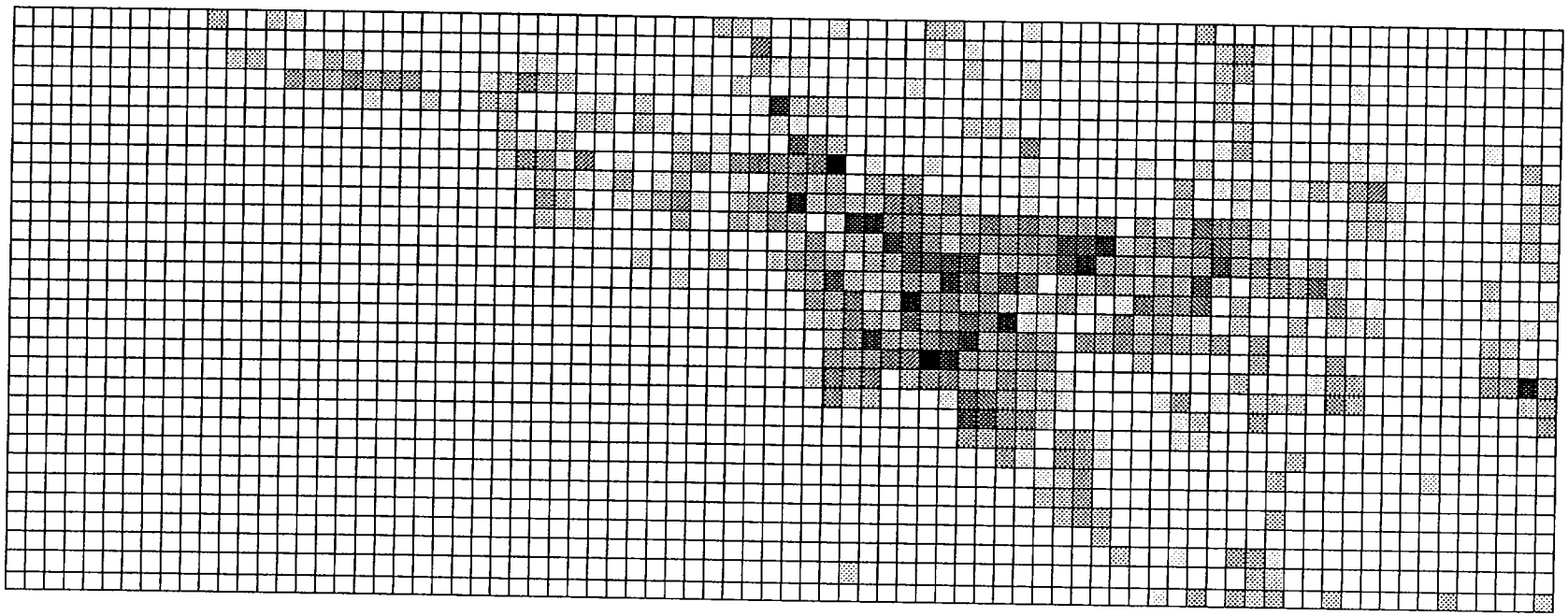

Figure 3.13

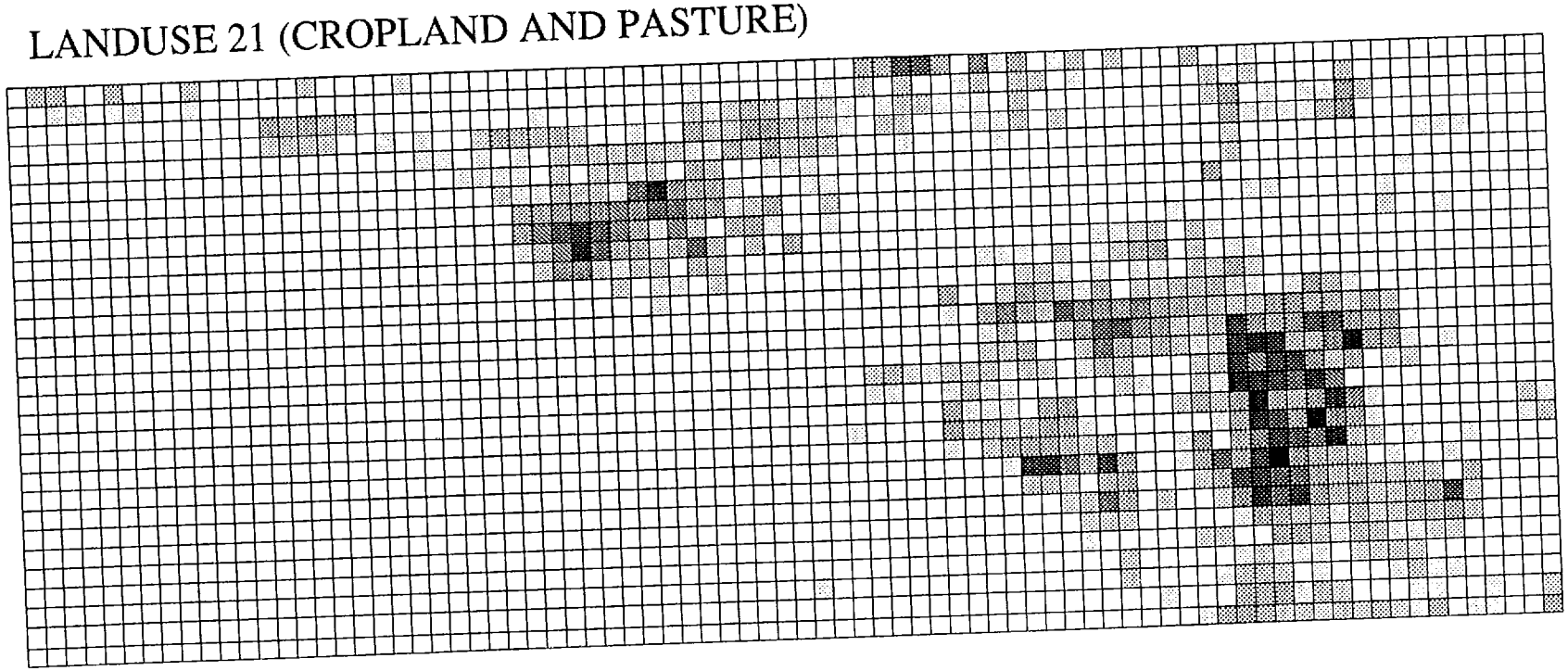

Figure 3.14

LANDUSE 22 (ORCHARDS, GROVES, VINEYARDS, NURSERIES AND ORNAMENTAL)

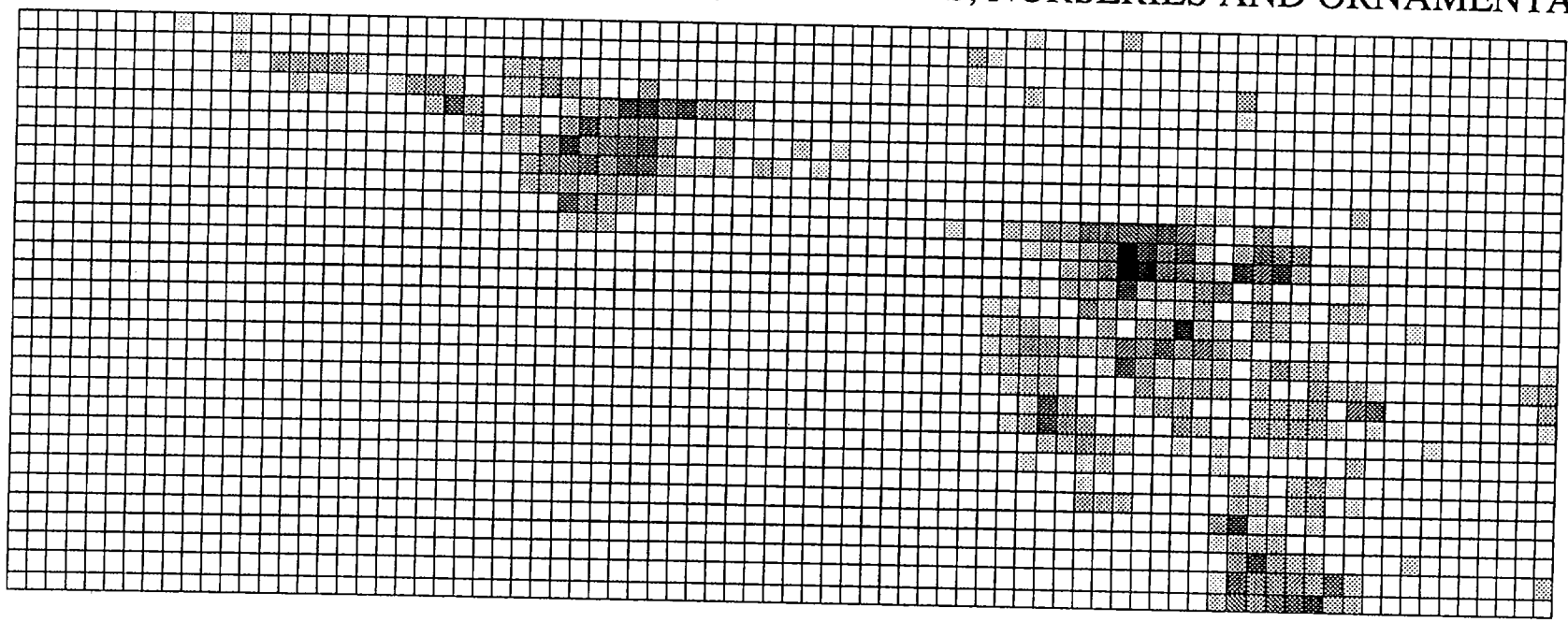

Figure 3.15

LANDUSE 23 (CONFINED FEEDING OPERATIONS)

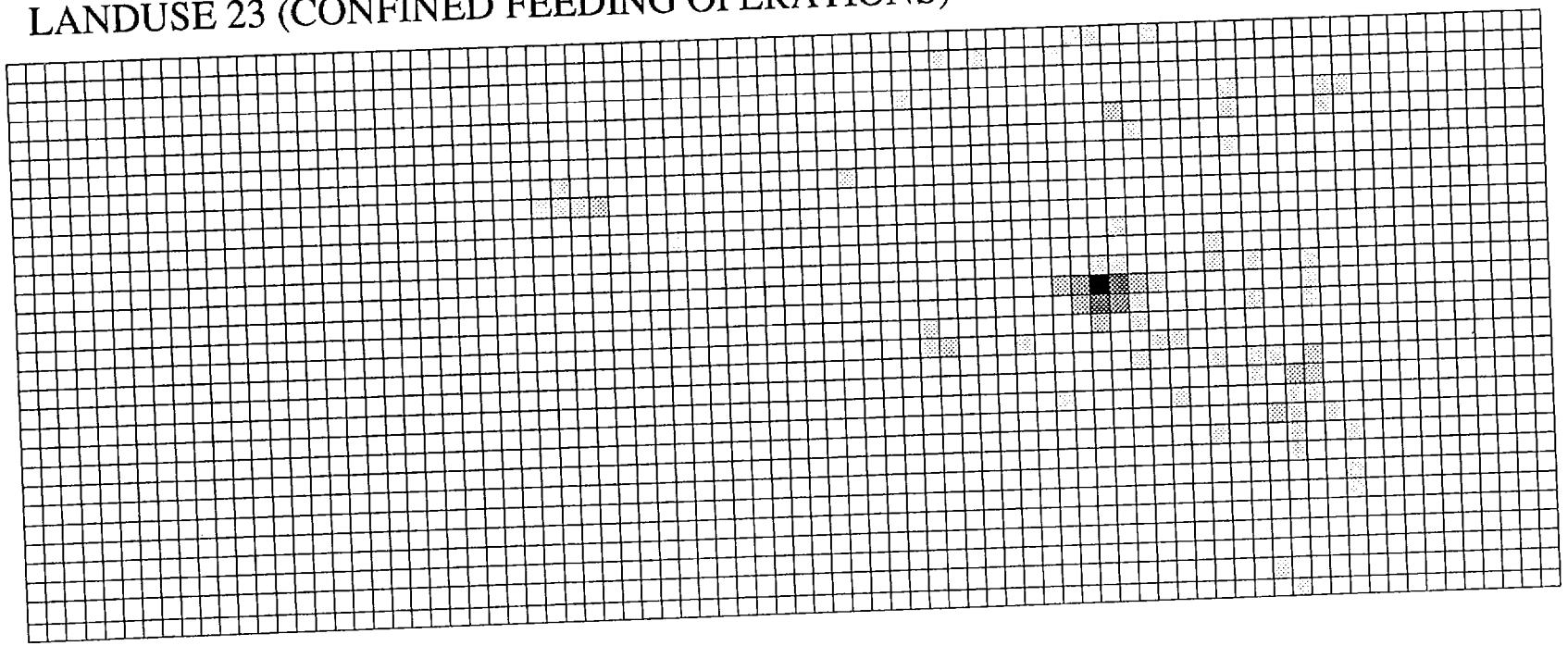

Figure 3.16

LANDUSE 24 (OTHER AGRICULTURAL LAND)

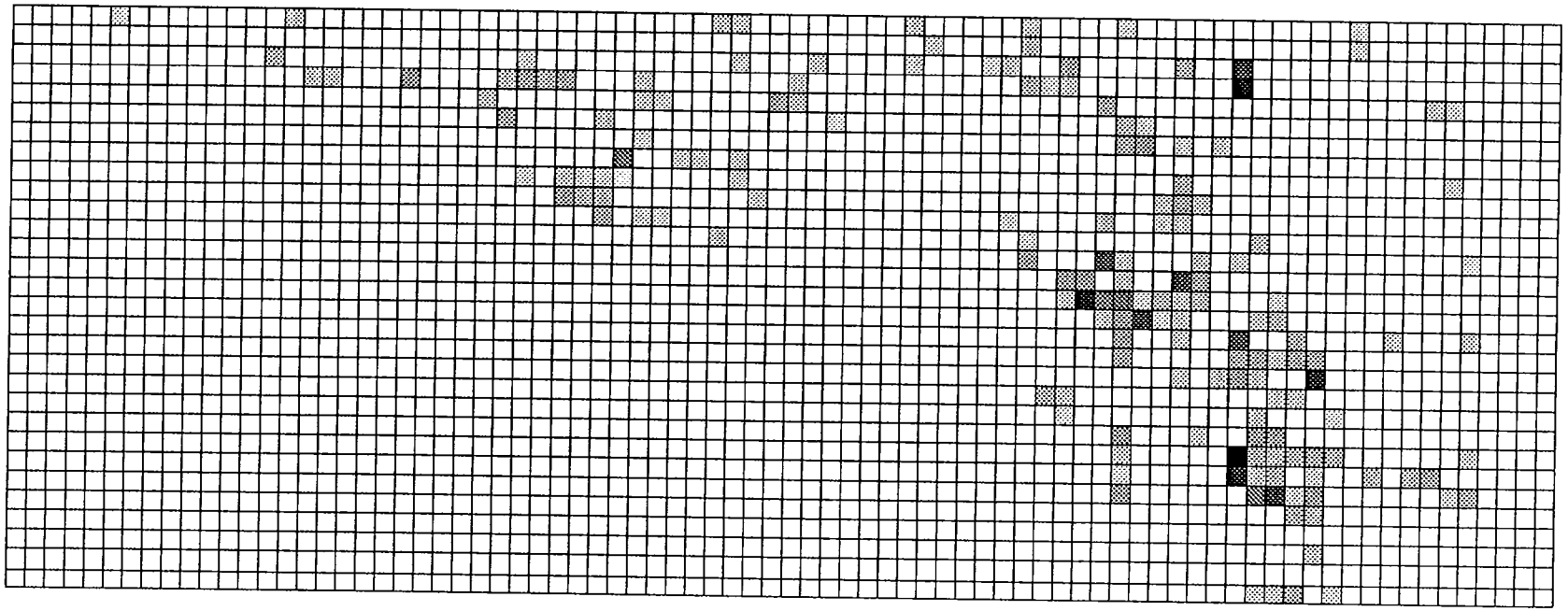

Figure 3.17

LANDUSE 31 (HERBACEOUS RANGELAND)

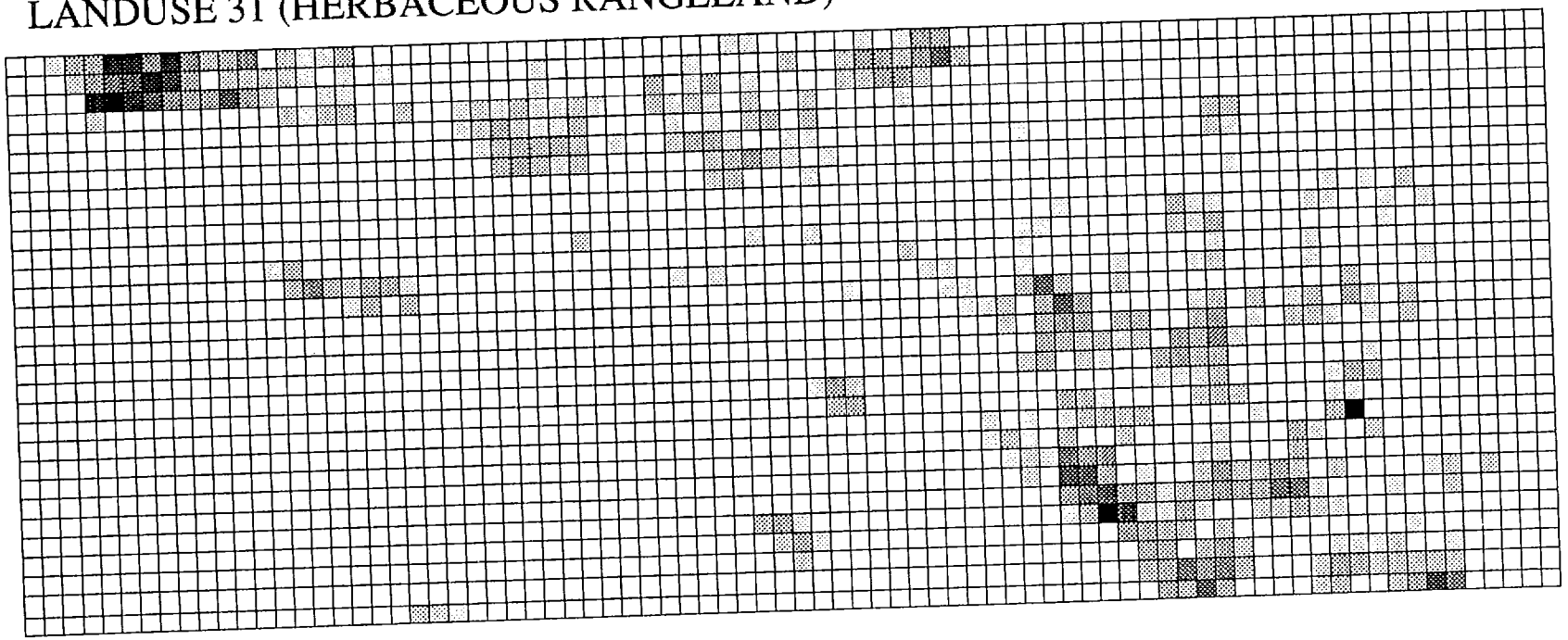

Figure 3.18

LANDUSE 32 (SHRUB AND BRUSH RANGELAND)

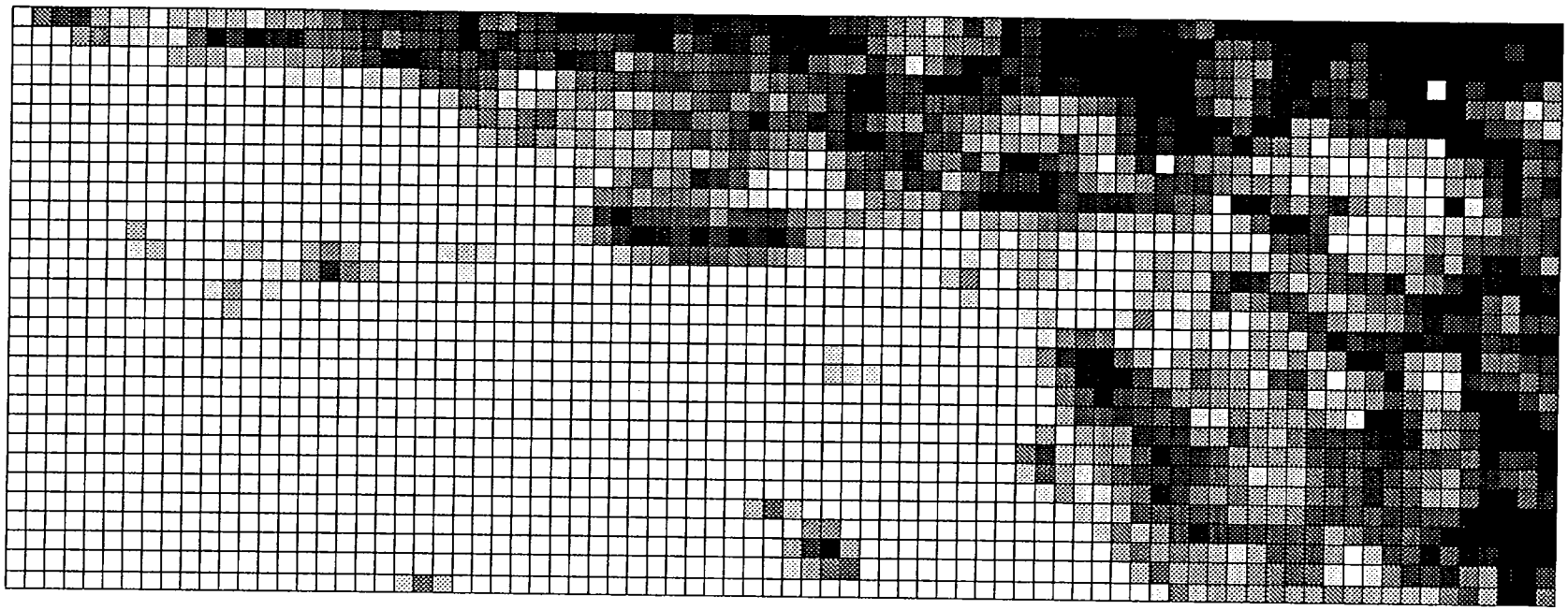

Figure 3.19

LANDUSE 33 (MIXED RANGELAND)

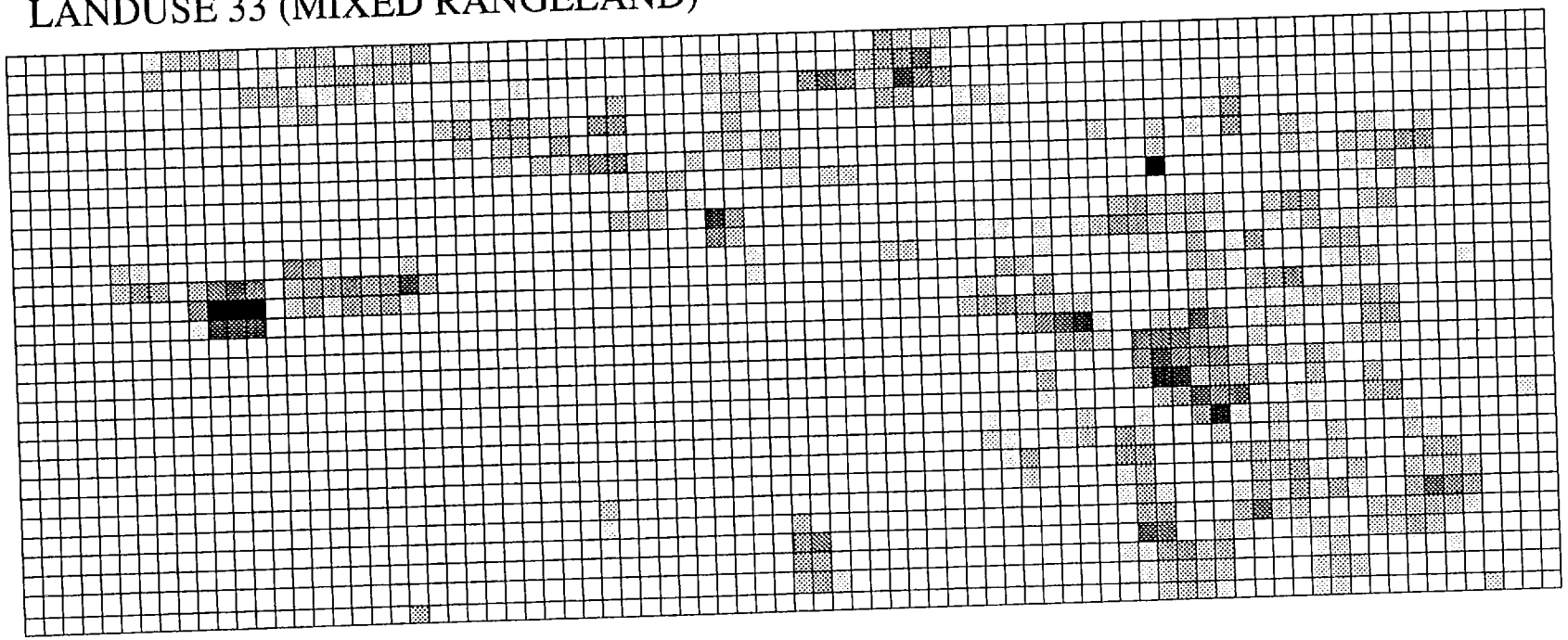

Figure 3.20

LANDUSE 41 (DECIDUOUS FOREST LAND)

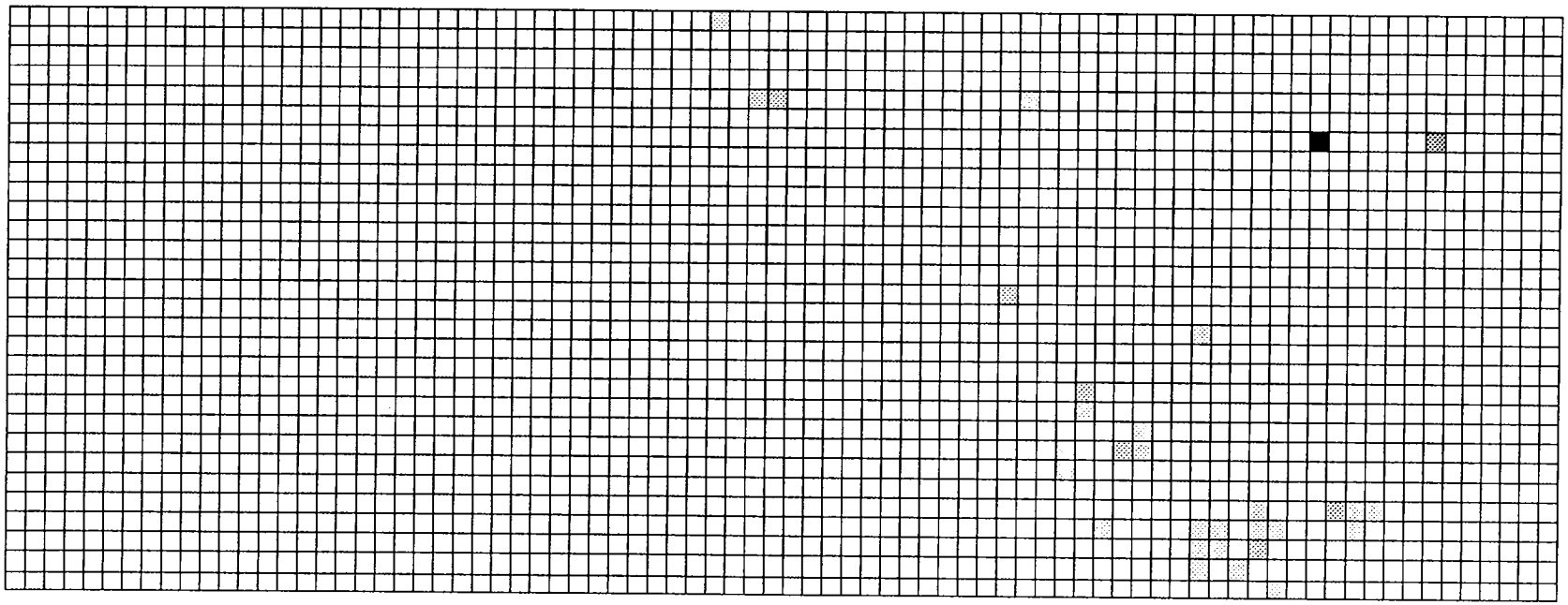

Figure 3.21

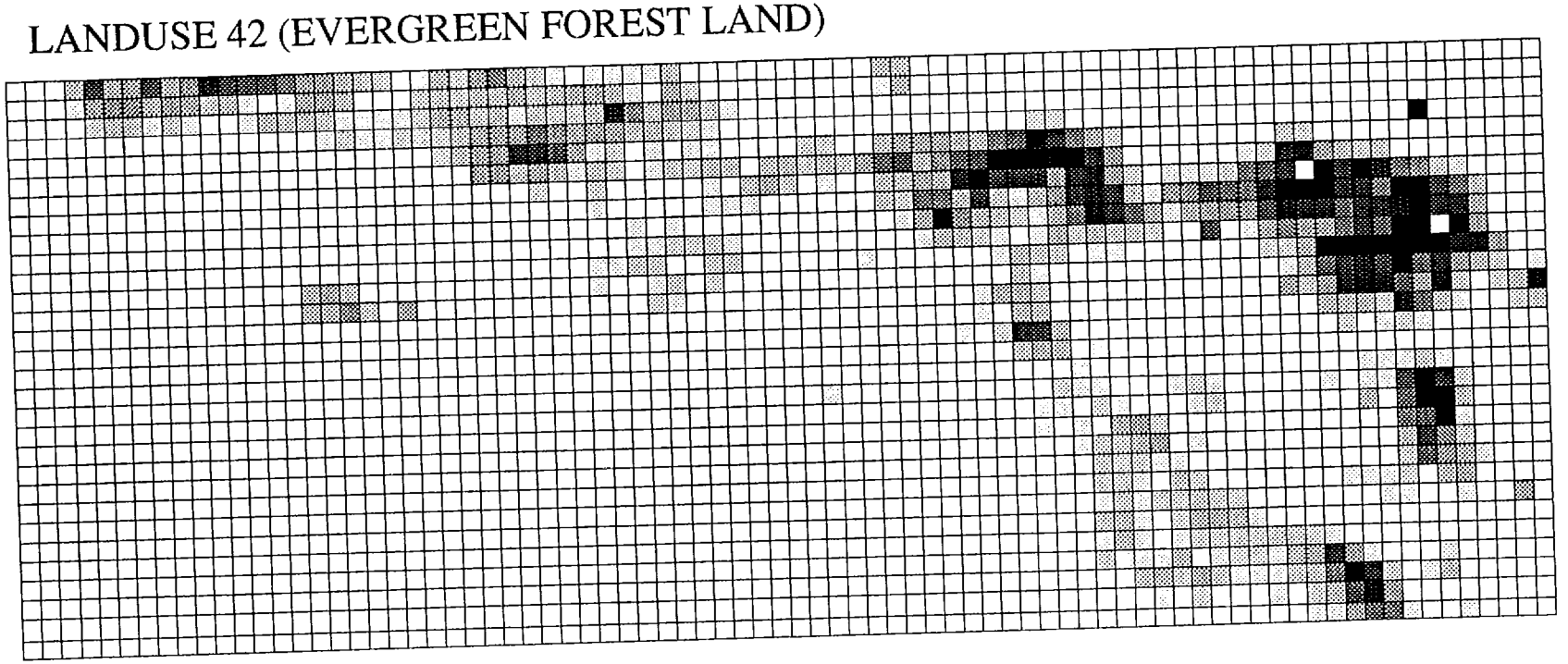

Figure 3.22

LANDUSE 43 (MIXED FOREST LAND)

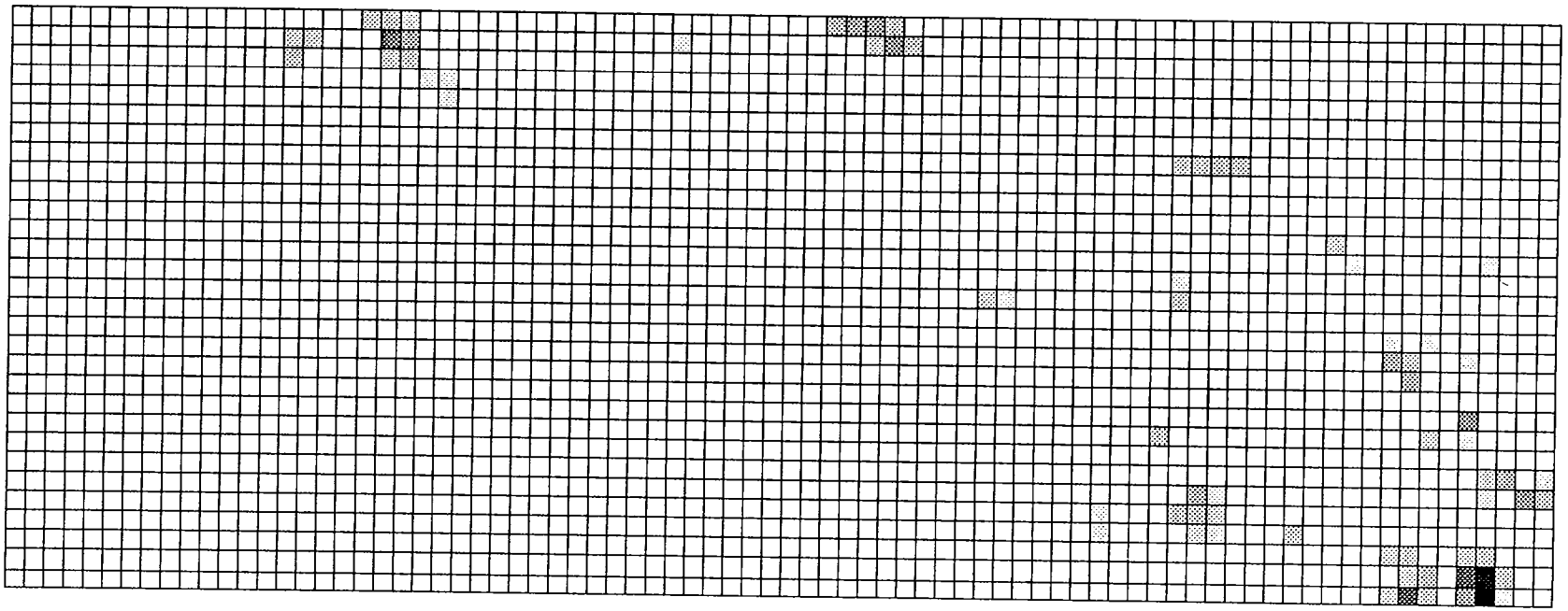

Figure 3.23

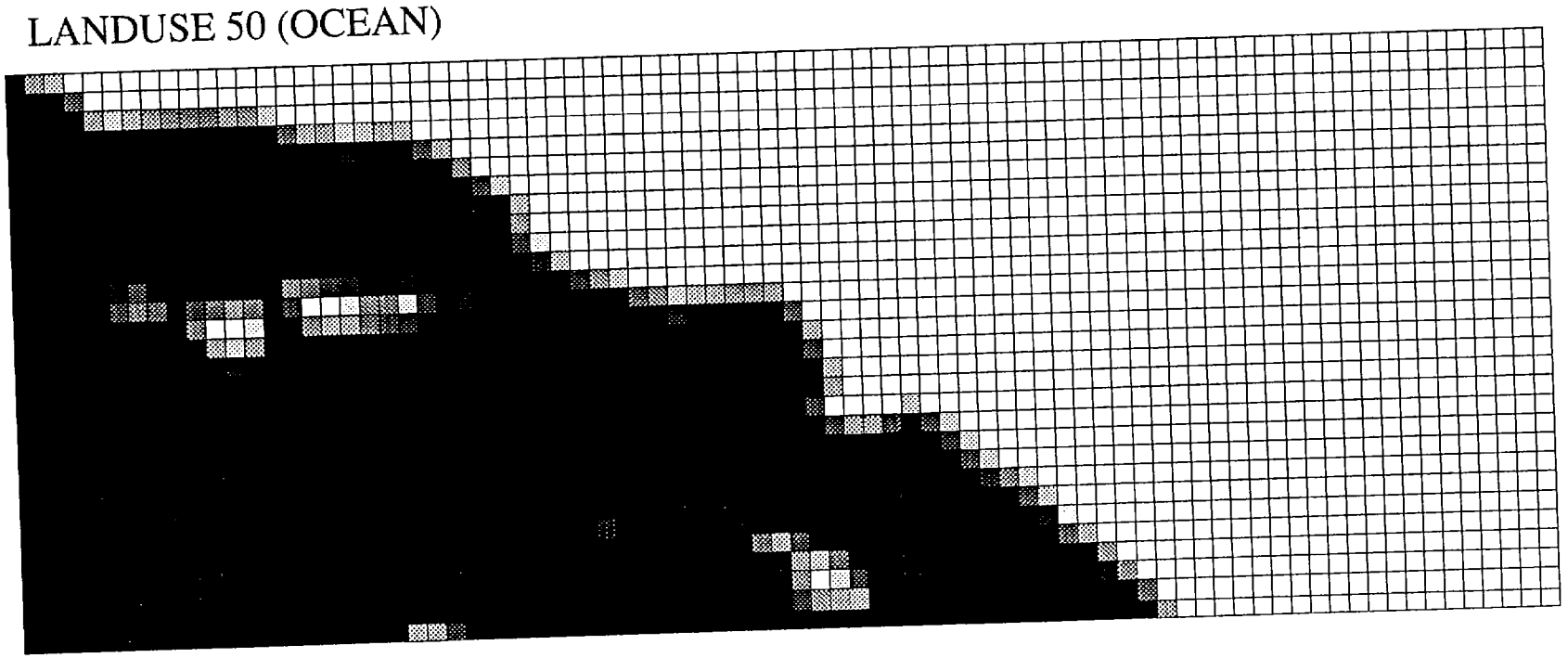

Figure 3.24

LANDUSE 51 (STREAMS AND CANALS)

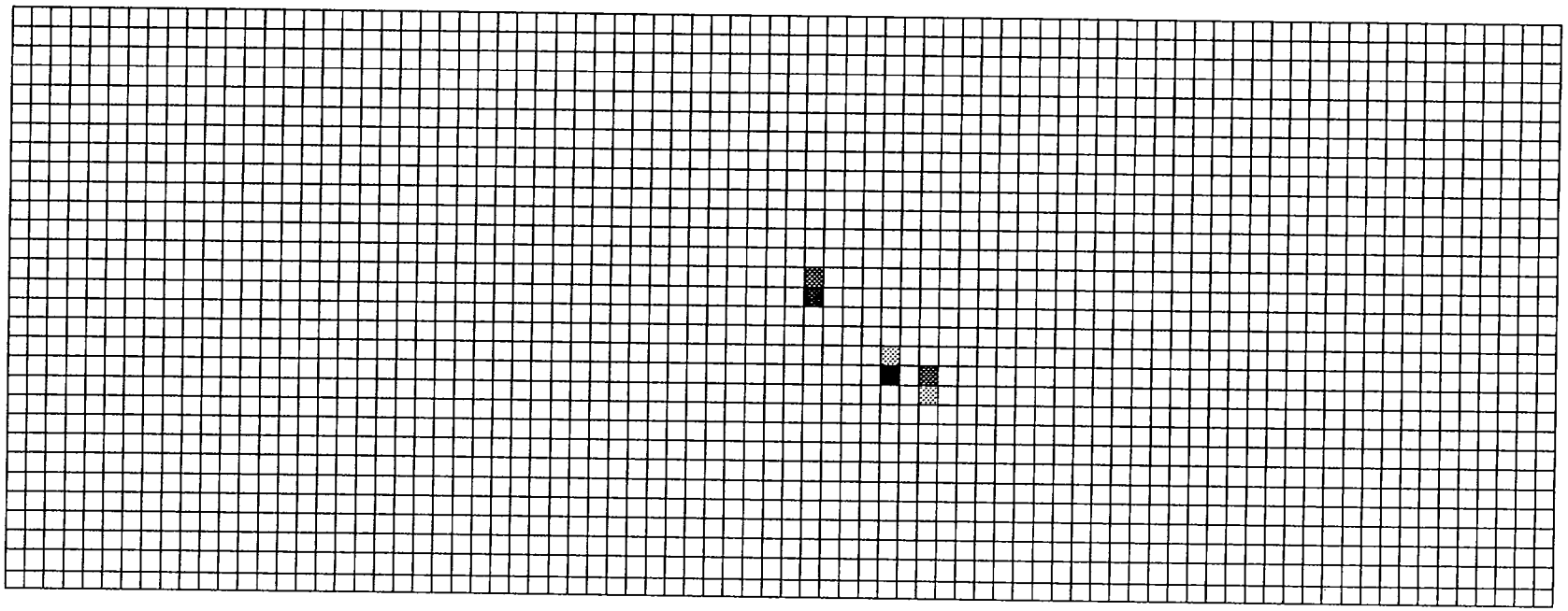

Figure 3.25

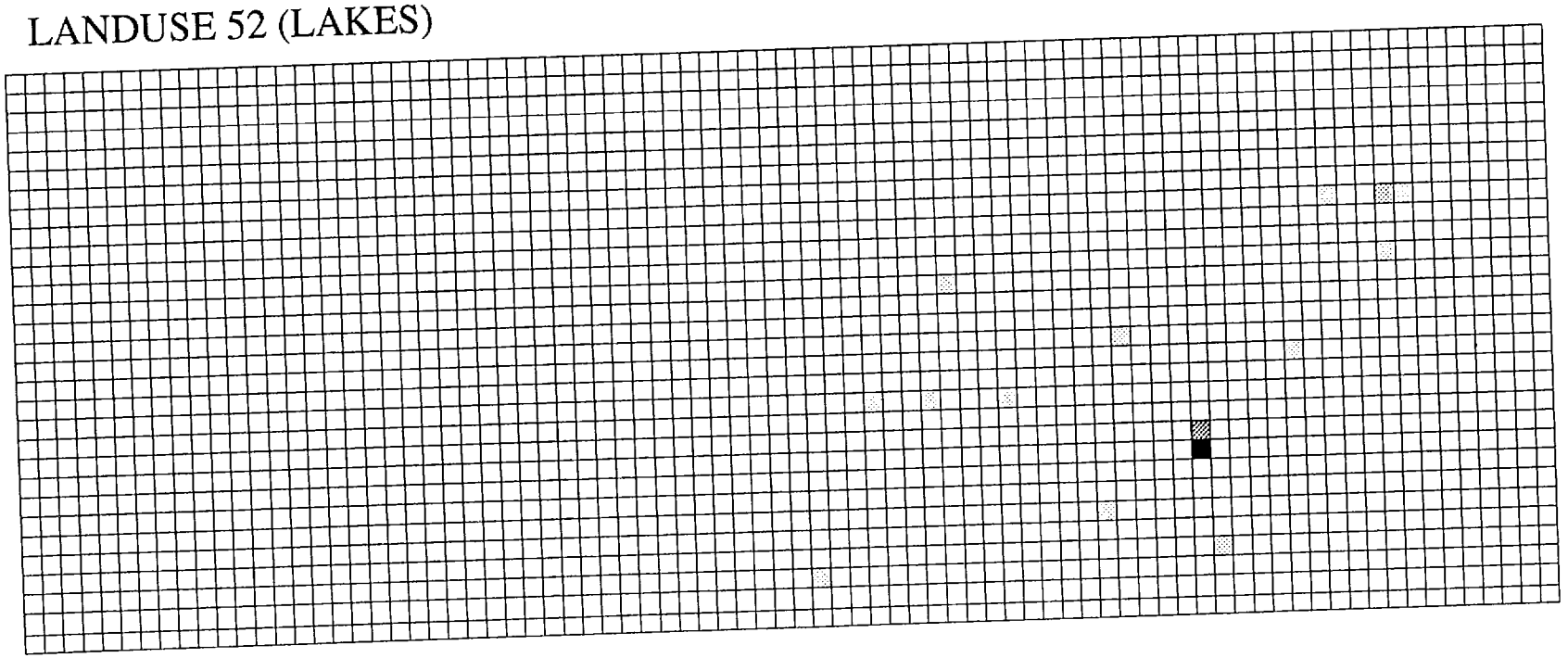

Figure 3.26

LANDUSE 53 (RESERVOIRS)

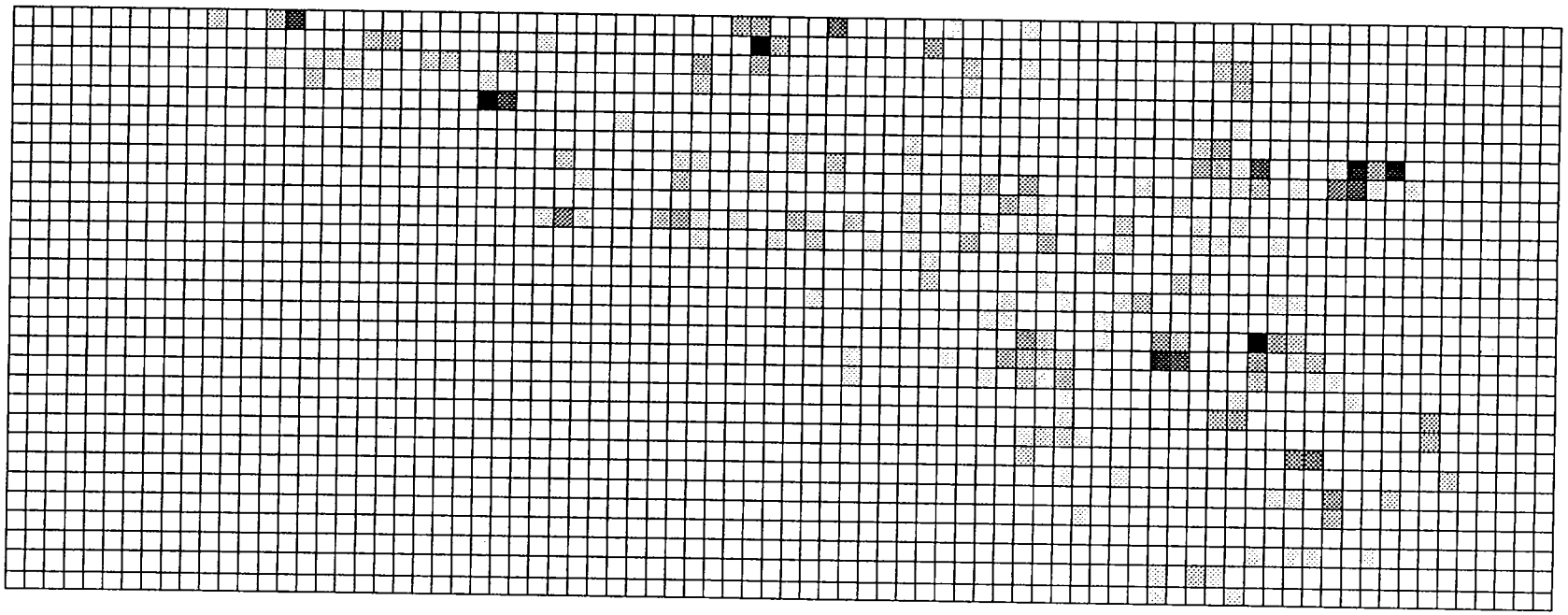

Figure 3.27

LANDUSE 54 (BAYS AND ESTUARIES)

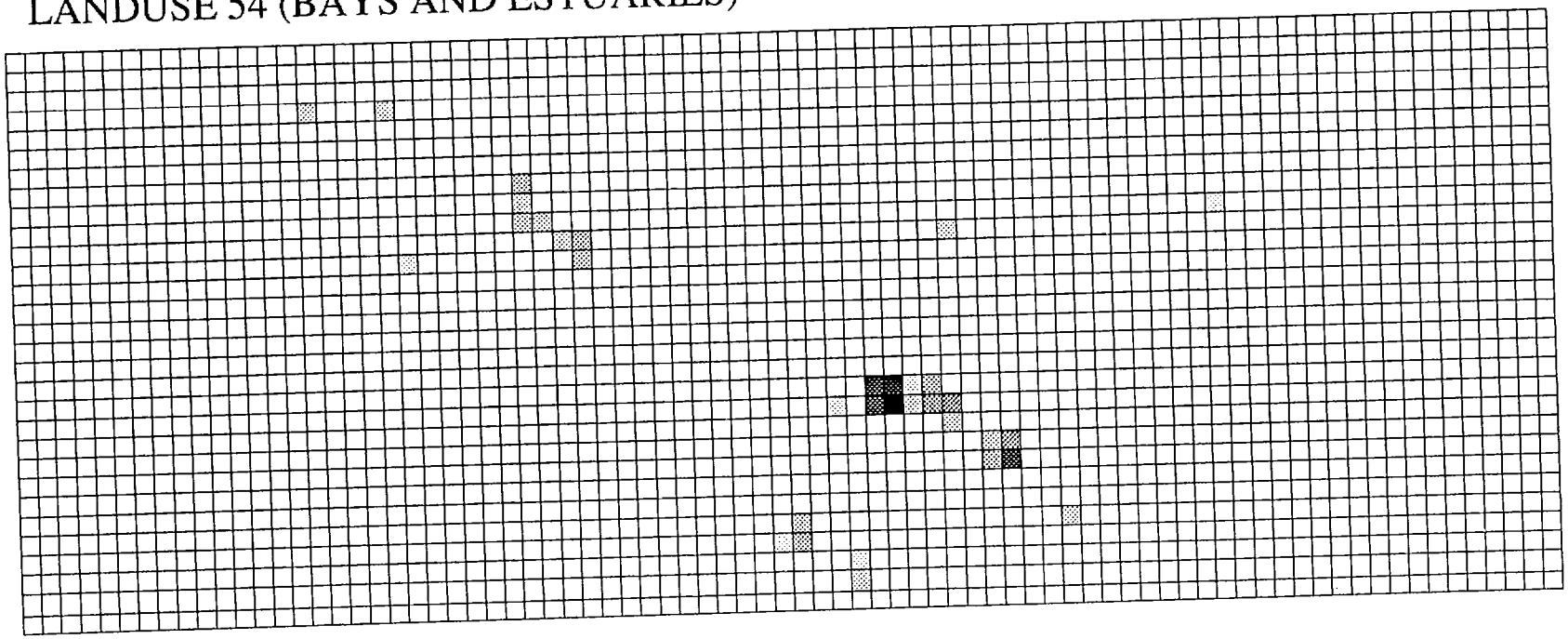

Figure 3.28

LANDUSE 61 (FORESTED WETLAND)

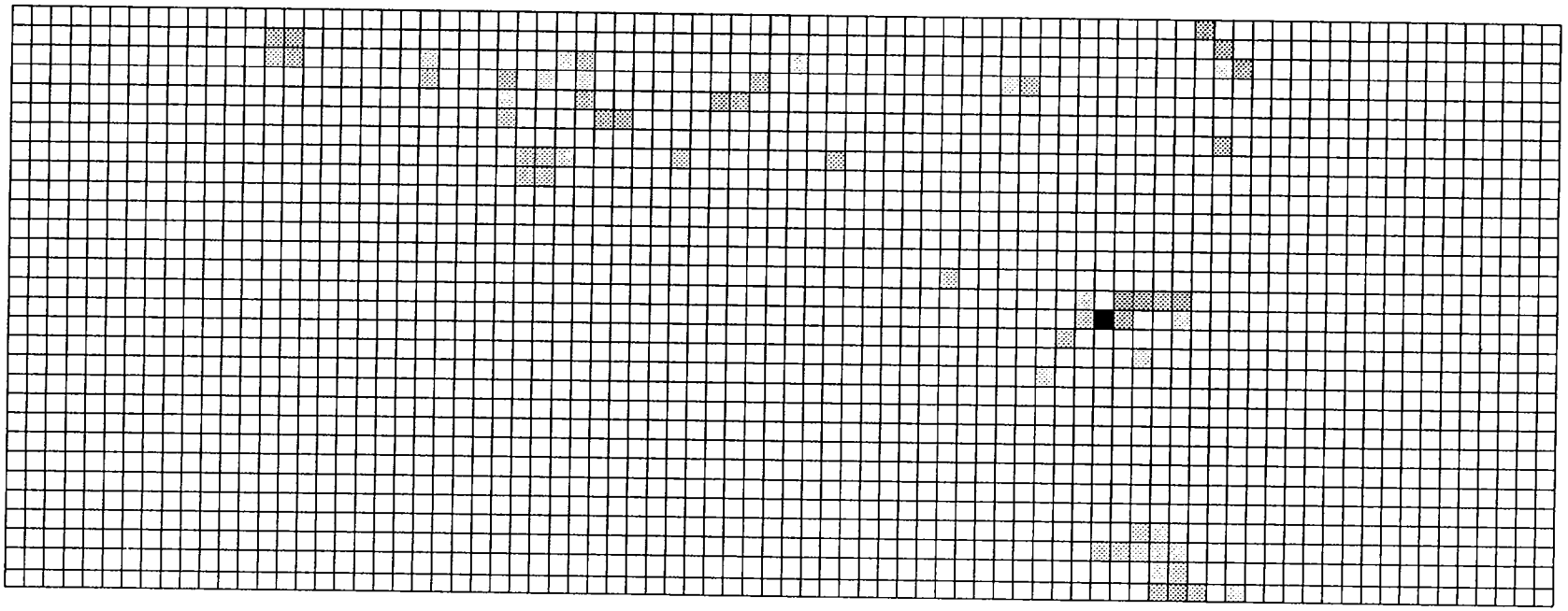

Figure 3.29

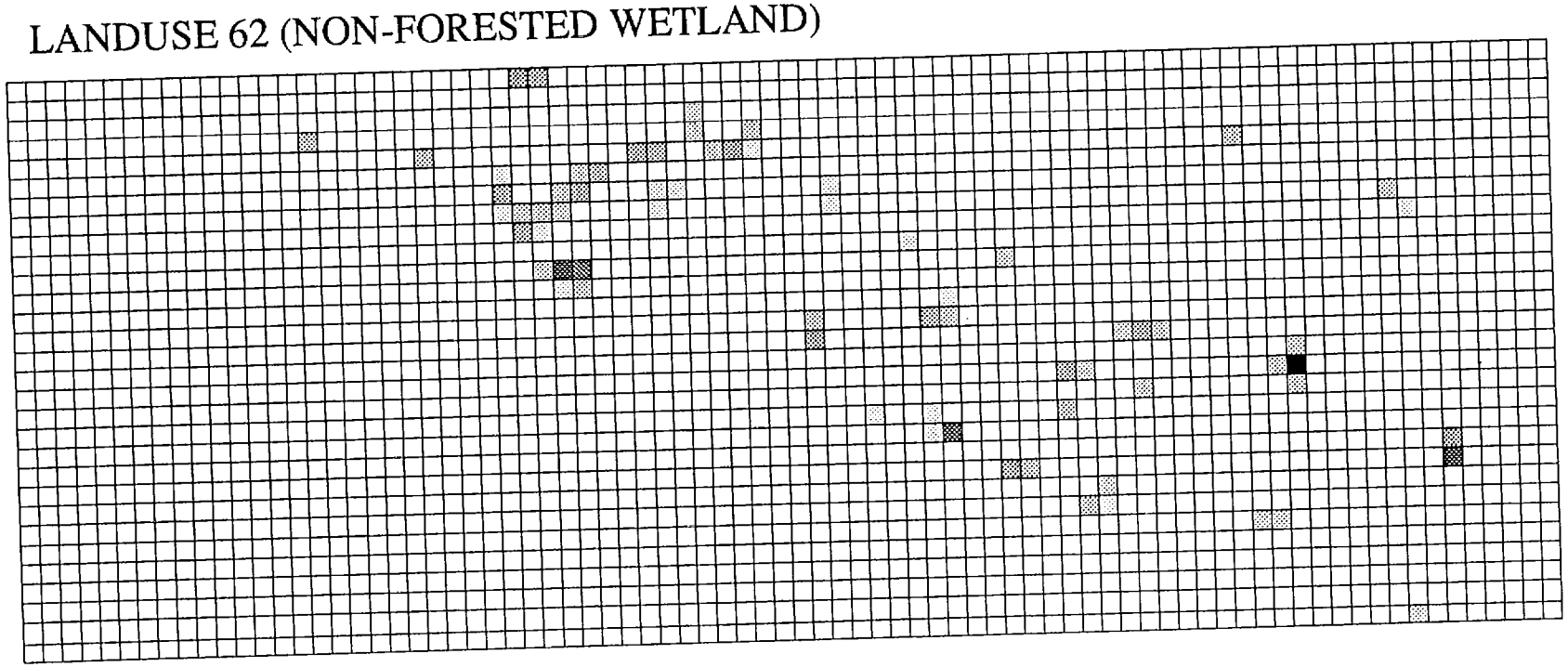

Figure 3.30

LANDUSE 71 (DRY SALT FLATS)

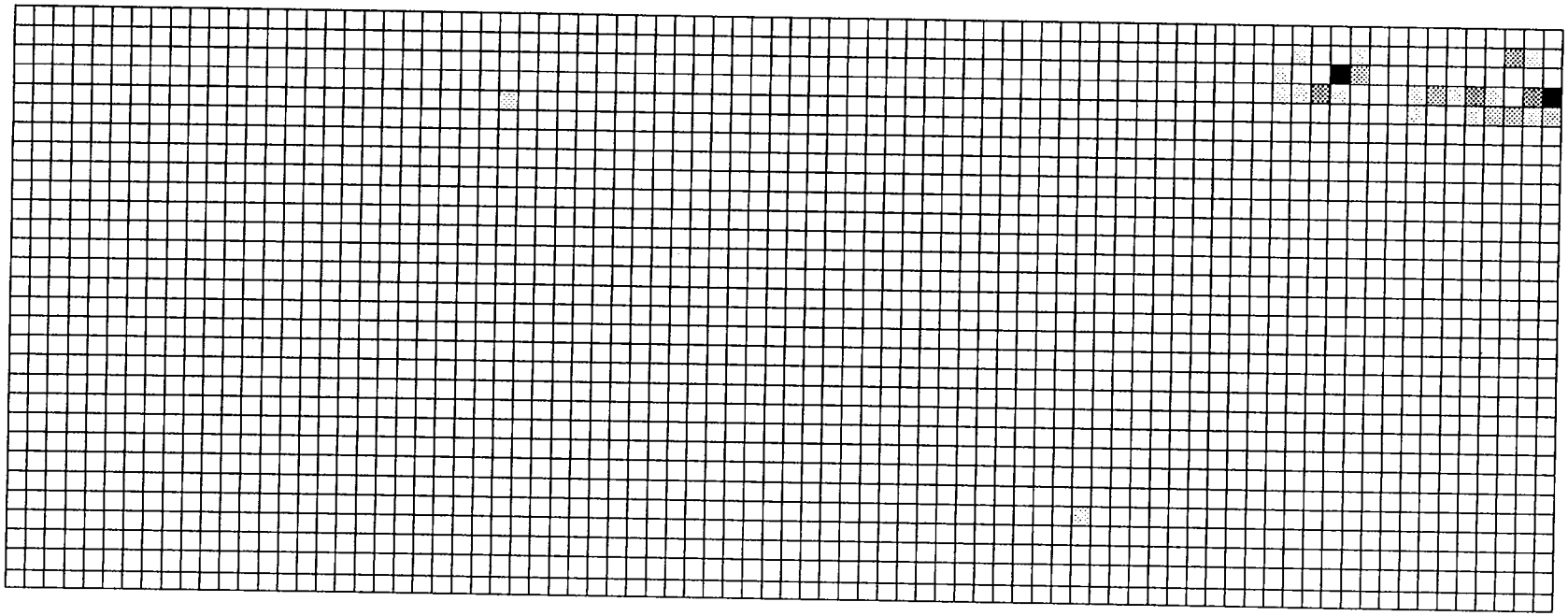

Figure 3.31

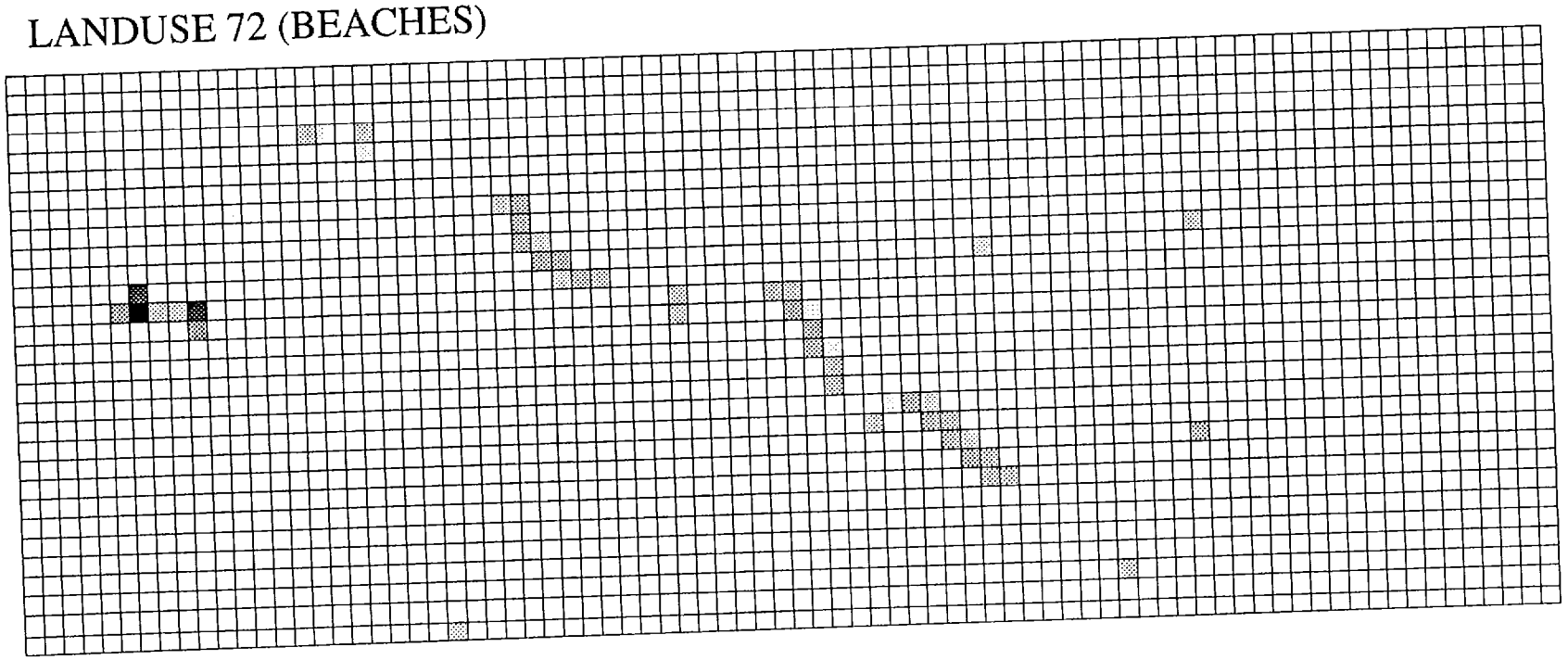

Figure 3.32

LANDUSE 73 (SANDY AREAS OTHER THAN BEACHES)

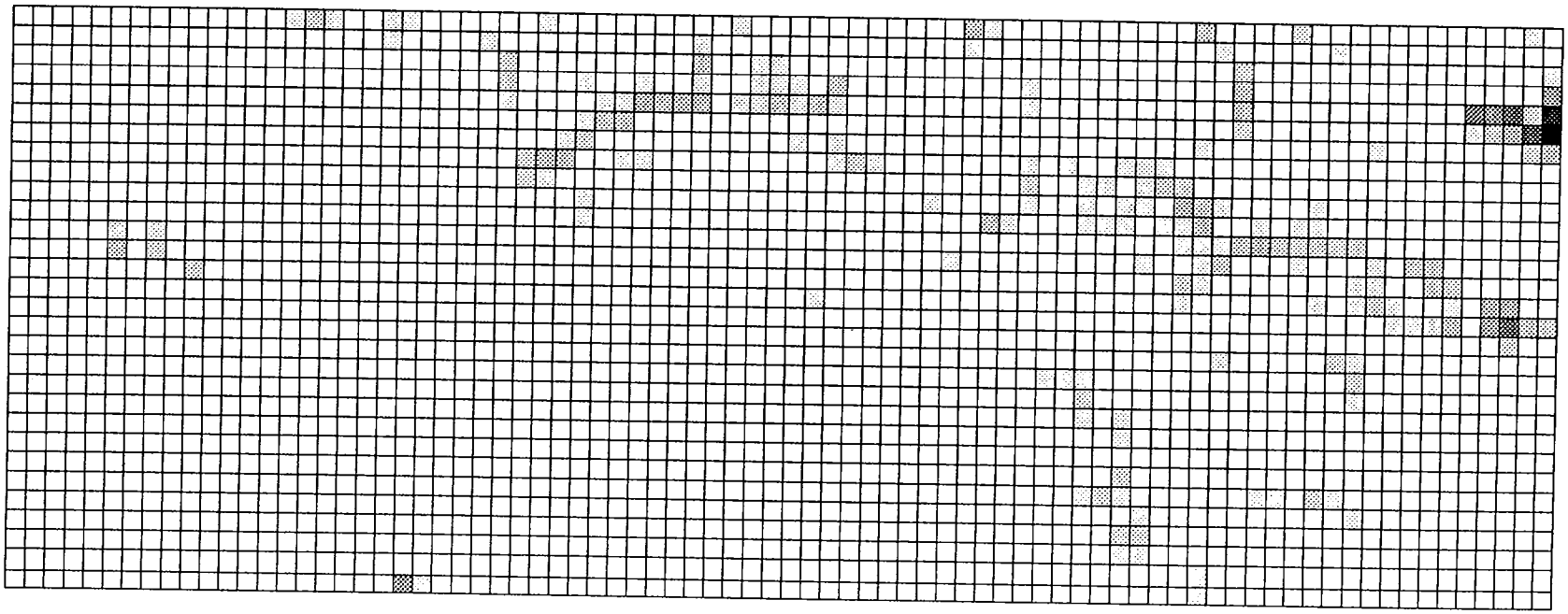

Figure 3.33

LANDUSE 74 (BARE EXPOSED ROCK)

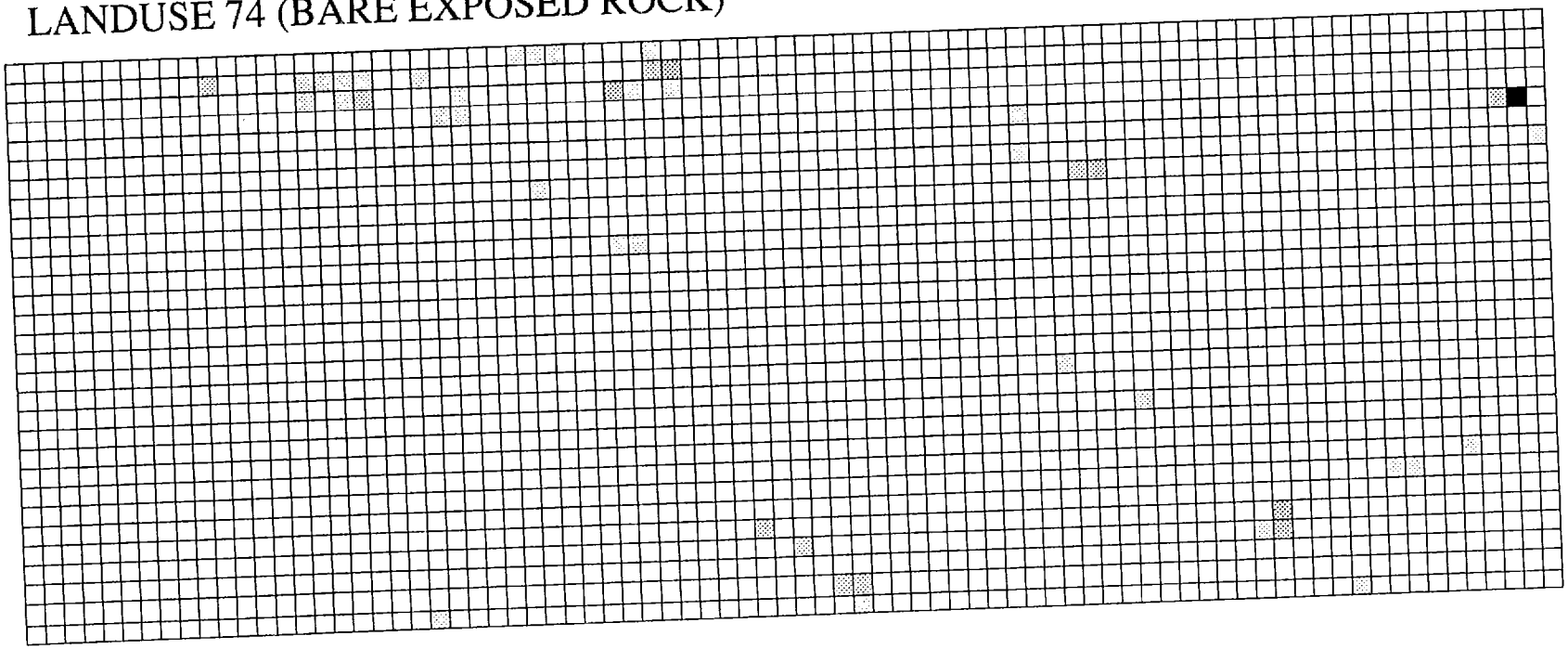

Figure 3.34

LANDUSE 75 (STRIP MINES, QUARRIES AND GRAVEL PITS)

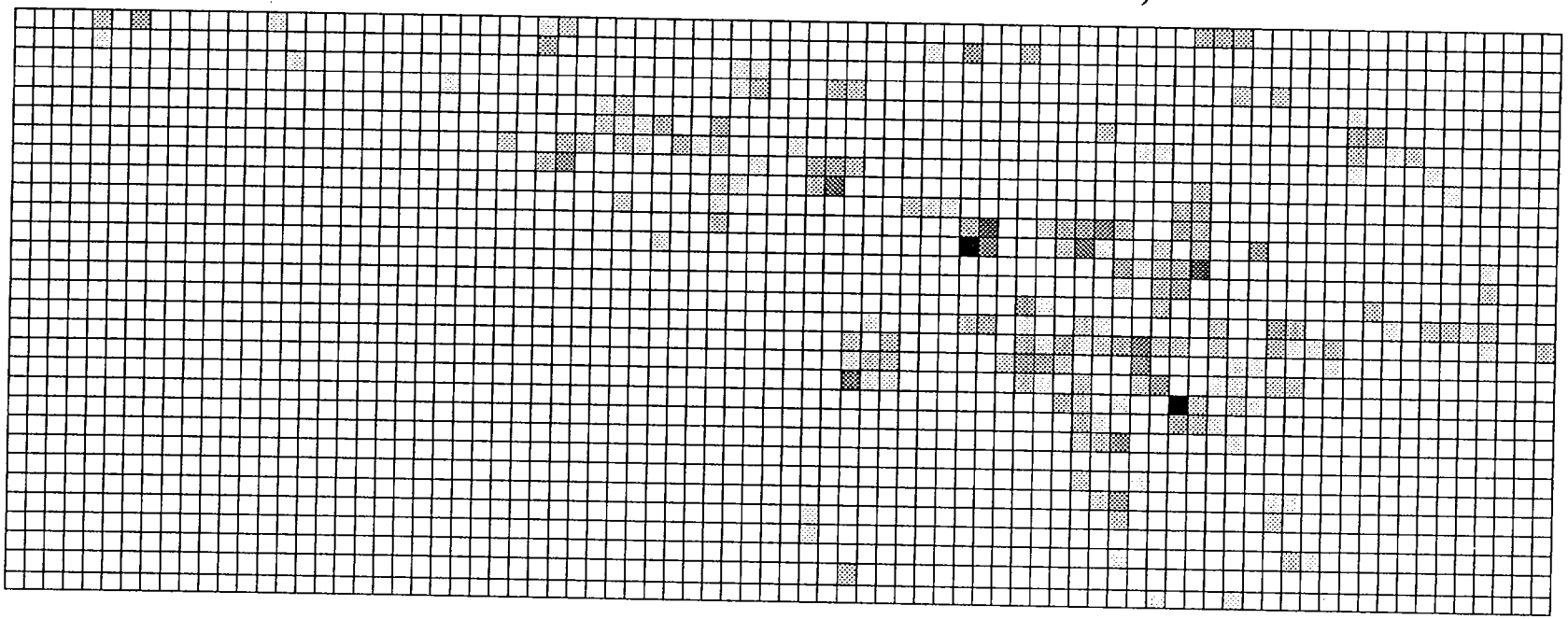

Figure 3.35

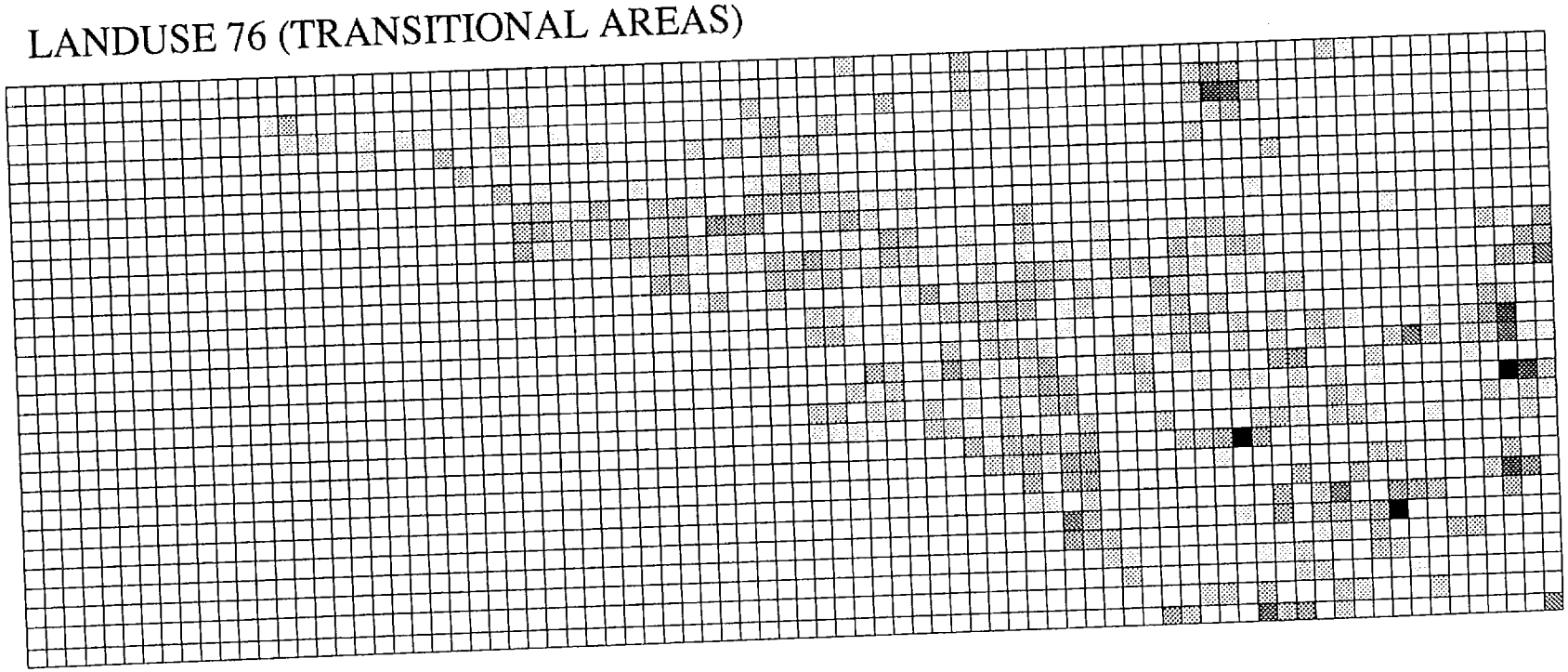

Figure 3.36

LANDUSE 77 (MIXED BARREN LAND)

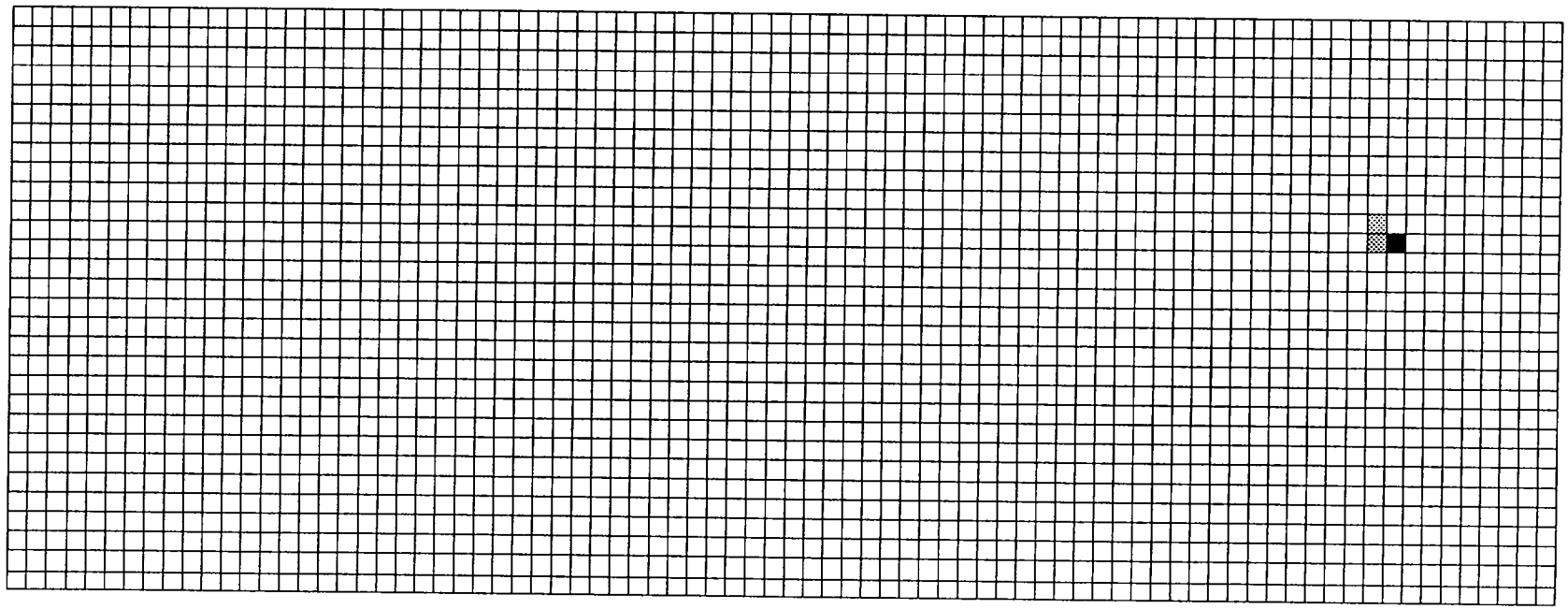

Cropland, pasture land, orchards, and vineyards (uses 21-22) are found largely in the eastern portion of the South Coast Air Basin, and in Ventura County. Confined animal feeding operations (use 23) are concentrated in the Chino area, coincident with the large spike in NH_3 emissions seen in Figure 3.2. Most of the hillside areas of the South Coast Air Basin are covered with shrub and brush rangeland (use 32). Evergreen forests are found on top of some of the mountainous areas. The shoreline and offshore islands are clearly indicated by reference to land use 50 (ocean).

3.4 CALCULATIONS THAT REFLECT THE SUBURBAN NATURE OF THE LOS ANGELES AREA

Review of Table 2.5 shows that ozone surface resistance values recommended by Sheih et. al. (1986) for urban areas, are as high as for bare dry land. It would appear that they envision residential areas like those in some cities in the eastern United States that are entirely built upon or paved over. In the Los Angeles area, however, aerial photographs show that a very large fraction of most residential, commercial and even some industrial areas consists of lawns and landscaping. By analogy to the surface resistance values given for grassy pasture land in Tables 2.2 and 2.5, a residential neighborhood with much lawn area should have a much lower surface resistance for many pollutants than would be true for an asphalt and building-covered urban core.

For this reason, aerial photographs were examined to determine the fraction of urban land in each land-use category that was not paved over and was not built upon. The results of this survey are shown in Table 3.3. Approximately 44% of the residential land in these photographs was not built upon or paved over. Similar amounts of open area were found for most other suburban land uses in Southern California. Therefore, in the modeling calculations that follow, deposition fluxes to "urban" areas are computed, using the urban surface resistance values in Tables 2.2, 2.5 and 2.6, only for that fraction of the "urban" land that is actually built-up or paved over. The flux to the remainder of the suburban landscape that is not built upon or paved over is computed as if that remaining land is landscaped with a surface resistance like that of cropland and pasture given in Tables 2.2 and 2.5. This representation of the suburban character of Southern California as a combination of high density urban coverage plus landscaping will be referred to as the "Suburban" version of the new dry deposition model.

Table 3.3 Fraction of Urban Land Not Paved Over and Not Built Upon

Highrise Urban	0.25
Residential	0.44
Commercial	0.34
Industrial	0.47
Utilities	0.55
Industrial/Commercial	0.40
Mixed Urban	0.43
Other Urban	0.43

3.5 USE OF THE REVISED DEPOSITION MODULE

The modified photochemical airshed model and deposition module defined in Chapter 2 with the suburban deposition scheme just described was tested by application to the South Coast Air Basin over the period August 30-31, 1982. The emissions data, meteorological fields, initial conditions and boundary conditions are identical to those used in the study just described and are documented in Appendix A.

Figures 3.37–3.50 show the spatial distribution of NO, NO_2, HNO_3, NH_3, aerosol nitrate, O_3 and PAN during the early morning hours (800 PST) and mid-afternoon (1400 PST) of the second day of simulation, as predicted by the modified airshed model. As seen in Figures 3.37–3.40, NO and NO_2 concentrations peak in the early morning on the western side of the air basin. NO concentrations above 0.25 ppm are predicted over central Los Angeles at 800 hours PST, while the peak NO_2 concentrations at that time occur in central Orange County. As the day progresses, NO is converted to NO_2 and is diluted by the rising mixing depth yielding NO concentrations that are everywhere below 0.05 ppm by mid-afternoon (Figure 3.38). Peak NO_2 concentrations also decline by mid-afternoon, and the NO_2 peak is advected inland by the wind yielding peak concentrations just above 0.05 ppm NO_2 in the middle of the air basin at 1400 hours (Figure 3.40).

Nitric acid vapor concentrations predicted by the revised model for the early hours of August 31 are significantly higher than those produced by the previous version of the model. HNO_3 concentrations approaching 25 ppb are seen in southern Orange County at 800 hours PST (Figure 3.41) compared to the previous model predictions of 10 ppb at that time, as seen in Figure 3.4. In the afternoon, HNO_3 levels as high as 25 ppb are predicted in the central portion of the air basin (Figure 3.42), compared to peak concentrations of about 15 ppb predicted previously. The possible causes of this increase in predicted HNO_3 concentrations will be discussed shortly.

Figures 3.41 and 3.42 show that HNO_3 concentrations fall below 5 ppb in an area just west of Riverside in the morning and below 10 ppb in the afternoon. That zone of low HNO_3 concentrations corresponds to the location of the very high NH_3 concentrations seen in Figures 3.43 and 3.44. The high morning NH_3 concentrations occur over the Chino dairy area, where livestock waste decomposition leads to high

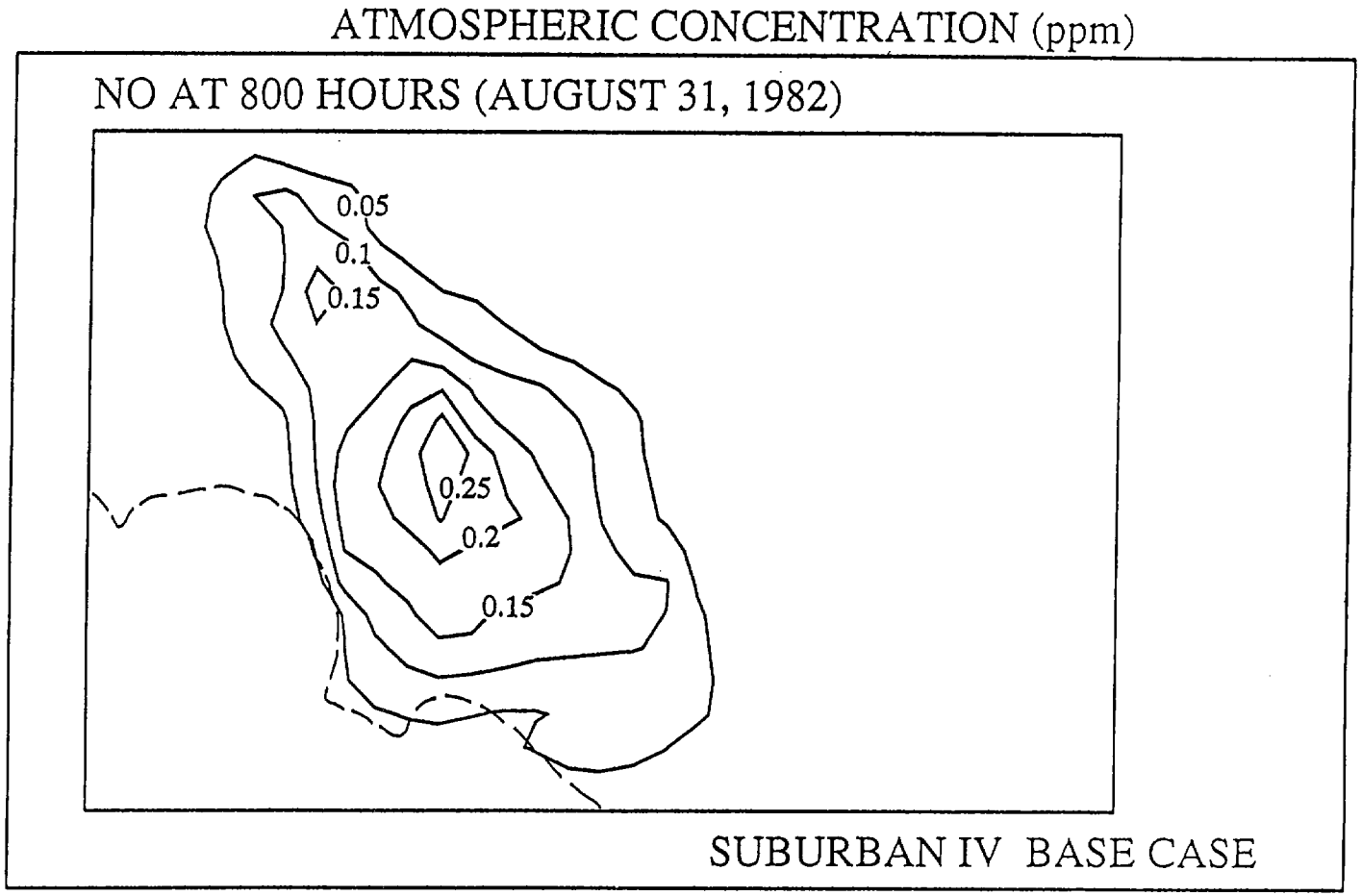
ATMOSPHERIC CONCENTRATION (ppm)
NO AT 800 HOURS (AUGUST 31, 1982)
0.05
0.1
0.15
0.25
0.2
0.15
SUBURBAN IV BASE CASE

Figure 3.37

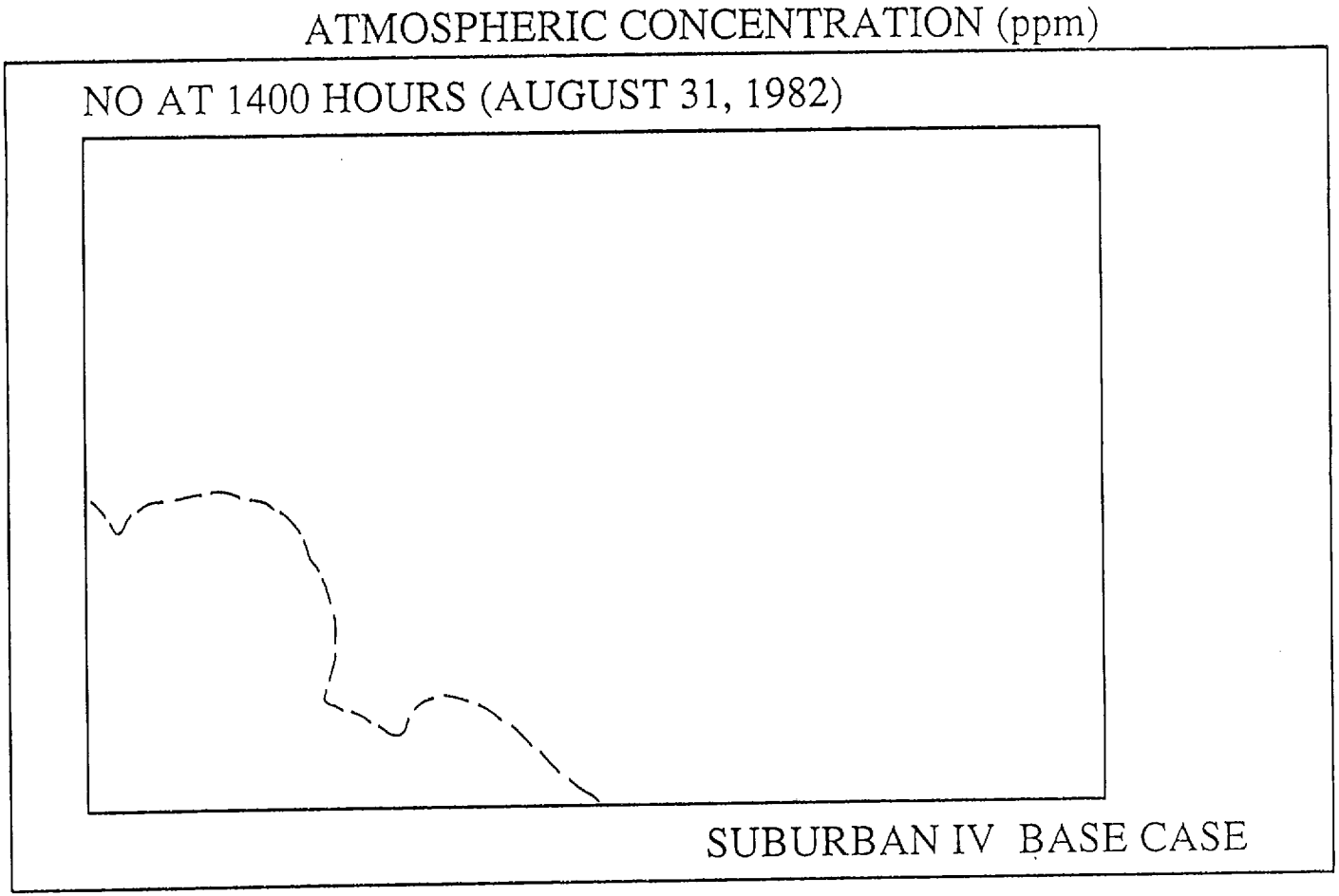
ATMOSPHERIC CONCENTRATION (ppm)
NO AT 1400 HOURS (AUGUST 31, 1982)
SUBURBAN IV BASE CASE

Figure 3.38

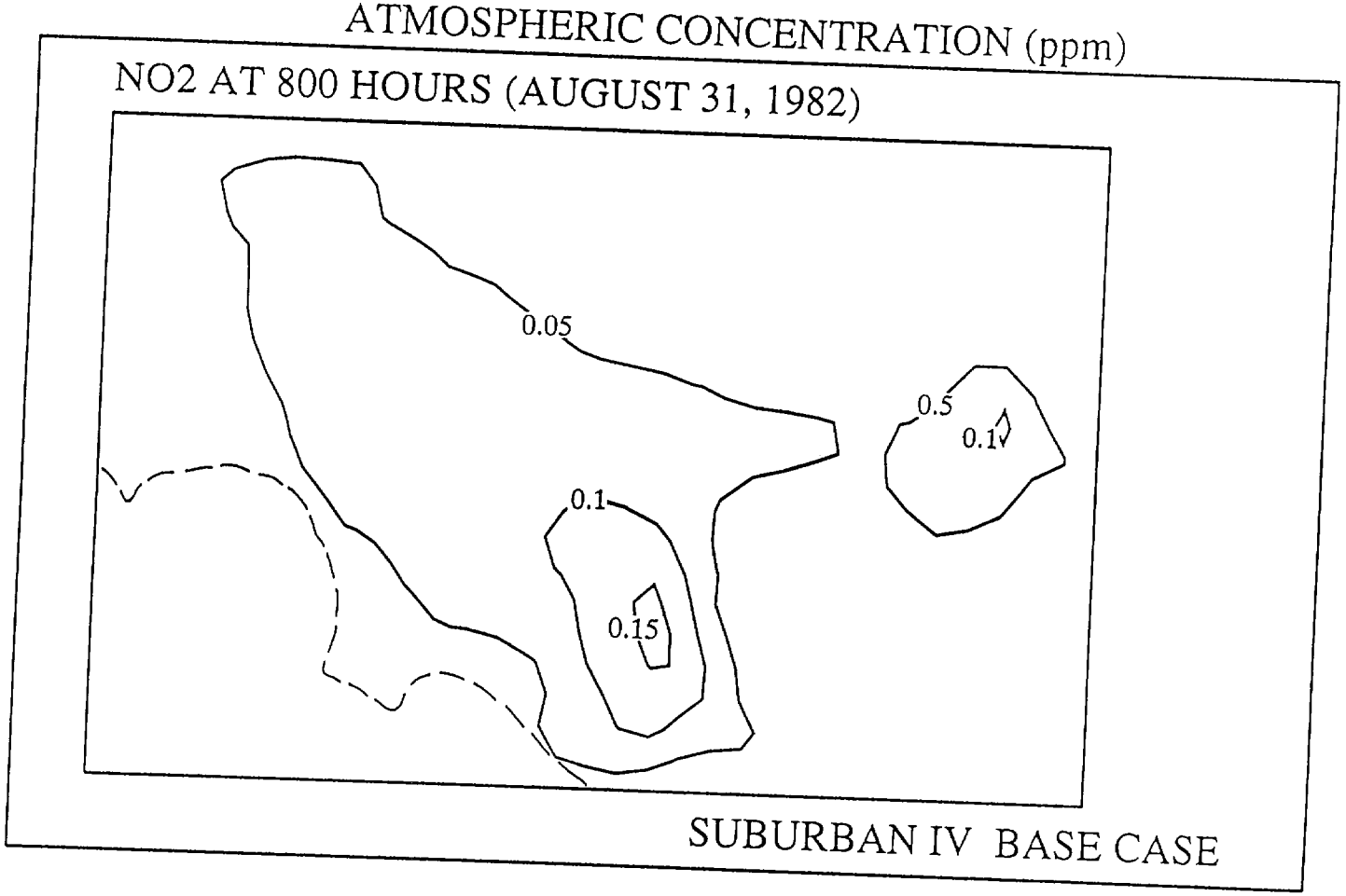
ATMOSPHERIC CONCENTRATION (ppm)
NO2 AT 800 HOURS (AUGUST 31, 1982)
0.05
0.5
0.1
0.1
0.15
SUBURBAN IV BASE CASE

Figure 3.39

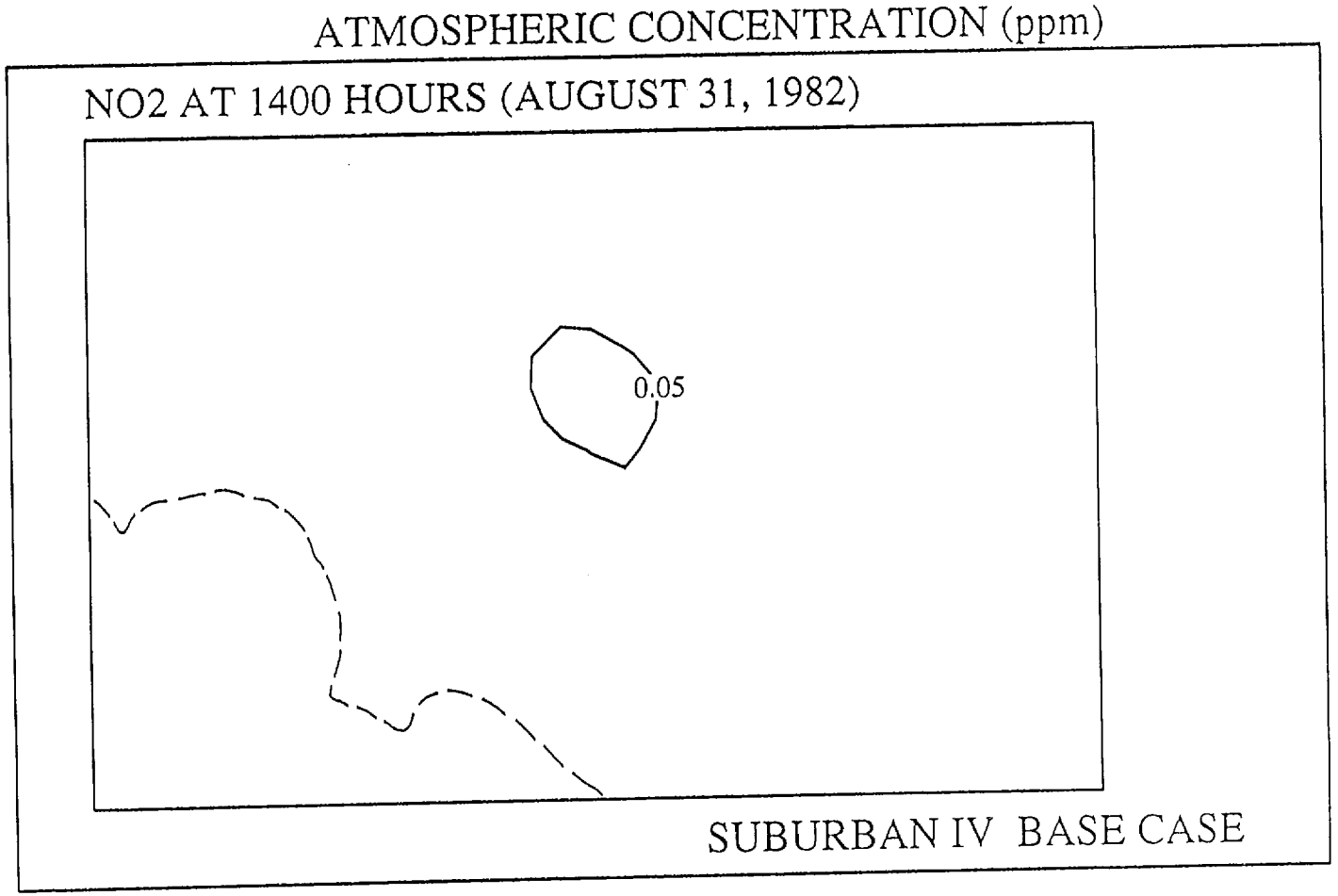
ATMOSPHERIC CONCENTRATION (ppm)
NO2 AT 1400 HOURS (AUGUST 31, 1982)
0.05
SUBURBAN IV BASE CASE

Figure 3.40

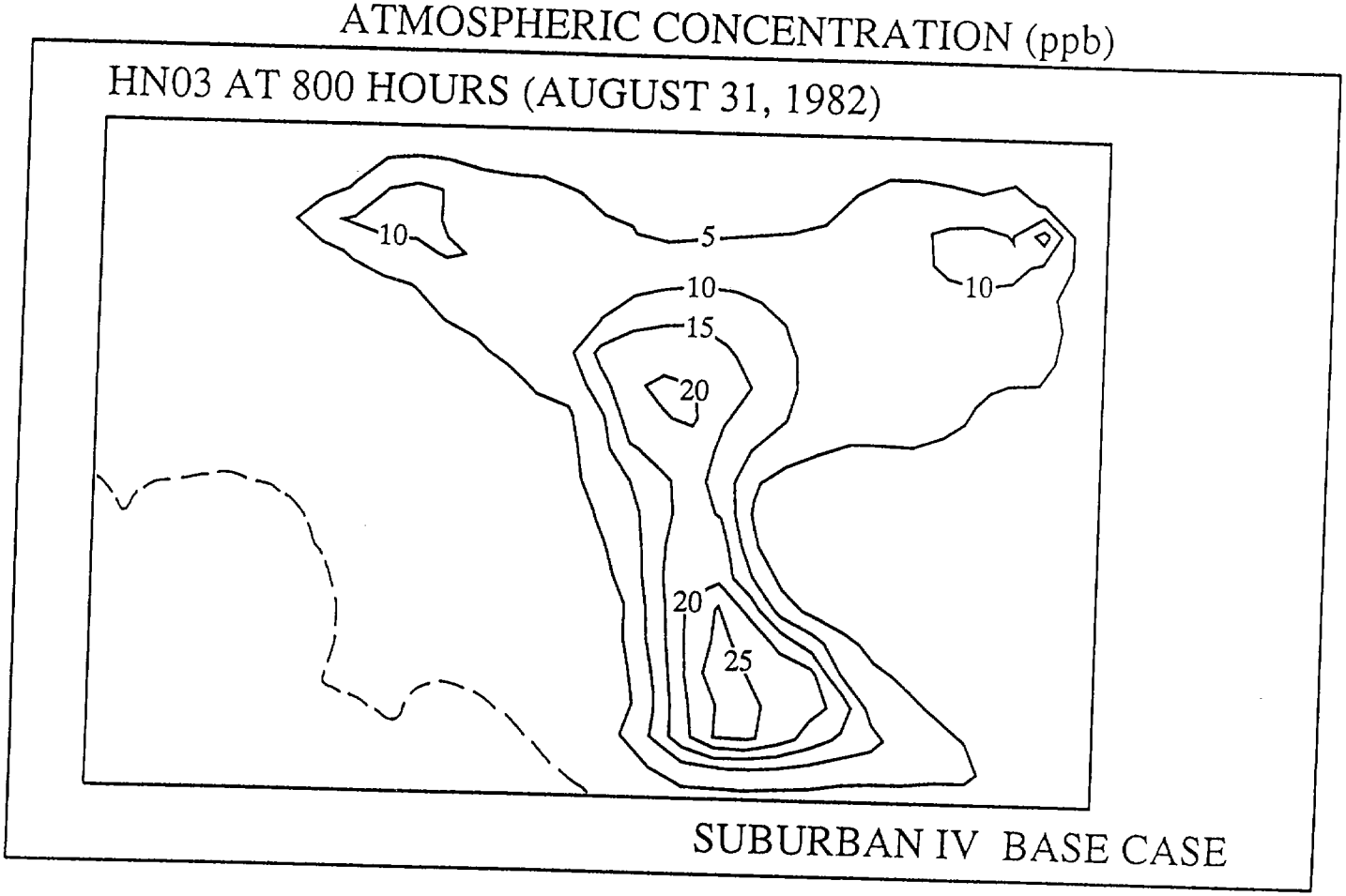
ATMOSPHERIC CONCENTRATION (ppb)
HN03 AT 800 HOURS (AUGUST 31, 1982)
10
5
10
10
15
20
20
25
SUBURBAN IV BASE CASE

Figure 3.41

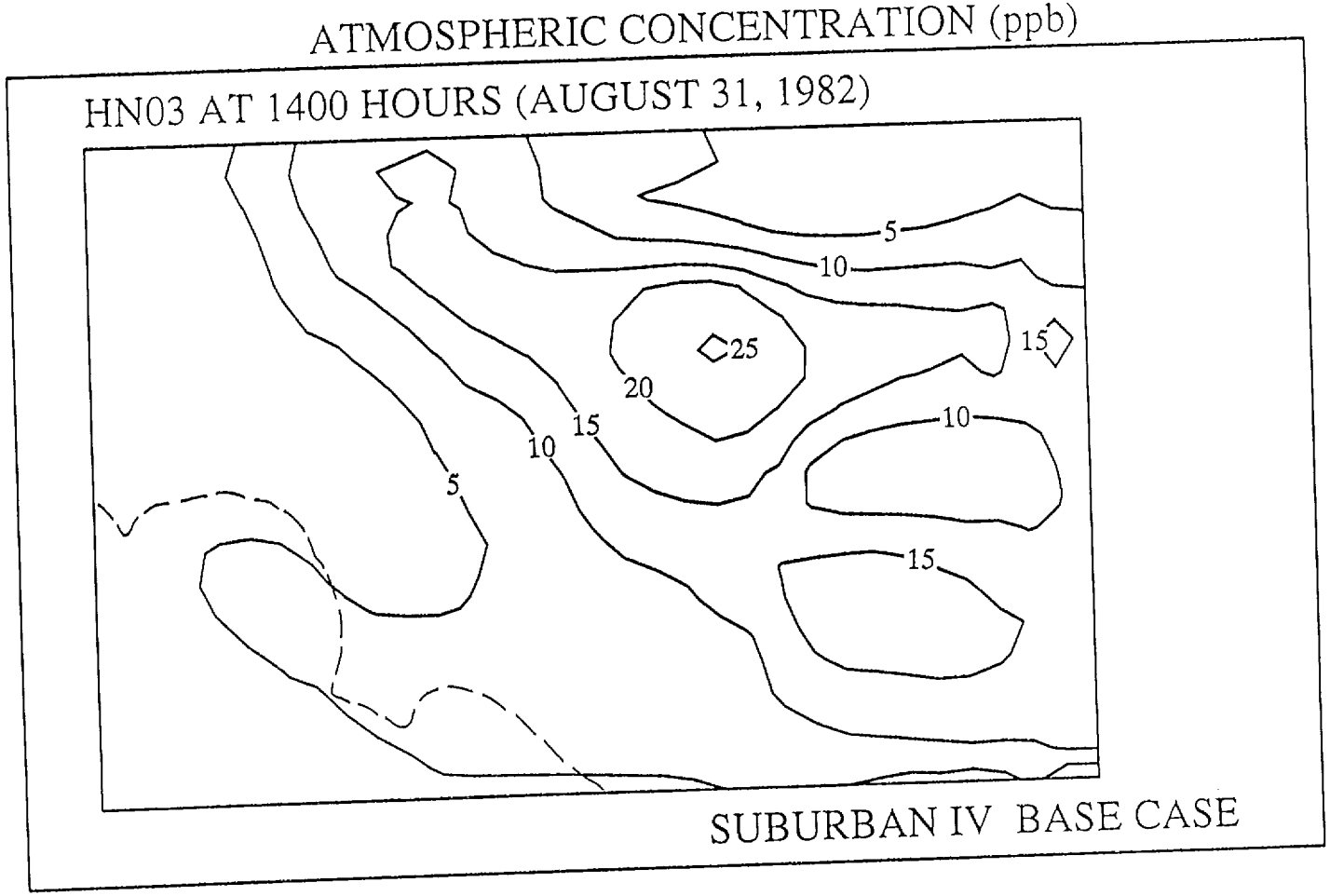
ATMOSPHERIC CONCENTRATION (ppb)
HN03 AT 1400 HOURS (AUGUST 31, 1982)
5
10
15
25
20
15
10
10
5
15
SUBURBAN IV BASE CASE

Figure 3.42

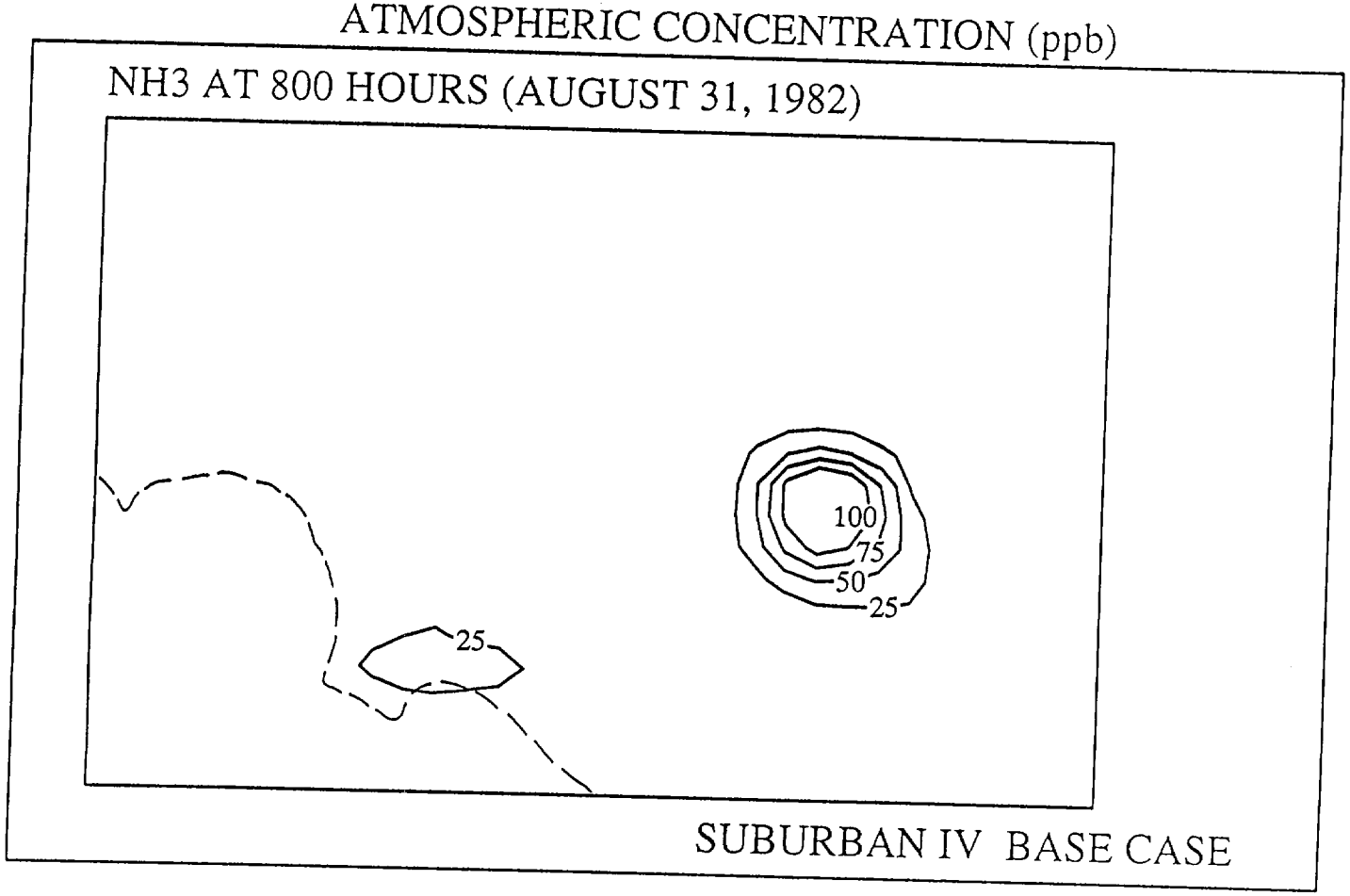
ATMOSPHERIC CONCENTRATION (ppb)
NH3 AT 800 HOURS (AUGUST 31, 1982)
100
75
50
25
25
SUBURBAN IV BASE CASE

Figure 3.43

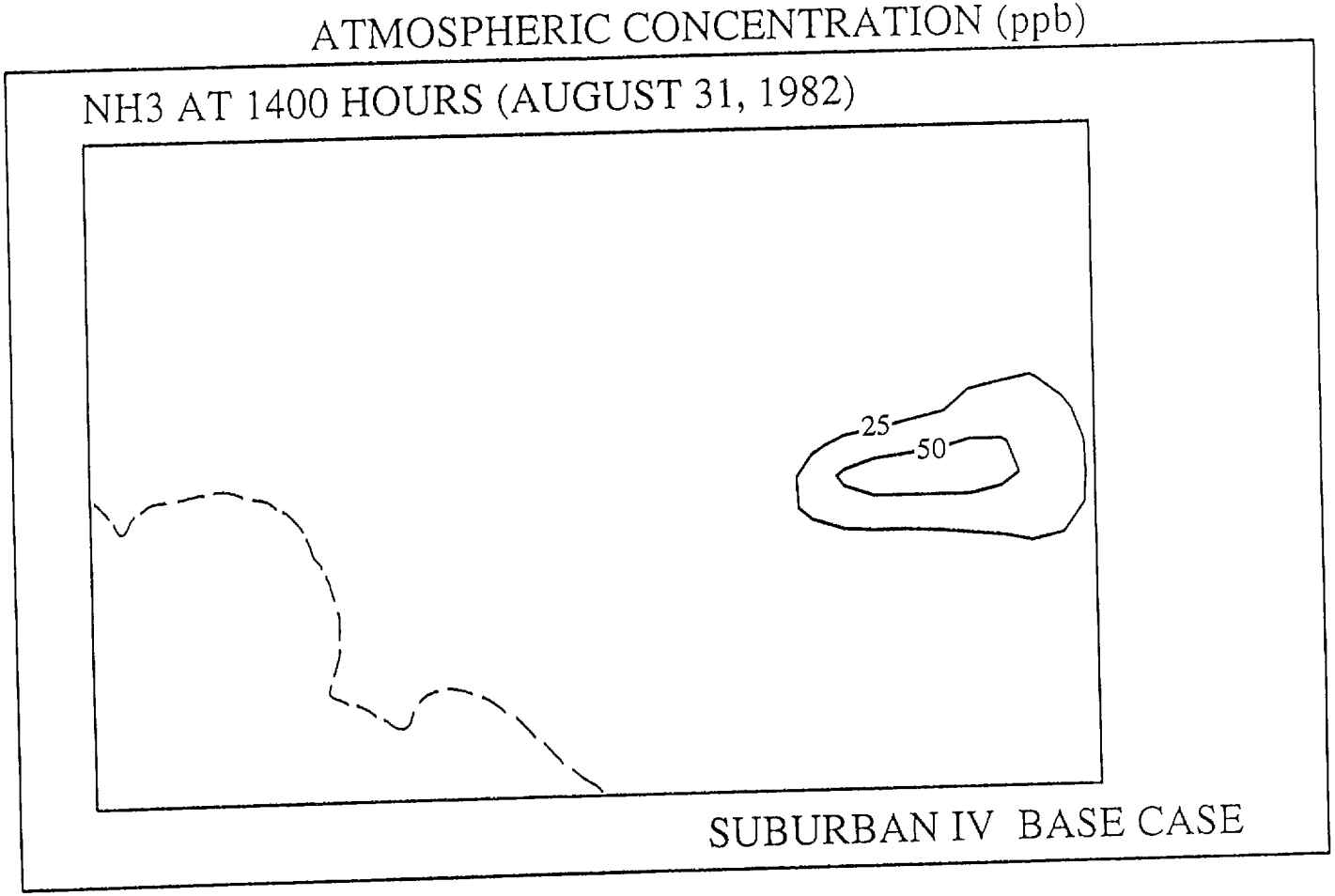
ATMOSPHERIC CONCENTRATION (ppb)
NH3 AT 1400 HOURS (AUGUST 31, 1982)
25
50
SUBURBAN IV BASE CASE

Figure 3.44

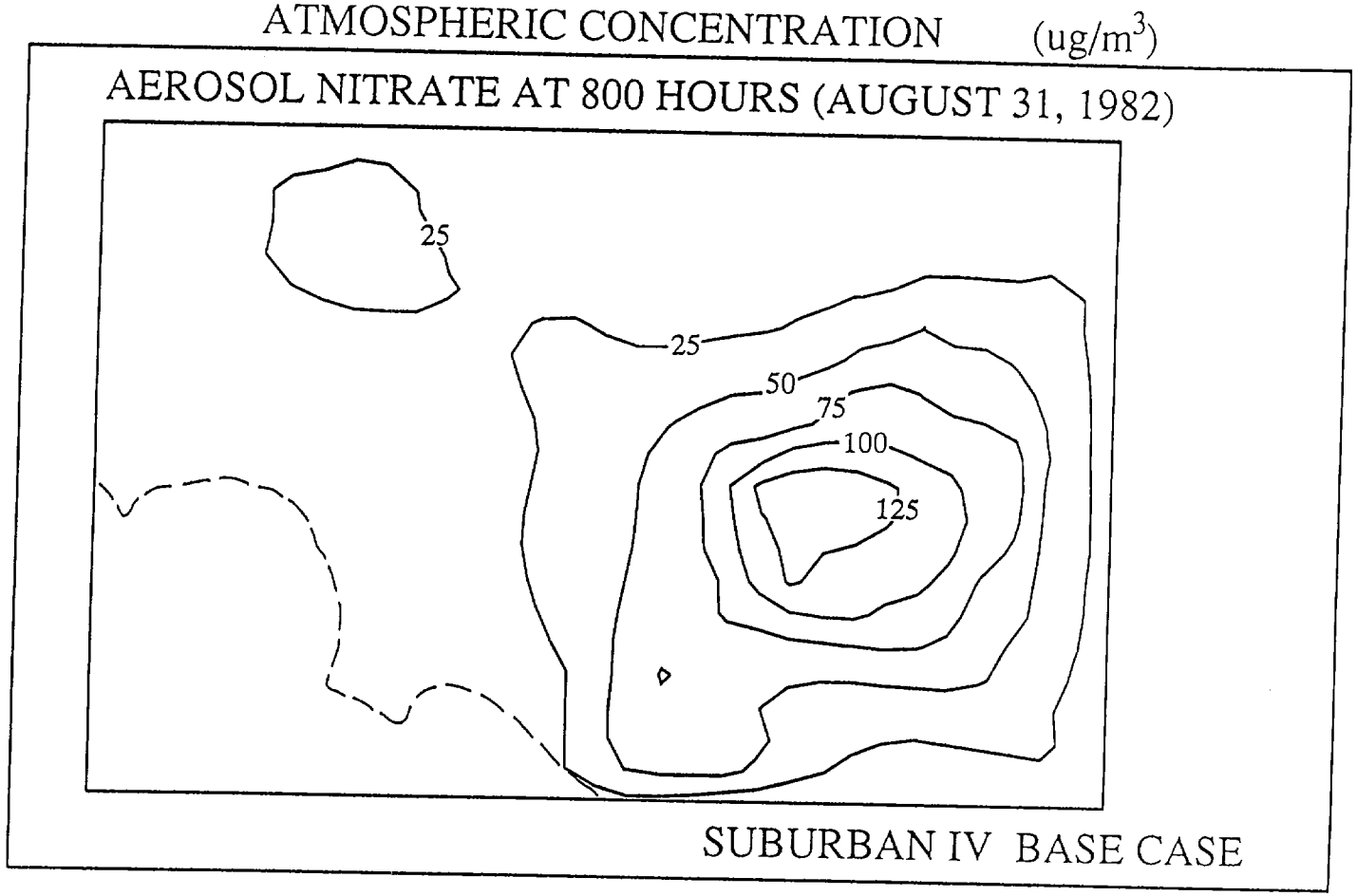
ATMOSPHERIC CONCENTRATION (ug/m3)
AEROSOL NITRATE AT 800 HOURS (AUGUST 31, 1982)
25
25
50
75
100
125
SUBURBAN IV BASE CASE

Figure 3.45

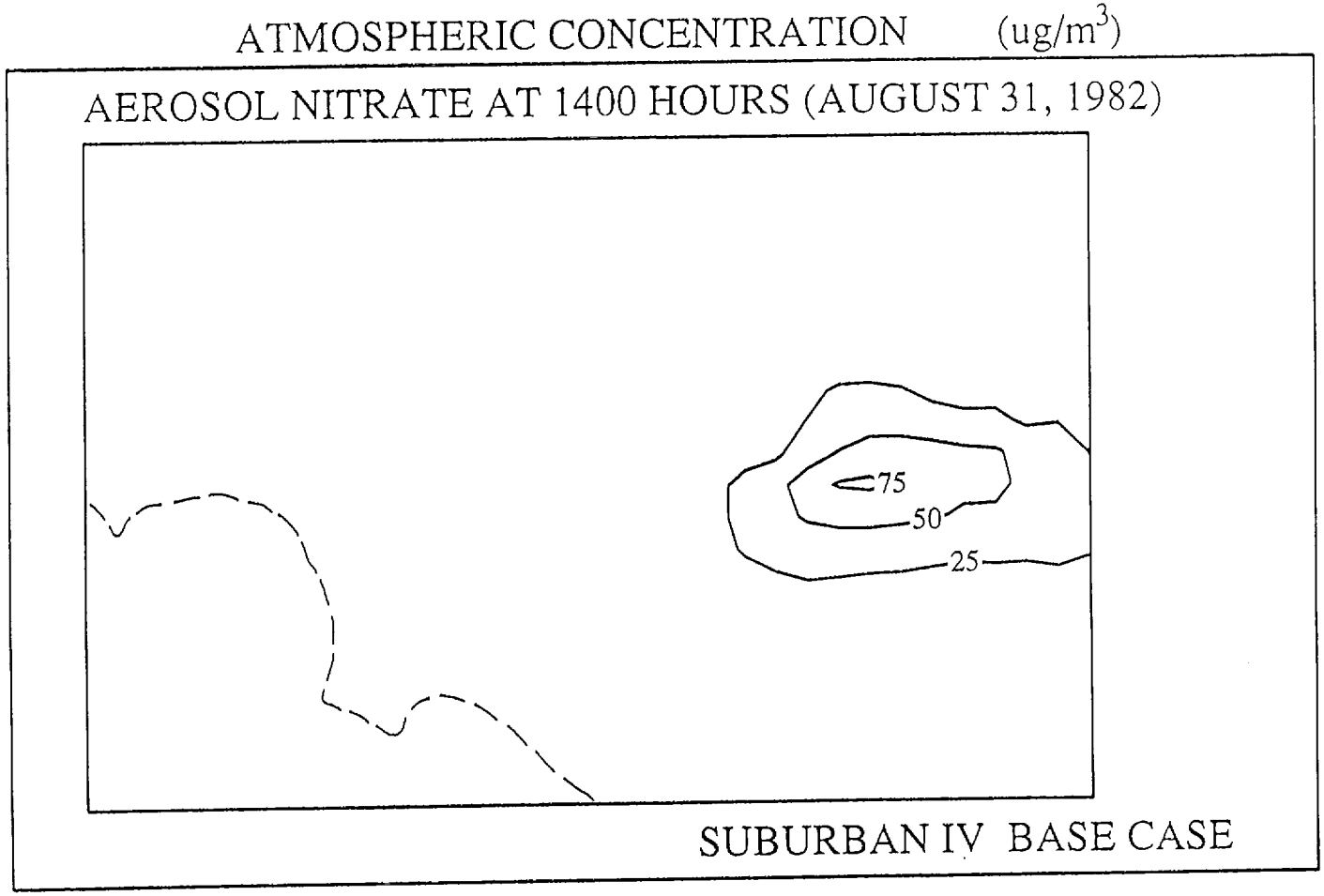
ATMOSPHERIC CONCENTRATION (ug/m3)
AEROSOL NITRATE AT 1400 HOURS (AUGUST 31, 1982)
75
50
25
SUBURBAN IV BASE CASE

Figure 3.46

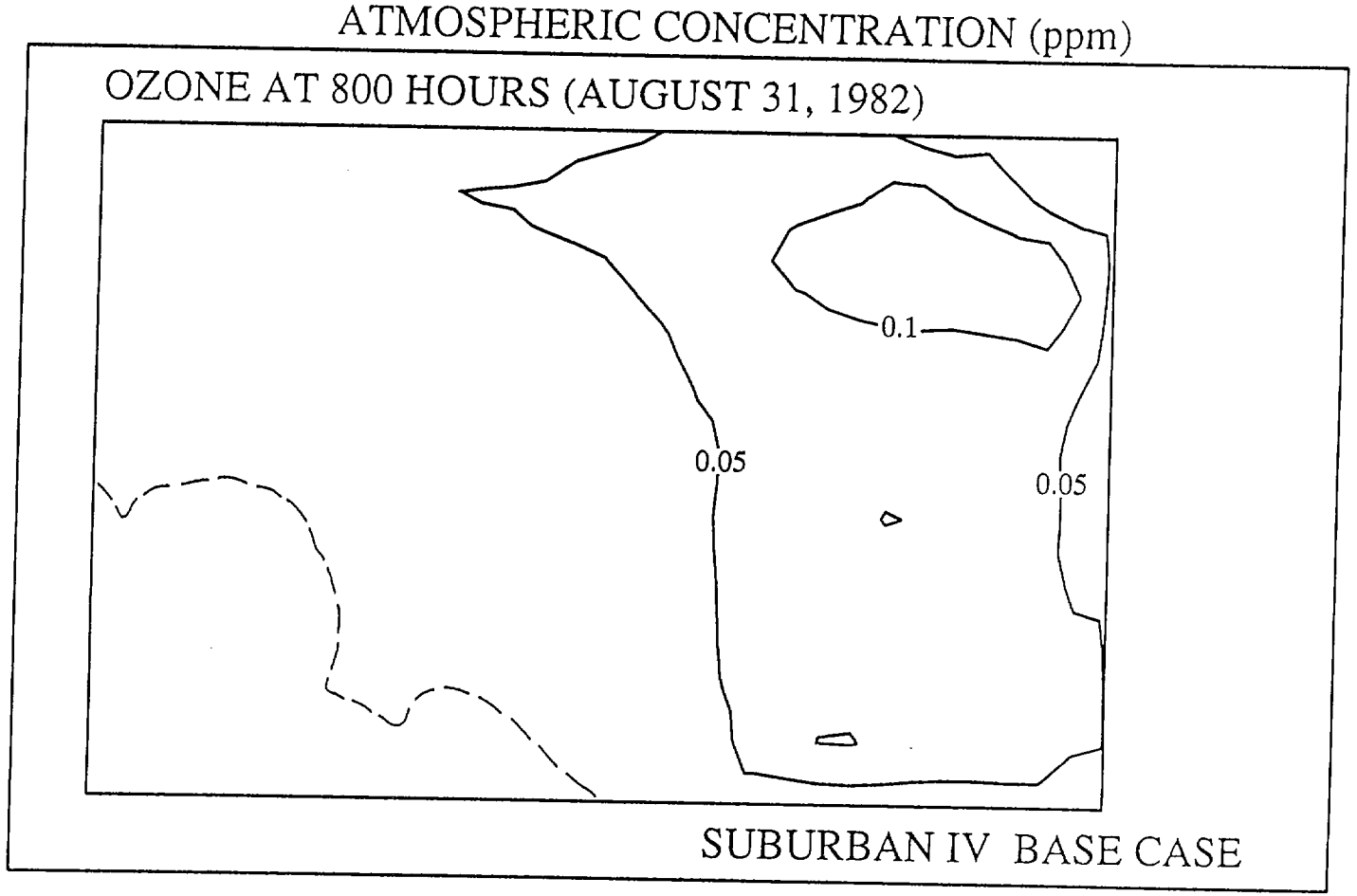
ATMOSPHERIC CONCENTRATION (ppm)
OZONE AT 800 HOURS (AUGUST 31, 1982)
0.1
0.05
0.05
SUBURBAN IV BASE CASE

Figure 3.47

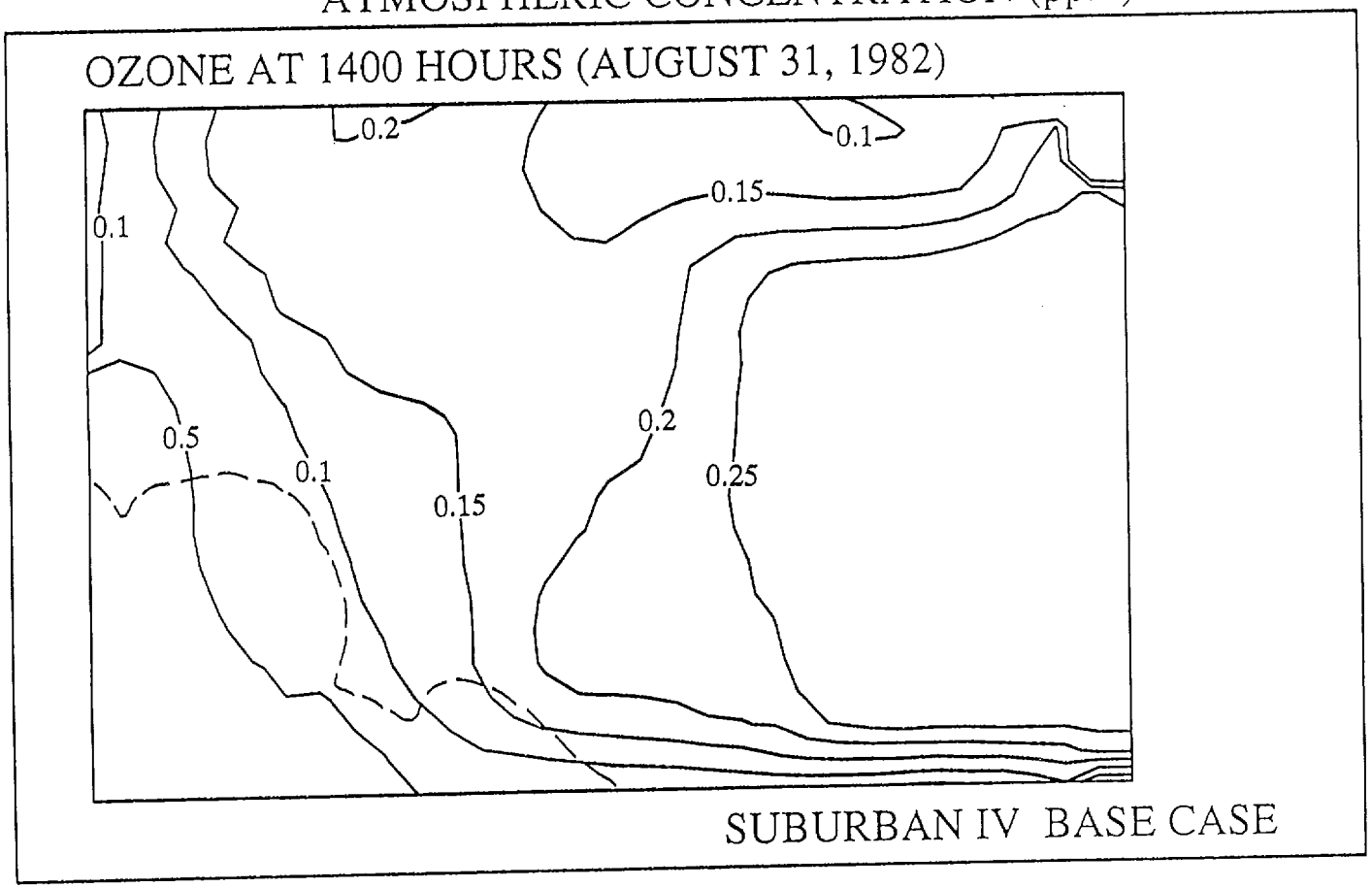
ATMOSPHERIC CONCENTRATION (ppm)
OZONE AT 1400 HOURS (AUGUST 31, 1982)
0.2
0.1
0.15
0.1
0.5
0.1
0.15
0.2
0.25
SUBURBAN IV BASE CASE

Figure 3.48

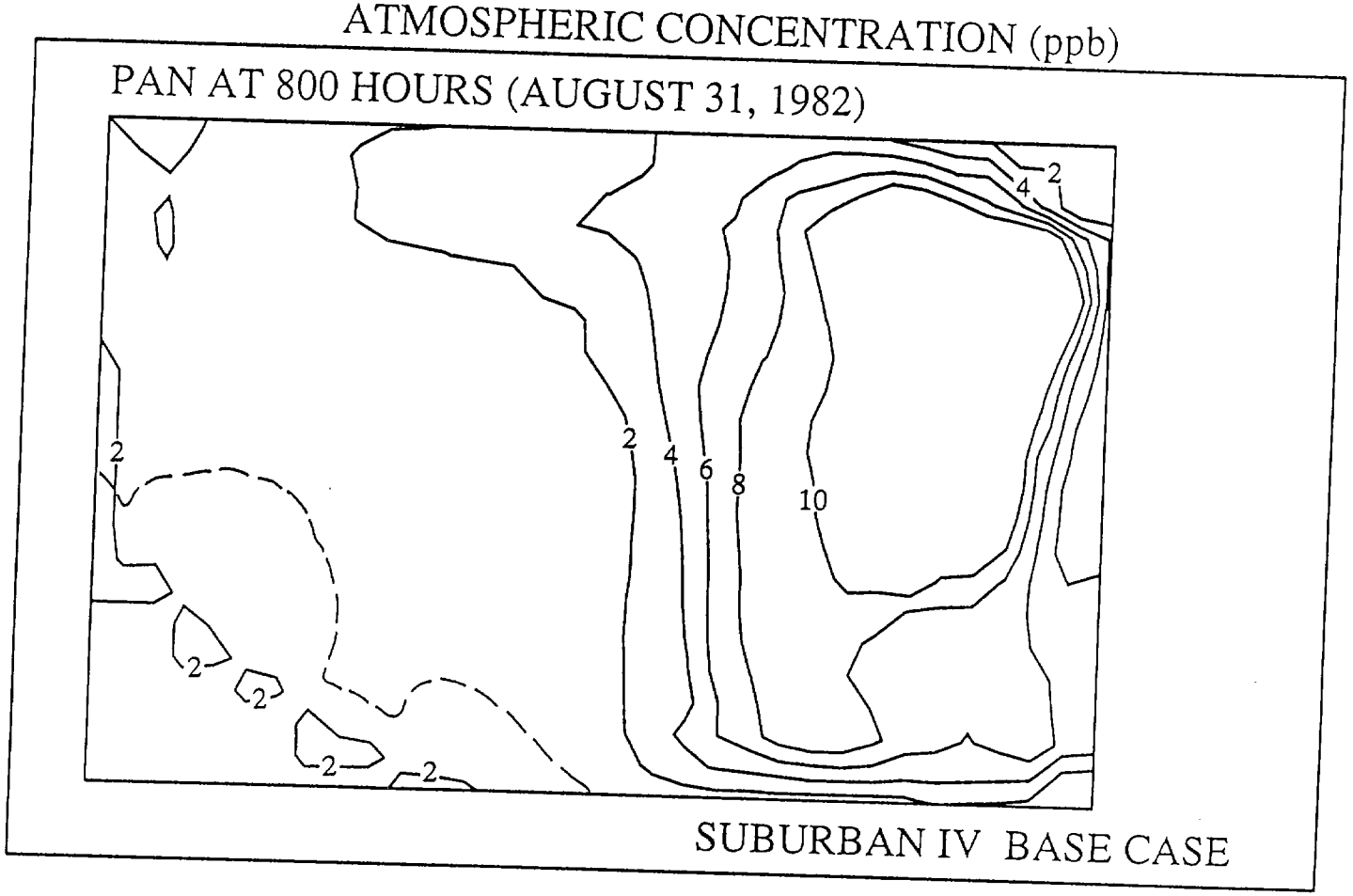
ATMOSPHERIC CONCENTRATION (ppb)
PAN AT 800 HOURS (AUGUST 31, 1982)
2
4
2
2
2
4
6
8
10
2
2
2
2
SUBURBAN IV BASE CASE

Figure 3.49

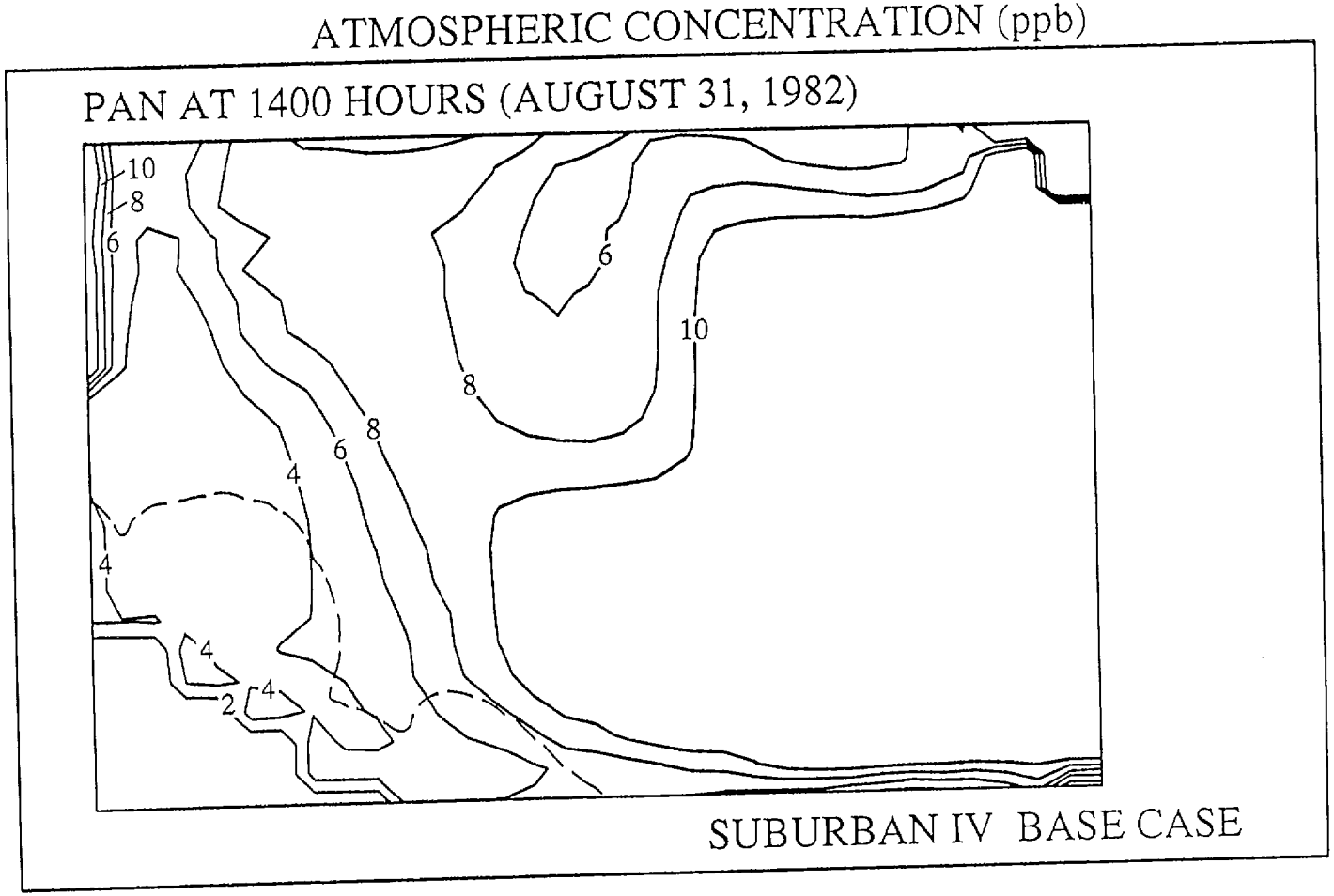
ATMOSPHERIC CONCENTRATION (ppb)
PAN AT 1400 HOURS (AUGUST 31, 1982)
10
8
6
6
10
8
8
6
4
4
4
4
2
SUBURBAN IV BASE CASE

Figure 3.50

NH_3 emissions (Figure 3.2). In the afternoon, the high NH_3 concentrations are shifted slightly downwind of Chino (compare Figures 3.43 and 3.44). Within this area of high NH_3 concentrations, NH_3 reacts with HNO_3 to produce high aerosol nitrate concentrations, thereby reducing ambient HNO_3 levels to values below that seen in adjacent areas. Aerosol nitrate concentrations predicted by the revised model are shown in Figures 3.45 and 3.46. The new aerosol nitrate predictions in the eastern portion of the air basin are higher than in the previous version of the model by a factor that is related directly to the increase in ambient nitric acid vapor predictions discussed earlier.

The spatial distributions of air quality model predictions for ozone and PAN are shown in Figures 3.47–3.50. Ozone concentrations in the early morning of August 31 are very low in the western portion of the air basin, while in the eastern area of the airshed, O_3 concentrations above 0.05 ppm prevail at 800 hours. Peak early morning O_3 concentrations exceed 0.1 ppm in the area north of San Bernardino at 800 hours on August 31. The spatial distribution of ground level O_3 concentrations at 800 hours is quite similar in both the previous and revised versions of the airshed model (compare Figures 3.4 and 3.47). Afternoon ozone levels predicted by the revised model are slightly higher than in the previous version of the model in the western area of the air basin. In the eastern portion of the basin, predicted ozone concentrations average about 0.24 ppm, about 0.05 ppm higher than the predictions of the previous model. For reference purposes, the basinwide O_3 peak that day was 0.26 ppm, observed at Glendora and at Riverside City College.

The spatial distribution of deposition velocity values predicted by the model likewise can be displayed, and this has been done in Figures 3.51–3.57. Nitric acid vapor is removed at a rate limited only by atmospheric transport, and therefore has the highest deposition velocity value predicted by the model at any time. In the middle of the afternoon of August 31, the deposition velocity for HNO_3 reached 10 cm/sec over southwestern Los Angeles County in an area of high wind speed and surface roughness, falling to less than 5 cm/sec in the less urbanized areas of the air basin at that time (Figure 3.51). Ozone and NO_2 with their significant surface resistances to dry deposition show lower deposition velocities, on the order of 1.0 to 0.7 cm/sec over much of the air basin at that time (see Figures 3.52 and 3.53). The surface resistances

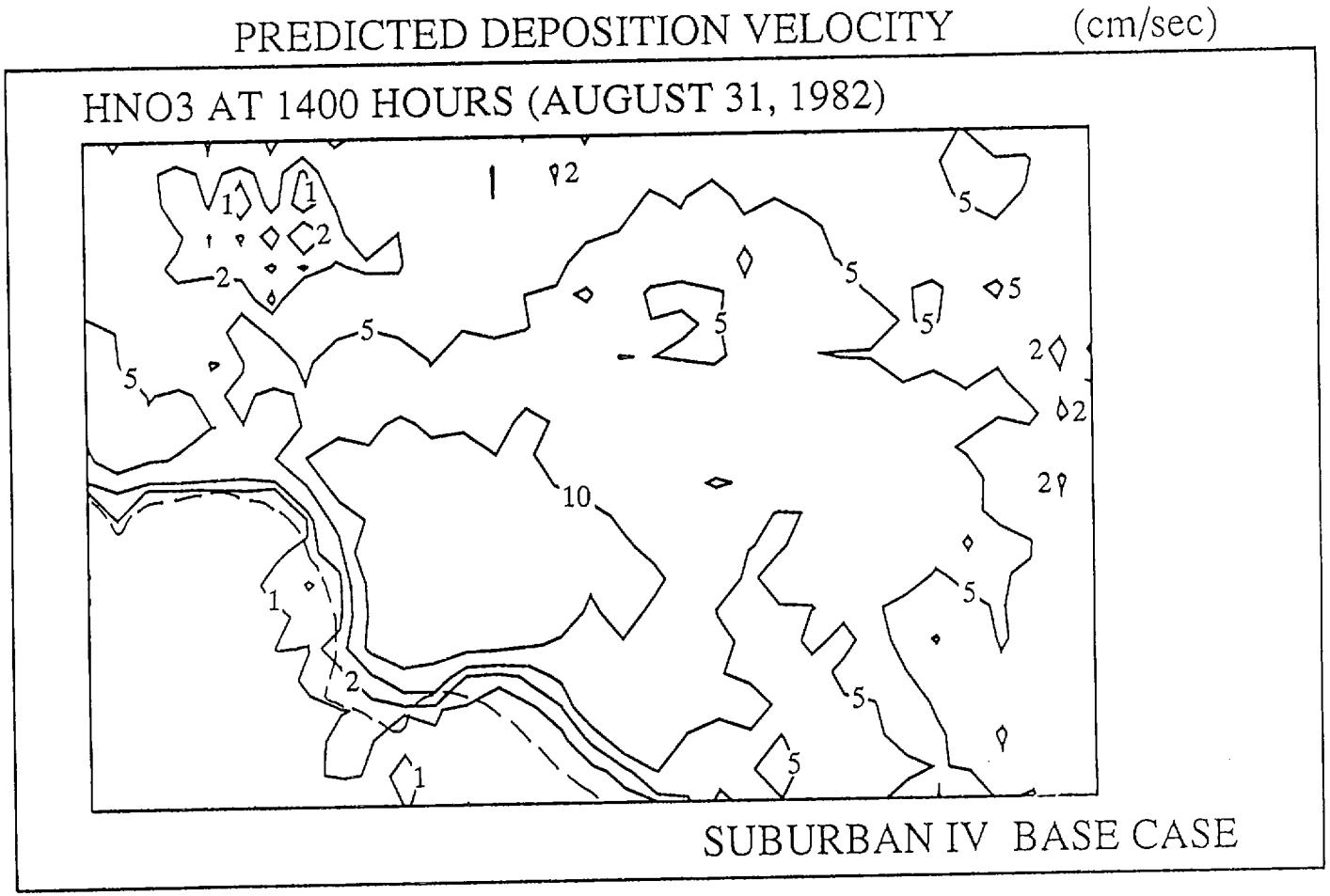
PREDICTED DEPOSITION VELOCITY (cm/sec)
HNO3 AT 1400 HOURS (AUGUST 31, 1982)
SUBURBAN IV BASE CASE

Figure 3.51

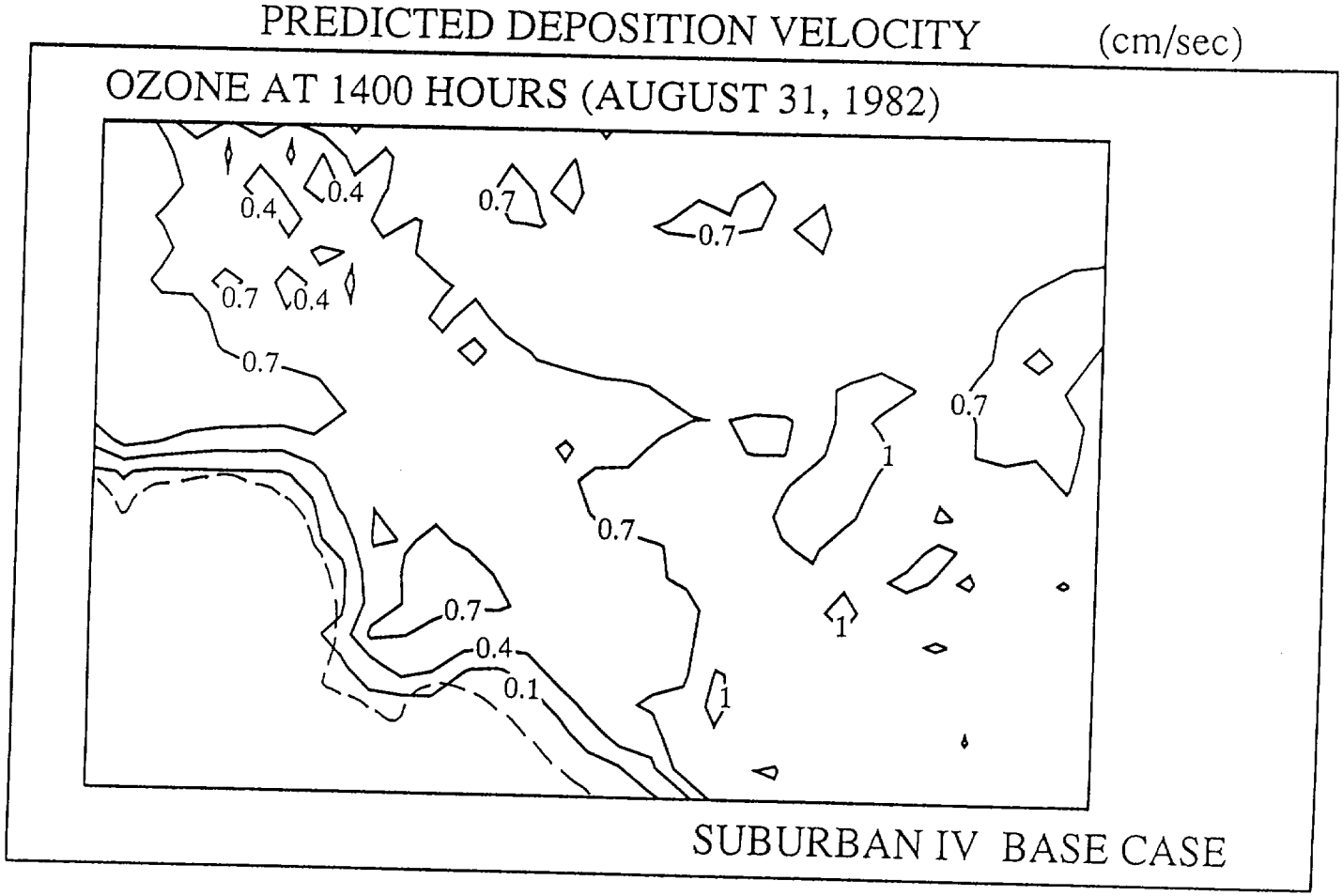
PREDICTED DEPOSITION VELOCITY (cm/sec)
OZONE AT 1400 HOURS (AUGUST 31, 1982)
0.4
0.4
0.7
0.7
0.7
0.4
0.7
0.7
1
0.7
0.7
1
0.7
0.4
0.1
1
SUBURBAN IV BASE CASE

Figure 3.52

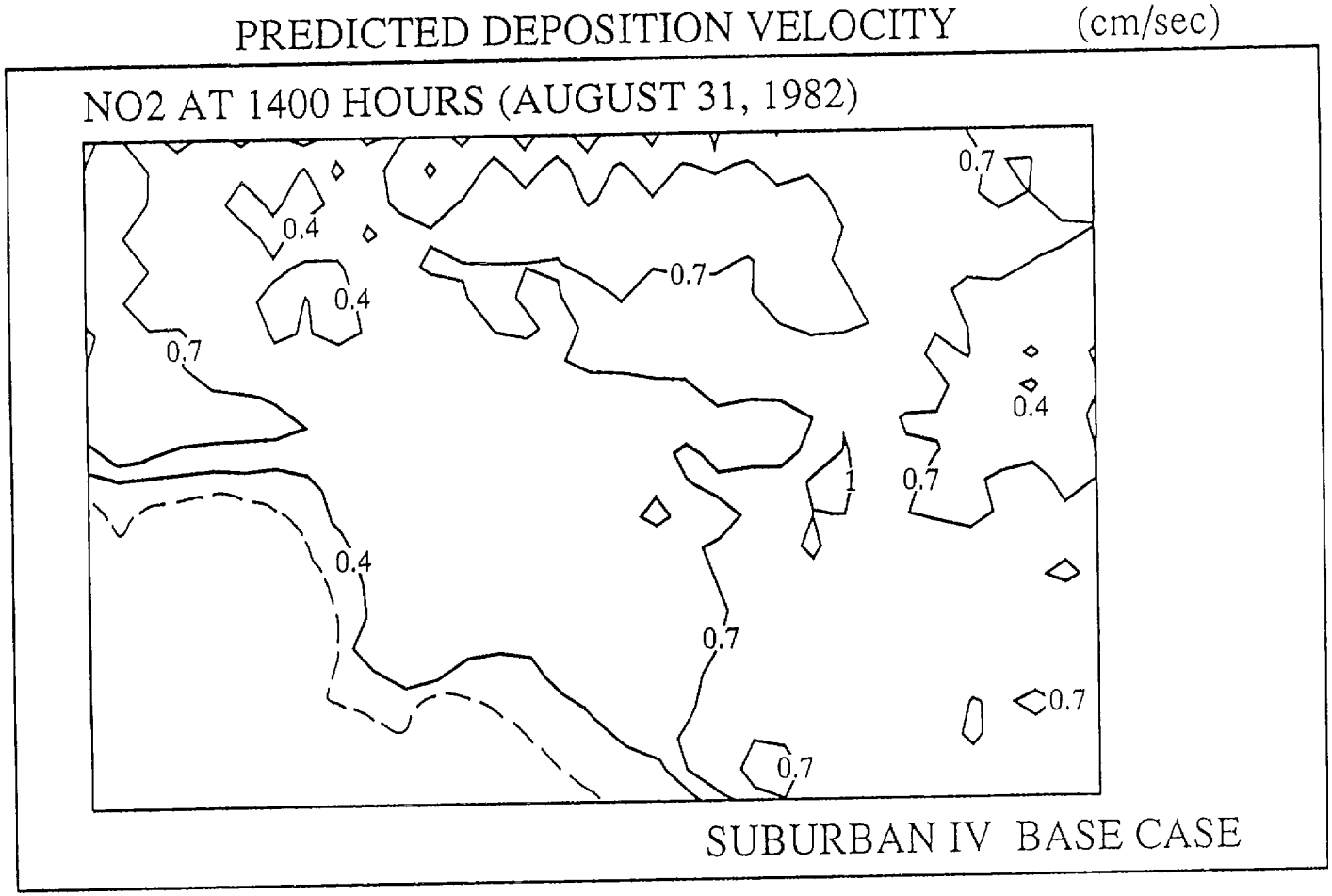
PREDICTED DEPOSITION VELOCITY (cm/sec)
NO2 AT 1400 HOURS (AUGUST 31, 1982)
0.4
0.4
0.7
0.7
0.7
0.4
1
0.7
0.4
0.7
0.7
0.7
SUBURBAN IV BASE CASE

Figure 3.53

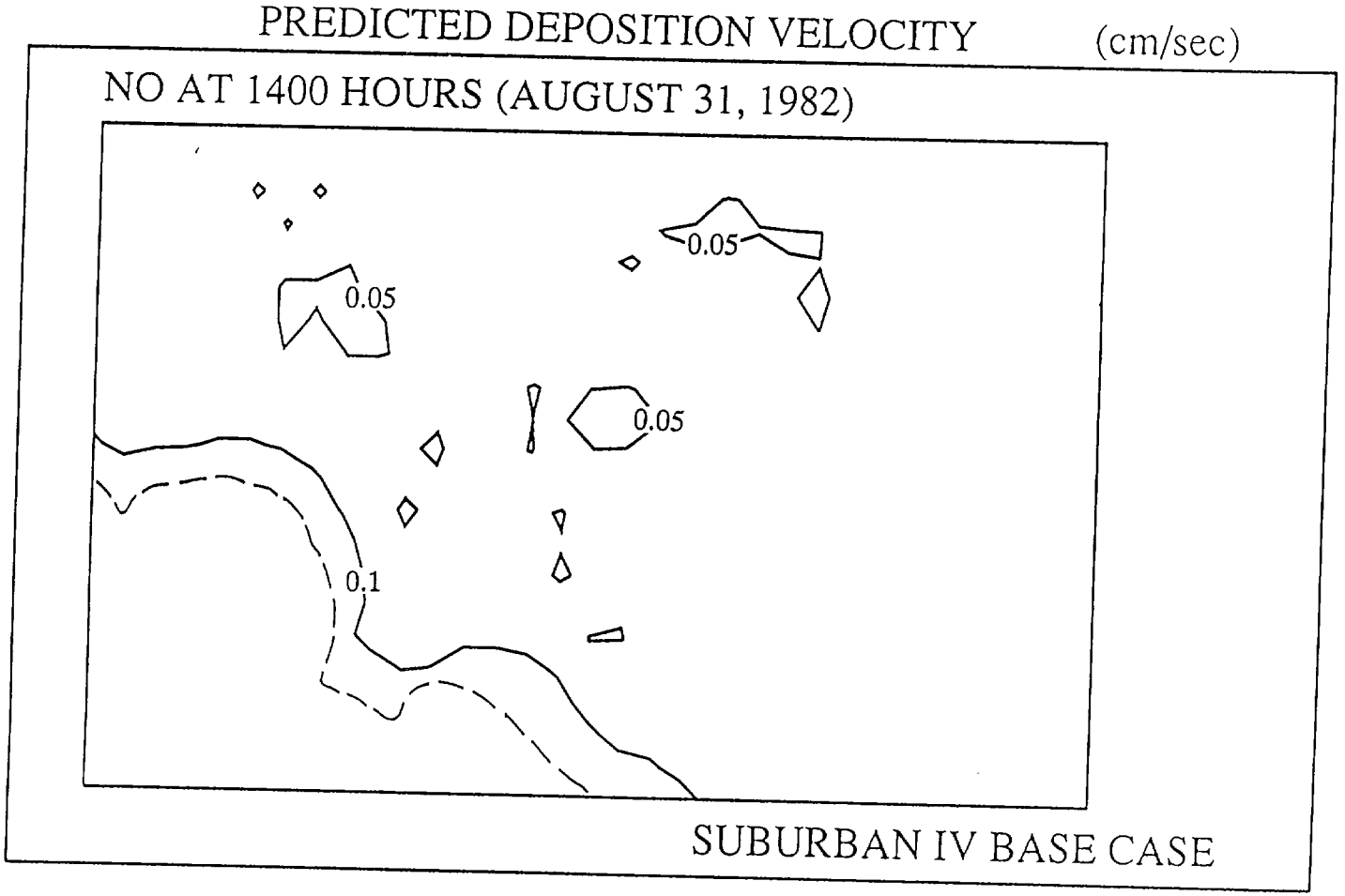
PREDICTED DEPOSITION VELOCITY (cm/sec)
NO AT 1400 HOURS (AUGUST 31, 1982)
0.05
0.05
0.05
0.1
SUBURBAN IV BASE CASE

Figure 3.54

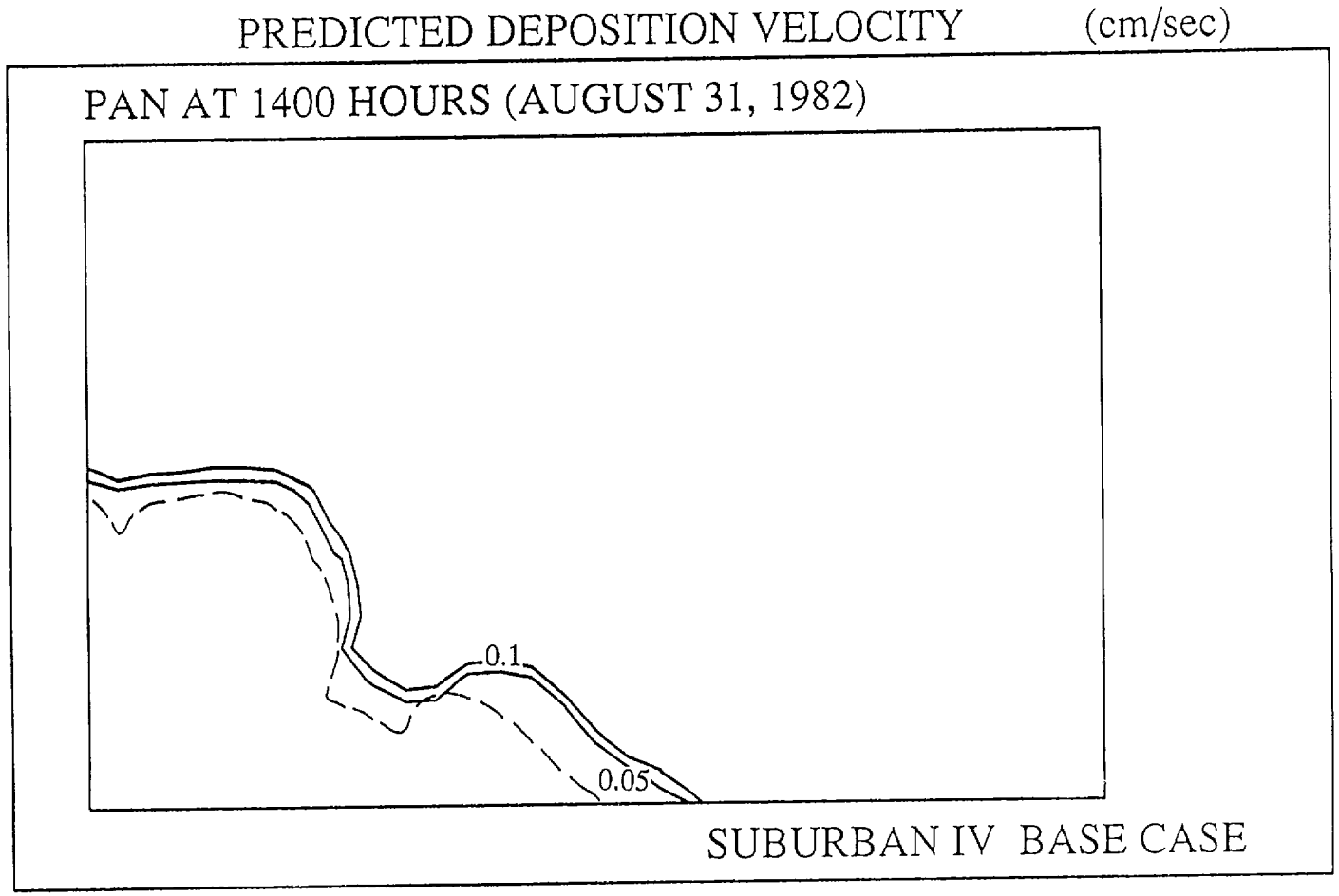
PREDICTED DEPOSITION VELOCITY (cm/sec)
PAN AT 1400 HOURS (AUGUST 31, 1982)
0.1
0.05
SUBURBAN IV BASE CASE

Figure 3.55

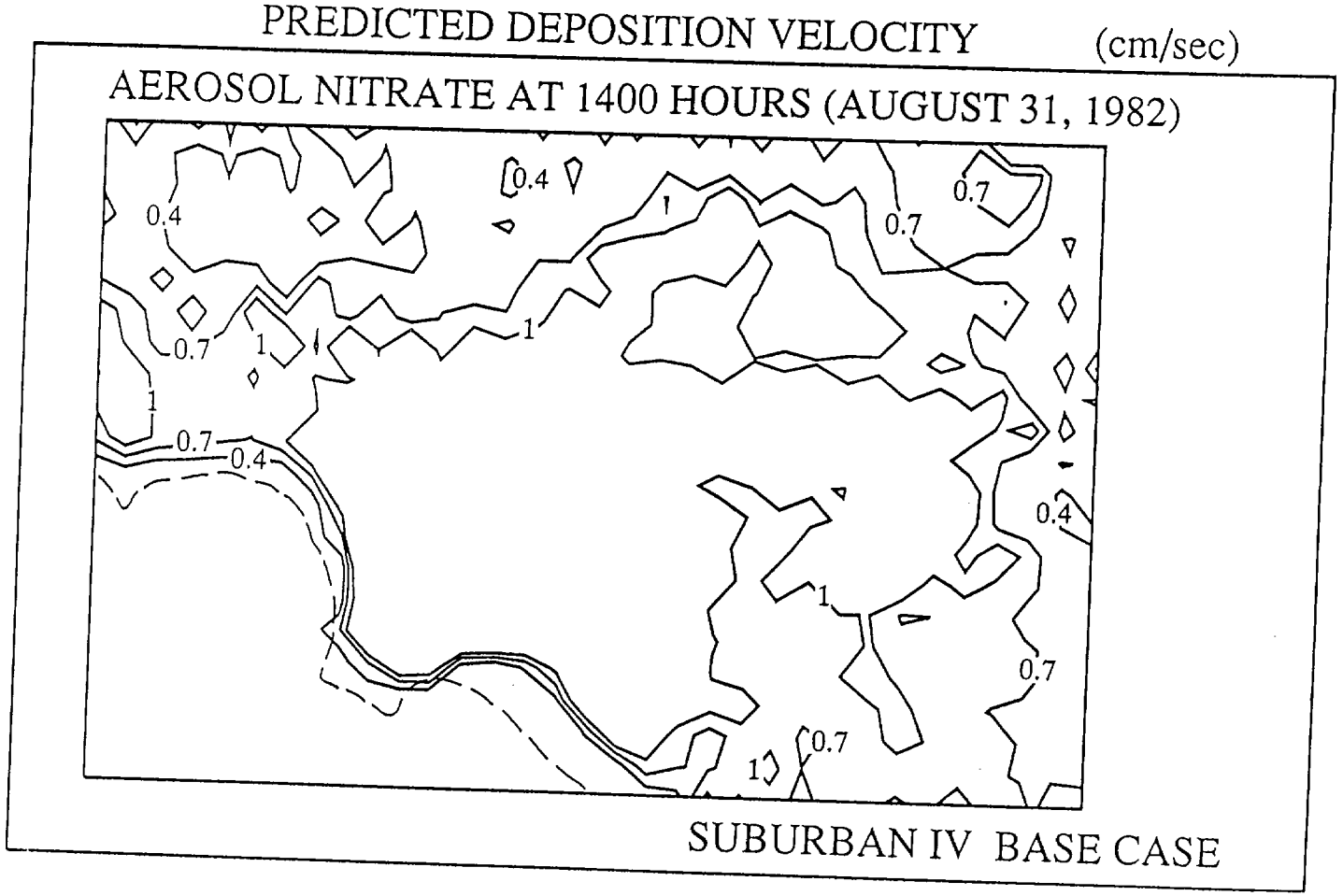
PREDICTED DEPOSITION VELOCITY (cm/sec)
AEROSOL NITRATE AT 1400 HOURS (AUGUST 31, 1982)
0.4
0.4
0.7
0.7
0.7
1
1
1
0.7
0.4
0.4
1
0.7
0.7
1
SUBURBAN IV BASE CASE

Figure 3.56

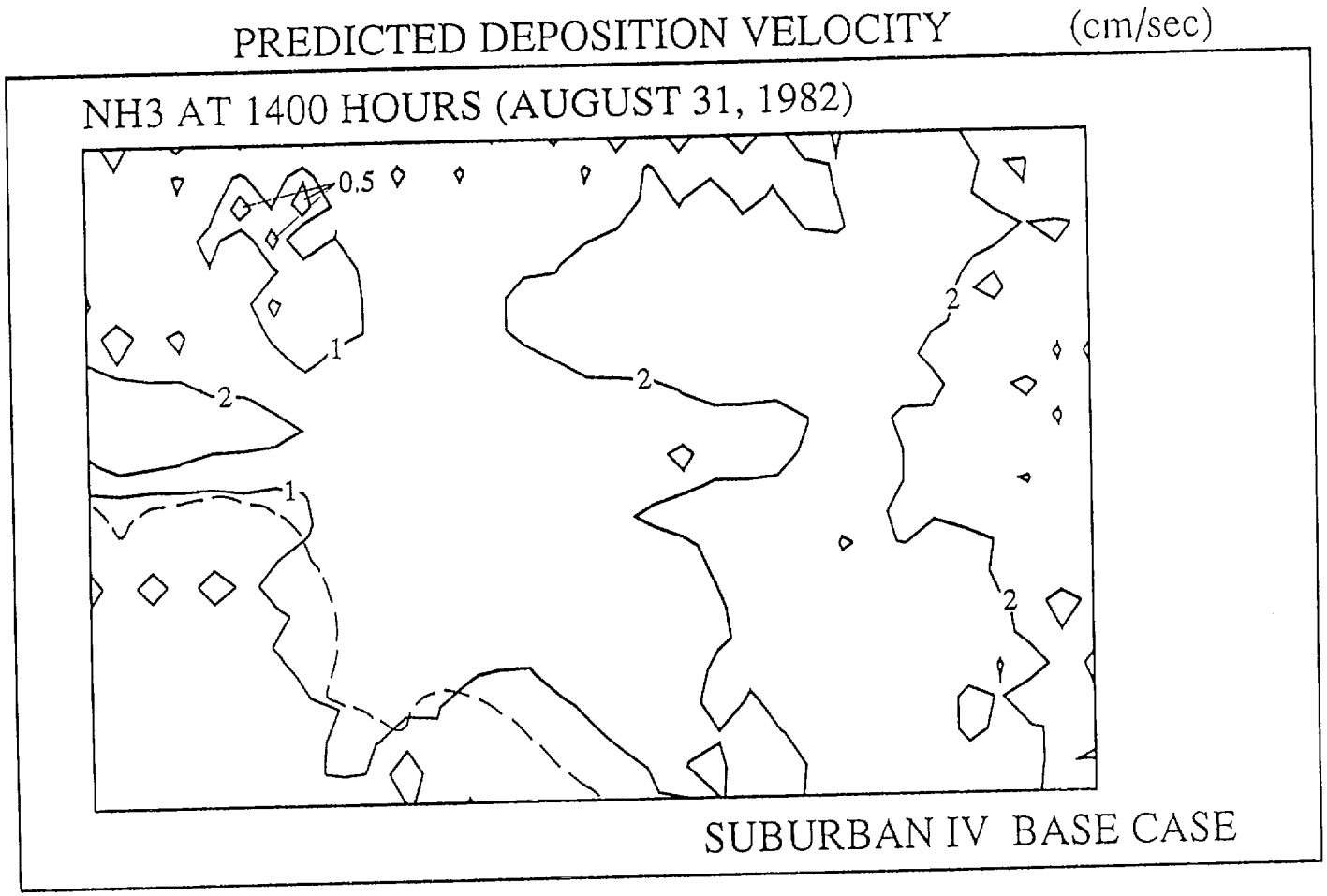
PREDICTED DEPOSITION VELOCITY (cm/sec)
NH3 AT 1400 HOURS (AUGUST 31, 1982)
0.5
1
2
2
2
1
2
SUBURBAN IV BASE CASE

Figure 3.57

for NO and PAN are much higher than for O_3, and their deposition velocities equal about 0.1 cm/sec in mid-afternoon, as shown in Figures 3.54 and 3.55. The spatial distribution of the aerosol nitrate dry deposition velocity shown in Figure 3.56 mirrors that of HNO_3 since the deposition velocity is calculated as a constant ratio to that of HNO_3 based on a rough analogy to field experimental data, as discussed earlier.

The spatial distribution of pollutant dry deposition fluxes next can be visualized. The deposition velocities are multiplied by the atmospheric concentrations, and contour plots of the deposition flux result. Deposition maps for the mid-afternoon of August 31 are shown in Figures 3.58–3.64 NO_x-derived species are removed predominantly as HNO_3. HNO_3 fluxes to the surface in the range 1.5–3 mg/m^2· hr are computed throughout the central portion of the air basin at that time (see Figure 3.58). NO_2 also makes a significant contribution to the flux of NO_x-derived species, as seen in Figure 3.59. Aerosol nitrate and ammonia fluxes are highest in the Rubidoux area, to the east of the zone of highest HNO_3 and NO_2 dry flux at that time (see Figures 3.60 and 3.61). NO and PAN concentrations make a smaller contribution to the dry deposition flux in the mid-afternoon (see Figures 3.62 and 3.63) because of their low deposition velocities (and, in the case of NO, its low concentration at that time of day). Ozone fluxes to the surface are very much larger than the fluxes of the other contaminants; as high as 25 mg/m^2· hr in portions of the eastern area of the air basin in mid-afternoon, as seen in Figure 3.64.

Under Base Case August 31, 1982, conditions, 247.1 metric tons/day of nitrogen is deposited by dry processes within the boundaries of the modeling region shown in Figure 3.1 (see the heavily outlined area in the center of that figure). As shown in Table 3.4, that dry flux is dominated by nitric acid, ammonia and NO_2. The ammonium nitrate flux includes nitrogen from both the ammonium and nitrate ions. The values in Table 3.4 differ from those in the graphs labeled as aerosol nitrate which only include the nitrogen contibuted by the nitrate ion. If the ammonia dry flux is set aside along with the ammonium content of the aerosol nitrate, then the flux of NO_x-derived species totals 175.5 metric tons/day, N, which is equivalent to 577 metric tons/day if stated at the molecular weight of NO_2. Since the NO_x emissions to the atmosphere of the air basin total about 1120 metric tons/day (see Table 3.1), the prediction is that 52% of the NO_x emitted will have been removed by dry deposition within the modeling region

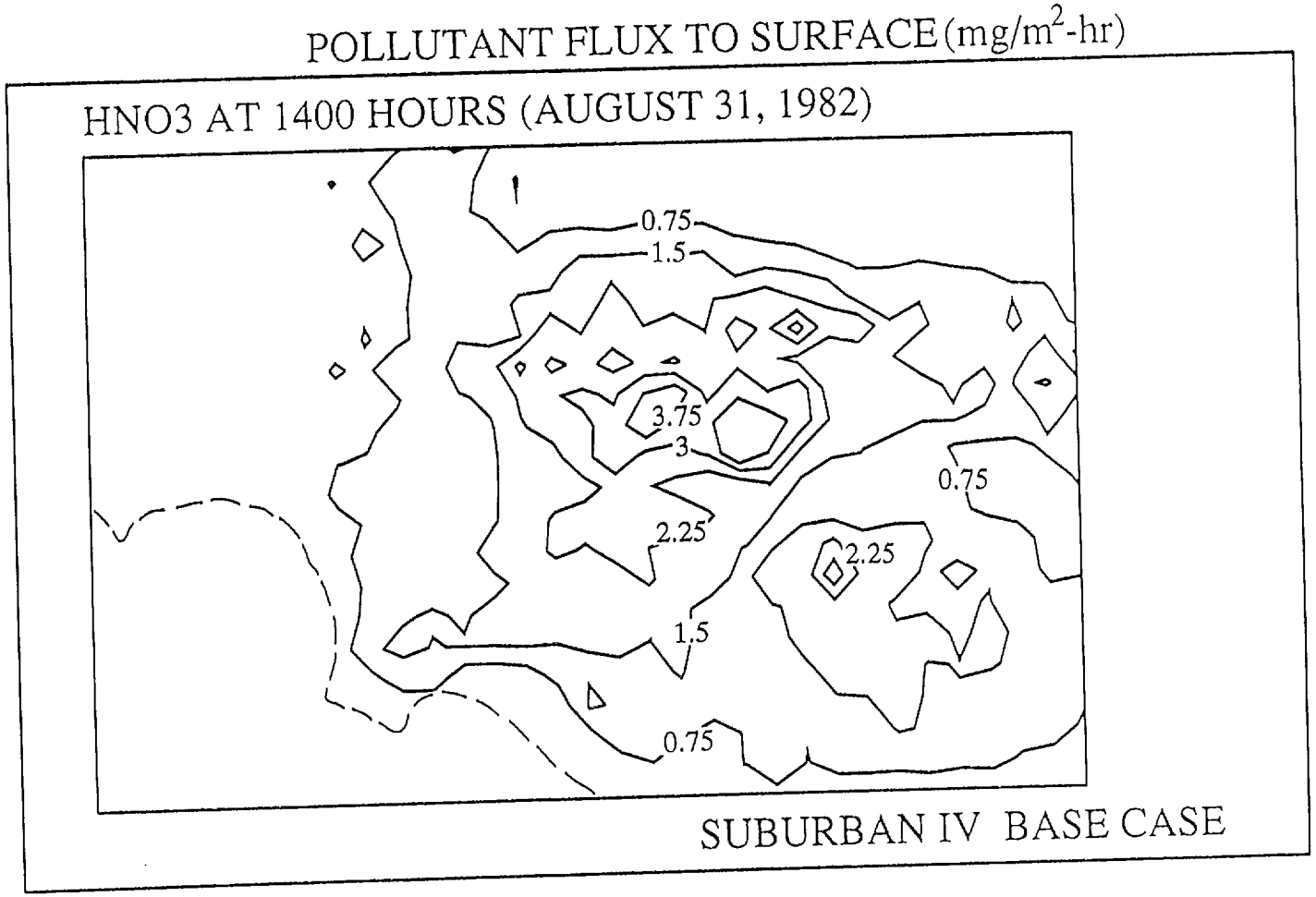
POLLUTANT FLUX TO SURFACE (mg/m2-hr)
HNO3 AT 1400 HOURS (AUGUST 31, 1982)
0.75
1.5
3.75
3
0.75
2.25
2.25
1.5
0.75
SUBURBAN IV BASE CASE

Figure 3.58

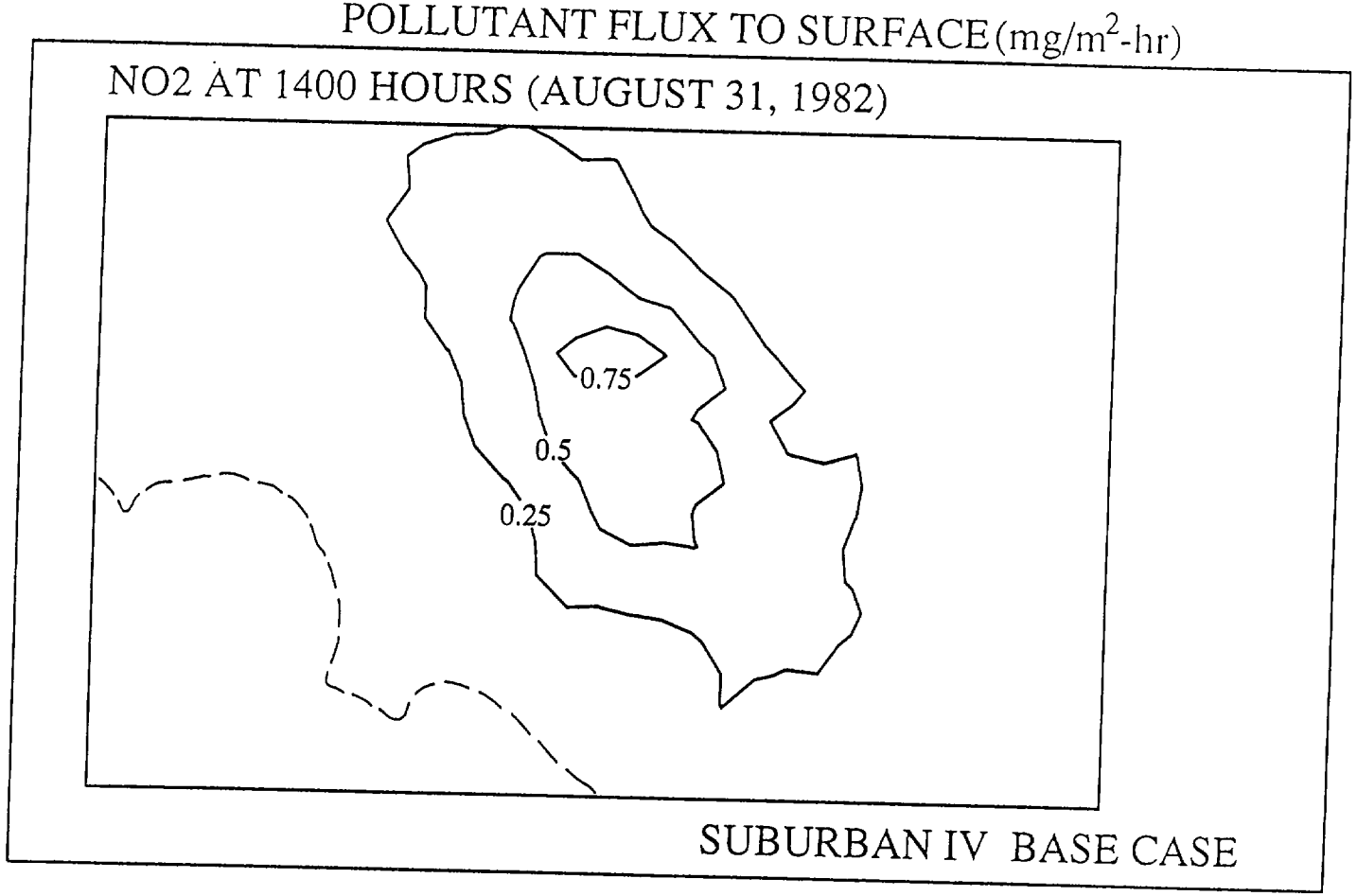
POLLUTANT FLUX TO SURFACE (mg/m2-hr)
NO2 AT 1400 HOURS (AUGUST 31, 1982)
0.75
0.5
0.25
SUBURBAN IV BASE CASE

Figure 3.59

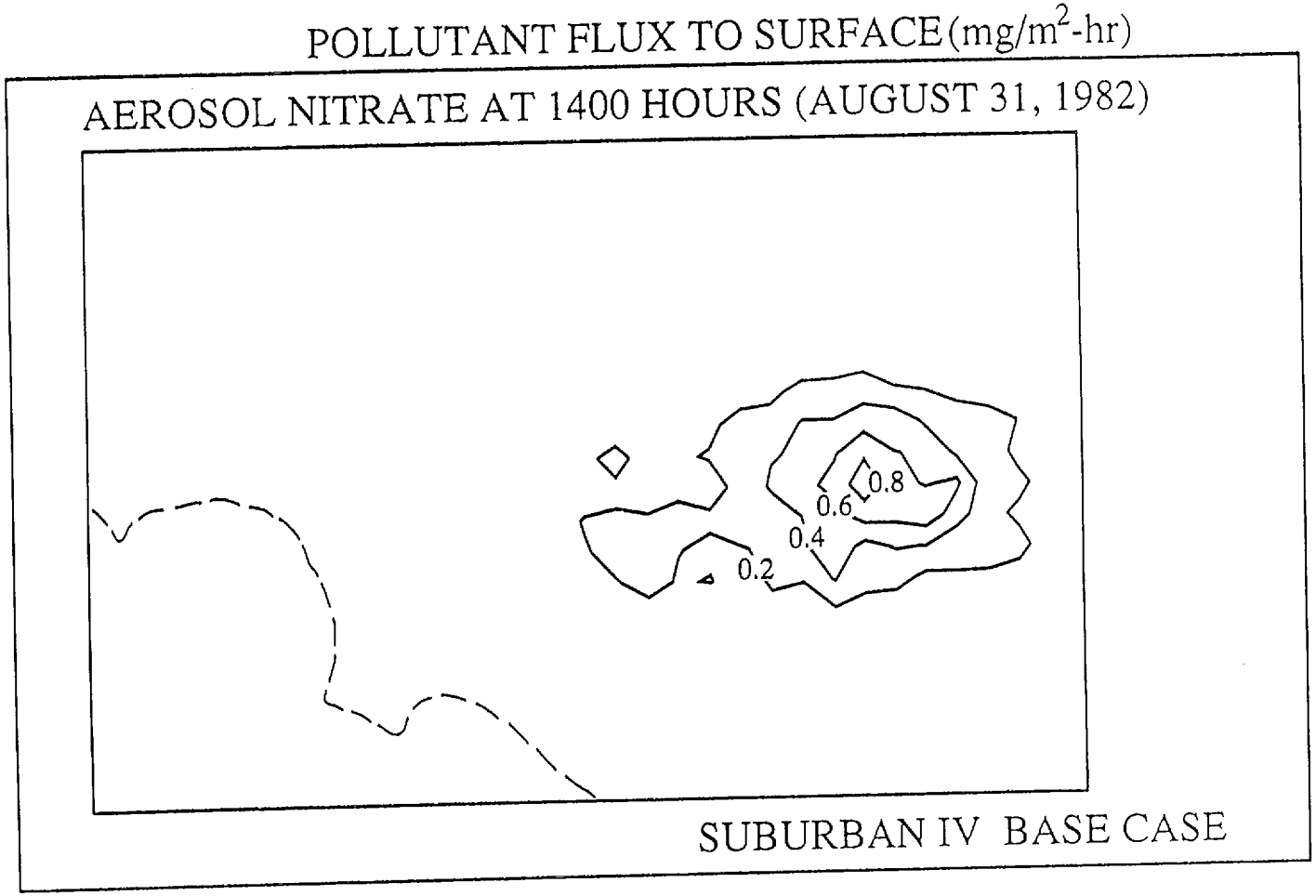
POLLUTANT FLUX TO SURFACE (mg/m2-hr)
AEROSOL NITRATE AT 1400 HOURS (AUGUST 31, 1982)
0.8
0.6
0.4
0.2
SUBURBAN IV BASE CASE

Figure 3.60

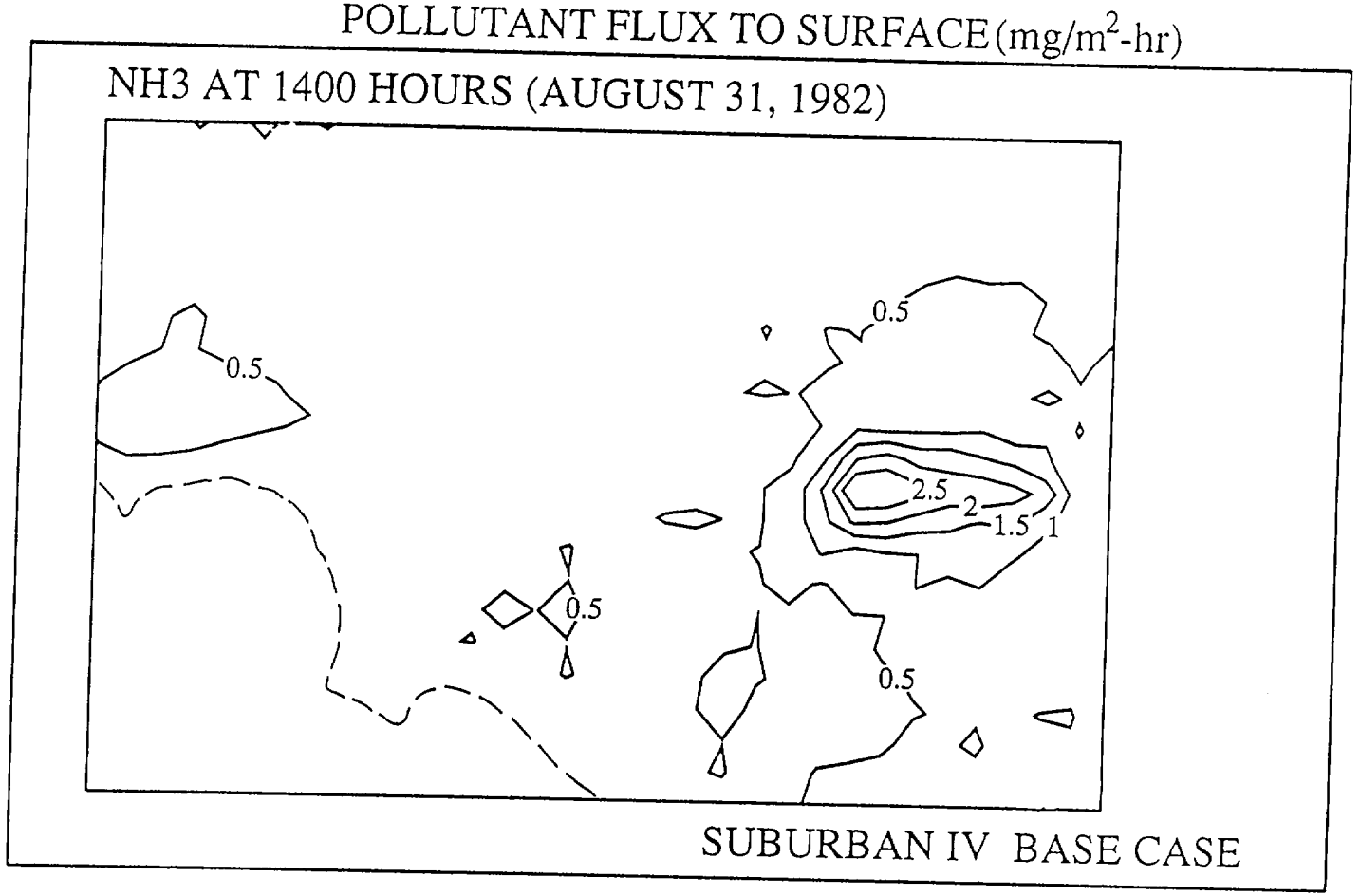
POLLUTANT FLUX TO SURFACE (mg/m2-hr)
NH3 AT 1400 HOURS (AUGUST 31, 1982)
0.5
0.5
2.5
2
1.5
1
0.5
0.5
SUBURBAN IV BASE CASE

Figure 3.61

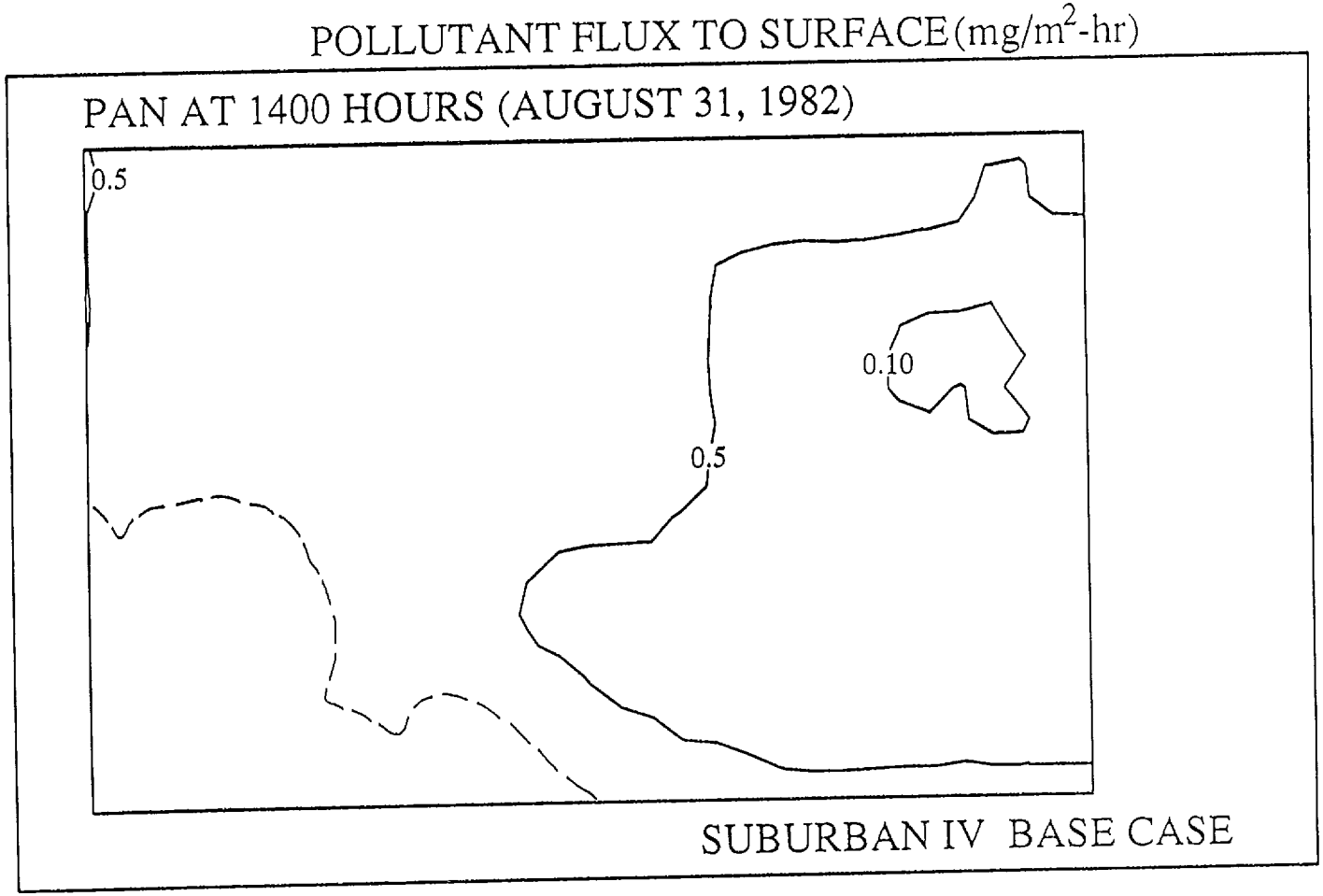
POLLUTANT FLUX TO SURFACE(mg/m2-hr)
PAN AT 1400 HOURS (AUGUST 31, 1982)
0.5
0.10
0.5
SUBURBAN IV BASE CASE

Figure 3.62

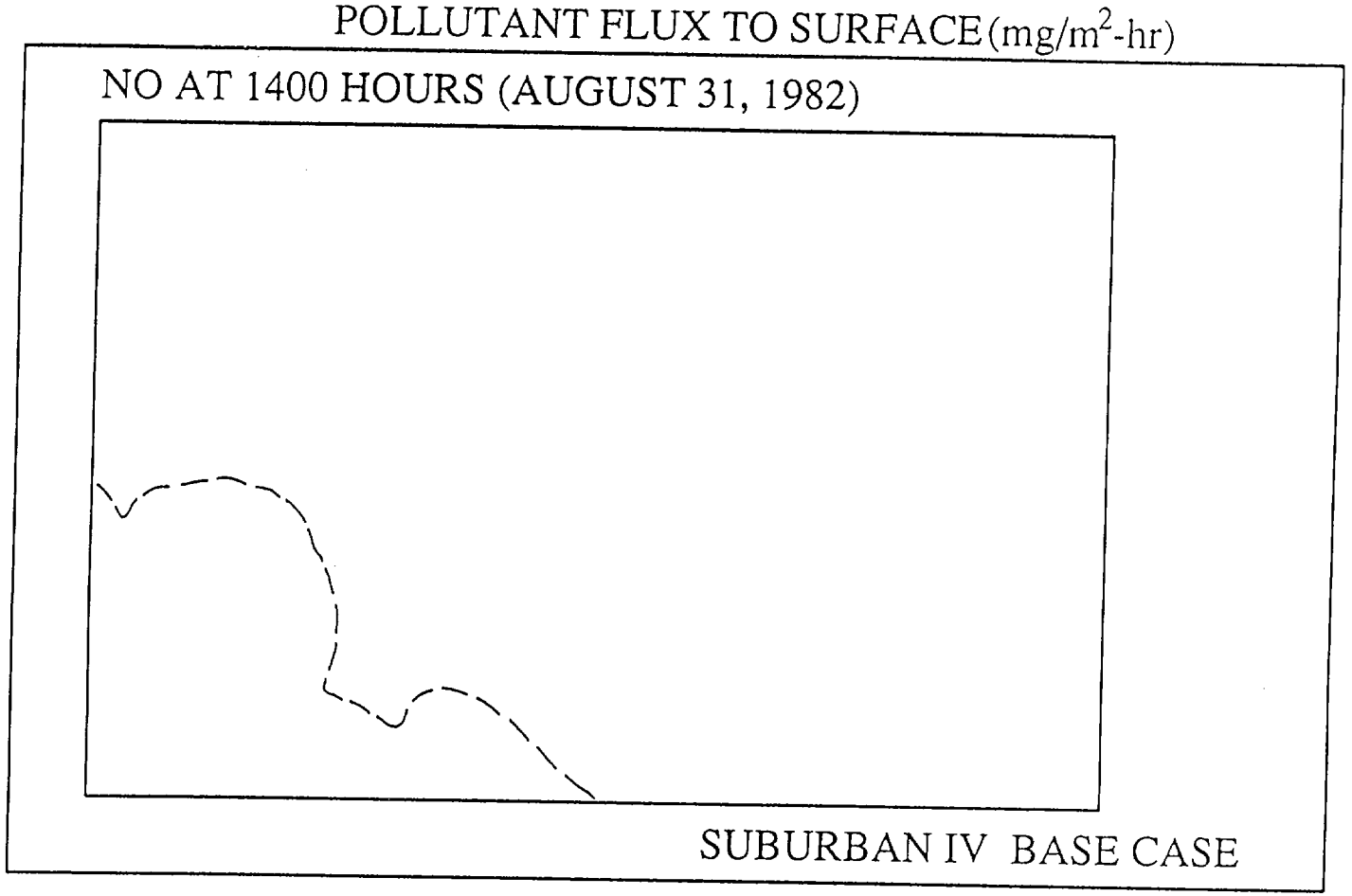
POLLUTANT FLUX TO SURFACE (mg/m2-hr)
NO AT 1400 HOURS (AUGUST 31, 1982)
SUBURBAN IV BASE CASE

Figure 3.63

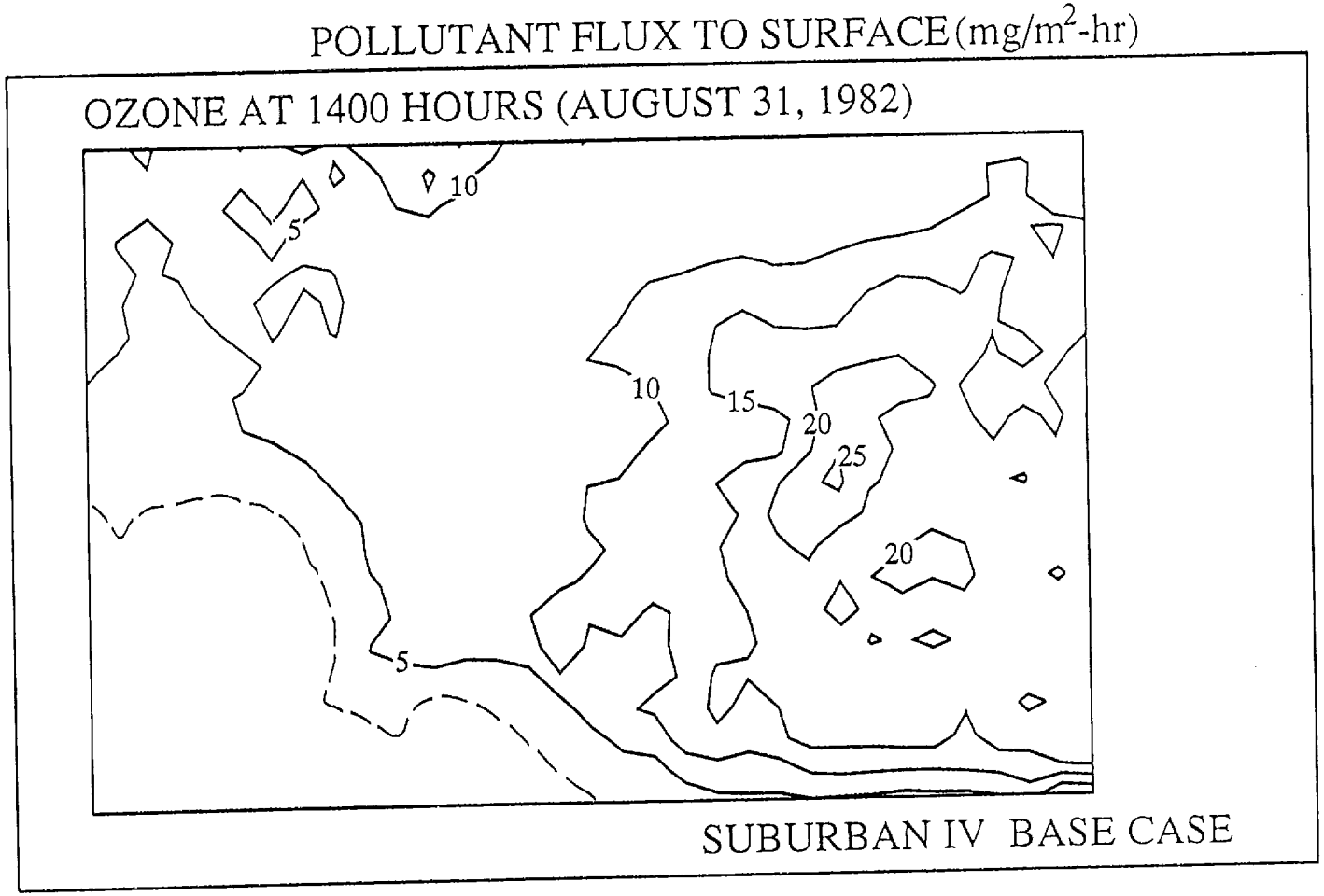
POLLUTANT FLUX TO SURFACE (mg/m2-hr)
OZONE AT 1400 HOURS (AUGUST 31, 1982)
5
10
10
15
20
25
20
5
SUBURBAN IV BASE CASE

Figure 3.64

Table 3.4 Dry Deposition Flux to the Surface of the Modeling Region – Base Case Conditions (Metric tons N/day for August 31, 1982)

Pollutant	Flux
NO	4.8
NO_2	49.1
PAN	7.2
HNO_3	101.4
NH_3	58.7
NH_4NO_3	25.9
Total	247.1

during a 24-hr. period like that studied here. This dry flux of NO_x-derived species is dominated by HNO_3 and NO_2, the sums of which considerably exceed the NH_3 dry flux.

Ozone concentration predictions in time series are given at stations spaced across the air basin in Figure 3.65. The absolute O_3 peaks at the high locations at Glendora and at Riverside are matched closely. For many hours of the day at sites in the eastern area of the air basin, O_3 concentration predictions are above the observed values, as shown for Riverside in Figure 3.65, such that the time-average of the predicted O_3 levels is above the observed average even when the peaks are closely reproduced.

Figure 3.66 compares "NO_2" as measured by a chemiluminescent NO_x monitor to the summation of the predicted concentrations of NO_2 plus PAN plus inorganic nitrate species, because such monitors measure those species as if they were NO_2. The resulting parameter will be referred to as "Total NO_2." Total NO_2 concentrations at the basinwide peak location at central Los Angeles are in good agreement with the observed values.

Predicted and observed ammonia, HNO_3 and aerosol nitrate values are shown at central Los Angeles in Figure 3.67, and the general magnitude of the predicted concentrations is in reasonable agreement with observations. Predicted NH_3 levels in the eastern portion of the air basin at Rubidoux are of about the right magnitude, as seen in Figure 3.68. Exact prediction of NH_3 concentrations is not expected because the spike in NH_3 emissions upwind of Rubidoux is so sharp that even a small error in wind direction will induce differences between predictions and observations. HNO_3 concentrations within this model are determined by the maximum amount of HNO_3 allowed in the the gas phase in equilibrium NH_4NO_3 at the prevailing NH_3 levels. With NH_3 concentrations above 50 ppb much of the time at Rubidoux, the HNO_3 concentrations will be forced to very low values by the great excess of NH_3. Predicted and observed HNO_3 concentrations at Rubidoux are in close agreement, as expected, since the HNO_3 level is governed by the NH_3 present (along with temperature and relative humidity) and the NH_3 values were predicted fairly closely. The excess inorganic nitrate production predicted by the revised model cannot remain in the gas phase in the presence of the high NH_3 levels at Rubidoux; instead, it appears as aerosol nitrate in considerable excess of observed values.

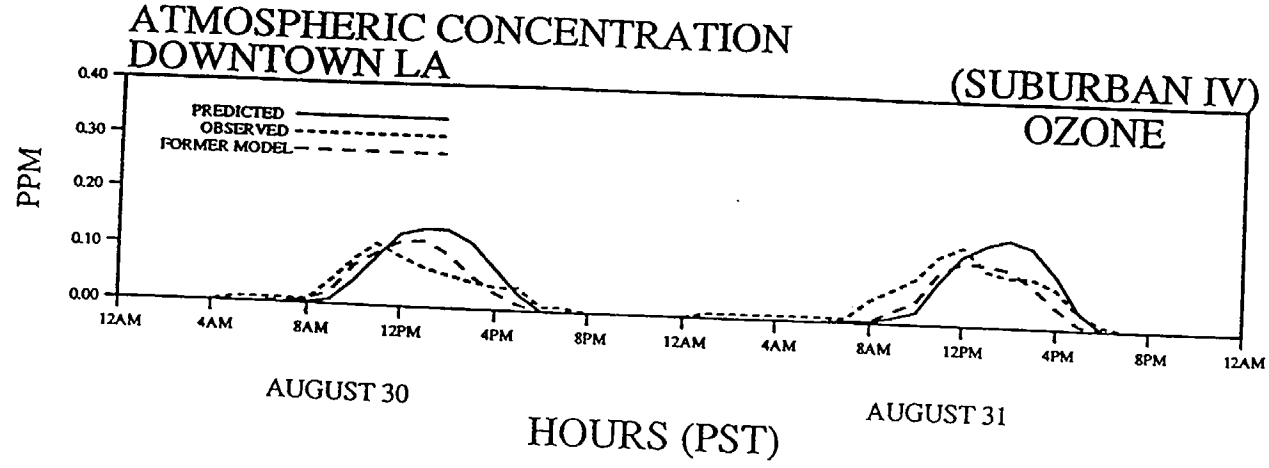
ATMOSPHERIC CONCENTRATION
DOWNTOWN LA
(SUBURBAN IV)
OZONE
PREDICTED
OBSERVED
FORMER MODEL
PPM
0.40
0.30
0.20
0.10
0.00
12AM
4AM
8AM
12PM
4PM
8PM
12AM
4AM
8AM
12PM
4PM
8PM
12AM
AUGUST 30
AUGUST 31
HOURS (PST)

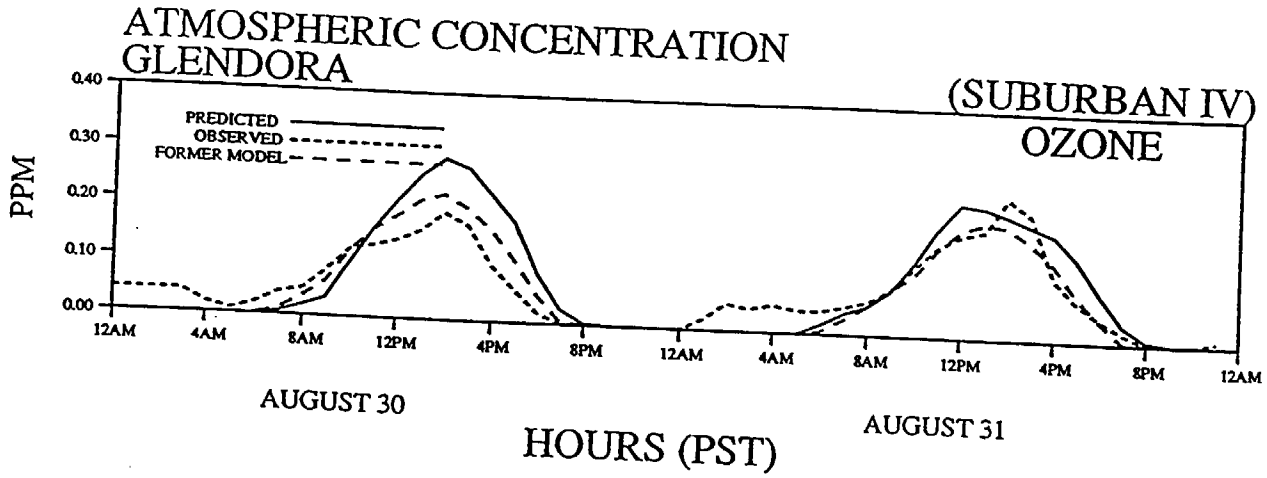
ATMOSPHERIC CONCENTRATION
GLENDORA
(SUBURBAN IV)
OZONE
PREDICTED
OBSERVED
FORMER MODEL
PPM
0.40
0.30
0.20
0.10
0.00
12AM
4AM
8AM
12PM
4PM
8PM
12AM
4AM
8AM
12PM
4PM
8PM
12AM
AUGUST 30
AUGUST 31
HOURS (PST)

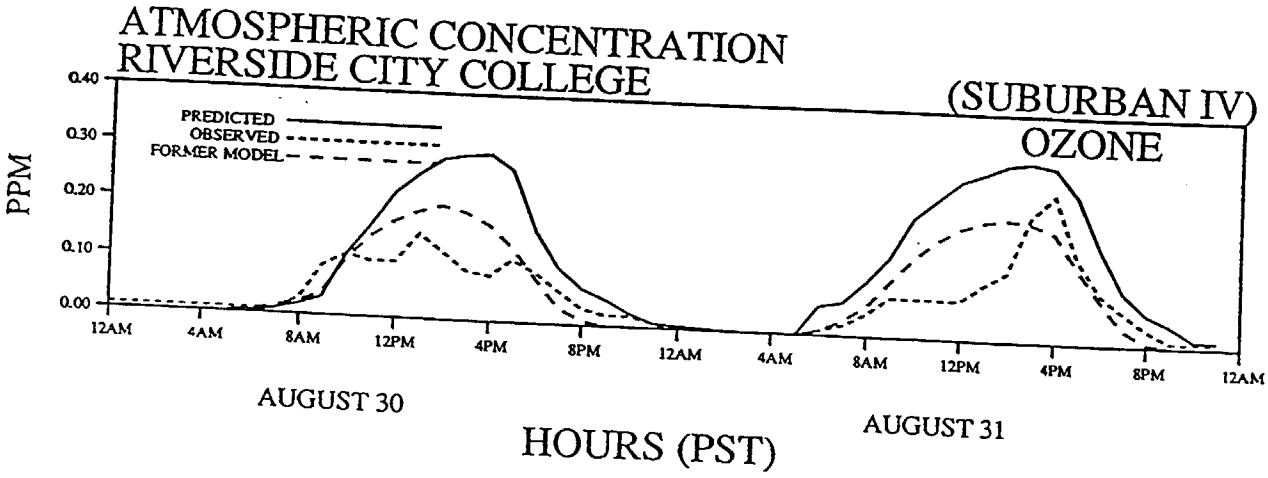
ATMOSPHERIC CONCENTRATION
RIVERSIDE CITY COLLEGE
(SUBURBAN IV)
OZONE
PREDICTED
OBSERVED
FORMER MODEL
PPM
0.40
0.30
0.20
0.10
0.00
12AM
4AM
8AM
12PM
4PM
8PM
12AM
4AM
8AM
12PM
4PM
8PM
12AM
AUGUST 30
AUGUST 31
HOURS (PST)

Figure 3.65

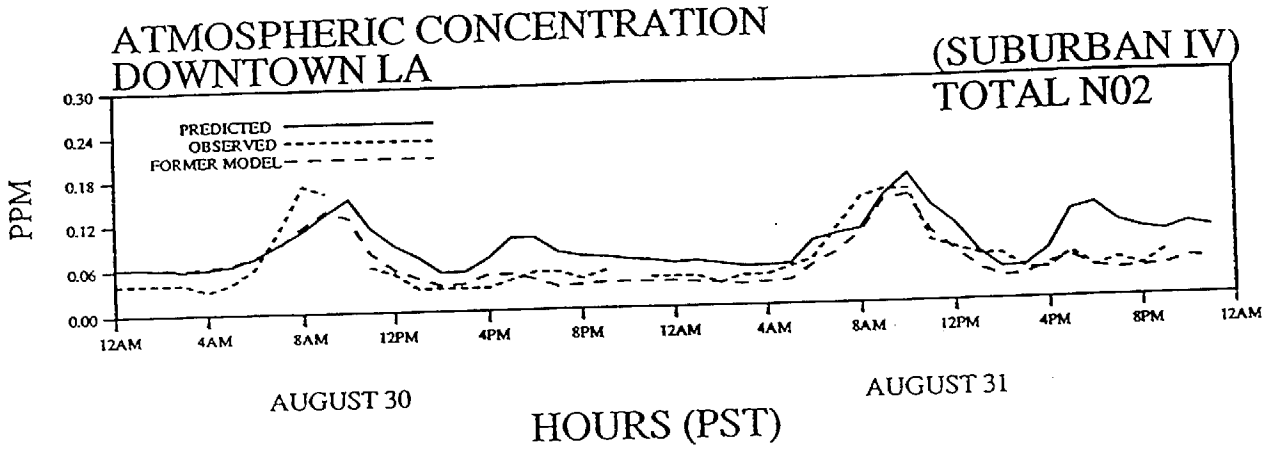
ATMOSPHERIC CONCENTRATION
DOWNTOWN LA
(SUBURBAN IV)
TOTAL N02
PREDICTED
OBSERVED
FORMER MODEL
PPM
0.30
0.24
0.18
0.12
0.06
0.00
12AM
4AM
8AM
12PM
4PM
8PM
12AM
4AM
8AM
12PM
4PM
8PM
12AM
AUGUST 30
AUGUST 31
HOURS (PST)

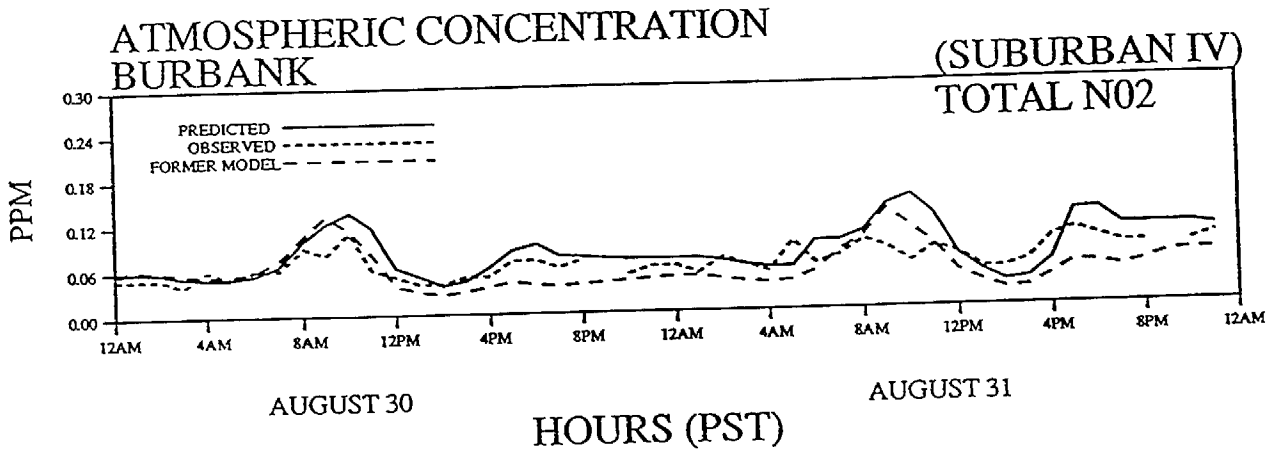
ATMOSPHERIC CONCENTRATION
BURBANK
(SUBURBAN IV)
TOTAL N02
PREDICTED
OBSERVED
FORMER MODEL
PPM
0.30
0.24
0.18
0.12
0.06
0.00
12AM
4AM
8AM
12PM
4PM
8PM
12AM
4AM
8AM
12PM
4PM
8PM
12AM
AUGUST 30
AUGUST 31
HOURS (PST)

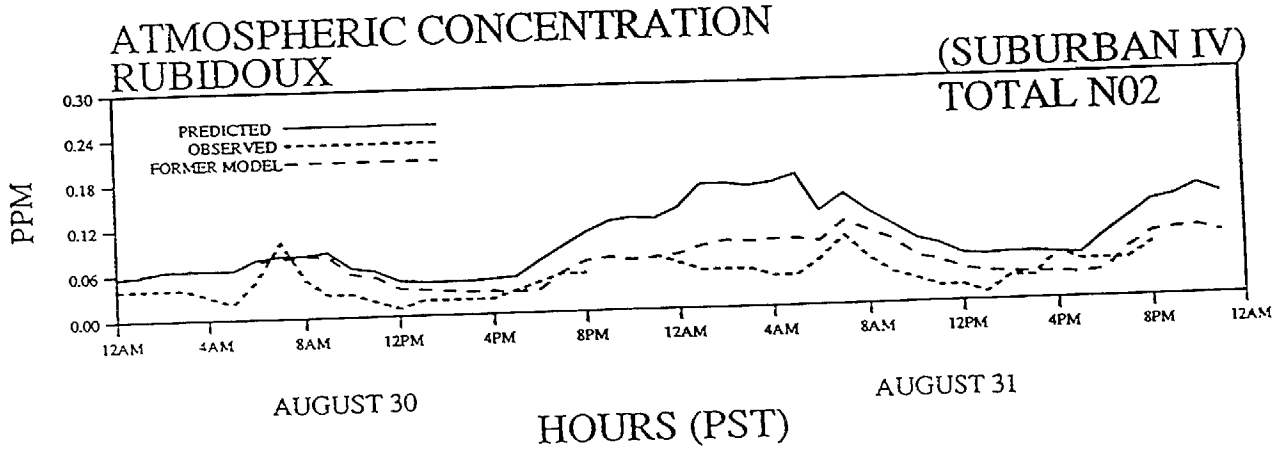
ATMOSPHERIC CONCENTRATION
RUBIDOUX
(SUBURBAN IV)
TOTAL N02
PREDICTED
OBSERVED
FORMER MODEL
PPM
0.30
0.24
0.18
0.12
0.06
0.00
12AM
4AM
8AM
12PM
4PM
8PM
12AM
4AM
8AM
12PM
4PM
8PM
12AM
AUGUST 30
AUGUST 31
HOURS (PST)

Figure 3.66

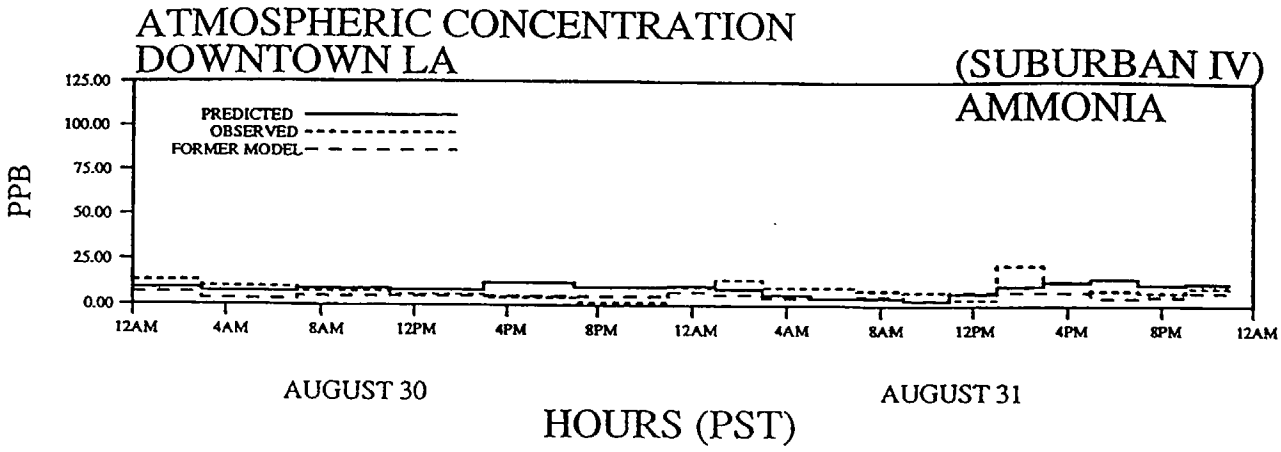
ATMOSPHERIC CONCENTRATION
DOWNTOWN LA
(SUBURBAN IV)
AMMONIA
PREDICTED
OBSERVED
FORMER MODEL
PPB
125.00
100.00
75.00
50.00
25.00
0.00
12AM
4AM
8AM
12PM
4PM
8PM
12AM
4AM
8AM
12PM
4PM
8PM
12AM
AUGUST 30
AUGUST 31
HOURS (PST)

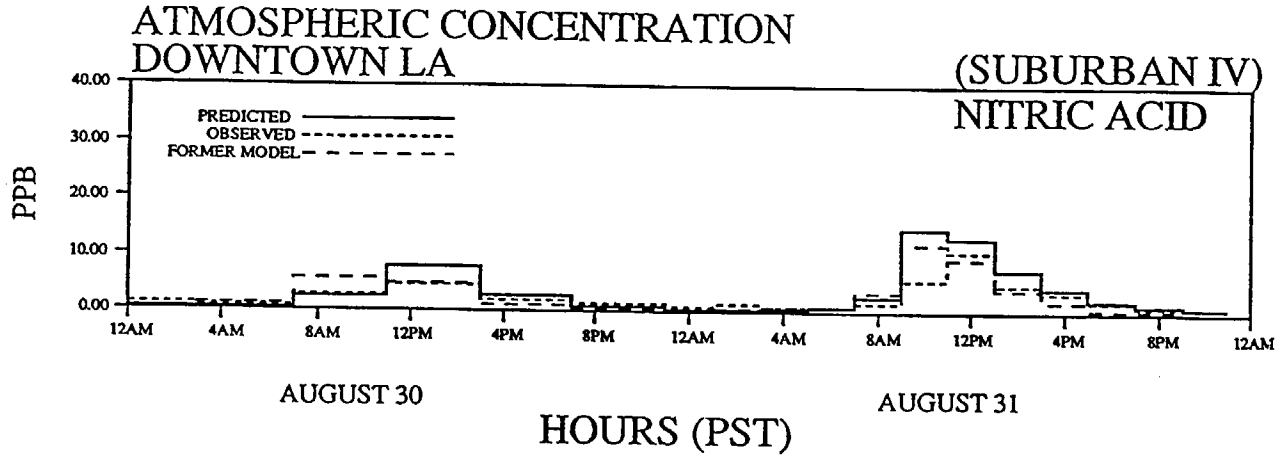
ATMOSPHERIC CONCENTRATION
DOWNTOWN LA
(SUBURBAN IV)
NITRIC ACID
PREDICTED
OBSERVED
FORMER MODEL
PPB
40.00
30.00
20.00
10.00
0.00
12AM
4AM
8AM
12PM
4PM
8PM
12AM
4AM
8AM
12PM
4PM
8PM
12AM
AUGUST 30
AUGUST 31
HOURS (PST)

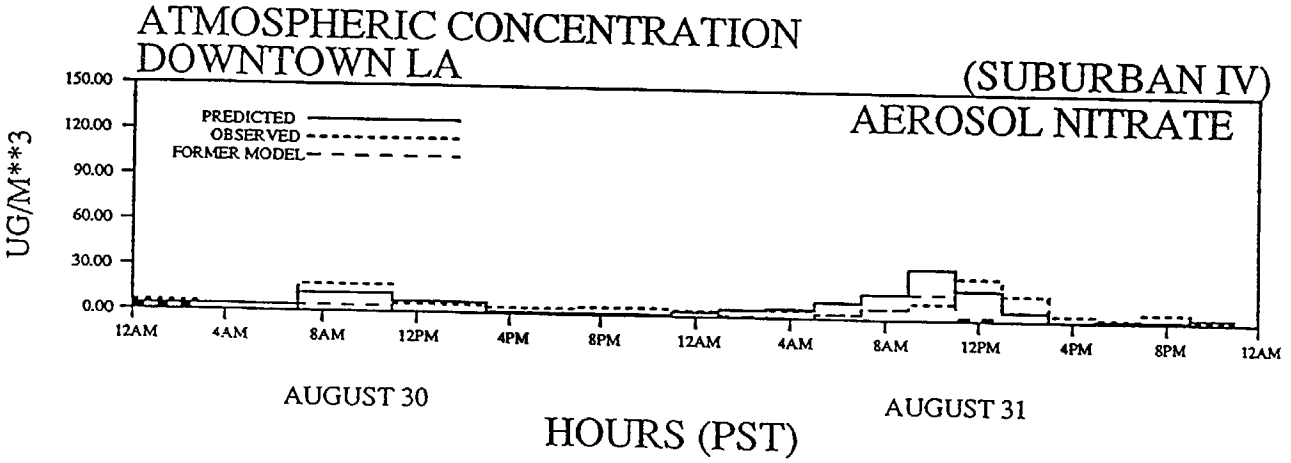
ATMOSPHERIC CONCENTRATION
DOWNTOWN LA
(SUBURBAN IV)
AEROSOL NITRATE
PREDICTED
OBSERVED
FORMER MODEL
UG/M**3
150.00
120.00
90.00
60.00
30.00
0.00
12AM
4AM
8AM
12PM
4PM
8PM
12AM
4AM
8AM
12PM
4PM
8PM
12AM
AUGUST 30
AUGUST 31
HOURS (PST)

Figure 3.67

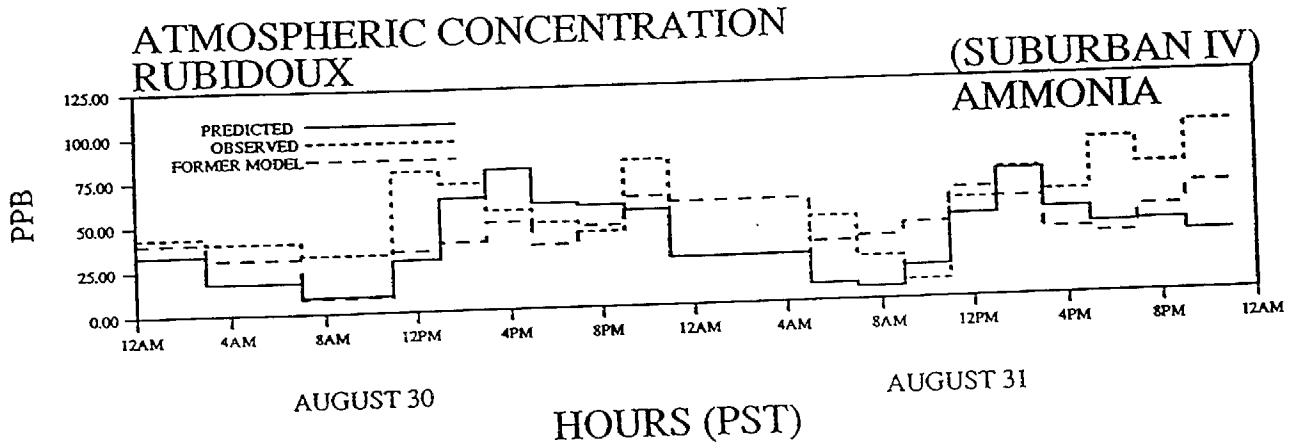
ATMOSPHERIC CONCENTRATION
RUBIDOUX
(SUBURBAN IV)
AMMONIA
PPB
125.00
100.00
75.00
50.00
25.00
0.00
PREDICTED
OBSERVED
FORMER MODEL
12AM
4AM
8AM
12PM
4PM
8PM
12AM
4AM
8AM
12PM
4PM
8PM
12AM
AUGUST 30
AUGUST 31
HOURS (PST)

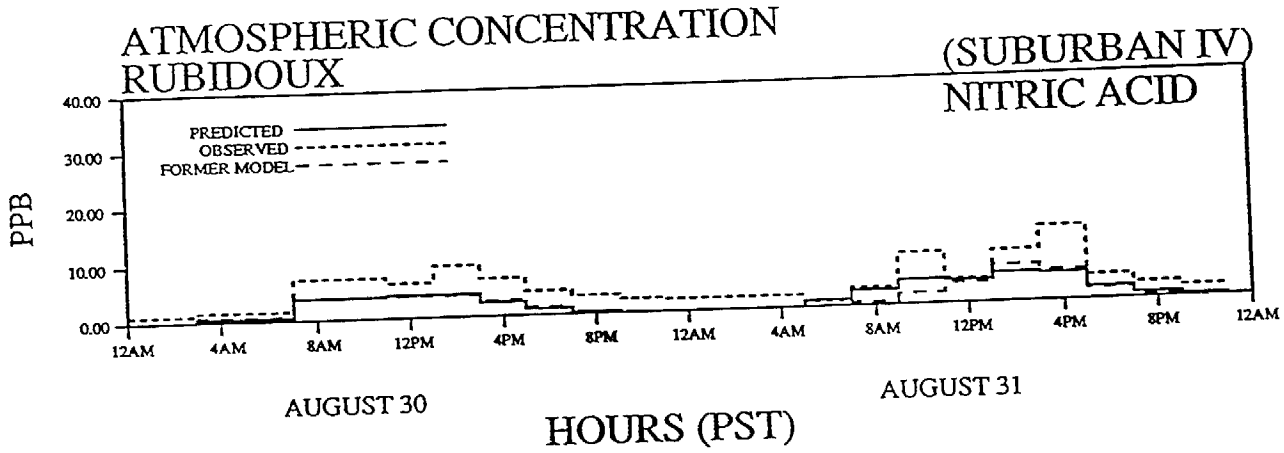
ATMOSPHERIC CONCENTRATION
RUBIDOUX
(SUBURBAN IV)
NITRIC ACID
PPB
40.00
30.00
20.00
10.00
0.00
PREDICTED
OBSERVED
FORMER MODEL
12AM
4AM
8AM
12PM
4PM
8PM
12AM
4AM
8AM
12PM
4PM
8PM
12AM
AUGUST 30
AUGUST 31
HOURS (PST)

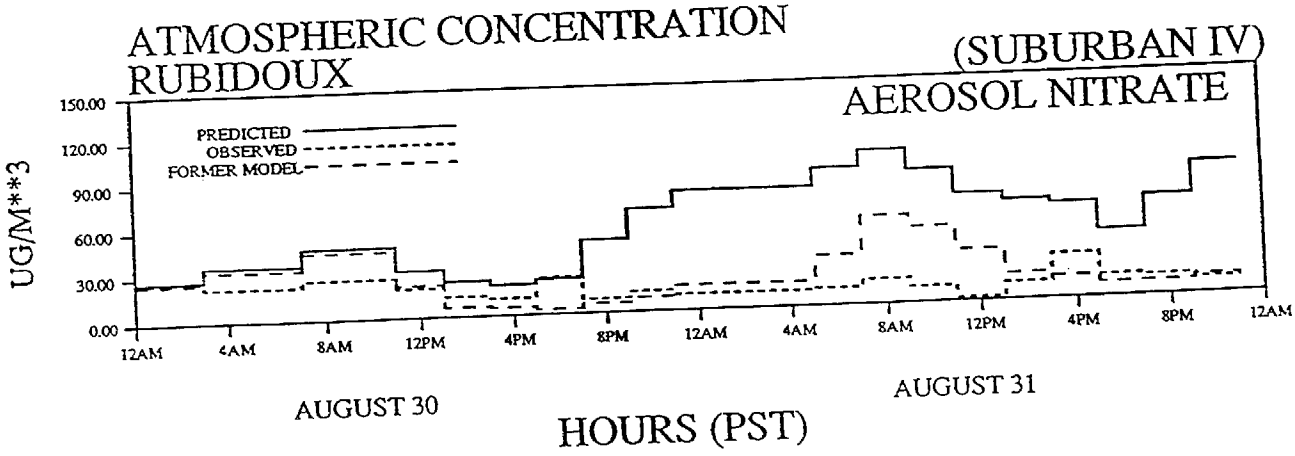
ATMOSPHERIC CONCENTRATION
RUBIDOUX
(SUBURBAN IV)
AEROSOL NITRATE
UG/M**3
150.00
120.00
90.00
60.00
30.00
0.00
PREDICTED
OBSERVED
FORMER MODEL
12AM
4AM
8AM
12PM
4PM
8PM
12AM
4AM
8AM
12PM
4PM
8PM
12AM
AUGUST 30
AUGUST 31
HOURS (PST)

Figure 3.68

These higher inorganic nitrate values than seen in prior model calculations are the result of greater inorganic nitrate accumulation overnight. This could be due either to a calculated increase in HNO_3 formation overnight due to nighttime chemical reactions or to a calculated decrease in dry deposition of HNO_3. Since HNO_3 is removed at a diffusion-limited rate in both the previous and present versions of the model, any calculated decrease in the HNO_3 dry flux to the ground is not due to an increase in the effective surface resistance value in the model. It is possible that the new surface roughness values calculated from the land use data have underestimated the actual surface roughness in the hilly areas of the central portion of the air basin, which would reduce the calculated HNO_3 dry flux.

An alternative possibility is that the higher HNO_3 accumulation overnight results from nighttime chemical reactions between O_3 and NO_2 to form HNO_3 via NO_3 and N_2O_5. The ozone concentrations predicted by the revised model are higher than from the prior model because the O_3 dry deposition rate is lower. Factors that could lead to underestimation of the O_3 dry flux include: (1) an overestimate of the surface resistance for dry deposition, particluarly for the urban areas for which experimental data are not available and (2) an underestimate of the effect of the surface area of buildings and other objects in urban areas that could act as a sink for O_3. As a result, O_3 concentrations aloft in the central and eastern portions of the air basin are higher at night than in the prior version of the model and also do not go to zero at ground level at night as quickly as was previously the case. One conclusion that can be drawn is that computed inorganic nitrate concentrations are very sensitive to even small changes in the deposition rates for HNO_3 or O_3.

A statistical comparison of model performance measures is presented in Tables 3.5 through 3.8 for those parameters that have been reported from the simulations conducted prior to changes in the dry deposition calculations. Concentration predictions resulting from the changes to the dry deposition module in the model generally are higher than from the previous version of the model. This is a consequence of the fact that estimated deposition rates from the surface resistance formulation of the deposition model are lower than before, given the estimates for surface resistances and roughnesses that are typically used by others in formulating such models. Present concentration predictions are clearly separated from the observations by no more than

the uncertainty of the parameters needed by the deposition module (as can be seen by reference to the prior model which is quite close to reproducing the observations with only a relatively small departure from the approach used here).

It must be noted that there are essentially zero data in the technical literature on the deposition rates for ozone and most other pollutants to urban land uses. All of the surface resistance parameter values used for urban landscapes in such models at present are essentially educated guesses. For that reason, we see no reason to restructure the model to force it to fit the observations. The structure of the model is believed to represent a major improvement upon prior applications in California. What is needed at this point to improve model performance is a program of field measurements necessary to determine the surface resistances for the large collection of pollutants and surface types that must be tracked by the photochemical airshed model. An experimental determination of the effect of the surface area of buildings and other roughness elements on the effective surface area for removal of pollutants also needs to be undertaken. It may be that the surface area for deposition should be increased above that presented by the horizontal plane of the model.

Table 3.5 Statistical Comparison of Model Performance for O_3 and NO_2 – Previous Model vs. Revised Deposition Module.

Performance Measure	Results of Test	
Ozone	Former Model	Revised Model
Mean of residuals, ppm (bias)	0.010	0.028
RMS error about the mean, ppm (σ of residuals)	0.037	0.055
Accuracy of peak prediction	0.262/0.26 =1.01	
Correlation coefficient	0.83	0.83
Linear least-squares fit $C_{obs} = MC_{pred} + B$	M=1.11 B=0.006	M=1.48 B=0.009
NO_2		
Mean of residuals, ppm (bias)	-0.002	0.020
RMS error about the mean, ppm (σ of residuals)	0.030	0.033
Accuracy of peak prediction	0.157/0.17 =0.92	
Correlation coefficient	0.43	0.43
Linear least-squares fit $C_{obs} = MC_{pred} + B$	M=0.47 B=0.026	M=0.57 B=0.045

Table 3.6 Statistical Comparison of Model Performance for Ammonia

Performance Measure (units are ppb)	Results of Test	
	Former Model	Revised Model
Mean of observations	13.86	13.86
Mean of predictions	14.6	13.5
Mean of residuals	0.7	-0.3
RMS error about the mean	16	12.2
Correlation coefficient	0.54	0.74
Regression analysis	M=0.54	M=0.52
$C_{pred} = MC_{obs} + B$	B=7.0	B=6.3

Table 3.7 Statistical Comparison of Model Performance for Nitric Acid Vapor

Performance Measure (units are μgm^{-3})	Results of Test	
	Former Model	Revised Model
Mean of observations	3.4	3.4
Mean of predictions	7.6	4.0
Mean of residuals	4.2	0.6
RMS error about the mean	7.8	4.1
Correlation coefficient	0.7	0.6
Regression analysis	M=1.7	M=0.8
C_{pred} =MC_{obs} + B	B=1.9	B=1.2

Table 3.8 Statistical Comparison of Model Performance for Aerosol Nitrate

Performance Measure (units are μgm^{-3})	Results of Test	
	Former Model	Revised Model
Mean of observations	9.5	9.5
Mean of predictions	8.0	20.5
Mean of residuals	-1.5	10.9
RMS error about the mean	12	24
Correlation coefficient	0.4	0.3
Regression analysis	M=0.74	M=0.99
C_{pred} =MC_{obs} + B	B=0.94	B=11.0

Chapter 4

Evaluation of the Effect of Emission Controls

4.1 INTRODUCTION

The model application described in Chapter 3 of this report forms a base case against which the effect of emission controls can be compared. Emission control measures that already have been examined for their effect on ambient pollutant concentrations by Russell et. al. (1988b) now will be evaluated for their effect on the dry deposition flux of nitrogen-containing species. The objective here is not to attempt to simulate the exact effect of a particular air quality management plan, but rather to examine the magnitude of the change in the dry deposition flux as emissions are lowered using control measures that have been discussed in recent years.

4.2 EMISSION CONTROL OPPORTUNITIES

The emission control measures that will be evaluated as part of this study are itemized in Table 4.1. Those control measures have been outlined previously by Russell et. al. (1988b), and that discussion will be repeated here for clarity.

Table 4.1 has been divided into 5 groups. Group 1 controls reflect a sub-set of the reduction possibilities that have been documented as part of the 1982 Air Quality Management Plan (AQMP) for the South Coast Air Basin that surrounds Los Angeles (South Coast Air Quality Management District, 1982). This group of controls approximates the effect of many of the emission reductions that can be expected to be implemented in the Los Angeles area in the years following the 1982 base year, but without extension of vehicular catalyst utilization or ammonia injection technology beyond that used in 1982. Group 2 and Group 3 controls simulate the effect of fleet-wide improvements in emissions from motor vehicles, at target levels that have been discussed by state and federal regulatory agencies (California Air Resources Board, n.d.; Environmental Protection Agency, 1984). Current standards for hydrocarbon emissions from new heavy trucks are in between the two levels of fleet-wide emissions studied here. Group 4 and Group 5 controls would further reduce NO_x emissions

Table 4.1

Specific Emission Control Measures and Their Effect if Applied to 1982 Emissions in the South Coast Air Basin

	1982 THC[a] emissns, ton/day	1982 NO_x emissns, ton/day	1982 NH_3 emissns, ton/day[n]	control measure	effect of controls: THC change, %[m]	NO_x change, %[m]	NH_3 change, %[m,n]	ref
				Group 1				
1 wood furniture finishing	16.6			use of water-based coatings and reduced overspray (B-5)	−54.1			3
2 auto refinishing	6.7			use of low solvent or water-based coatings (B-8)	−21.0			3
3 wood flatstock coating	1.5			afterburners on drying and curing ovens (B-1)	−75.0			3
4 industrial maintenance coatings	6.3			use of low solvent or water-based coatings (B-2)	−39.3			3
5 marine coatings	2.4			use of low solvent or more durable coatings (B-3)	−82.8			3
6 motor vehicle manufacturing (painting)	8.2			electrostatic coating and high solids paint (B-4)	−41.2			3
7 metal parts manufacturing (coatings)	25.8			substitute coatings (B-6)	−28.6			3
8 aerospace coatings	4.6			use of low solvent coatings (B-7)	−40.5			3
9 oil and gas well leak reduction	27.3			semiannual inspection and maintenance (A-3)	−50.0			3
10 pesticide application	12.9			changes in formulation and application methods (C-3)	−27.3			3
11 metal and nonmetal parts cleaning	40.6			covers on circuit board degreasers; fewer exemptions (C-1)	−12.8			3
12 paper and fabric coating	10.6			afterburners or activated carbon adsorption on curing ovens (D-2)	−50.0			3
13 dry cleaning	17.9			reduced transfer emissions (wash and dry in a single unit) (G-3)	−35.8			3
14 landfill gas recovery	778.0[o]			methane recovery (F-1)	−46.1[o]			3
15 rubber products manufacturing	3.6			incineration or carbon adsorption on fugitive organics emissions (D-3)	−10.3			3
16 synthetic chemical manufacturing	2.1			chemical absorbers, carbon adsorption, and process changes (G-1)	−90.9			3
17 marine fuel transfer	0.4			vapor recovery systems (A-7)	−90.9			3
18 graphic arts industry	11.9			high solids or waterborne ink; incineration or adsorption (G-2)	−85.0			3
19 refinery boilers and heaters		40.3		combustion modification		−8.0		4
20 residential water heaters		10.3		intermittent ignition devices and stack vent valves (N-18)		−25.0		3
21 nonrefinery industrial boilers		35.0		combustion modification (G-11)		−25.0		3
22 cement kilns		9.7		combustion modification (G-7)		−40.0		3
23 glass furnaces		3.2		process modification		−45.3		5
24 light-duty highway vehicle exhaust	439.0	427.0		inspection and maintenance (no-load idle test and repair)	−11.3	−9.4		6
				Group 2 Additional Mobile Source Control				
25 light-duty highway vehicle exhaust	439.0	427.0	2.8	entire fleet meets 0.7 g/mi NO_x and 0.41 g/mi THC objective; NH_3 emissions reach 0.0035 g/km; inspection and maintenance program continued	−84.8	−73.3	222	*b*, 7, 8
26 heavy-duty diesel highway vehicle exhaust	25.8	157.0	0.02	entire fleet meets objective of 10.7 g NO_x/BHP-h and 2.65 g/mi THC	−30.0	−25.9		*c*, 9
27 heavy-duty gasoline highway vehicle exhaust	18.6	35.7	(0.1)	entire fleet meets objective of 10.7 g NO_x/BHP-h and 2.65 g/mi THC	−49.2	−34.8	0	*d*, 9
28 medium-duty highway vehicle exhaust (gasoline and diesel)	32.6	38.7	(0.3)	entire fleet meets 1.5 g/mi NO_x and 0.6 g/mi THC objective (NH_3 emissions reach 0.035 g/km)	−82.0	−62.1	(+83)	*e*, 8, 9
				Group 3 Stringent Mobile Source Control				
29 light-duty highway vehicle exhaust	439.0	427.0	2.8	entire fleet meets objective of 0.40 g/mi NO_x and 0.41 g/mi THC (NH_3 emissions held at 0.035 g/km)	−84.8	−84.8	+222	*f*, 7, 8
30 heavy-duty diesel highway vehicle exhaust	25.8	157.0	0.02	entire fleet meets objective of 5.1 g NO_x/BHP-h and 2.65 g/mi THC	−30.0	−65	0	*f*, 9
31 heavy-duty gasoline highway vehicle exhaust	18.6	35.7	(0.1)	entire fleet meets objective of 5.1 g NO_x/BHP-h and 2.65 g/mi THC	−49.2	−69	0	*f*, 9
				Group 4 Stationary Source NO_x Control–Noncatalytic NH_3 Injection				
32 refinery boilers and heaters		40.3	(0.5)	direct NH_3 injection		−50	+869	*g*, 4
33 utility boilers		57.6	(1.6)	direct NH_3 injection		−40	+344	*h*, 10

Table 4.1 (continued)

		1982 THC[a] emissns, ton/day	1982 NO_x emissns, ton/day	1982 NH_3 emissns, ton/day[n]	control measure	THC change, %[m]	effect of controls NO_x change, %[m]	NH_3 change, %[m,n]	ref
34	nonrefinery industrial boilers		35.0	(0.65)	direct NH_3 injection + combustion modification		−55	+392	*i*, 10
35	cement kilns			9.7	direct NH_3 injection		−50	+	11
36	glass melting furnaces			3.2	direct NH_3 injection		−50	+	5
	Group 5 Stationary Source NO_x Control–Selective Catalytic Reduction								
37	refinery boilers and heaters		40.3	(0.5)	selective catalytic reduction		−44	+small	*j*, 12
38	utility boilers		57.6	(1.6)	selective catalytic reduction		−90	+small	*k*, 13
39	nonrefinery industrial boilers		35.0	(0.65)	SCR plus combustion modification		−92	+small	*l*, 13
40	cement kilns			9.7	selective catalytic reduction		−90	+small	11
41	stationary industrial IC engines			74.2	use of catalytic converters		−66.7	+small	14
42	glass melting furnaces		3.2		selective catalytic reduction		−90.0	+small	5

[a] THC equals total hydrocarbon emissions; in all cases except landfill gas leak reduction and oil and gas well leak reduction, THC ≃ RHC (reactive hydrocarbon emissions). Landfill emissions are mostly methane, with only 1.4% non-methane hydrocarbons. Only the non-methane hydrocarbon (NMHC) data are used by the air quality model, and the percent of control shown applies to the NMHC content of the emissions only. [b] Computed by multiplying vehicle miles traveled (VMT) per day × 0.7 g/mi NO_x and 0.41 g/mi THC. NH_3 emissions become 9.14 metric tons/day. [c] Computed by taking emissions from a new (undeteriorated) 1984 heavy diesel truck as representing 6.5 g/BHP-h NO_x and also as equaling 10.31 g/mi NO_x. Ratio gives scale factor of 1.59 g mi^{-1}/(g/BHP-h) NO_x. If entire fleet achieves 10.7 g/BHP-h NO_x (representing a fleet average of 1984 trucks with deterioration) then emissions factor for entire fleet would be 17.0 g/mi. Emissions computed by multiplying VMT for heavy diesel vehicles × 17.0 g/mi. Hydrocarbon emissions obtained by multiplying 2.65 g/mi × heavy diesel vehicle VMT. [d] A new 1984 heavy gasoline truck emits 4.25 g/mi NO_x corresponding to 6.94 g/BHP-h. Calculation proceeds as in *c* above. [e] Computed by multiplying medium truck VMT per day × 1.5 g/mi NO_x and 0.6 g/mi THC. NH_3 emissions become 0.55 metric tons/day. [f] Emission reductions computed by procedure analogous to that for group 2 Mobile Source Controls (see footnotes *b*, *c*, or *d*). [g] NH_3 breakthrough is assumed to be 50 ppm NH_3 for reduction of 75 ppm NO_x (50%). Final NH_3 emission is 5.04 metric tons/day. [h] NH_3 breakthrough is 50 ppm NH_3 giving total NH_3 emissions of 7.1 metric tons/day. [i] Estimated based on utility boiler performance, see *h* and ref 10. [j] SCR achieves 90% NO_x control but is applied only to the largest units, yielding 44% reduction relative to the entire source class. [k] Ammonia bleed-through is 12 ppm. [l] 25% control by combustion modification plus 90% control via SCR, see *k* and also control measure 21 in Table I above. Rule-making process would probably choose to exclude smaller boilers, but no indication is yet given of where the line would be drawn. NH_3 break-through assumed to be 12 ppm. [m] Percent change in emissions is defined as follows: −84% implies that (1 − 84/100) = 0.16 × original 1982 emission rate remains after control; +222% implies that (1 + 222/100) = 3.22 × original 1982 emission rate remains after control. [n] NH_3 emission values in parentheses estimated from data of ref 8.

References for Table 4.1 can be found in Appendix B.

from stationary sources through the use of non-catalytic ammonia injection or selective catalytic reduction (SCR) technology.

The 1982 emission inventory employed during the model verification effort of Chapter 3 of this study will be referred to as the Base Case. The 1982 Base Case emissions from each source class that will be considered for control are given in Table 4.1, along with the percentage reduction in those emissions that would result if the control measures had been in effect during 1982 (i.e. 84% reduction implies that (1-84/100)=0.16 times the Base Case emissions from a stated source class would remain if the stated control measure had been implemented). Although several of the control measures cited are cross- referenced to the 1982 AQMP planning document, the base year emission inventory of the present study (1982) differs from the 1979, forecast 1977 and forecast year 2000 inventories used in the 1982 AQMP. The objective of the present study is to provide information on the air quality effects that would be observed if the controls listed in Table 4.1 had been applied during the 1982 Base Case model verification days in the amounts specified. No attempt will be made to simulate the effect of emission controls during some hypothetical future year.

The largest number of control measures in Group 1 of Table 4.1 (those designated B-1 through B-8) are aimed at reducing solvent vapor emissions from painting and surface coating operations, usually through reformulation of the coating material or through reduced overspray during application. Reduction in fugitive hydrocarbon emissions from landfill gas leaks and oil and gas field fixture leaks is anticipated. The remaining hydrocarbon controls would suppress solvent losses from cleaning operations and pesticide application, or capture certain industrial process emissions using incineration, activated carbon adsorption or other vapor recovery methods.

Stationary source oxides of nitrogen controls included in Group 1 involve relatively straightforward modification of combustion system design, but without the use of ammonia injection or selective catalytic reduction technology. The effect of a mandatory vehicle inspection and maintenance program involving a no-load idle test, followed by repairs to the vehicle designed to correct defects observed also is included among the relatively simple control measures in Group 1.

Two further levels of mobile source NO_x control were considered. At the Group 2 level in Table 4.1, the entire light duty vehicle fleet was assumed to have achieved a

NO_x emission rate of 0.7g mi^{-1}, and the NO_x emissions from heavy duty trucks were assumed to be reduced to 10.7 g/BHP-hr. There are two ways that one could view this case with 0.7 g $mi^{-1}NO_x$ emitted from the light duty vehicle fleet. Until very recently, new cars sold in California were required to meet a 0.7 g $mi^{-1}NO_x$ standard. This level of control could be used to approximate a successful completion of conversion of the entire vehicle fleet to meet such a regulatory objective for new cars, in combination with a high level of catalyst system durability and maintenance. In the absence of high durability and maintenance, catalyst system deterioration can be expected to increase actual on-road emissions to levels above legal objectives. The 0.7 g/mile NO_x fleet-wide emission rate employed here closely approximates the introduction of a fleet of cars initially set to achieve the current regulatory requirement of 0.4 g/mi NO_x when new, followed by a typical degree of control system deterioration in the hands of the final consumer. The 10.7 g/BHP-hr. NO_x objective for heavy duty trucks reflects an intermediate level of control proposed by the U.S. Environmental Protection Agency (1984).

Mobile source controls shown in Group 3 reflect the emissions pattern that would result if the 0.4 g/mi NO_x and 0.41 g/mi total hydrocarbon (THC) emission rate for light duty vehicles called for under the Clean Air Act in fact were achieved and maintained by the vehicle fleet. Increased control system durability or maintenance would be needed for this event to occur. Further NO_x reductions from heavy duty vehicles have been added to Group 3, at the most stringent level discussed by the federal government (Environmental Protection Agency, 1984).

NO_x emission reductions from stationary combustion sources can be achieved by non-catalytic ammonia injection into the stack exhaust within a narrow exhaust temperature range. This direct NH_3 injection technology has been demonstrated on a utility boiler in the Los Angeles area (Dziegiel et. al. 1982). NO_x emission reductions in the vicinity of 50% are observed, accompanied by significant bleed-through of NH_3 into the atmosphere. Group 4 controls in Table 4.1 simulate the installation of such controls on all of the largest stationary combustion sources in the South Coast Air Basin.

Selective catalytic reduction (SCR) technology involves NO_x abatement by injection of NH_3 into stationary source exhaust in the presence of a catalyst. Control

efficiencies are generally higher than in the case of the direct non-catalytic NH_3 injection systems cited in control Group 4, and NH_3 bleed-through into the atmosphere is reduced. The effect of SCR technology applied to a variety of stationary sources in the Los Angeles area is indicated in Group 5 of Table 4.1.

By applying the controls in Table 4.1 in various combinations, a matrix of control opportunities can be constructed that represents the trade-off between increasingly stringent stationary source control vs. increasingly stringent mobile source control, as shown in Table 4.2. Nine cases will be defined. Beginning near the upper left corner of Table 4.2, the Base Case 1982 emission inventory first will be perturbed by applying the Group 1 controls from Table 4.1 to the emissions sources. Moving from left to right across the top of the table, increasingly stringent mobile source controls are added to the Group 1 stationary source controls. Moving from top to bottom along the left edge of the table, increasingly demanding stationary source NO_x controls are added to a minimal motor vehicle control program. At the lower right corner of that table, the intersection of all of the most stringent mobile and stationary source controls is applied. The headings aligned with the columns and rows of Table 4.2 suggest the maximum cumulative degree of NO_x control achieved in each case; the hydrocarbon controls shown in Table 4.1 also are included.

4.3 THE EFFECT OF EMISSION CONTROLS

The grid-based air quality model evaluated in Chapter 3 of this study was used to determine the effects on the dry deposition flux that could be expected if each of the combinations of emission control measures defined in Table 4.2 were applied in the South Coast Air Basin (SoCAB). For each set of control measures considered, the Base Case 1982 emission inventory for the SoCAB as presented in Tables 3.1 and 3.2 was modified to reflect the addition of that particular group of control measures. Then the air quality modeling calculations were executed over two days of simulation using the modified emission inventory along with the meteorological conditions observed during the Base Case model verification days (August 30-31, 1982).

The initial conditions and boundary conditions supplied to the air quality model in each case were identical to those observed during August 30-31, 1982, as described by Russell et. al. (1988a). The purpose of the first day of each two-day simulation

Table 4.2

Combinations of Mobile and Stationary Source Controls That Will Be Examined for Their Effect on Air Quality in the South Coast Air Basin[a]

BASE CASE 1982 EMISSIONS (tons/day) THC = 2416 RHC = 1224 NO_x = 1120 NH_3 = 164	MOBILE SOURCE CONTROLS VEHICLE INSPECTION AND MAINTENANCE	LIGHT DUTY FLEET 0.41 g/mi THC; 0.7g/mi NO_x HEAVY DUTY FLEET 2.65g/mi THC 10.7g/bhp-hr NO_x	LIGHT DUTY FLEET 0.41g/mi THC; 0.4g/mi NO_x HEAVY DUTY FLEET 2.65g/mi THC 5.1 g/bhp-hr NO_x
STATIONARY SOURCE CONTROLS AQMP EVAPORATIVE CONTROLS & COMBUSTION MODIFICATION	CONTROL MEASURES: 1-24 EFFECT ON EMISSIONS: RHC -9.3% NO_x -5.4% NH_3 NO CHANGE	CONTROL MEASURES: 1-28 EFFECT ON EMISSIONS: RHC -37.2% NO_x -36.6% NH_3 +3.9%	CONTROL MEASURES: 1-24,28-31 EFFECT ON EMISSIONS: RHC -37.2% NO_x -47.6% NH_3 +3.9%
AQMP + NON-CATALYTIC AMMONIA INJECTION	CONTROL MEASURES: 1-18,20,24,32-36 EFFECT ON EMISSIONS: RHC -9.3% NO_x -10.0% NH_3 +8.7%	CONTROL MEASURES: 1-18,20,24-28,32-36 EFFECT ON EMISSIONS: RHC -37.2% NO_x -41.2% NH_3 +12.7%	CONTROL MEASURES: 1-18,20,24,28-36 EFFECT ON EMISSIONS: RHC -37.2% NO_x -52.2% NH_3 +12.7%
AQMP + SELECTIVE CATALYTIC REDUCTION	CONTROL MEASURES: 1-18,20,24,37-42 EFFECT ON EMISSIONS: RHC -9.3% NO_x -18.4% NH_3 +0.7%	CONTROL MEASURES: 1-18,20,24-28,37-42 EFFECT ON EMISSIONS: RHC -37.2% NO_x -49.6% NH_3 +4.7%	CONTROL MEASURES: 1-18,20,24,28-31,37-42 EFFECT ON EMISSIONS: RHC -37.2% NO_x -60.6% NH_3 +4.7%

[a]Control measures refer to the control measures numbered in Table 4.1. Labels on columns and rows of this table are indicative of the maximum degree of NO_x control required.

was to establish initial conditions for the second day of calculations that reflect the altered emissions into the air basin. The effect of emission controls on dry deposition then was determined by comparison between Base Case and post-control deposition flux predictions for the second day of each two-day simulation. As changes in emission controls might affect the boundary conditions supplied to the model, a perturbation analysis of the effect of altered boundary conditions was conducted by Russell et. al. (1988b). Reducing the inflow O_3 boundary conditions from those observed on August 30-31, 1982, to 0.04 ppm all around the border of the modeling region reduced Base Case peak O_3 concentrations by only 0.01 ppm. Inflow NO_x boundary conditions on August 30-31, 1982, were examined and found to be very low except along a small stretch of the southeast corner of the grid system. In summary, predicted changes in deposition flux on the second day of simulation are determined predominantly by changes in emissions into the model and not by altered initial or boundary conditions.

The effect of emission controls now can be examined. The upper left-hand corner of Table 4. 2. shows that completion of the vehicle inspection and maintenance program plus evaporative hydrocarbon controls and combustion modifications would lower reactive hydrocarbon emissions by 9.3% and would lower NO_x emissions by 5.4%. In response to those controls, the dry flux of NO_x-derived species would decline by 2% to 7%, as shown in the upper left corner of Table 4.3. The ammonia flux would increase slightly. Less aerosol nitrate is formed while NH_3 emissions remain unchanged; thus, NH_3 concentrations will increase and so will the NH_3 dry flux. Table 4.4 shows the computed dry flux to the surface of the modeling region in that case. The dry flux in the presence of the Group 1 controls totals 242 metric tons/day of nitrogen, of which 170 metric tons/day N is derived from NO_x emissions.

Moving to the right across the top row of Tables 4.3 and 4.4, the effect of progressively more stringent controls on motor vehicles is seen in the presence of a minimal stationary source control program. In response to a 37% reduction in both reactive hydrocarbon emissions and NO_x emissions (top row, center column), dry fluxes of NO and NO_2 decline by amounts that are slightly greater than proportional to the gross emissions change (-42% and -39%, respectively). HNO_3 and NH_4NO_3 fluxes decline by 28% to 30%. The NH_3 flux increases as NH_4NO_3 formation in the atmosphere is suppressed due to the lower atmospheric HNO_3 concentrations.

Table 4.3

CHANGE IN FLUX TO SURFACE OF MODELING REGION
(PERCENT)

BASE CASE	VEHICLE INSPECTION AND MAINTENANCE	VEHICLE FLEET MEETS: 0.7 g/mi LIGHT DUTY 10.7 g/bhp-hr HEAVY DUTY	VEHICLE FLEET MEETS: 0.4 g/mi LIGHT DUTY 5.1 g/bhp-hr HEAVY DUTY
COMBUSTION MODIFICATION	NO -7% NO_2 -5% PAN -2% HNO_3 -3% NH_3 +2% NH_4NO_3 -4%	NO -42% NO_2 -39% PAN -11% HNO_3 -28% NH_3 +17% NH_4NO_3 -30%	NO -54% NO_2 -51% PAN -9% HNO_3 -36% NH_3 +22% NH_4NO_3 -43%
THERMAL DE NO_x ™	NO -11% NO_2 -7% PAN -1% HNO_3 -7% NH_3 +7% NH_4NO_3 -1%	NO -46% NO_2 -41% PAN -11% HNO_3 -32% NH_3 +23% NH_4NO_3 -29%	NO -58% NO_2 -55% PAN -9% HNO_3 -39% NH_3 +28% NH_4NO_3 -43%
SELECTIVE CATALYTIC REDUCTION	NO -26% NO_2 -14% PAN +2% HNO_3 -10% NH_3 +6% NH_4NO_3 -11%	NO -58% NO_2 -47% PAN -9% HNO_3 -35% NH_3 +22% NH_4NO_3 -40%	NO -69% NO_2 -59% PAN -9% HNO_3 -43% NH_3 +27% NH_4NO_3 -53%

SUBURBAN IV

Table 4.4

CALCULATED FLUX TO SURFACE OF MODELING REGION
AUGUST 31, 1982
(METRIC TONS N/DAY)

BASE CASE	VEHICLE INSPECTION AND MAINTENANCE	VEHICLE FLEET MEETS: 0.7 g/mi LIGHT DUTY 10.7 g/bhp-hr HEAVY DUTY	VEHICLE FLEET MEETS: 0.4 g/mi LIGHT DUTY 5.1 g/bhp-hr HEAVY DUTY
COMBUSTION MODIFICATION	NO 5 NO_2 47 PAN 7 HNO_3 98 NH_3 60 NH_4NO_3 25	NO 3 NO_2 30 PAN 6 HNO_3 73 NH_3 69 NH_4NO_3 18	NO 2 NO_2 24 PAN 7 HNO_3 65 NH_3 72 NH_4NO_3 15
THERMAL DE NO_x ™	NO 4 NO_2 46 PAN 7 HNO_3 94 NH_3 63 NH_4NO_3 26	NO 3 NO_2 29 PAN 6 HNO_3 69 NH_3 72 NH_4NO_3 18	NO 2 NO_2 23 PAN 7 HNO_3 62 NH_3 75 NH_4NO_3 15
SELECTIVE CATALYTIC REDUCTION	NO 4 NO_2 42 PAN 7 HNO_3 91 NH_3 62 NH_4NO_3 23	NO 2 NO_2 26 PAN 7 HNO_3 66 NH_3 72 NH_4NO_3 16	NO 2 NO_2 20 PAN 7 HNO_3 58 NH_3 75 NH_4NO_3 12

SUBURBAN IV

With a further decrease in NO_x emissions from motor vehicles (far right column of Table 4.2), basinwide NO_x emissions would be reduced by close to 48%. As seen in Tables 4.3–4.4, the dry fluxes of NO and NO_2 would decline by more than 50%, while the HNO_3 dry flux declines by 36% relative to the base case.

Moving down the left-hand column of Tables 4.2–4.4, the effect of progressively more stringent NO_x controls on the stationary sources is examined. With highly effective selective catalytic reduction (SCR) systems applied to the largest stationary NO_x sources plus evaporative hydrocarbon controls and a minimal motor vehicle control program, NO_x emissions would decline by 18.4% and reactive hydrocarbon emissions would decline by 9.3%. The results of such a control program would include a 26% decline in the NO dry flux, a 14% decline in the NO_2 dry flux and a 10%–11% decline in the dry flux of HNO_3 and NH_4NO_3.

If the most stringent combination of stationary source controls and mobile source controls studied here is applied, then NO_x emissions would decline by more than 60%, accompanied by a 37% reduction in reactive hydrocarbon emissions. The effect of this maximum control case is shown in the box in the lower right-hand corner of Tables 4.3 and 4.4. The total flux of nitrogen- containing species in that case is predicted to decline from 247 metric tons/day N in the Base Case to 174 tons/day of nitrogen in the Maximum Control Case studied. Of that total, 87 tons/day of nitrogen is derived from acid gases plus PAN and 75 tons/day of nitrogen is dry deposited as NH_3. The remaining 12 tons/day of nitrogen is deposited as ammonium nitrate. Although the balance between deposited NH_3 and acid gases is nearly equal in this case, the reader is cautioned to remember that the spatial distribution of the dry flux of these species is different, with the NH_3 dry flux occurring predominantly in the high NH_3 concentration areas of the eastern portion of the air basin. The temporal character of the change in the dry deposition flux in the presence of the maximum level of control studied is shown in Figures 4.1–4.5. Dry flux reductions in response to emission controls are largest in an absolute sense in the middle of the day when the deposition velocities are at their highest values. The spatial distribution of the dry flux values is given in Figures 4.6–4.12 during the high flux afternoon hours of August 31, and can be compared to the pre-control case that was pictured in Figures 3.58–3.64.

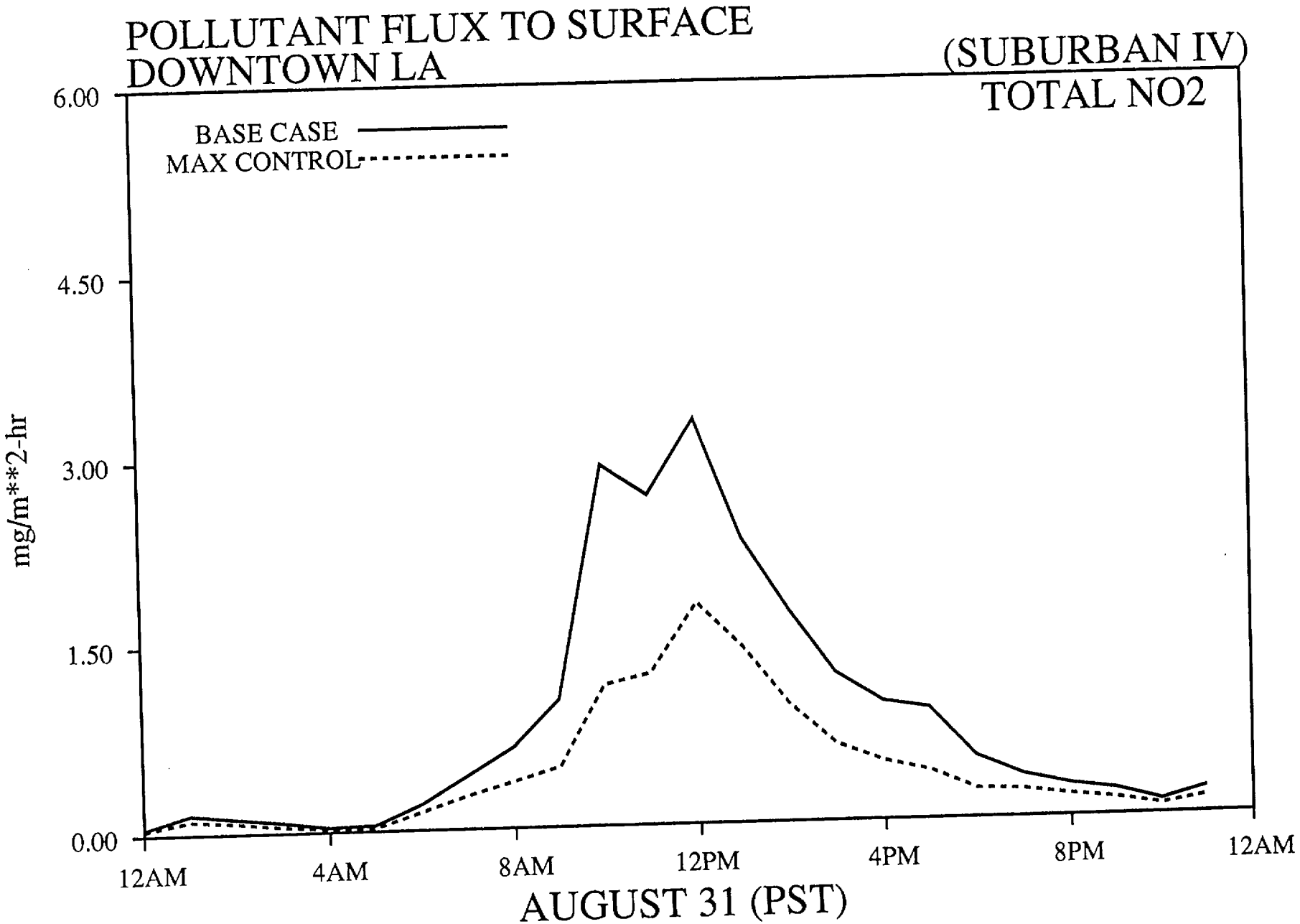
POLLUTANT FLUX TO SURFACE
DOWNTOWN LA
(SUBURBAN IV)
TOTAL NO2
BASE CASE
MAX CONTROL
6.00
4.50
3.00
1.50
0.00
mg/m**2-hr
12AM
4AM
8AM
12PM
4PM
8PM
12AM
AUGUST 31 (PST)

Figure 4.1

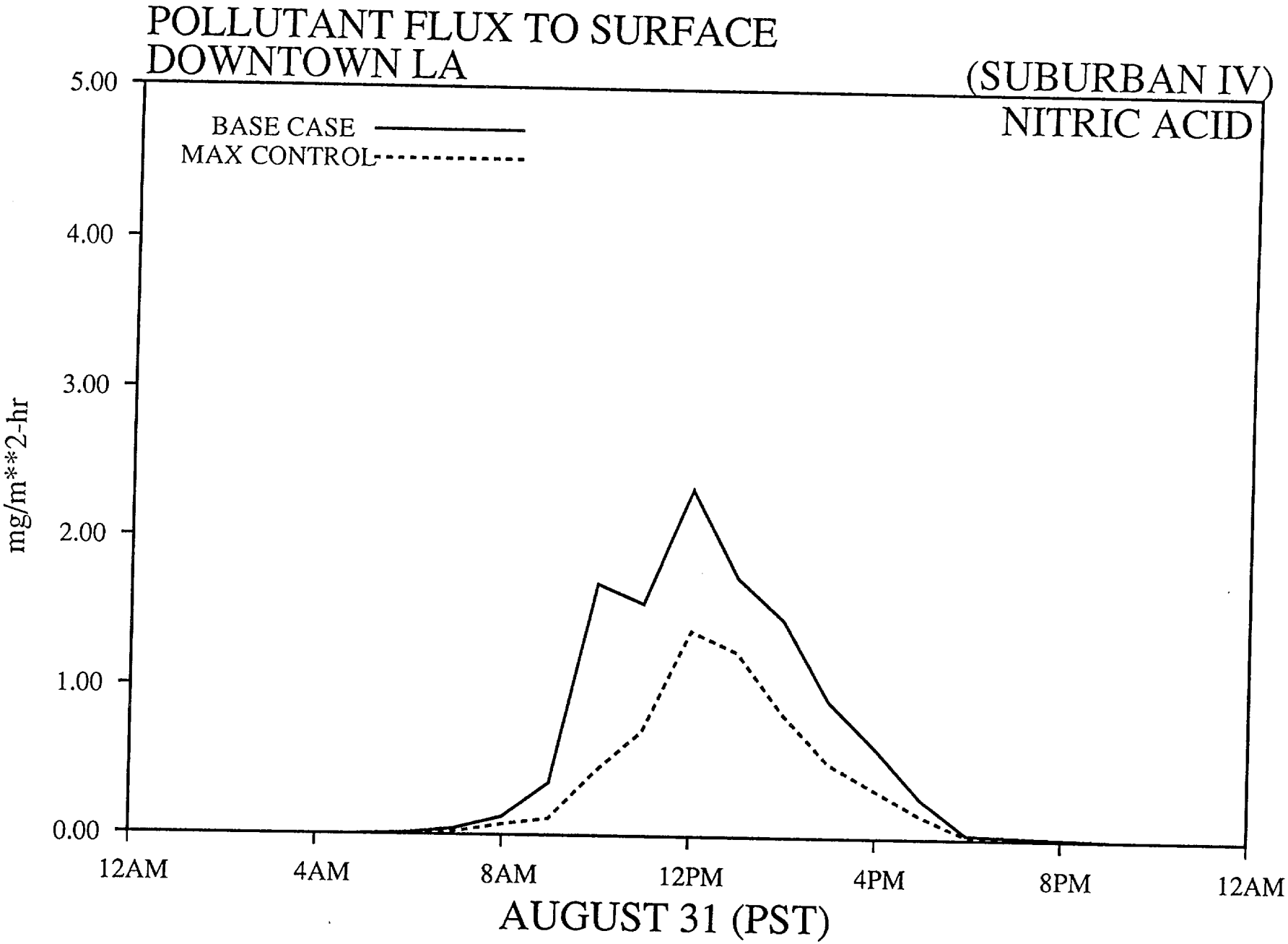
POLLUTANT FLUX TO SURFACE
DOWNTOWN LA
(SUBURBAN IV)
NITRIC ACID
BASE CASE
MAX CONTROL
5.00
4.00
3.00
2.00
1.00
0.00
mg/m**2-hr
121
12AM
4AM
8AM
12PM
4PM
8PM
12AM
AUGUST 31 (PST)

Figure 4.2

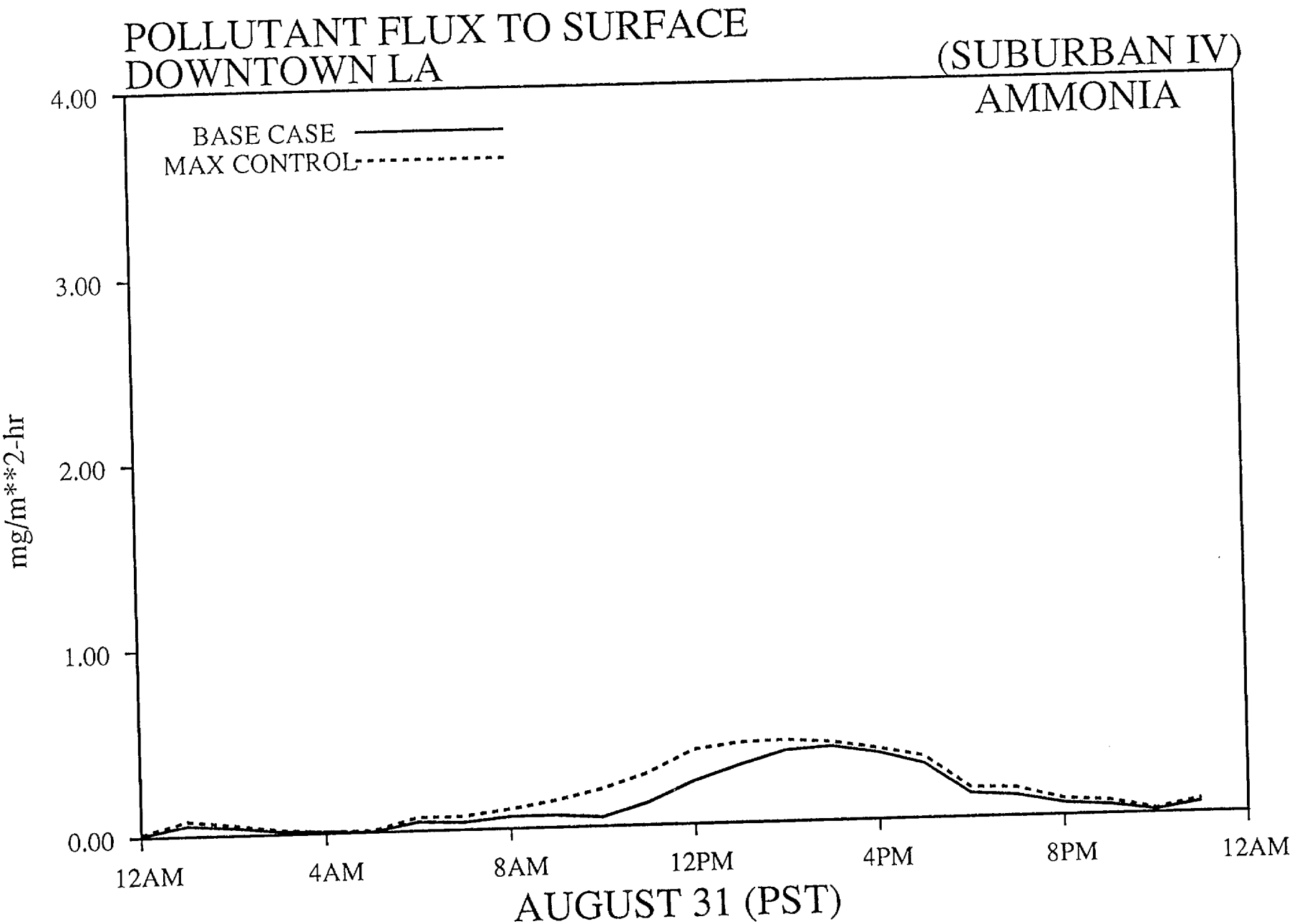
POLLUTANT FLUX TO SURFACE
DOWNTOWN LA
(SUBURBAN IV)
AMMONIA
BASE CASE
MAX CONTROL
4.00
3.00
2.00
1.00
0.00
mg/m**2-hr
12
12AM
4AM
8AM
12PM
4PM
8PM
12AM
AUGUST 31 (PST)

Figure 4.3

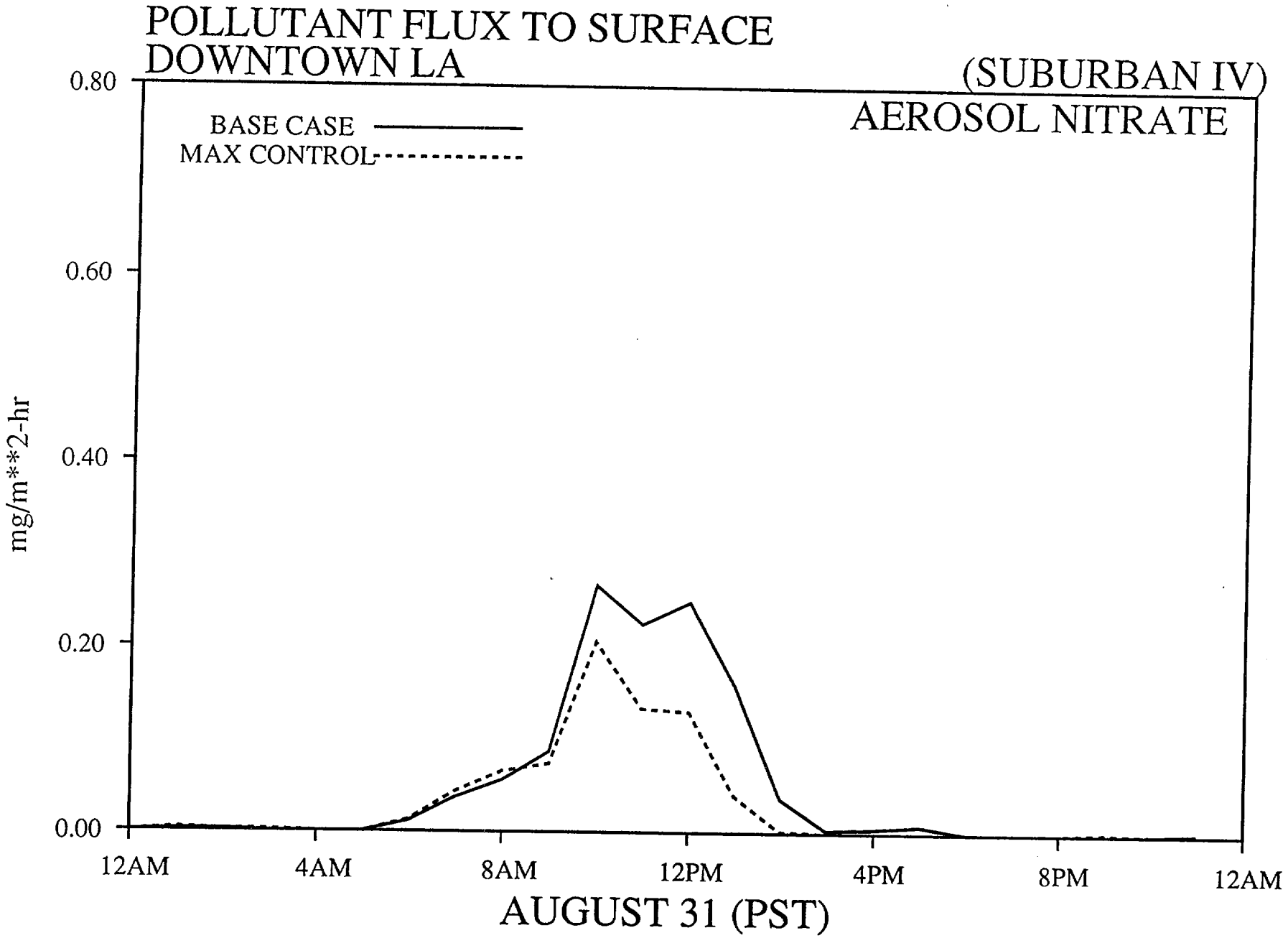
POLLUTANT FLUX TO SURFACE
DOWNTOWN LA
(SUBURBAN IV)
AEROSOL NITRATE
BASE CASE
MAX CONTROL
0.80
0.60
0.40
0.20
0.00
mg/m**2-hr
123
12AM
4AM
8AM
12PM
4PM
8PM
12AM
AUGUST 31 (PST)

Figure 4.4

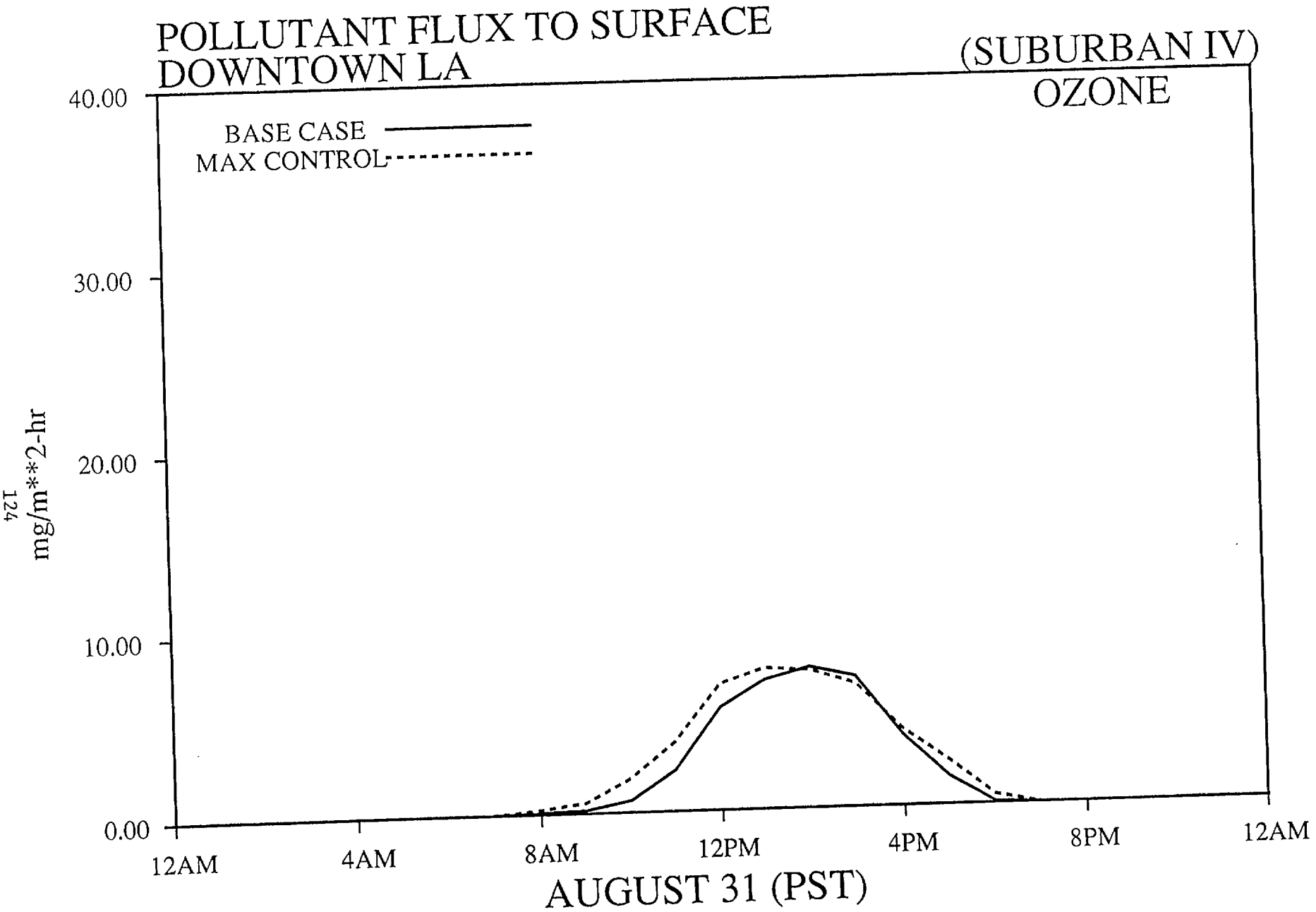
POLLUTANT FLUX TO SURFACE
DOWNTOWN LA
(SUBURBAN IV)
OZONE
BASE CASE
MAX CONTROL
40.00
30.00
20.00
10.00
0.00
mg/m**2-hr
12AM
4AM
8AM
12PM
4PM
8PM
12AM
AUGUST 31 (PST)

Figure 4.5

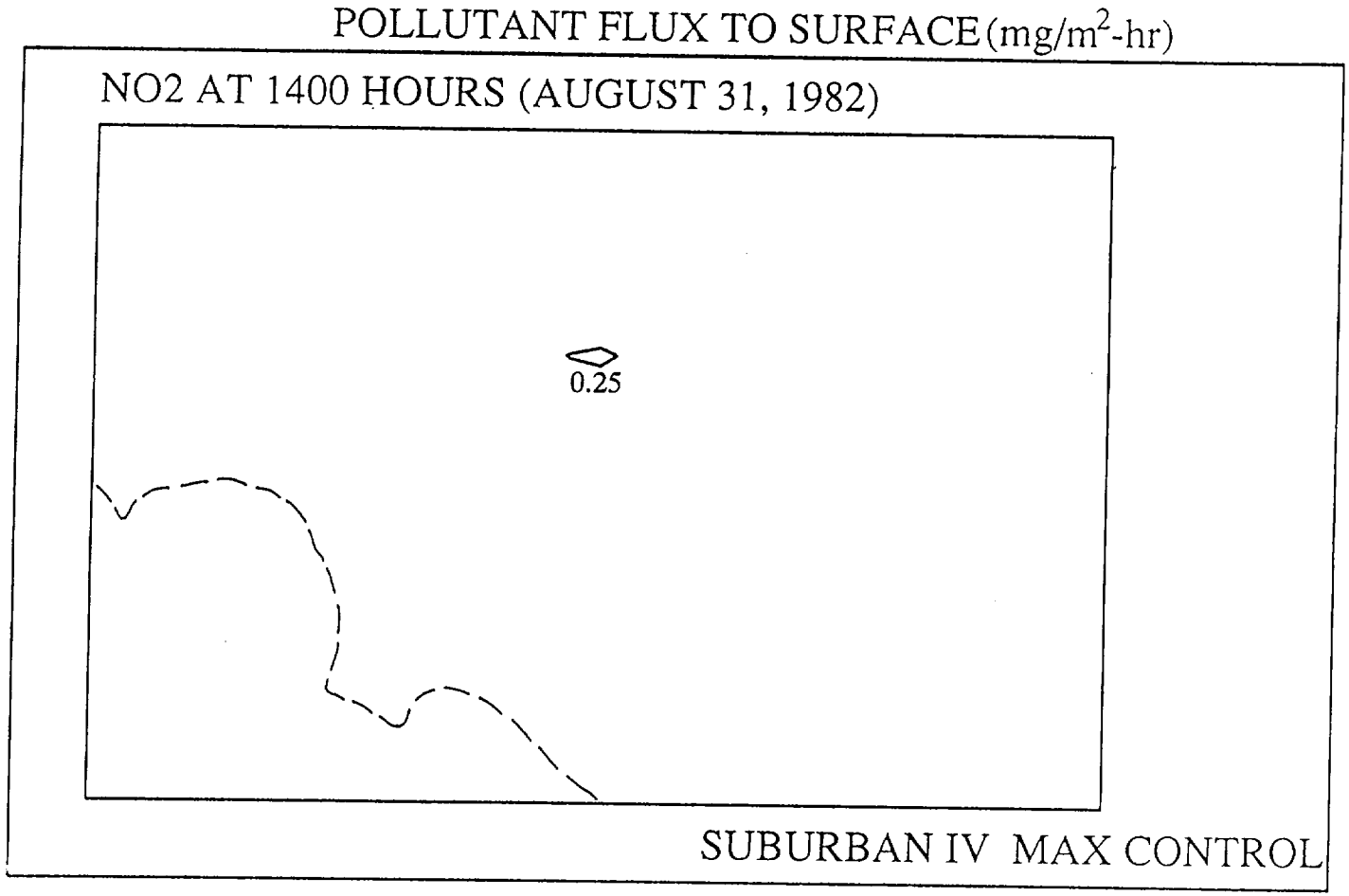
POLLUTANT FLUX TO SURFACE (mg/m2-hr)
NO2 AT 1400 HOURS (AUGUST 31, 1982)
0.25
SUBURBAN IV MAX CONTROL

Figure 4.6

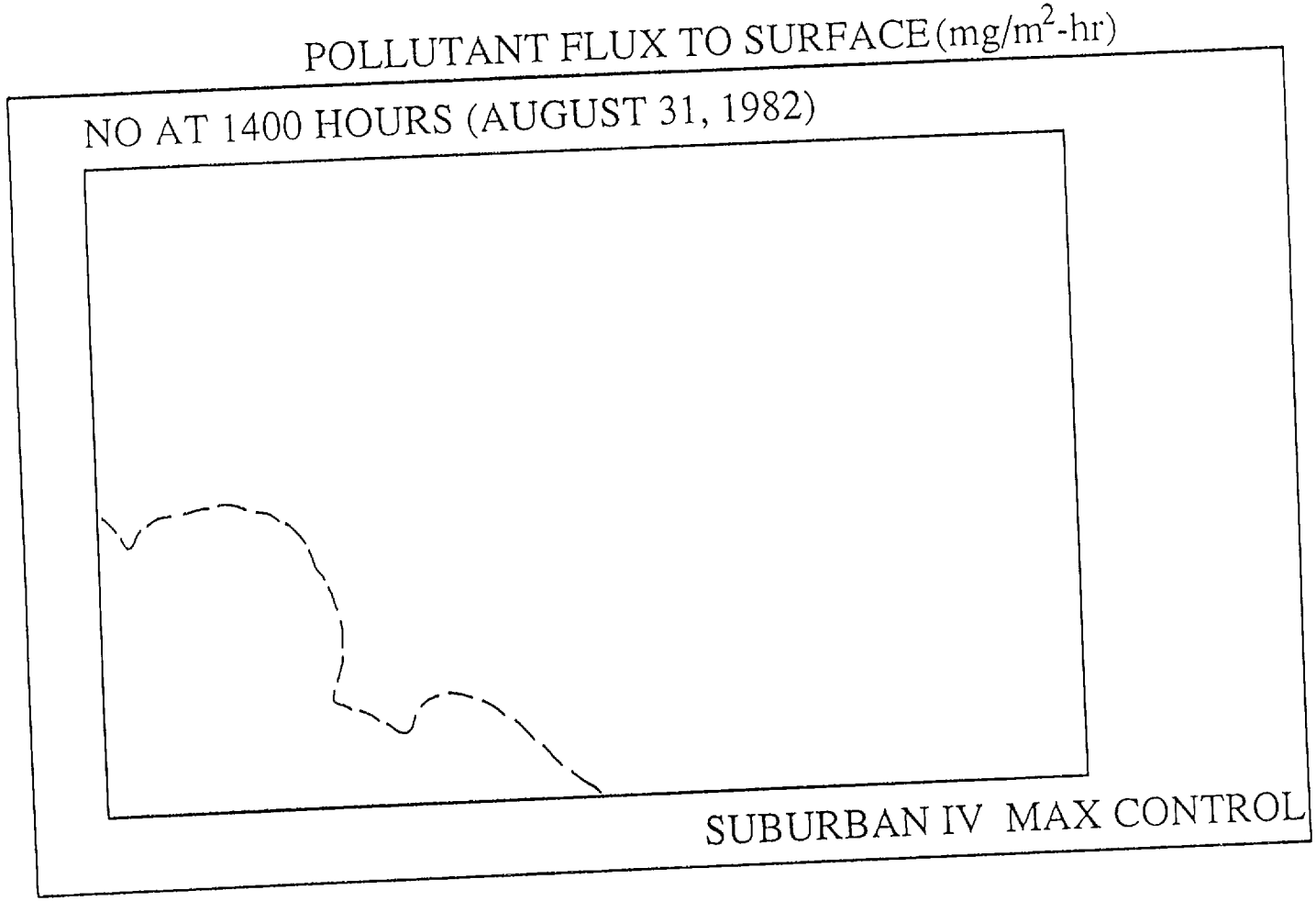
POLLUTANT FLUX TO SURFACE (mg/m2-hr)
NO AT 1400 HOURS (AUGUST 31, 1982)
SUBURBAN IV MAX CONTROL

Figure 4.7

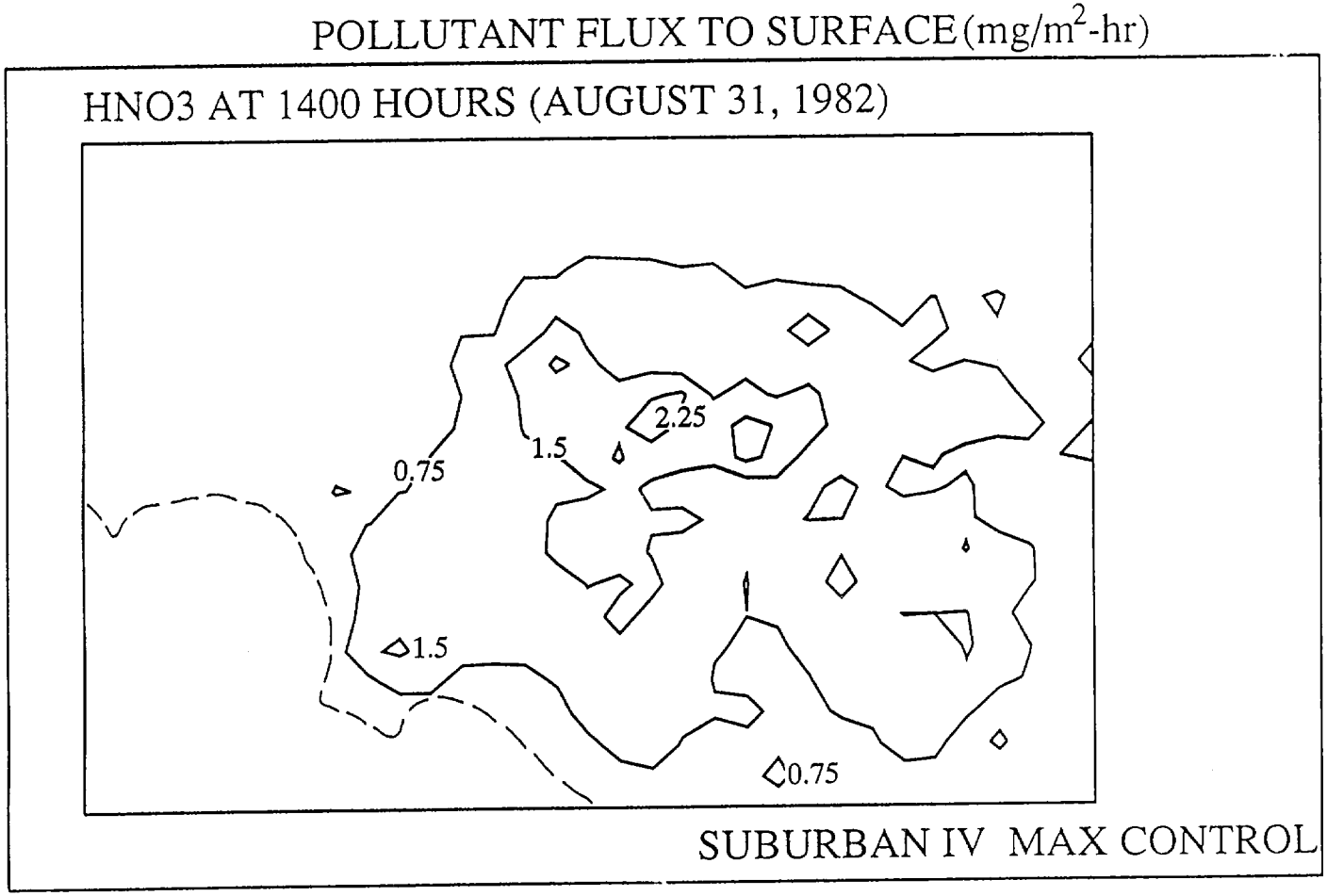
POLLUTANT FLUX TO SURFACE (mg/m2-hr)
HNO3 AT 1400 HOURS (AUGUST 31, 1982)
2.25
1.5
0.75
1.5
0.75
SUBURBAN IV MAX CONTROL

Figure 4.8

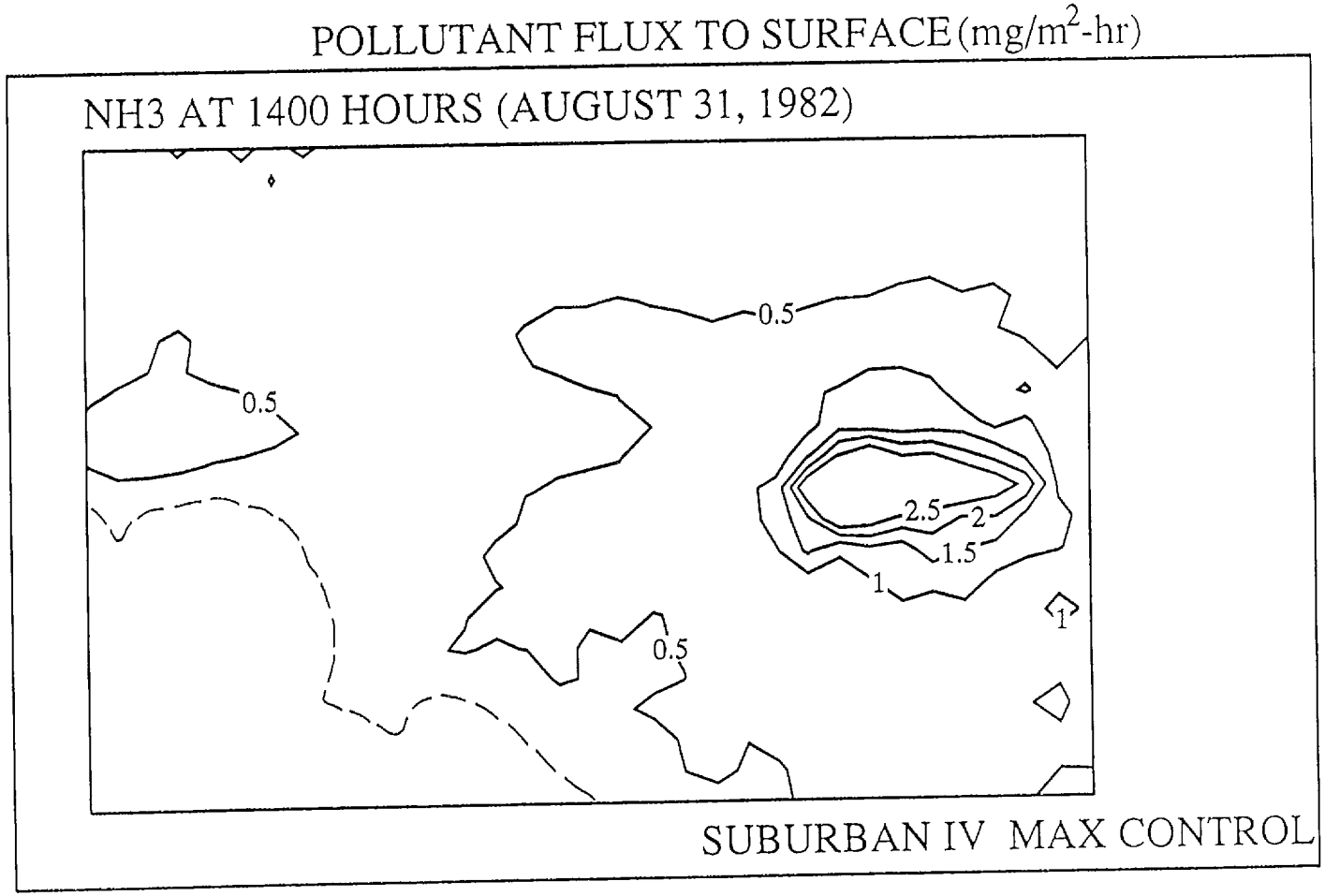
POLLUTANT FLUX TO SURFACE (mg/m2-hr)
NH3 AT 1400 HOURS (AUGUST 31, 1982)
0.5
0.5
2.5
2
1.5
1
1
0.5
SUBURBAN IV MAX CONTROL

Figure 4.9

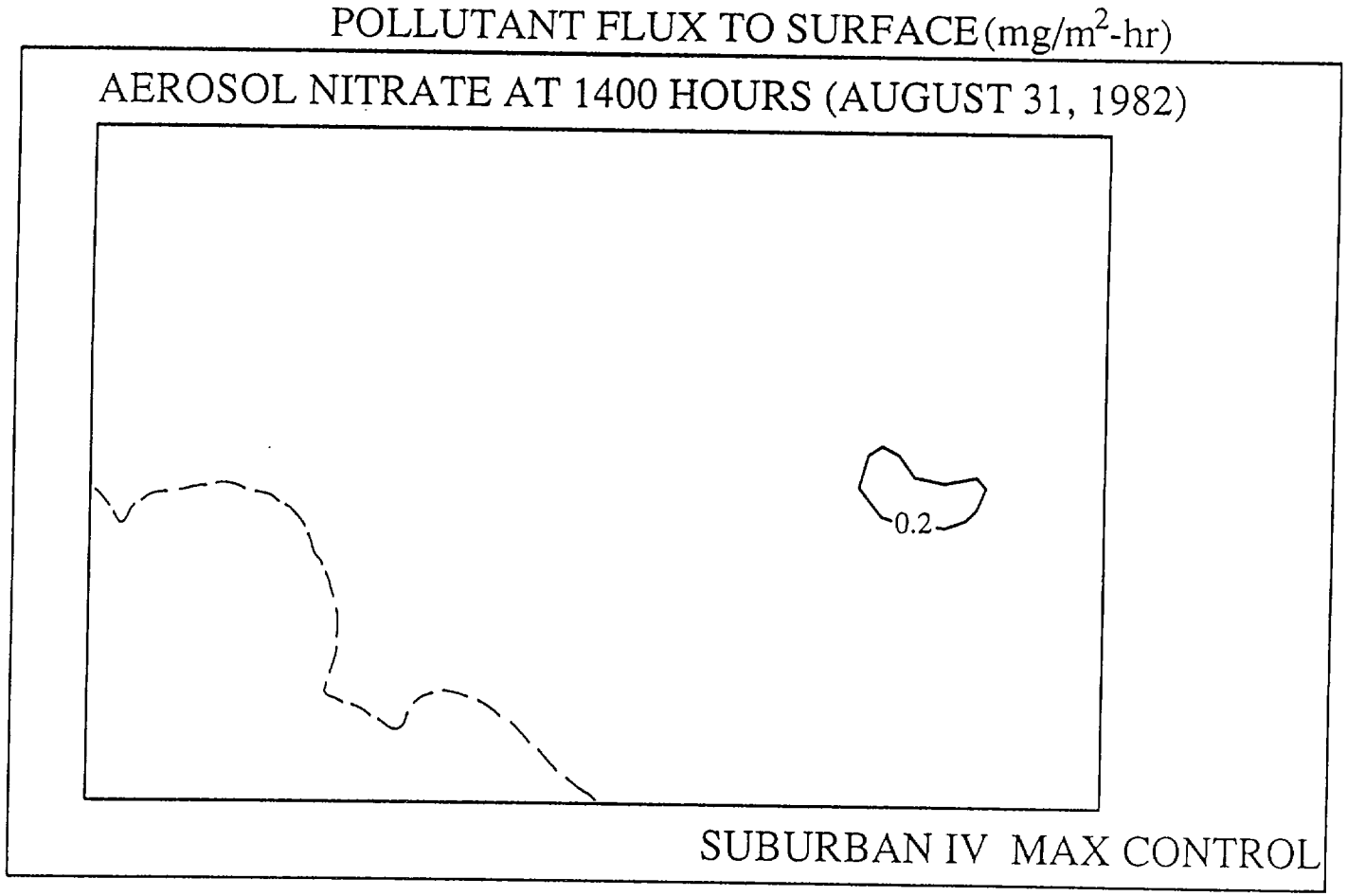
POLLUTANT FLUX TO SURFACE (mg/m2-hr)
AEROSOL NITRATE AT 1400 HOURS (AUGUST 31, 1982)
0.2
SUBURBAN IV MAX CONTROL

Figure 4.10

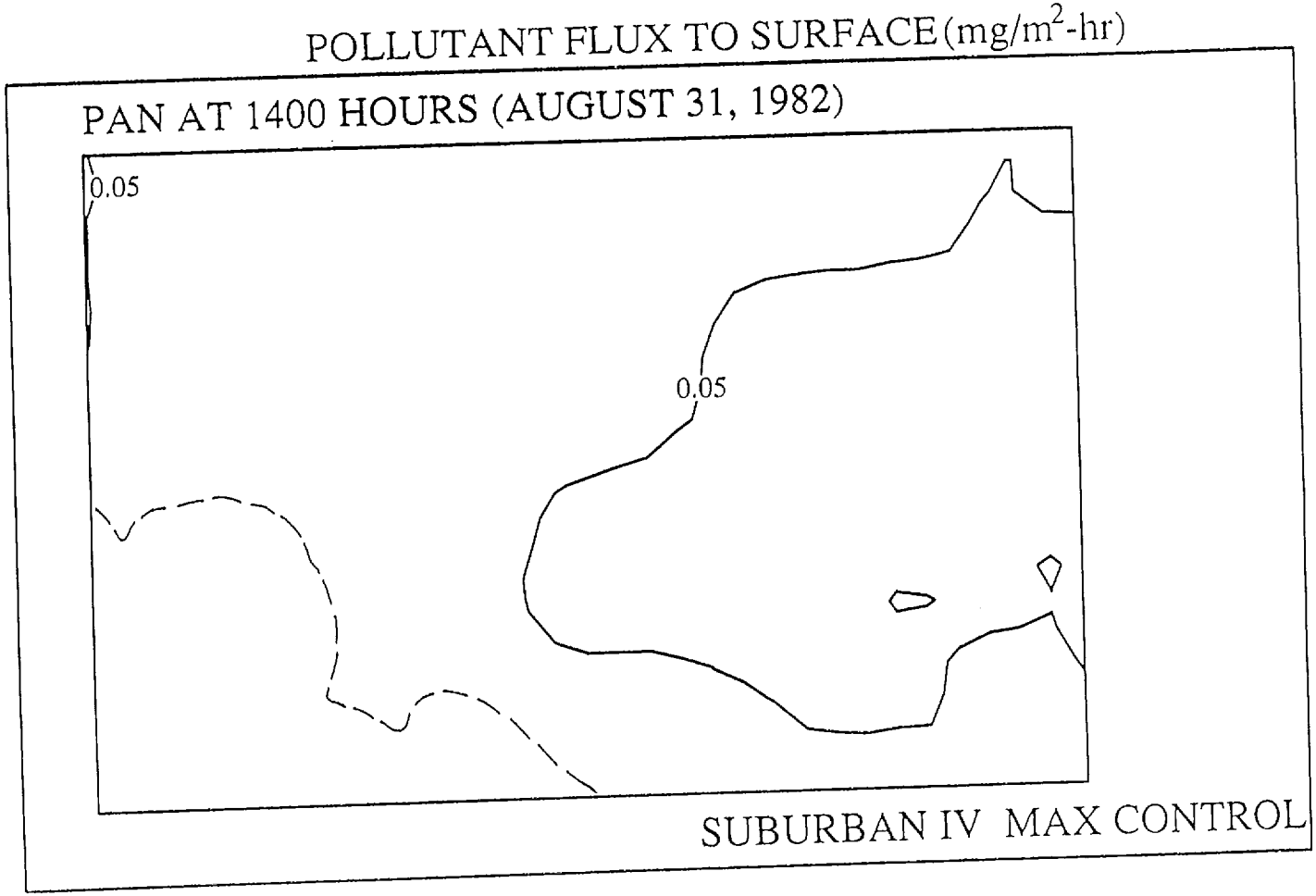
POLLUTANT FLUX TO SURFACE (mg/m2-hr)
PAN AT 1400 HOURS (AUGUST 31, 1982)
0.05
0.05
SUBURBAN IV MAX CONTROL

Figure 4.11

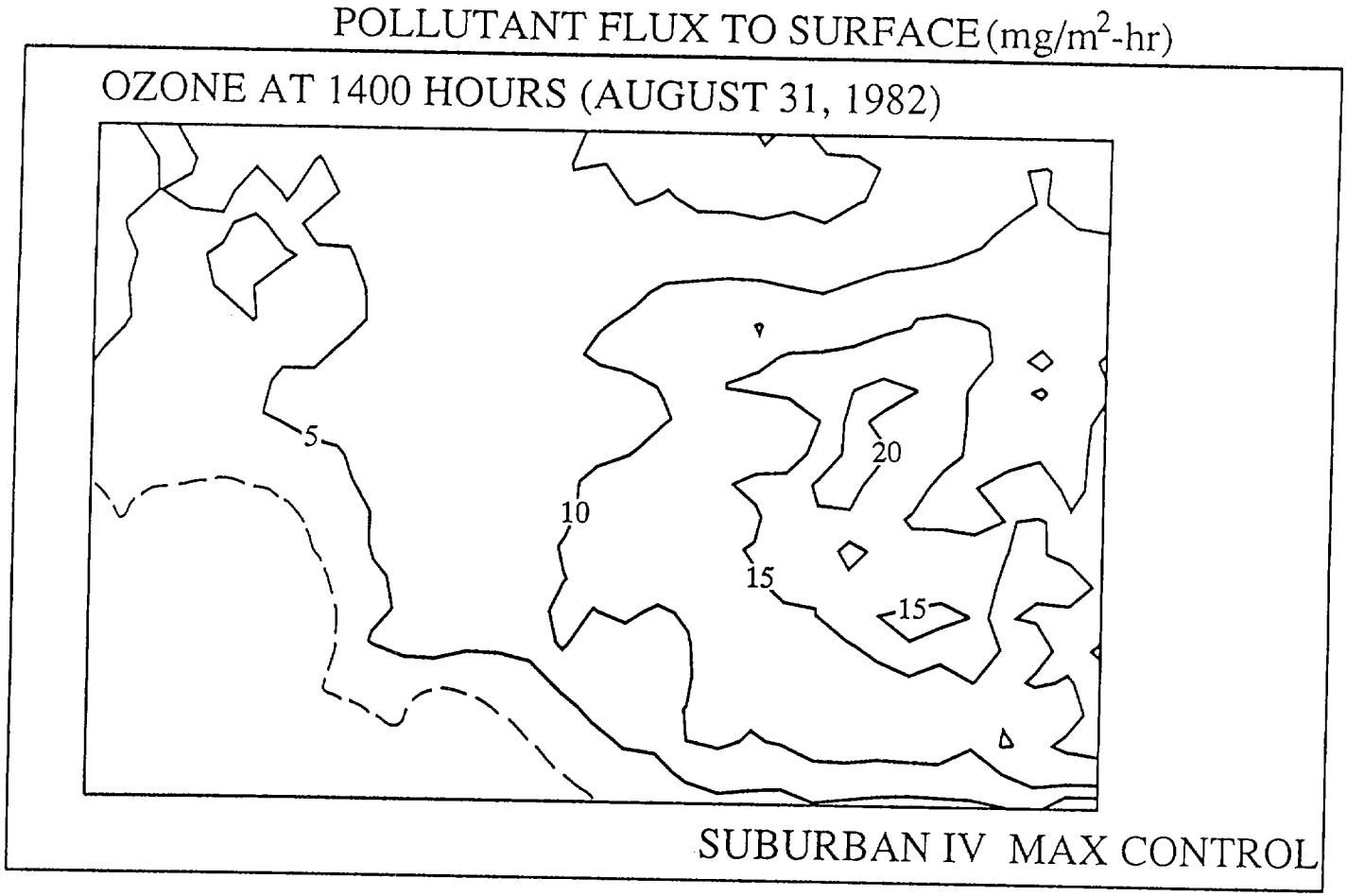
POLLUTANT FLUX TO SURFACE (mg/m2-hr)
OZONE AT 1400 HOURS (AUGUST 31, 1982)
5
10
15
20
15
SUBURBAN IV MAX CONTROL

Figure 4.12

Chapter 5

Conclusions

The approximately 1000 tons of nitrogen oxides emitted per day to the atmosphere of the South Coast Air Basin are converted by chemical reactions into an entire family of nitrogen-containing pollutants, including NO_2, HNO_3, PAN and aerosol nitrates. Eventually, these pollutants are removed by wet or dry deposition at the earth's surface. The dry deposition flux of nitrogen-containing pollutants to the surface of the modeling region was calculated for 1982 base case conditions. NO_x emissions accounted for 175.5 tons/day of the total 247.1 tons/day deposited nitrogen, while the remainder originated from ammonia emissions. That 175.5 tons/day of nitrogen would be equivalent to 577 metric tons/day of NO_x emissions if stated at the molecular weight of NO_2, which corresponds to more than half of the NO_x daily emissions to the air basin. Gas phase species deliver 90% of the nitrogen to the surface.

The revised dry deposition model was employed to examine the nature of the effects that would occur if emission controls were applied to the NO_x and hydrocarbon sources in the South Coast Air Basin as they existed in 1982. At the highest level of control studied (37% reactive hydrocarbon reduction, 61% NO_x reduction), the nitrogen dry flux would be reduced from 247 tons per day N in the pre-control Base Case to 174 tons/day N after control. Of that 174 tons/day N, 87 tons/day N would be derived from deposition of acid gases plus PAN, while 75 tons/day N would be deposited as NH_3. The remaining 12 tons/day N would be deposited as ammonium nitrate. In general, as emission controls are applied to reactive hydrocarbons and NO_x, the dry flux of acid gases declines while the dry flux of NH_3 increases (due to greater NH_3 emissions and due to higher NH_3 concentrations that result from lowered aerosol nitrate formation).

Model verification studies show that atmospheric ozone and inorganic nitrate concentrations are over-predicted when the new dry deposition code is used in place of the former Caltech airshed model dry deposition code. The new dry deposition code requires data on the surface resistance to dry deposition as a function of land use type for a very large number of surface types. For pollutants other than SO_2, the

experimental data simply do not exist that accurately specify the surface resistance values needed to perform such detailed calculations with high precision. In particular, the scientific literature contains nothing more than educated estimates of the surface resistance values for large urban areas. This is a critical matter when evaluating the South Coast Air Basin, where most of the surface of the center of the air basin consists of a giant urban area. A program of experiments is needed to measure the surface resistance parameters required by the present model. An experimental determination of the effect of the surface area of buildings and other roughness elements on the effective surface area for removal of pollutants also is needed.

REFERENCES

Brutsaert, W. 1975. The Roughness Length for Water Vapor, Sensible Heat, and Other Scalars. *Journal of Atmospheric Science* 31:2028-2031.

Businger, J. A., J.C. Wyngaard, Y. Izumi and E.F. Bradley. 1971. Flux Profile Relationships in the Atmospheric Surface Layer. *Journal of Atmospheric Science* 28:181-189.

California Air Resources Board. "Report to the Legislature on the Feasibility of a 0.4 Gram per Mile Oxide of Nitrogen Exhaust Emission Standard for Passenger Cars and Light Trucks;" California Air Resources Board: Sacramento, CA.

Chang, J. S., R. A. Brost, I. S. A. Isaksen, S. Madronich, P. Middleton, W. R. Stockwell and C. J. Walcek. 1987. A Three-Dimensional Eulerian Acid Deposition Model: Physical Concepts and Formulation. *Journal of Geophysical Research* 92:14681-14700.

Derwent, R., and O. Hov. 1988. Application of Sensitivity and Uncertainty Analysis Techniques to a Photochemical Ozone Model. *Journal of Geophysical Research* 93:5185-5199.

Dolske, D. A., and D. F. Gatz. 1985. A Field Intercomparison of Methods for the Measurement of Particle and Gas Dry Deposition. *Journal of Geophysical Research* 90:2076-2084.

Dziegiel, H. T., T. B. Aure, and D. W. Anderson. 1982. "The Thermal DeNO$_x$ Demonstration Project." Los Angeles Department of Water and Power: Los Angeles, CA. Presented at the Joint Symposium on Stationary Combustion NO$_x$ Control, Dallas, TX, Nov. 1-4, 1982, Figures 11, 12 and 13.

Environmental Protection Agency. 1984. "Control of Air Pollution from New Motor Vehicles and New Motor Vehicle Engines; Gaseous Emission Regulations for 1987 and Later Model Year Light-Duty Vehicles, and for 1988 and Later Model Year Light-Duty Trucks and Heavy-Duty Engines; Particulate Emission Regulations for 1988 and Later Model Year Heavy-Duty Diesel Engines;" U.S. Environmental Protection Agency: Washington, D.C., 1984; *Federal Register* 40 CFR, Parts 86 and 600.

Finlayson-Pitts, B. J., and J. N. Pitts, Jr. 1986. "Atmospheric Chemistry: Fundamentals and Experimental Techniques." New York, Wiley.

Garland, J. A. 1976. Dry Deposition of SO_2 and Other Gases. In "Atmosphere–Surface Exchange of Particulate and Gaseous Pollutants (1974)," R. J. Engelman and G. A. Sehmel (co-ordinators), Technical Information Center, Office of Public Affairs, U.S. Energy Research and Development Administration.

Garland, J. A., and S. A. Penkett. 1976. Absorption of Peroxy Acetyl Nitrate and Ozone by Natural Surfaces. *Atmospheric Environment* 10:1127-1131.

Hildemann, L. M., A. G. Russell, and G. R. Cass. 1984. Ammonia and Nitric Acid Concentrations in Equilibrium with Atmospheric Aerosols: Experiment vs. Theory. *Atmospheric Environment* 18:1737-50.

Hill, A. C., and E. M. Chamberlain, Jr. 1976. The Removal of Water Soluble Gases from the Atmosphere by Vegetation. In "Atmosphere–Surface Exchange of Particulate and Gaseous Pollutants (1974)," R. J. Engelman and G. A. Sehmel (co-ordinators), Technical Information Center, Office of Public Affairs, U.S. Energy Research and Development Administration.

Huebert, B. J., and C. H. Robert. 1985. The Dry Deposition of Nitric Acid to Grass. *Journal of Geophysical Research* 90:2085-2090.

Liljestrand, H. M. 1979. Atmospheric Transport of Acidity in Southern California by Wet and Dry Mechanisms. Ph.D. thesis, California Institute of Technology, Pasadena.

McRae, G. J., and A. G. Russell. 1984. Dry Deposition of Nitrogen-Containing Species. In "Deposition Both Wet and Dry," B. B. Hicks (editor) Acid Precipitation Series–Volume 4, J. I. Teasley (series editor), Butterworths (Ann Arbor Science), Boston.

McRae, G. J., W. R. Goodin, and J. H. Seinfeld. 1982a. Development of a Second Generation Mathematical Model for Urban Air Pollution–I: Model Formulation. *Atmospheric Environment* 16:679-96.

McRae, G. J., W. R. Goodin and J. H. Seinfeld. 1982b. Mathematical Modeling of Photochemical Air Pollution. Environmental Quality Laboratory Report 18, California Institute of Technology, Pasadena, CA.

Nazaroff, W. W., and G. R. Cass. 1986. Mathematical Modeling of Chemically Reactive Pollutants in Indoor Air. *Environmental Science and Technology* 20:924-934.

Pierson, W. R., W. W. Brachaczek, S. M. Japar, G. R. Cass and P. A. Solomon. 1988. Dry Deposition and Dew Chemistry in Claremont, California, During the 1985 Nitrogen Species Methods Comparison Study. *Atmospheric Environment* 22:1657-1663.

Russell, A. G., and G. R. Cass. 1986. Verification of a Mathematical Model for Aerosol Nitrate and Nitric Acid Formation, and Its Use for Control Measure Evaluation. *Atmospheric Environment* 20:2011-25.

Russell, A. G., and G. R. Cass. 1984. Acquisition of Regional Air Quality Model Validation Data for Nitrate, Sulfate, Ammonium Ion and Their Precursors. *Atmospheric Environment* 18:1815-27.

Russell, A. G., K. F. McCue, and G. R. Cass. 1988a. Mathematical Modeling of the Formation of Nitrogen-Containing Air Pollutants-1. Evaluation of an Eulerian Photochemical Model. *Environmental Science & Technology* 22:263-271.

Russell, A. G., K. F. McCue and G. R. Cass. 1988b. Mathematical Modeling of the Formation of Nitrogen-Containing Pollutants-2. Evaluation of the Effect of Emission Controls. *Environmental Science and Technology* 22:1336-1347.

Russell, A. G., G. J. McRae, and G. R. Cass. 1983. Mathematical Modeling of the Formation and Transport of Ammonium Nitrate Aerosol. *Atmospheric Environment* 17:949-64.

Russell, A. G., G. J. McRae, and G. R. Cass. 1984. Acid Deposition of Photochemical Oxidation Products — A Study Using a Lagrangian Trajectory Model. In *Air Pollution Modeling and Its Application III*, C. de Wispelaere (editor), Plenum Publishing, New York.

Russell, A. G., G. J. McRae, and G. R. Cass. 1985. The Dynamics of Nitric Acid Production and the Fate of Nitrogen Oxides. *Atmospheric Environment* 19:893-903.

Sehmel. G. A. 1980. Particle and Gas Dry Deposition: A Review. *Atmospheric Environment* 14:983-1011.

Sheih, C. M., M. L. Wesely, and C. J. Walcek. 1986. A Dry Deposition Module for Regional Acid Deposition, Atmospheric Sciences Research Laboratory, Office of Research and Development, U.S. Environmental Protection Agency, Research Triangle Park, N.C.; produced under interagency agreement DW 89930060-0 to the U.S. Department of Energy.

South Coast Air Quality Management District. 1982. "Final Air Quality Management Plan 1982 Revision–Final Appendix No. VII-A–Short Range Tactics for the South Coast Air Basin;" South Coast Air Quality Management District: El Monte, CA.

Walcek, C. J., R. A. Brost, J. S. Chang, and M. L. Wesely. 1986. SO_2, Sulfate and HNO_3 Deposition Velocities Computed Using Regional Landuse and Meteorological Data. *Atmospheric Environment* 20:949-964.

Wesely, M. L., J. A. Eastman, D. H. Stedman, and E. D. Yalvac. 1982. An Eddy-Correlation Measurement of NO_2 Flux to Vegetation and Comparison to O_3 Flux. *Atmospheric Environment* 16:815-820.

Wesely, M. L., and B. B. Hicks. 1977. Some Factors that Affect the Deposition Rates of Sulfur Dioxide and Similar Gases on Vegetation. *Journal of the Air Pollution Control Association* 27:1110-1116.

Appendix A

Mathematical Modeling of the Formation of Nitrogen-Containing Air Pollutants. 1. Evaluation of an Eulerian Photochemical Model

Reprinted from ENVIRONMENTAL SCIENCE & TECHNOLOGY, Vol. 22, Page 263, March 1988

Mathematical Modeling of the Formation of Nitrogen-Containing Air Pollutants. 1. Evaluation of an Eulerian Photochemical Model

Armistead G. Russell

Department of Mechanical Engineering, Carnegie-Mellon University, Pittsburgh, Pennsylvania 15213

Kenneth F. McCue and Glen R. Cass*

Environmental Quality Laboratory, California Institute of Technology, Pasadena, California 91125

■ A grid-based, Eulerian airshed model has been used to study the formation and control of gas- and aerosol-phase nitrogen-containing air pollutants. The performance of the model was assessed by comparison against field measurements made for this purpose in the Los Angeles area over the period 30–31 August 1982. Model predictions for O_3 and peroxyacetyl nitrate (PAN) concentrations are in good agreement with observations. The absolute values of the total inorganic nitrate, NH_3, and HNO_3 predictions on the average are within a few ppb of the observations. Lacking an inventory of ionic and alkaline aerosol emissions, accurate apportionment of total inorganic nitrate between the aerosol and gas phases is not possible at coastal locations. At midbasin sites like Anaheim, where NH_4NO_3 is the dominant nitrate aerosol species present, the aerosol nitrate levels predicted by the model are in good agreement with observed values.

Introduction

Nitrogen-containing air pollutants like HNO_3, aerosol nitrates, and peroxyacetyl nitrate (PAN) are formed as further reaction products of NO_2 in the atmosphere. HNO_3 is implicated as a major contributor to the acid deposition flux in the western U.S., aerosol nitrates contribute to visibility deterioration, and PAN is a well-known plant toxicant. Therefore, there is considerable interest in how these pollutants would respond to the imposition of emission controls.

In a previous study, a mathematical model based on the Lagrangian trajectory formulation of the atmospheric diffusion equation was used to test the effects of emissions reductions on the resulting nitric acid, aerosol nitrate, and O_3 concentrations at a receptor site in the Los Angeles basin of California (*1*). Though a trajectory model is a very valuable tool for determining the probable outcome at a single predetermined location, it may not be the most effective method of determining the basinwide consequences of emission changes or even the consequences at a large number of sites within a given airshed. In this paper an Eulerian, grid-based model is used to describe the transport and formation of pollutants, including O_3, NO_2, nitric acid, aerosol nitrate, and PAN. Predictions of this model are compared against a set of field experimental data for the 30–31 August 1982 period (*2*), a data set expressly designed for use in evaluating this type of model. In paper 2 of this series, the model will be used to test the effects of emission reductions resulting from specific emission control strategies.

Model Description

The mathematical model employed by this study is based on numerical solution of the semiempirical atmospheric diffusion equation for the ensemble mean concentration $\langle C_i \rangle$ of each pollutant species i within the chemical reaction mechanism R:

$$\frac{\partial \langle C_i \rangle}{\partial t} + \nabla(\bar{u}\langle C_i \rangle) = \nabla(K\nabla\langle C_i \rangle) + R_i(\langle C_1 \rangle, \langle C_2 \rangle, ..., \langle C_n \rangle) \quad (1)$$

where $\bar{u}$ is the wind velocity at the point of interest and K is the atmospheric eddy diffusivity tensor (*3*). Aside from the improvements detailed below, the methods used for solving eq 1 are as described by McRae et al. (*4*, *5*) and Russell et al. (*6*) and will not be repeated here.

In previous studies, operator splitting techniques were used to decouple the horizontal transport, vertical transport, and chemical reaction components of the atmospheric diffusion equation. In this study, the vertical diffusion remains coupled to the chemical reaction component, so that the resulting sequence is

$$C^{n+1} = A_x A_y [A_{z,c}(2\Delta t)] A_y A_x C^{n-1} \quad (2)$$

where A_x and A_y are the numerical approximations to the horizontal transport operators, $A_{z,c}$ is the approximation to the combined, simultaneous vertical transport and chemical reaction operator, n is the time level, and Δt is the time step.

A second major difference between this study and the earlier studies is that the chemical reaction mechanism and the associated rate constants have been updated. Because this study concerns itself not only with the formation of O_3 and NO_2 but also with the production of nitric acid, aerosol nitrate, and PAN, it is necessary to treat the N_xO_y chemistry in much greater detail. The chemical reaction mechanism tracks 30 pollutant species (Table I) and includes 58 reactions (Table II). Of particular importance is the expanded treatment of reactions involving the NO_3 radical and N_2O_5, which can be important at night (*9*). The

0013-936X/88/0922-0263$01.50/0

Table I. Definition of Chemical Species Symbols Used in the Chemical Mechanism of Table II

symbol	definition
NO	nitric oxide
NO_2	nitrogen dioxide
O_3	ozone
HCHO	formaldehyde
RCHO	lumped aldehyde
OLE	lumped olefin
ALK	lumped alkane
ARO	lumped aromatic
C_2H_4	ethylene
PAN	peroxyacetyl nitrate
N_2O_5	dinitrogen pentoxide
HNO_2	nitrous acid
NO_3	nitrate radical
RONO	lumped nitrate
RNO_4	lumped peroxynitrate (RO_2NO_2)
HNO_4	peroxy nitrous acid (HO_2NO_2)
HO_2	hydroperoxyl radical
RO	alkoxyl radical
RO_2	peroxyalkyl radical
RCO_3	peroxyacyl radical
O	atomic oxygen
OH	hydroxyl radical
CO	carbon monoxide
H_2O_2	hydrogen peroxide
CO_2	carbon dioxide
HNO_3	nitric acid
NH_3	ammonia
NH_4NO_3	ammonium nitrate aerosol
RNO_3	alkyl nitrate
RPN	nitroxyperoxyalkyl nitrates and dinitrates

ability of a Lagrangian trajectory model employing this chemical mechanism to predict the concentrations of O_3, NO_2, NO_3, HNO_3, and PAN has been verified in previous studies (*1*, *9*).

Ammonium nitrate aerosol concentrations (NH_4NO_3, Table I) are calculated in the model as being at thermodynamic equilibrium with HNO_3 and NH_3 (*11*) according to the scheme outlined in ref 6. The apportionment of total inorganic nitrate (TN = HNO_3 + aerosol NO_3^-) and ammonia between the gas and aerosol phases is calculated at every second time step ($2\Delta t$) and is important because of the different depositional rates of aerosol and reactive gases. In this paper, NH_4NO_3 is the only aerosol nitrate species considered due to the lack of an emission inventory for alkaline aerosol that might be available to act as a "sink" for gaseous HNO_3 (see ref 1).

Modeling Region

Figure 1 shows the extent of the modeling region used in this study and the boundaries of the South Coast Air Basin (SoCAB) of California. Meteorological fields, topographical details, and emission inventory data were developed over the 150 km × 400 km system of 5 km × 5 km grid cells shown in Figure 1. In the vertical dimension, the model is subdivided into five cells. Starting from ground level, the vertical cell dimensions are 38, 116, 154, 363, and 429 m, reaching an aggregate height of 1100 m above ground level.

Meteorological Fields

Meteorological fields required for model evaluation were calculated by interpolating individual measurements available from the South Coast Air Quality Management District (SCAQMD), the California Air Resources Board (CARB), and the National Weather Service (NWS) over the computational grid (*12*) as described in an earlier

Table II. Kinetic Mechanism (*4*, *7–10*)

	reaction	rate constant, ppm min K units
1	$NO_2 + h\nu \rightarrow NO + O(^3P)$	*a*
2	$O(^3P) + O_2 + M \rightarrow O_3 + M$	$0.346T^{-2}\exp(510/T)$
3	$O_3 + NO \rightarrow NO_2 + O_2$	$1.04 \times 10^6 T^{-1}\exp(-1450/T)$
4	$NO_2 + O(^3P) \rightarrow NO + O_2$	$3.99 \times 10^6 T^{-1}$
5	$NO + O(^3P) \rightarrow NO_2$	$1.67 \times 10^5 T^{-1}\exp(584/T)$
6	$NO_2 + O(^3P) \rightarrow NO_3$	$1.07 \times 10^6 T^{-1}$
7	$O_3 + NO_2 \rightarrow NO_3 + O_2$	$5.19 \times 10^4 T^{-1}\exp(-2450/T)$
8	$NO_3 + NO \rightarrow 2NO_2$	$8.05 \times 10^6 T^{-1}$
9	$NO + OH \rightarrow HNO_2$	$5.07 \times 10^6 T^{-1}$
10	$HNO_2 + h\nu \rightarrow NO + OH$	*a*
11	$HO_2 + NO_2 \rightarrow HNO_2 + O_2$	$17.37T^{-1}\exp(1006/T)$
12	$HNO_2 + OH \rightarrow H_2O + NO_2$	$2.91 \times 10^6 T^{-1}$
13	$NO_2 + HO_2 \rightarrow HNO_4$	$1.73 \times 10^4 T^{-1}\exp(1006/T)$
14	$HNO_4 \rightarrow HO_2 + NO_2$	$1.80 \times 10^{15}\exp(-9950/T)$
15	$HO_2 + NO \rightarrow NO_2 + OH$	$3.58 \times 10^6 T^{-1}$
16	$RO_2 + NO \rightarrow NO_2 + RO$	$3.58 \times 10^6 T^{-1}$
17	$RCO_3 + NO \rightarrow NO_2 + RO_2 + CO_2$	$3.36 \times 10^6 T^{-1}$
18	$NO_2 + OH \rightarrow HNO_3$	$4.53 \times 10^6 T^{-1}$
19	$CO + OH\ (+O_2) \rightarrow HO_2 + CO_2$	$1.31 \times 10^5 T^{-1}$
20	$O_3 + h\nu \rightarrow O(^3P) + O_2$	*a*
21	$HCHO + h\nu\ (+2O_2) \rightarrow 2HO_2 + CO$	*a*
22	$HCHO + h\nu \rightarrow H_2 + CO$	*a*
23	$HCHO + OH\ (+O_2) \rightarrow HO_2 + H_2O + CO$	15000
24	$RCHO + h\nu \rightarrow HO_2 + RO_2 + CO$	*a*
25	$RCHO + OH\ (+O_2) \rightarrow RCO_3 + H_2O$	23600
26	$C_2H_4 + OH \rightarrow RO_2$	12000
27	$C_2H_4 + O(^3P) \rightarrow HO_2 + RO_2$	1219
28	$OLE + OH \rightarrow RO_2$	89142
29	$OLE + O(^3P) \rightarrow RO_2 + RCO_3$	22118
30	$OLE + O_3 \rightarrow 0.5RCHO + 0.5HCHO + 0.3HO_2 + 0.31RO_2 + 0.14OH + 0.03RO$	0.136
31	$ALK + OH \rightarrow RO_2$	5800
32	$ALK + O(^3P) \rightarrow RO_2 + OH$	99.8
33	$ARO + OH \rightarrow RO_2 + RCHO$	10112
34	$RO \rightarrow HO_2 + 0.5HCHO + RCHO$	2.0×10^5
35	$RONO + h\nu \rightarrow RO + NO$	*a*
36	$RO + NO \rightarrow RONO$	$4.38 \times 10^6 T^{-1}$
37	$RO + NO_2 \rightarrow RNO_3$	$2.19 \times 10^6 T^{-1}$
38	$RO + NO_2 \rightarrow RCHO + HNO_2$	$1.91 \times 10^5 T^{-1}$
39	$NO_2 + RO_2 \rightarrow RNO_4$	$1.64 \times 10^6 T^{-1}$
40	$H_2O_2 + OH \rightarrow HO_2 + H_2O$	2.50×10^3
41	$RNO_4 \rightarrow NO_2 + RO_2$	$1.80 \times 10^{15}\exp(-9950/T)$
42	$RCO_3 + NO_2 \rightarrow PAN$	$2.05 \times 10^6 T^{-1}$
43	$PAN \rightarrow RCO_3 + NO_2$	$4.77 \times 10^{16}\exp(-12516/T)$
44	$NO_2 + NO_3 \rightarrow N_2O_5$	$7.40 \times 10^5 T^{-1}$
45	$N_2O_5 \rightarrow NO_2 + NO_3$	$4.06 \times 10^{16}\exp(-11080/T)$
46	$H_2O + N_2O_5 \rightarrow 2HNO_3$	$5.66 \times 10^{-4} T^{-1}$
47	$O_3 + OH \rightarrow HO_2 + O_2$	$6.62 \times 10^5 T^{-1}\exp(-1000/T)$
48	$O_3 + HO_2 \rightarrow OH + 2O_2$	$4.85 \times 10^3 T^{-1}\exp(-580/T)$
49	not used	
50	$HO_2 + HO_2 \rightarrow H_2O_2 + O_2$	$2.5 \times 10^4 T^{-1}\exp(1150/T) + [5.8 \times 10^{-5} T^{-2}\exp(5800/T)][H_2O]$
51	$H_2O_2 + h\nu \rightarrow 2OH$	*a*
52	$RO_2 + RO_2 \rightarrow 2RO + O_2$	$2.04 \times 10^4 T^{-1}\exp(223/T)$
53	$NO_3 + HCHO\ (+O_2) \rightarrow HNO_3 + HO_2 + CO$	0.43
54	$NO_3 + RCHO\ (+O_2) \rightarrow HNO_3 + RCO_3$	1.98
55	$NO_3 + h\nu \rightarrow NO_2 + O(^3P)$	*a*
56	$NO_3 + OLE \rightarrow RPN$	$1826.7T^{-1}$
57	$NO_2 + NO_3 \rightarrow NO_2 + NO + O_2$	0.59
58	$HNO_3 + NH_3 \rightarrow NH_4NO_3$	*b*

[a] Photolytic reaction; see McRae (*10*). [b] See ref 6.

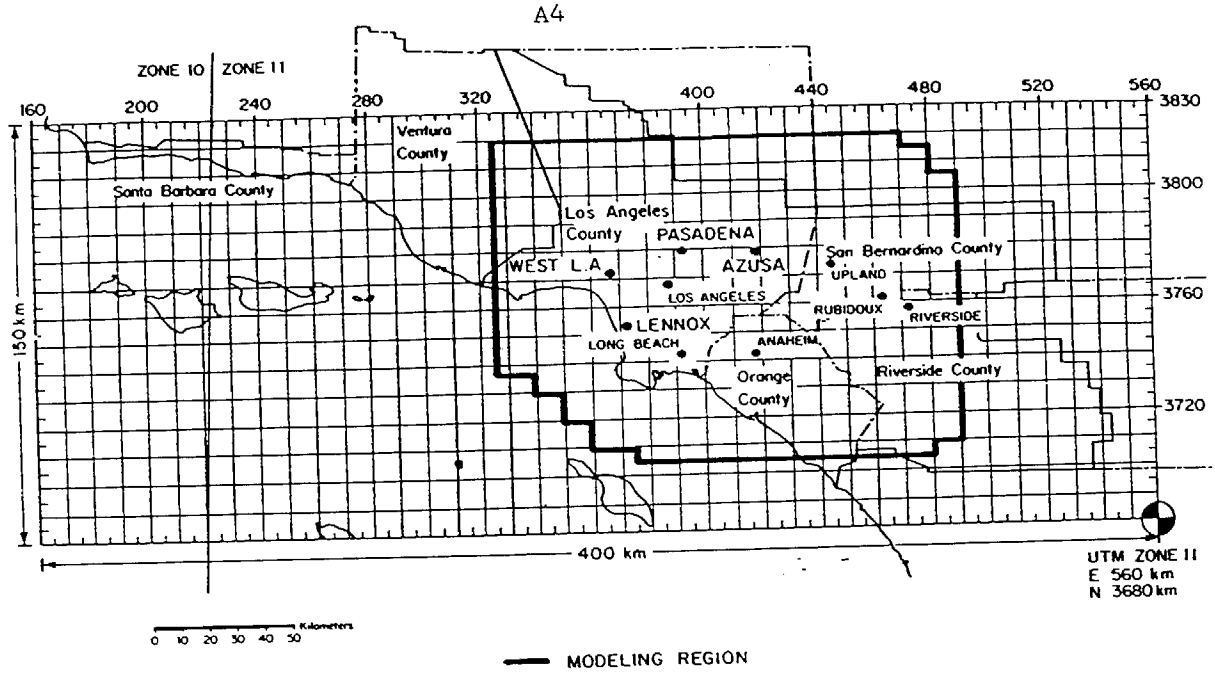

Figure 1. South Coast Air Basin of California, plus Ventura and coastal Santa Barbara Counties. Emissions and meteorological data fields are developed over the 150 km × 400 km gridded area. Air monitoring sites at which HNO_3, NH_3, and aerosol nitrate data are available from ref 2 are shown by (●). Air quality modeling calculations are performed within the region bounded by the heavy solid line in the center of the map.

trajectory model evaluation study (*1*). Additional hourly, three-dimensional wind fields were developed with use of the two-dimensional ground-level wind fields and upper-level wind measurements gathered from seven locations at a variety of times throughout the day. Solar radiation measurements were obtained at Pasadena, Upland, and central Los Angeles from the Jet Propulsion Laboratory, CARB, and SCAQMD, respectively. These data, along with cloud cover observations, were used to determine the insolation levels within the modeling region.

Pollutant Emissions

NO_x, speciated hydrocarbons, and CO emissions were calculated for every hour and grid in the SoCAB from the 1982 forecast emission inventory provided by CARB (*13*, *14*). A 1982 ammonia emissions inventory was developed for use in this study (*15*). These emission data are presented in detail by Russell and Cass (*1*) and, therefore, will not be repeated here. Actual NO_x emissions data for each electric utility generating station were obtained for the two days modeled from SCAQMD along with August 1982 emission data for fuel burning at the petroleum refineries. These data replaced the CARB forecast emissions from electric utility and refinery fuel burning, lowering the total areawide emissions of NO_x from 1134 metric tons/day given in ref. 1 down to 1120 metric tons/day. The spatial distribution of pollutant emissions is shown in Figure 2.

Initial and Boundary Conditions

Concentrations of O_3, NO_2, NO, SO_2, CO, and total hydrocarbons (THC) are measured throughout the basin, and hourly averaged values are recorded by SCAQMD. The concentrations of HNO_3(g), NH_3(g), PAN, aerosol nitrate, and ammonium ion on 30–31 August 1982 were measured as part of a field experiment conducted specifically to acquire model verification data (*2*). These values then were interpolated to form a two-dimensional ground-level initial concentration field over the basin for those pollutants at 0000 Pacific Standard Time (PST), 30 August 1982. The initial concentration of PAN (which was measured at only one location at the beginning of the experiment) was set to one-tenth of the initial O_3 level (on a ppm basis). Upper-level O_3 initial conditions were set to the previous 1400 PST ground-level O_3 concentrations

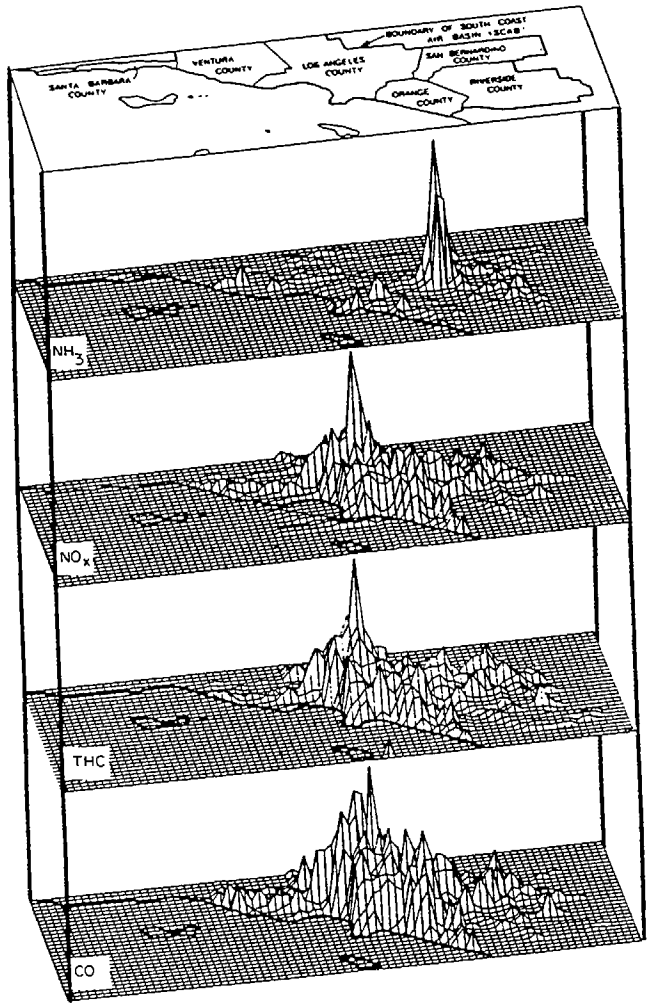

Figure 2. Spatial distribution of NH_3, NO_x, total hydrocarbons, and CO emissions within the grid system for the summer of 1982.

Table III. Hydrocarbon Splitting Factors

	urban	rural	ocean
HCHO	0.0037	0.0010	0.0010
RCHO	0.0033	0.0020	0.0050
OLE	0.0042	0.0006	0.0001
ALK	0.0675	0.0226	0.0096
ARO	0.0177	0.0052	0.0017
C_2H_4	0.0061	0.0040	0.0060

following the results of Blumenthal et al. (*16*) and Edinger (*17*). Trajectory simulations and the experimental results of Sonoma Technology (*18*) indicated that the NO and NO_2 levels above the mixed layer at 0000 PST would be very low, and the initial concentrations of those species aloft were set to zero.

Total hydrocarbon measurements taken by SCAQMD are not speciated into the different organic compounds actually present. Thus, a set of factors must be developed to split the measured initial hydrocarbon concentrations into the six hydrocarbon classes used by the model. This process is complicated by the need to split the hydrocarbons into the six classes over three distinct regions in which one would expect a very different chemical composition: the urban area, rural surroundings, and over the ocean. Three sets of splitting factors were developed, one for each of the different regions, and are shown in Table III. Urban area factors were derived from the measurements of Grosjean and Fung (*19*), and the ocean and rural factors were calculated from measurements (*18*) and previous modeling analysis (*7*). The effect of these assumptions about initial conditions on the resulting predictions is minimized by conducting multiday calculations (since subsequent emissions into the model are fully speciated).

Ground-level boundary conditions are derived from the interpolated pollutant concentration fields discussed earlier. Those concentration fields start with Pacific Ocean background values (in ppb: O_3, 40; NO_2, 10; NO, 10; CO, 100; HNO_3, 1; NH_3, 1; THC, 1000) at the western edge of the large grid shown in Figure 1 and rise to match the on-land values at near-coastal monitoring sites. The smaller modeling region shown in Figure 1 is superimposed on these concentration fields, and the surface-level boundary conditions supplied to the model are defined by the values of the interpolated concentration fields that prevail at the edges of the modeling region. Boundary conditions above the mixed layer at the western, upwind boundary of the modeling region over the ocean were set to a column average of 60 ppb O_3, 250 ppb reactive hydrocarbons, 0.0 ppb NO and NO_2, 1 ppb HNO_3, 4 ppb NH_3, and 3.25 $\mu g\ m^{-3}$ aerosol nitrate. The hydrocarbon value was derived from reports by Sonoma Technology (*18*) and Killus (*20*), while the O_3, NO, and NO_2 values were based on work by Sonoma Technology (*18*). Upper-level, downwind boundary conditions are set as a function of the predicted pollutant concentrations in air advected out of the basin.

Model Application on 30–31 August 1982

Prediction of pollutant concentrations as a function of time began at 0000 PST, 30 August 1982, and was continued for 48 h. Of the species being modeled, particular attention is paid to NO, NO_2, O_3, PAN, HNO_3, aerosol nitrate, and NH_3, for which ambient measurements are available for comparison. Previous grid model evaluation studies have relied on comparison of measurements to predicted concentrations of O_3 and, at times, NO_2. This study provides a much more stringent test of the photochemical model as it compares results for HNO_3, aerosol NO_3^-, NH_3, and PAN as well as NO_2 and O_3.

The August 30–31 data set (*2*) used in this study is the only model evaluation data set in existence with regionwide short-time average observations on all of the unregulated nitrogen-containing pollutants of interest here: HNO_3, NH_3, aerosol nitrate, and PAN. For that reason, the August 30–31, 1982, time period is the best choice for a model evaluation study of NO_x-derived unregulated pollutants. Ozone concentration predictions are an interesting byproduct of this study. While these days were not chosen primarily for their ozone data, it can be noted that the representativeness of the August 31 period as an O_3 modeling event in the Los Angeles area has been examined by Horie (*21*). August 31, 1982, was found to fall within one of the two most common types of high O_3 event days in the Los Angeles area. That class of events is characterized by a strong temperature inversion, a west to northwest morning wind at Los Angeles International Airport, and an average peak O_3 concentration of 0.235 ppm. If the characteristics of days of this type are ranked by their deviation from the mean of all similar days, August 31, 1982, would fall within the closest 25% of the days to the group norm.

Results from the model calculation for the two days are presented in two formats. First, a series of concentration isopleths are given for O_3, NO_2, HNO_3, aerosol nitrate, and NH_3 for the second day (31 August) of the simulation in Figure 3. This provides a convenient means for studying the temporal and spatial evolution of the pollutants, making it easier to judge where the highest concentrations of the pollutants can be expected. A second method for presenting the results allows for visual evaluation by plotting the predicted concentrations as a function of time along with the measurements from a monitoring station in the same grid location. This has been done for a number of locations across the Los Angeles basin (Figures 4–7).

Figure 3 shows the predicted spatial distribution of pollutant concentrations at 3-h intervals throughout the day of 31 August. NO_2 levels peak in the early morning in the western and coastal part of the basin, followed by declining values throughout the remainder of the day. HNO_3 concentrations begin at low levels throughout the basin at 0800 PST. By 1100 PST, NO_2 oxidation to form nitric acid accompanied by higher ambient air temperatures leads to the accumulation of HNO_3(g) concentrations above 15 ppb within a zone stretching from central Orange County through the Pomona, San Gabriel, and San Fernando Valleys in eastern and northern Los Angeles County. At the same time, very low HNO_3 concentrations (below 3 ppb) occur in adjacent portions of Riverside and San Bernardino Counties. That zone of low HNO_3 levels is centered over the Chino dairy area where high levels of NH_3 (see the NH_3 concentration predictions in Figure 3 and the tall spike in the NH_3 emissions inventory in Figure 2) from decomposition of livestock waste and from farm-related fertilizer use act to drive the inorganic nitrate present into the aerosol phase. By 1400 PST, the HNO_3(g) concentrations are declining, with the highest remaining levels in north Los Angeles County between Azusa and Claremont (near Upland). By 1700 PST in the late afternoon, HNO_3(g) concentrations have returned to very low values.

Ozone concentration predictions are compared to observations in the time series at six widely spaced monitoring sites in Figure 4. At some near-coastal sites, ozone predictions exceed observations in a manner similar to the results shown for Anaheim in Figure 4. However, at the midbasin and inland monitoring stations where high ozone

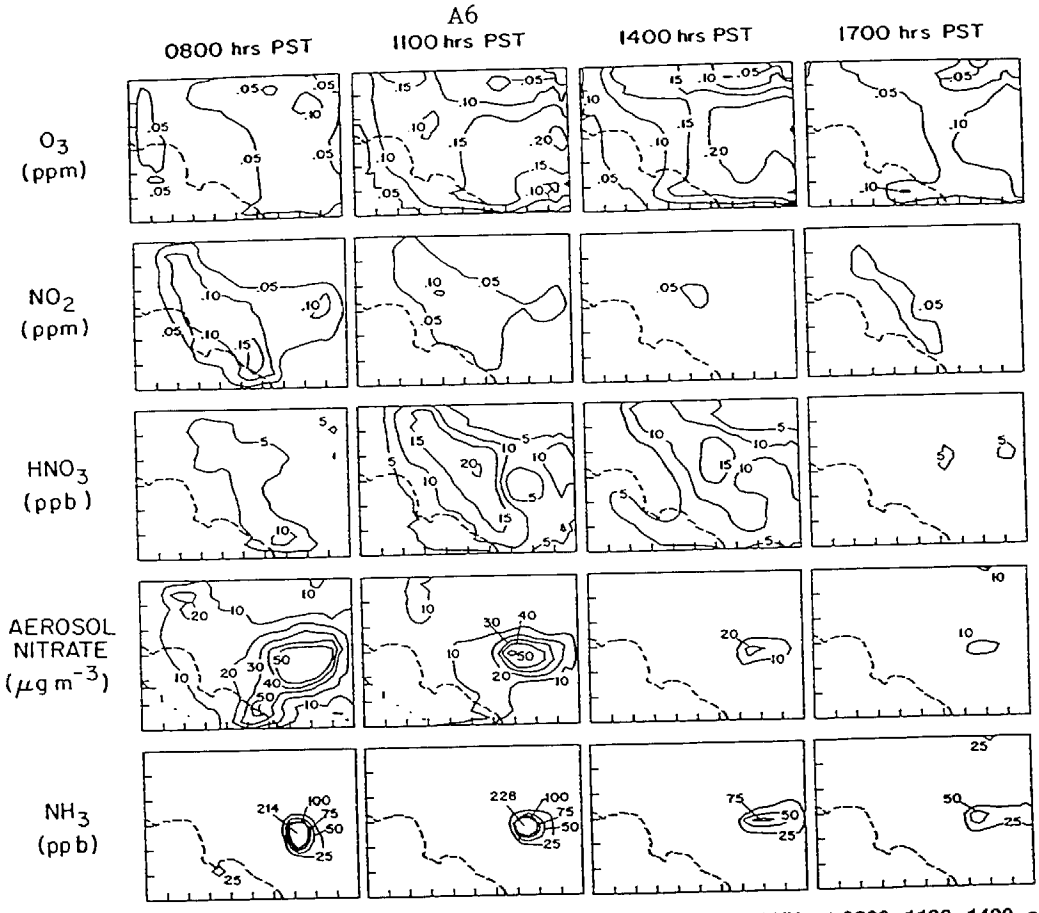

Figure 3. Spatial distribution of predicted concentrations of O_3, NO_2, HNO_3, aerosol nitrate, and NH_3 at 0800, 1100, 1400, and 1700 PST, 31 August 1982.

concentrations occur, model predictions are generally in excellent agreement with measured ozone values.

Figures 5–7 show the time series of model predictions and experimental observations for nitrogen-containing pollutants at locations moving from west to east across the air basin. At central Los Angeles, predicted and observed NO_2 and TN values are generally in good agreement except that the timing of the TN peak occurs one interval prior to the time of the observed peak. At Los Angeles and at the coastal sites in the western portion of the air basin, the partition of TN between HNO_3(g) and aerosol nitrate by the model results in more HNO_3 and less aerosol than is actually observed. This is consistent with the previous analysis of the aerosol data at the coastal sites (22) that showed that the nitrate aerosol present near the coast is not pure NH_4NO_3 aerosol. Near the coast, sea salt (or other alkaline aerosol) has stripped the HNO_3(g) forming non-NH_4NO_3 aerosol nitrate. In a prior analysis of aerosol nitrate formation using a trajectory version of this photochemical model, the heterogeneous reaction between HNO_3 and preexisting sink aerosol (such as NaCl) was simulated (*1*). In the present study, only the reaction between NH_3 and HNO_3 was included because an accurate description of the chemical composition of aerosol emissions across the entire SoCAB was unavailable. With this heterogeneous reaction step missing, we do not expect to be able to fully account for the partition of total inorganic nitrate between the aerosol and gas phases. This explains why aerosol nitrate is underpredicted at the near-coastal sites (Lennox, Long Beach, West Los Angeles, and central Los Angeles) by the present model that incorporates only NH_4NO_3 formation.

Total inorganic nitrate concentrations (TN) measured at 10 monitoring stations vary from low values at coastal locations to higher values inland near Rubidoux. The predicted TN concentrations follow the same geographic trends. Since TN accounts for only a very small portion of airborne NO_x-related species, very small absolute differences between the observed and the predicted partition of the total oxidized nitrogen in the system between NO_2, PAN, and TN have the appearance of a large relative difference between observed and predicted TN; in an absolute sense, TN predictions are close to the observations at most sites, as will be discussed under Statistical Evaluation of Model Results. At four sites, the predicted TN concentration peaks earlier in the morning than does the measured TN concentration. Though the reasons for this result are not certain, this effect could be achieved if the mixing depth as modeled is lower than the actual mixing depth at those times, trapping more nitrate close to the ground. It is difficult to estimate mixing depths precisely during the morning as the inversion base is rising rapidly. The early peak in TN levels also could be produced by faster than actual oxidation of NO_2 by the OH radical to from HNO_3. OH radical concentration measurements are scarce, and none were available against which to compare model predictions. Predicted midday OH concentrations ranged from 8×10^{-8} to 1.6×10^{-7} ppm, while predicted midday HO_2 levels ranged from 1×10^{-5} to 5×10^{-5} ppm.

Differences between predicted and observed HNO_3(g) are governed by the problems inherent in distributing total inorganic nitrate between the aerosol and gas phases. At midbasin sites like Anaheim, both TN and NH_3 are predicted to be close to the observed values, and an ion balance on the composition of the measured aerosol (22) shows that NH_4NO_3 is present. In that case, the major assumptions of the model are satisfied, and the observed and predicted HNO_3 and aerosol nitrate values also are

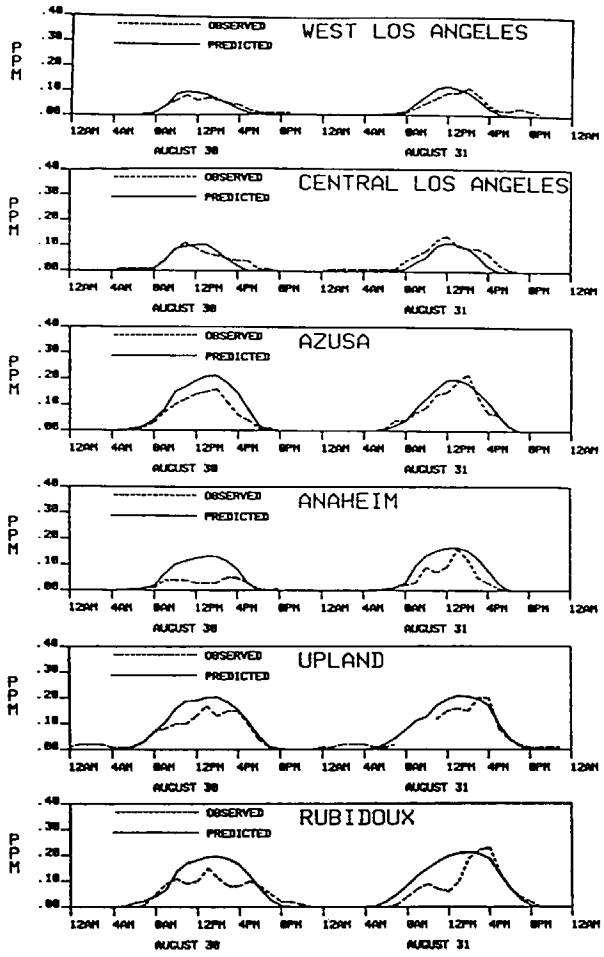

Figure 4. Comparison of predicted and observed ozone concentrations in the South Coast Air Basin, 30–31 August 1982.

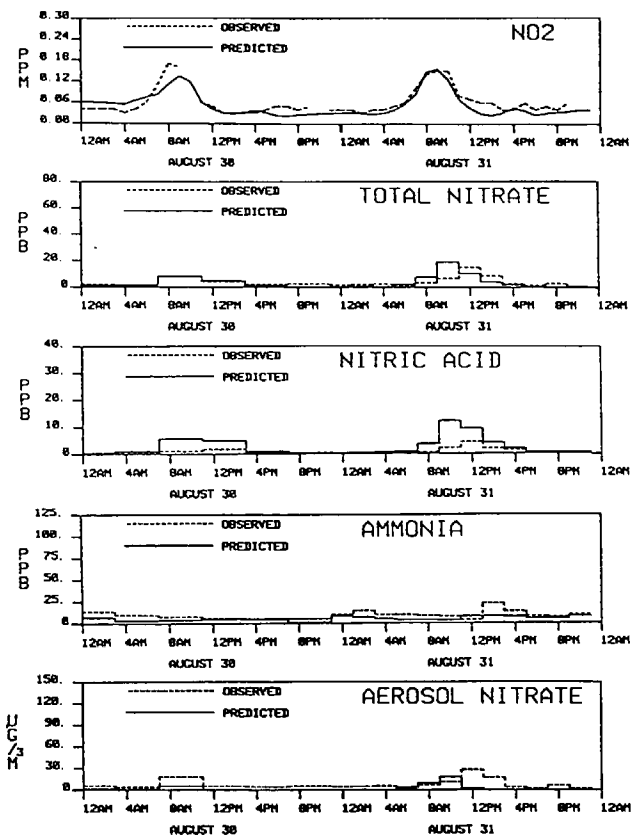

Figure 5. Comparison of predicted and observed concentrations of NO_2, TN, HNO_3, aerosol nitrate, and NH_3 at central Los Angeles on 30–31 August 1982.

close to the observed values. Far downwind, overpredictions of aerosol nitrate at Rubidoux and Upland occur due to the overprediction of total inorganic nitrate formation just discussed. HNO_3 levels predicted at Rubidoux are still close to the observed values in spite of the overprediction of TN because the NH_3 concentration and the temperature modulate the $HNO_3(g)$ concentrations via the NH_4NO_3 equilibrium dissociation constant and the NH_3 is in great excess at that site.

PAN measurements were taken at two sites during the August 1982 field experiment: the University of California at Riverside (UCR) and the California Institute of Technology (Caltech) in Pasadena. The peak-measured PAN concentration was 17 ppb at UCR between 1400 and 1500 PST, 31 August. The predicted PAN peak at UCR was 16 ppb between 1200 and 1300 PST the same day. The predicted PAN concentration at the time of the measured peak was 15 ppb. At Caltech, the measured maximum PAN concentration on August 31 was 9 ppb between 1300 and 1500 PST, which compares well to the predicted maximum of 7 ppb occurring during the same time period. The agreement between predicted and measured PAN concentrations for the two days at Pasadena is excellent, as shown in Figure 8.

Statistical Evaluation of Model Results

Visual inspection of graphs showing predicted and observed pollutant concentrations provides one method for assessing air quality model performance. However, when the number of monitoring sites to be examined grows large, the amount of information to be absorbed and evaluated by that means can become overwhelming. A number of investigators have addressed the problem of objective evaluation of model performance and have proposed a variety of statistical tests that can be applied to judge the quality of the model's results (*23–25*). In this study, a wide range of performance measures is presented following the format of McRae and Seinfeld (*7*); for brevity, the significance and relevance of each test is given only for those tests not described in that study. A statistical description of model performance for O_3 and NO_2 is given in Table IV. Corresponding statistics for total inorganic nitrate, NH_3, HNO_3, and aerosol nitrate are given separately in Table V.

As seen in Table IV, the model performance measures for O_3 are excellent. In the case of NO_2, the predictions are unbiased, and the absolute accuracy [root mean square (RMS) error, peak prediction, percent residuals within 0.05 ppm] is good, much better than would be expected if one looked only at a correlation analysis. The low correlation coefficient is due to two factors: (1) the predicted NO_2 peaks occur at a slightly different time than the observed peaks (typically the timing of the observed and predicted morning NO_2 peaks differ by 1–2 h) and (2) measurements at some locations are anomalous (e.g., NO_2 concentrations reported at the Pasadena SCAQMD station over time do not track the observations at surrounding stations). The correlation coefficient and least-squares coefficients are extremely sensitive to any offset between predicted and observed peaks (*7*, *24*). Residual frequency plots (Figure 9) show that the residual differences between the predicted and observed concentrations of O_3 and NO_2 center about zero (little or no bias) in approximately a Gaussian form. The RMS error values given in Table IV provide a measure of the spread of the O_3 and NO_2 residual histograms in Figure 9.

Table IV. Statistical Evaluation of Model Performance for O_3 and NO_2[a]

performance measure	results of test: O_3	results of test: NO_2	remarks
mean of residuals, ppm (bias)	0.010 (20%)	−0.002 (−5%)	predictions and measurements agree closely on the average
RMS error about the mean, ppm (σ of residuals)	0.037	0.030	root mean square error about the mean is lower than in previous studies
accuracy of peak prediction[b]	0.262/0.26 = 1.01	0.157/0.17 = 0.92	magnitudes of the peak predictions are in excellent agreement for both O_3 and NO_2
correlation coefficient	0.83	0.43	predicted and measured O_3 values agree closely; low correlation for NO_2 is due to the prediction that the NO_2 peaks occur at slightly different times than the measured peaks
linear least-squares fit, $C_{obsd} = MC_{pred} + B$	M = 1.11, B = 0.006	0.47, 0.026	again the O_3 results are excellent; NO_2 results suffer from the peak timing problem detailed above
% of residuals ≤ bounds = 0.05 ppm	86	93	there are very few outliers

[a] McRae and Seinfeld (7) explain the significance of the performance measures. [b] The predicted and observed peak values occur near each other but not necessarily at exactly the same air monitoring site.

Table V. Statistical Evaluation of Model Performance for Total Inorganic Nitrate, Ammonia, Aerosol Nitrate, and Nitric Acid

performance measure	TN, $\mu g\ m^{-3}$	NH_3, ppb	AN, $\mu g\ m^{-3}$	HNO_3, $\mu g\ m^{-3}$
mean of observations	12.9	13.8	9.5	3.4
mean of predictions	15.6	14.6	8.0	7.6
mean of residuals	2.7	0.7	−1.5	4.2
RMS error about the mean	14	16	12	7.8
correlation coefficient	0.6	0.6	0.4	0.7
regression analysis, $C_{prep} = MC_{obsd} + B$	M = 1.15, B = 0.7	M = 0.54, B = 7.0	M = 0.74, B = 0.94	M = 1.7, B = 1.9

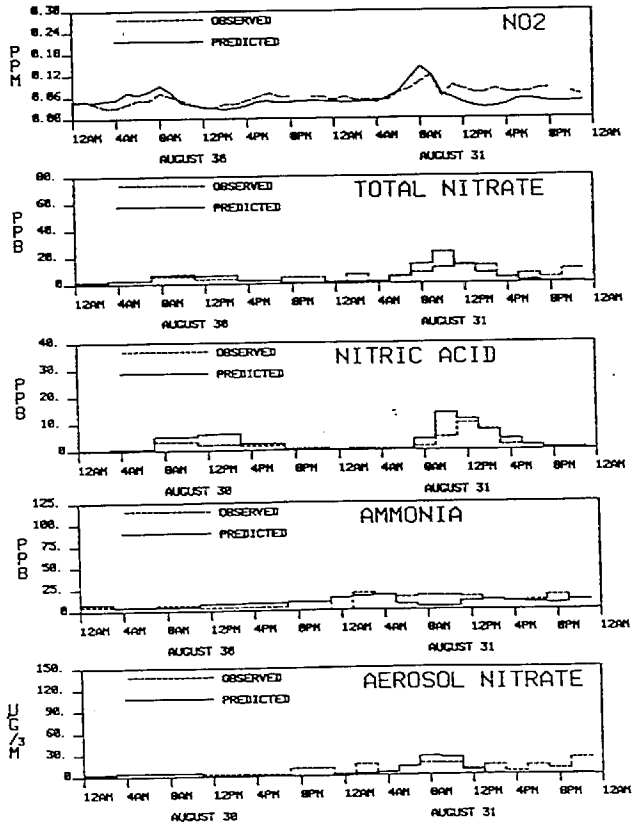

Figure 6. Comparison of predicted and observed concentrations of NO_2, TN, HNO_3, aerosol nitrate, and NH_3 at Anaheim on 30–31 August 1982.

Evaluation of the model's ability to predict nitrate-containing species concentrations can be broken into three steps: (1) the ability to predict correctly the formation of

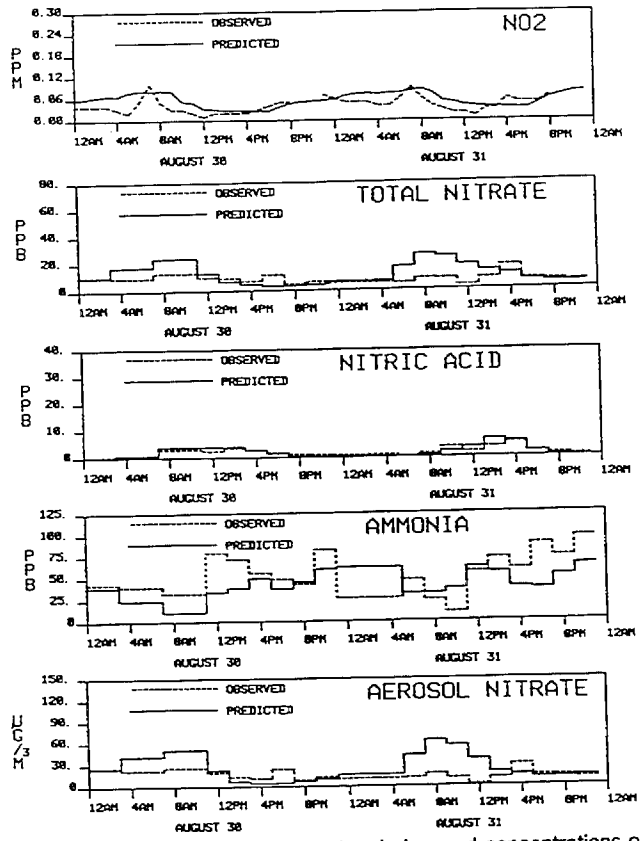

Figure 7. Comparison of predicted and observed concentrations of NO_2, TN, HNO_3, aerosol nitrate, and NH_3 at Rubidoux on 30–31 August 1982.

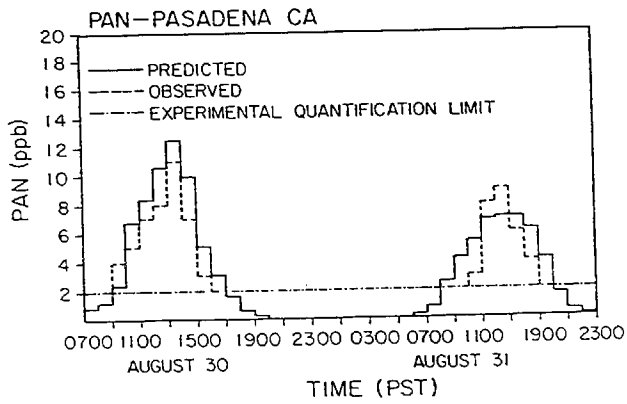

Figure 8. Comparison of predicted and observed PAN concentrations at Pasadena on 30–31 August 1982.

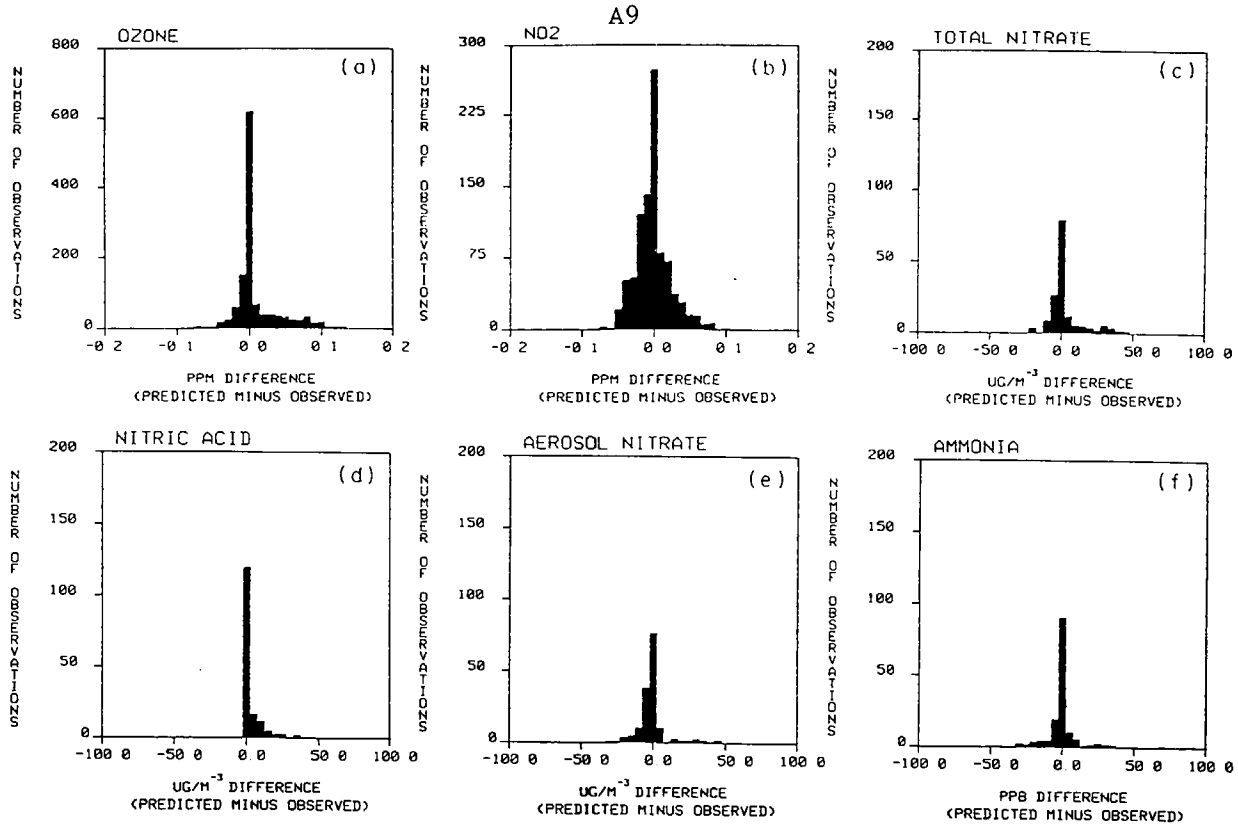

Figure 9. Histogram of concentration residuals (predicted minus observed) determined over all times and locations of the 2-day period, 30–31 August 1982: (a) O_3, (b) NO_2, (c) total inorganic nitrate, (d) nitric acid, (e) aerosol nitrate, and (f) ammonia.

total inorganic nitrate (this is a test of the photochemical, gas-phase mechanism); (2) the ability to reproduce correctly the NH_3 concentrations (this evaluates the accuracy of the ammonia emissions inventory and transport calculations); (3) given that the first two steps are handled adequately, use of the predicted NH_3 concentrations to apportion the TN between the gas and aerosol phases. Approaching the problem in this order, a statistical comparison of the paired predicted and observed TN concentrations was constructed and is summarized in Table V. The average of the predicted TN concentrations was 15.6μg m^{-3}, and the average of the observations was 12.9 μg m^{-3}, showing good agreement with little model bias. Regression analysis of TN predictions on observations also showed good agreement (slope 1.15, intercept 0.7 μg m^{-3}). Residual frequency histograms for TN, AN, HNO_3, and NH_3 are shown in Figure 9. This analysis indicates that the model is adequately predicting the TN concentrations. Improved correlations between predictions and observations over time would be achieved if the morning TN peaks that occur as the mixing depth is increasing rapidly were predicted more accurately. The residual histograms for AN and NH_3 are very similar to that for TN. While most HNO_3 predictions are within a few micrograms per cubic meter of the observations, Figure 9 shows that HNO_3 is overpredicted more often than it is underpredicted.

Given the spatial distribution of emissions as shown in Figure 2 and the generally westerly winds, one would expect that the greatest NH_3 concentrations would be found in the eastern portion of the air basin. Comparison of measured and predicted NH_3 levels confirms that speculation (e.g., compare NH_3 levels in Figure 5 to those in Figure 7). Statistical analysis of that comparison at all monitoring sites is shown in Table V. Given the possible uncertainties in the NH_3 inventory (as discussed in ref 1), the model accurately predicts the NH_3 levels throughout the basin.

Having completed steps 1 and 2 above, the final test is to determine how well the model apportions the inorganic nitrate between the gas and aerosol phases. Since it was impossible to include the heterogeneous reaction between nitric acid and preexisting aerosol within this modeling framework due to the lack of an emissions inventory for alkaline and ionic aerosols, one does not expect that the aerosol nitrate formation calculation will work well at all sites. This expectation is confirmed in Table V. However, aerosol nitrate concentration predictions do match observations closely at sites like Anaheim where an ion balance on measured aerosol composition shows that NH_4NO_3 is present (22) and where TN levels were predicted correctly.

Conclusions

An Eulerian grid-based photochemical airshed model has been employed to study the formation of nitrogen-containing air pollutants. Comparison of model predictions to observations in California's South Coast Air Basin over 2 days in August 1982 shows that the model predictions for O_3, total inorganic nitrate, and PAN match observations closely. Predicted NO_2 levels showed little bias when compared to the measurements, and predicted peak NO_2 concentrations also matched measurements in magnitude. Apportionment of the inorganic nitrate between the gas and aerosol phases at near-coastal sites is hindered by the absence of an emission inventory for preexisting aerosol that is available to react with HNO_3(g).

Results from the present grid-based modeling study may be compared to a previous trajectory modeling study (*1*). The trajectory version employing the same chemical mechanism and the same input data applied to the same days in 1982 produces results at Rubidoux that match observations more closely than the grid-based version of the same model. The reasons for these differences must be due to fundamental differences in the transport cal-

culations, including the better vertical resolution of the trajectory model, the absence of horizontal numerical diffusion in the trajectory model, and the effect of boundary and initial conditions on the grid model. The grid-based version of the photochemical airshed model tested here has the advantage of increased spatial coverage when compared to the trajectory model and, thus, can be used to efficiently examine the basinwide consequences of emissions changes. In paper 2 of this series, the effect of a variety of candidate emission control programs on Los Angeles nitrate air quality will be examined.

Registry No. PAN, 2278-22-0; NH_4NO_3, 6484-52-2; O_3, 10028-15-6; NO_2, 10102-44-0; NH_3, 7664-41-7; HNO_3, 7697-37-2.

Literature Cited

(1) Russell, A. G.; Cass, G. R. *Atmos. Environ.* **1986**, *20*, 2011–2025.
(2) Russell, A. G.; Cass, G. R. *Atmos. Environ.* **1984**, *18*, 1815–1827.
(3) Seinfeld, J. H. *Air Pollution: Physical and Chemical Fundamentals*; McGraw-Hill: New York, 1975.
(4) McRae, G. J.; Goodin, W. R.; Seinfeld, J. H. *Atmos. Environ.* **1982**, *16*, 679–696.
(5) McRae, G. J.; Tilden, J. W.; Seinfeld, J. H. *Comput. Chem. Eng.* **1982**, *6*, 15–25.
(6) Russell, A. G.; McRae, G. J.; Cass, G. R. *Atmos. Environ.* **1983**, *17*, 949–964.
(7) McRae, G. J.; Seinfeld, J. H. *Atmos. Environ.* **1983**, *17*, 501–522.
(8) Baulch, D. L.; et al. *J. Phys. Chem. Ref. Data* **1982**, *11*, 327–496.
(9) Russell, A. G.; McRae, G. J.; Cass, G. R. *Atmos. Environ.* **1985**, *19*, 893–903.
(10) McRae, G. J. Ph.D. Thesis, California Institute of Technology, Pasadena, CA, 1981.
(11) Stelson, A. W.; Seinfeld, J. H. *Atmos. Environ.* **1982**, *16*, 983–992.
(12) Goodin, W. R.; McRae, G. J.; Seinfeld, J. H. *J. Appl. Meteorol.* **1979**, *18*, 761–771.
(13) Ranzieri, A. "1982-SCAB Point and Area Source Emissions"; forwarded magnetic tape AR3288; California Air Resources Board: Sacramento, CA, 1983; personal communication.
(14) Ranzieri, A. "1982-SCAB Mobile Source Emissions"; forwarded magnetic tape AR3292; California Air Resources Board: Sacramento, CA, 1984; personal communication.
(15) Cass, G. R.; Gharib, S. "Ammonia Emissions In The South Coast Air Basin 1982."; open file report 84-2; Environmental Quality Laboratory, California Institute of Technology: Pasadena, CA, 1984.
(16) Blumenthal, D. L.; White, W. H.; Smith, T. B. *Atmos. Environ.* **1978**, *12*, 893–907.
(17) Edinger, J. G. *Environ. Sci. Technol.* **1973**, *7*, 247–252.
(18) Blumenthal, D. L., Sonoma Technology, personal communication, 1984.
(19) Grosjean, D.; Fung, K. *J. Air Pollut. Control Assoc.* **1984**, *34*, 537–543.
(20) Killus, J. P. Presented at the XVth Informal Conference on Photochemistry, Stanford, CA, June 27–July 1, 1984.
(21) Horie, Y. *Ozone Episode Representativeness Study for the South Coast Air Basin*; Valley Research Corp.: Van Nuys, CA, 1987.
(22) Hildemann, L. M.; Russell, A. G.; Cass, G. R. *Atmos. Environ.* **1984**, *18*, 1737–1750.
(23) Bencala, K. E.; Seinfeld, J. H. *Atmos. Environ.* **1979**, *13*, 1181–1185.
(24) Fox, D. *Bull. Am. Meteorol. Soc.* **1981**, *62*, 599–609.
(25) Rao, S. T.; Visalli, J. R. *J. Air Pollut. Control Assoc.* **1981**, *31*, 851–860.

Received for review December 8, 1986. Accepted July 9, 1987. This work was supported by the California Air Resources Board under Agreement A2-150-32 and by gifts to the Environmental Quality Laboratory.

Appendix B

Mathematical Modeling of the Formation of Nitrogen-Containing Air Pollutants. 2. Evaluation of the Effect of Emission Controls

Reprinted from ENVIRONMENTAL SCIENCE & TECHNOLOGY, Vol. 22, Page 1336 November 1988

Mathematical Modeling of the Formation of Nitrogen-Containing Pollutants. 2. Evaluation of the Effect of Emission Controls

Armistead G. Russell

Department of Mechanical Engineering, Carnegie Mellon University, Pittsburgh, Pennsylvania 15213

Kenneth F. McCue and Glen R. Cass*

Environmental Engineering Science Department and Environmental Quality Laboratory, California Institute of Technology, Pasadena, California 91125

■ A grid-based Eulerian airshed model is used to study the effect of specific emission control measures on ambient NO_2, total inorganic nitrate (TN), HNO_3, aerosol nitrate, PAN, NH_3, and ozone concentrations in the Los Angeles area. NO_x and reactive hydrocarbon (RHC) emission reductions of up to 61 and 37%, respectively, are examined. NO_2 and TN concentration reductions in excess of 50% averaged over 20 monitoring sites are achieved at the highest level of emission control studied. The distribution of TN air quality improvements between HNO_3 and aerosol nitrate is affected by the NH_3 emission rate of the NO_x control technologies employed. Peak 1-h O_3 concentrations at many sites in the eastern portion of the air basin studied decline by more than 25% at the highest NO_x and RHC control levels studied.

Introduction

In part 1 of this series, the performance of a grid-based photochemical airshed model for NO_2, total inorganic nitrate (TN), PAN, HNO_3, NH_3, aerosol nitrate (AN), and ozone formation and transport was evaluated (*1*). Model predictions were compared against experimental observations made for this purpose in the Los Angeles area over the period August 30–31, 1982. It was found that O_3 and PAN concentration predictions were in excellent agreement with observations and that NO_2 predictions were in closer agreement with observed values than in many previous studies. On average, TN, NH_3, and HNO_3 concentration predictions differed from observations by very small absolute amounts: 2.7 $\mu g\ m^{-3}$ (1.1 ppb), 0.7 ppb; and 4.2 $\mu g\ m^{-3}$ (1.65 ppb), respectively.

In this paper, that model will be used to explore the effect of specific emission control measures on the HNO_3/NH_3/aerosol nitrate system. Newly adopted ambient air quality standards for particulate matter in sizes less than 10-μm diameter (PM_{10}) have focused attention on the importance of aerosol nitrate control. Recent measurements of PM_{10} concentrations and chemical composition in the Los Angeles area show a peak 24-h average PM_{10} concentration of 299 $\mu g/m^3$ at Rubidoux near Riverside, CA, during the year 1986 (*2*). That PM_{10} concentration is approximately twice as high as allowed by the newly adopted PM_{10} standards of the U.S. Environmental Protection Agency, and 6 times higher than the State of California 24-h average PM_{10} ambient air quality standard. On the peak day in question (October 29, 1986), aerosol nitrate plus associated ammonium ion accounted for more than 40% of the observed PM_{10} peak value (*2*). Clearly, it will not be possible to attain compliance with PM_{10} air quality standards in the Riverside area without considering the approaches available to reduce aerosol nitrate concentrations via emission controls. Key questions that must be addressed include: (1) What effects would controls on reactive hydrocarbons (RHC) and oxides of nitrogen (NO_x) emissions have on aerosol nitrate concentrations? (2) How would controls on ammonia emissions affect HNO_3 and NH_4NO_3 concentrations? (3) If NH_3 injection technology is used for NO_x control at stationary sources, would the NH_3 emissions from such systems aggravate the NH_4NO_3 aerosol control problem? While the principal focus of this work is directed at examining the effect of emission controls on the $HNO_3/NH_3/NH_4NO_3$ system, further information on the response of NO_2, O_3, and PAN concentrations to emission controls is obtained as a byproduct of the analysis.

Emission Control Opportunities

Emission control measures evaluated as part of this study are itemized in Table I. That table has been divided into five groups. Group 1 controls reflect a subset of the reduction possibilities that have been documented as part of the 1982 Air Quality Management Plan (AQMP) for the South Coast Air Basin that surrounds Los Angeles (*3*). This group of controls approximates the effect of many of the emission reductions that were expected to be implemented in the Los Angeles area in the years following the 1982 base year, but without extension of vehicular catalyst utilization or ammonia injection technology beyond that used in 1982. Group 2 and group 3 controls simulate the effect of fleetwide improvements in emissions from motor vehicles at target levels that have been discussed by state and federal regulatory agencies (*7*, *9*). Group 4 and group 5 controls would further reduce NO_x emissions from stationary sources through the use of noncatalytic ammonia injection or selective catalytic reduction (SCR) technology.

The 1982 emission inventory employed during the model verification effort of part 1 of this study (*1*, *15*) will be referred to as the base case. The 1982 base case emissions from each source class that will be considered for control are given in Table I, along with the percentage reduction in those emissions that would result if the control measures

 0013-936X/88/0922-1336$01.50/0

had been in effect during 1982 [i.e., 84% reduction implies that (1–84/100) = 0.16 times the base case emissions from a stated source class would remain if the stated control measure had been implemented]. Although several of the control measures cited are cross-referenced to the AQMP planning document, the base year emission inventory of the present study (1982) differs from the 1979, forecast 1987, and forecast year 2000 inventories used in the AQMP. The objective of the present study is to provide information on the air quality effects that would be observed if the controls listed in Table I had been applied during the 1982 base case model verification days in the amounts specified. No attempt will be made to simulate the effect of emission controls during some hypothetical future year.

The largest number of control measures in group 1 of Table I (those designated B-1–B-8) are aimed at reducing solvent vapor emissions from painting and surface coating operations, usually through reformulation of the coating material or through reduced overspray during application. Reduction in fugitive hydrocarbon emissions from landfill gas leaks and oil and gas field fixture leaks is anticipated. The remaining hydrocarbon controls would suppress solvent losses from cleaning operations and pesticide application or capture certain industrial process emissions by using incineration, activated carbon adsorption, or other vapor recovery methods.

Stationary source oxides of nitrogen controls included in group 1 involve relatively straightforward modification of combustion system design, but without the use of ammonia injection or selective catalytic reduction technology. The effect of a mandatory vehicle inspection and maintenance program involving a no-load idle test, followed by repairs to the vehicle designed to correct defects observed, also is included among the relatively simple control measures in group 1.

Two further levels of mobile source NO_x control were considered. At the group 2 level in Table I, the entire light-duty vehicle fleet was assumed to have achieved a NO_x emission rate of 0.7 g/mi, while the NO_x emissions from medium-duty trucks were assumed to be reduced to 1.5 g/mi, and the NO_x emissions from heavy-duty trucks were assumed to be reduced to 10.7 g/BHP-h. There are two ways that one could view this case with 0.7 g/mi NO_x emitted from the light-duty vehicle fleet. Since new cars sold in California must presently meet a 0.7 g/mi NO_x standard, this level of control could be used to approximate a successful completion of conversion of the entire vehicle fleet to meet current regulatory objectives for new cars, in combination with a high level of catalyst system durability and maintenance. In the absence of high durability and maintenance, catalyst system deterioration can be expected to increase actual on-road emissions to levels above legal objectives. The 0.7 g/mi NO_x fleetwide emission rate employed here closely approximates the introduction of a fleet of cars initially set to achieve 0.4 g/mi NO_x when new, followed by a typical degree of control system deterioration in the hands of the final consumer. The 10.7 g/BHP-h NO_x objective for heavy-duty trucks reflects an intermediate level of control proposed by the U.S. Environmental Protection Agency (*9*).

Mobile source controls shown in group 3 reflect the emission pattern that would result if the 0.4 g/mi NO_x and 0.41 g/mi total hydrocarbon (THC) emission rate for light-duty vehicles called for under the Clean Air Act in fact were achieved and maintained by the vehicle fleet. Increased control system durability or maintenance would be needed for this event to occur. Further NO_x reductions from heavy-duty vehicles have been added to group 3, at the most stringent level discussed by the federal government (*9*).

NO_x emission reductions from stationary combustion sources can be achieved by noncatalytic ammonia injection into the stack exhaust within a narrow exhaust temperature range. This direct NH_3 injection technology has been demonstrated on a utility boiler in the Los Angeles area (*10*). NO_x emission reductions in the vicinity of 50% are observed, accompanied by significant bleed-through of NH_3 into the atmosphere. Group 4 controls in Table I simulate the installation of such controls on all of the largest stationary combustion sources in the South Coast Air Basin. A major objective of our analysis of this group of controls is to determine if aerosol nitrate formation would be suppressed or enhanced by this NO_x emission reduction combined with NH_3 emission increase.

Selective catalytic reduction (SCR) technology involves NO_x abatement by injection of NH_3 into stationary source exhaust in the presence of a catalyst. Control efficiencies are generally higher than in the case of the direct noncatalytic NH_3 injection systems cited in control group 4, and NH_3 bleed-through into the atmosphere is reduced. The effect of SCR technology applied to a variety of stationary sources in the Los Angeles area is indicated in group 5 of Table I.

By applying the controls of Table I in various combinations, a matrix of control opportunities can be constructed that represents the trade-off between increasingly stringent stationary source control vs increasingly stringent mobile source control, as shown in Table II. Ten cases will be defined. Beginning near the upper left corner of Table II, the base case 1982 emission inventory first will be perturbed by applying the group 1 controls from Table I to the emission sources. Moving from left to right across the top of the table, increasingly stringent mobile source controls are added to the group 1 stationary source controls. Moving from top to bottom along the left edge of the table, increasingly demanding stationary source NO_x controls are added to a minimal motor vehicle control program. At the lower right corner of that table, the intersection of all of the most stringent mobile and stationary source controls is applied. The headings aligned with the columns and rows of Table II are suggestive of the maximum cumulative degree of NO_x control achieved in each case; the hydrocarbon controls shown in Table I also are included.

The 10th perturbed case examined here explores the effect of NH_3 emission reduction alone. The base case 1982 emission inventory for NO_x and hydrocarbons remains untouched, but all of the NH_3 emissions from livestock waste decomposition and farming activities in the air basin are removed. This perturbation completely eliminates the large spike in the NH_3 inventory centered over the Chino dairy area in western Riverside and San Bernardino Counties (see Figure 2 of ref 1). That emission reduction may occur in the near future without the action of governmental air pollution control agencies. Rapid urban development in that area of both counties could displace the dairy industry within a few years.

Effect of Emission Controls

The grid-based air quality model evaluated in part 1 of this study (*1*) was used to determine the effects on air quality that could be expected if each of the combinations of emission control measures defined in Table II were applied in the South Coast Air Basin (SoCAB). For each set of control measures considered, the base case 1982 emission inventory for the SoCAB discussed in ref 1 and

Table I. Specific Emission Control Measures and Their Effect if Applied to 1982 Emissions in the South Coast Air Basin

		1982 THC[a] emissns, ton/day	1982 NO_x emissns, ton/day	1982 NH_3 emissns, ton/day[a]	control measure	effect of controls: THC change, %[m]	NO_x change, %[m]	NH_3 change, %[m,n]	ref
					Group 1				
1	wood furniture finishing	16.6			use of water-based coatings and reduced overspray (B-5)	−54.1			3
2	auto refinishing	6.7			use of low solvent or water-based coatings (B-8)	−21.0			3
3	wood flatstock coating	1.5			afterburners on drying and curing ovens (B-1)	−75.0			3
4	industrial maintenance coatings	6.3			use of low solvent or water-based coatings (B-2)	−39.3			3
5	marine coatings	2.4			use of low solvent or more durable coatings (B-3)	−82.8			3
6	motor vehicle manufacturing (painting)	8.2			electrostatic coating and high solids paint (B-4)	−41.2			3
7	metal parts manufacturing (coatings)	25.8			substitute coatings (B-6)	−28.6			3
8	aerospace coatings	4.6			use of low solvent coatings (B-7)	−40.5			3
9	oil and gas well leak reduction	27.3			semiannual inspection and maintenance (A-3)	−50.0			3
10	pesticide application	12.9			changes in formulation and application methods (C-3)	−27.3			3
11	metal and nonmetal parts cleaning	40.6			covers on circuit board degreasers; fewer exemptions (C-1)	−12.8			3
12	paper and fabric coating	10.6			afterburners or activated carbon adsorption on curing ovens (D-2)	−50.0			3
13	dry cleaning	17.9			reduced transfer emissions (wash and dry in a single unit) (G-3)	−35.8			3
14	landfill gas recovery	778.0[a]			methane recovery (F-1)	−46.1[a]			3
15	rubber products manufacturing	3.6			incineration or carbon adsorption on fugitive organics emissions (D-3)	−10.3			3
16	synthetic chemical manufacturing	2.1			chemical absorbers, carbon adsorption, and process changes (G-1)	−90.9			3
17	marine fuel transfer	0.4			vapor recovery systems (A-7)	−90.9			3
18	graphic arts industry	11.9			high solids or waterborne ink; incineration or adsorption (G-2)	−85.0			3
19	refinery boilers and heaters		40.3		combustion modification		−8.0		4
20	residential water heaters		10.3		intermittent ignition devices and stack vent valves (N-18)		−25.0		3
21	nonrefinery industrial boilers		35.0		combustion modification (G-11)		−25.0		3
22	cement kilns		9.7		combustion modification (G-7)		−40.0		3
23	glass furnaces		3.2		process modification		−45.3		5
24	light-duty highway vehicle exhaust	439.0	427.0		inspection and maintenance (no-load idle test and repair)	−11.3	−9.4		6
					Group 2 Additional Mobile Source Control				
25	light-duty highway vehicle exhaust	439.0	427.0	2.8	entire fleet meets 0.7 g/mi NO_x and 0.41 g/mi THC objective; NH_3 emissions reach 0.0035 g/km; inspection and maintenance program continued	−84.8	−73.3	222	*b*, 7, 8
26	heavy-duty diesel highway vehicle exhaust	25.8	157.0	0.02	entire fleet meets objective of 10.7 g NO_x/BHP-h and 2.65 g/mi THC	−30.0	−25.9		*c*, 9
27	heavy-duty gasoline highway vehicle exhaust	18.6	35.7	(0.1)	entire fleet meets objective of 10.7 g NO_x/BHP-h and 2.65 g/mi THC	−49.2	−34.8	0	*d*, 9
28	medium-duty highway vehicle exhaust (gasoline and diesel)	32.6	38.7	(0.3)	entire fleet meets 1.5 g/mi NO_x and 0.6 g/mi THC objective (NH_3 emissions reach 0.035 g/km)	−82.0	−62.1	(+83)	*e*, 8, 9
					Group 3 Stringent Mobile Source Control				
29	light-duty highway vehicle exhaust	439.0	427.0	2.8	entire fleet meets objective of 0.40 g/mi NO_x and 0.41 g/mi THC (NH_3 emissions held at 0.035 g/km)	−84.8	−84.8	+222	*f*, 7, 8
30	heavy-duty diesel highway vehicle exhaust	25.8	157.0	0.02	entire fleet meets objective of 5.1 g NO_x/BHP-h and 2.65 g/mi THC	−30.0	−65	0	*f*, 9
31	heavy-duty gasoline highway vehicle exhaust	18.6	35.7	(0.1)	entire fleet meets objective of 5.1 g NO_x/BHP-h and 2.65 g/mi THC	−49.2	−69	0	*f*, 9
					Group 4 Stationary Source NO_x Control–Noncatalytic NH_3 Injection				
32	refinery boilers and heaters		40.3	(0.5)	direct NH_3 injection		−50	+869	*g*, 4
33	utility boilers		57.6	(1.6)	direct NH_3 injection		−40	+344	*h*, 10

Table I (Continued)

		1982 THC[a] emissns, ton/day	1982 NO_x emissns, ton/day	1982 NH_3 emissns, ton/day[n]	control measure	THC change, %[m]	effect of controls NO_x change, %[m]	NH_3 change, %[m,n]	ref
34	nonrefinery industrial boilers		35.0	(0.65)	direct NH_3 injection + combustion modification		−55	+392	*i*, 10
35	cement kilns			9.7	direct NH_3 injection		−50	+	11
36	glass melting furnaces			3.2	direct NH_3 injection		−50	+	5
	Group 5 Stationary Source NO_x Control–Selective Catalytic Reduction								
37	refinery boilers and heaters		40.3	(0.5)	selective catalytic reduction		−44	+small	*j*, 12
38	utility boilers		57.6	(1.6)	selective catalytic reduction		−90	+small	*k*, 13
39	nonrefinery industrial boilers		35.0	(0.65)	SCR plus combustion modification		−92	+small	*l*, 13
40	cement kilns			9.7	selective catalytic reduction		−90	+small	11
41	stationary industrial IC engines			74.2	use of catalytic converters		−66.7	+small	14
42	glass melting furnaces		3.2		selective catalytic reduction		−90.0	+small	5

[a] THC equals total hydrocarbon emissions; in all cases except landfill gas leak reduction and oil and gas well leak reduction, THC ≃ RHC (reactive hydrocarbon emissions). Landfill emissions are mostly methane, with only 1.4% non-methane hydrocarbons. Only the non-methane hydrocarbon (NMHC) data are used by the air quality model, and the percent of control shown applies to the NMHC content of the emissions only. [b] Computed by multiplying vehicle miles traveled (VMT) per day × 0.7 g/mi NO_x and 0.41 g/mi THC. NH_3 emissions become 9.14 metric tons/day. [c] Computed by taking emissions from a new (undeteriorated) 1984 heavy diesel truck as representing 6.5 g/BHP-h NO_x and also as equaling 10.31 g/mi NO_x. Ratio gives scale factor of 1.59 g mi^{-1}/(g/BHP-h) NO_x. If entire fleet achieves 10.7 g/BHP-h NO_x (representing a fleet average of 1984 trucks with deterioration) then emissions factor for entire fleet would be 17.0 g/mi. Emissions computed by multiplying VMT for heavy diesel vehicles × 17.0 g/mi. Hydrocarbon emissions obtained by multiplying 2.65 g/mi × heavy diesel vehicle VMT. [d] A new 1984 heavy gasoline truck emits 4.25 g/mi NO_x corresponding to 6.94 g/BHP-h. Calculation proceeds as in *c* above. [e] Computed by multiplying medium truck VMT per day × 1.5 g/mi NO_x and 0.6 g/mi THC. NH_3 emissions become 0.55 metric tons/day. [f] Emission reductions computed by procedure analogous to that for group 2 Mobile Source Controls (see footnotes *b*, *c*, or *d*). [g] NH_3 breakthrough is assumed to be 50 ppm NH_3 for reduction of 75 ppm NO_x (50%). Final NH_3 emission is 5.04 metric tons/day. [h] NH_3 breakthrough is 50 ppm NH_3 giving total NH_3 emissions of 7.1 metric tons/day. [i] Estimated based on utility boiler performance, see *h* and ref 10. [j] SCR achieves 90% NO_x control but is applied only to the largest units, yielding 44% reduction relative to the entire source class. [k] Ammonia bleed-through is 12 ppm. [l] 25% control by combustion modification plus 90% control via SCR, see *k* and also control measure 21 in Table I above. Rule-making process would probably choose to exclude smaller boilers, but no indication is yet given of where the line would be drawn. NH_3 break-through assumed to be 12 ppm. [m] Percent change in emissions is defined as follows: −84% implies that (1 − 84/100) = 0.16 × original 1982 emission rate remains after control; +222% implies that (1 + 222/100) = 3.22 × original 1982 emission rate remains after control. [n] NH_3 emission values in parentheses estimated from data of ref 8.

15 was modified to reflect the addition of that particular group of control measures. Then the air quality modeling calculations were executed over 2 days of simulation by using the modified emission inventory along with the meteorological conditions observed during the base case model verification days (August 30–31, 1982).

The initial conditions and boundary conditions supplied to the air quality model in each case were identical with those observed during August 30–31, 1982, as described in ref 1. The purpose of the first day of each 2-day simulation was to establish initial conditions for the second day of calculations that reflect the altered emissions into the air basin. The effect of emission controls on air quality then was determined by comparison between base case and postcontrol air quality predictions for the second day of each 2-day simulation. As changes in emission controls might affect the boundary conditions supplied to the model, a perturbation analysis of the effect of altered upper level boundary conditions was conducted. Reducing the upper level inflow O_3 boundary conditions from those estimated for August 30–31, 1982, to 0.04 ppm all around the border of the modeling region reduced base case peak O_3 concentrations on August 31 by only 0.01 ppm. Inflow NO_x boundary conditions on August 30–31, 1982, were examined and found to be very low except along a small stretch of the southeast corner of the grid system. In summary, predicted changes in air quality on the second day of simulation are determined predominantly by changes in emissions into the model and not by altered initial or boundary conditions.

The results of this comparison of alterative emission control strategies are presented in several formats. First, an account of the changes in basinwide peak 1-h average pollutant concentrations is given in Table III. Base case peak pollutant levels as they were calculated for August 31, 1982, in the absence of further emission controls are stated in the upper left-hand corner of that table. Then for each combination of emission controls as defined in Table II, the predicted basinwide peak values are given, both in absolute concentration units and as a percent deviation from the precontrol base case. Since the effect of some control measures is to change the location or timing of the basinwide peaks, the values shown in Table III may not be typical of the effects seen at most air monitoring sites. Therefore in Table IV, the average change in the peak 1-h pollutant concentrations at the 20 sites shown in Figure 1 is given, along with the range of the changes observed between the least affected and most affected air monitoring stations.

As seen in the upper left corner of the matrix of control opportunities in Table II, completion of the stationary source evaporative hydrocarbon controls that are a part of the 1982 AQMP for the Los Angeles area plus stationary source combustion modifications and a vehicle maintenance program would result in a 5.4% reduction in basinwide NO_x emissions and a 9.3% reduction in reactive hydrocarbon (RHC) emissions. Comparison with Table IV shows that the 1-h peak levels of NO_2 and TN typically drop by an amount that is roughly proportional to the change in NO_x emissions. The greatest percentage decreases in total inorganic nitrate (TN) levels occur in the eastern portion of the air basin [from Pomona (TN = −5.5%) to Rubidoux (TN = −7.4%)], while TN levels decline by only 3–5% in the western part of the air basin. The effect on HNO_3 and AN levels likewise is highest in the eastern portion of the air basin. Basinwide maximum O_3 and PAN levels in this case decline by only 1.6 and 2.2% at the location of the basinwide 1-h peak (Table III),

Table II. Combinations of Mobile and Stationary Source Controls That Will Be Examined for Their Effect on Air Quality in the South Coast Air Basin[a]

STATIONARY SOURCE CONTROLS	MOBILE SOURCE CONTROLS: BASE CASE (1982 EMISSIONS (tons/day): THC = 2416; RHC = 1224; NO_x = 1120; NH_3 = 164)	VEHICLE INSPECTION AND MAINTENANCE: LIGHT DUTY FLEET 0.41 g/mi THC; 0.7 g/mi NO_x; HEAVY DUTY FLEET 2.65 g/mi THC 10.7 g/bhp-hr NO_x	VEHICLE INSPECTION AND MAINTENANCE: LIGHT DUTY FLEET 0.41 g/mi THC; 0.4 g/mi NO_x; HEAVY DUTY FLEET 2.65 g/mi THC 5.1 g/bhp-hr NO_x
AQMP EVAPORATIVE CONTROLS & COMBUSTION MODIFICATION	CONTROL MEASURES: 1-24 EFFECT ON EMISSIONS: RHC −9.3% NO_x −5.4% NH_3 NO CHANGE	CONTROL MEASURES: 1-28 EFFECT ON EMISSIONS: RHC −37.2% NO_x −36.6% NH_3 +3.9%	CONTROL MEASURES: 1-24,28-31 EFFECT ON EMISSIONS: RHC −37.2% NO_x −47.6% NH_3 +3.9%
AQMP + NON-CATALYTIC AMMONIA INJECTION	CONTROL MEASURES: 1-18,20,24,32-36 EFFECT ON EMISSIONS: RHC −9.3% NO_x −10.0% NH_3 +8.7%	CONTROL MEASURES: 1-18,20,24-28,32-36 EFFECT ON EMISSIONS: RHC −37.2% NO_x −41.2% NH_3 +12.7%	CONTROL MEASURES: 1-18,20,24,28-36 EFFECT ON EMISSIONS: RHC −37.2% NO_x −52.2% NH_3 +12.7%
AQMP + SELECTIVE CATALYTIC REDUCTION	CONTROL MEASURES: 1-18,20,24,37-42 EFFECT ON EMISSIONS: RHC −9.3% NO_x −18.4% NH_3 +0.7%	CONTROL MEASURES: 1-18,20,24-28,37-42 EFFECT ON EMISSIONS: RHC −37.2% NO_x −49.6% NH_3 +4.7%	CONTROL MEASURES: 1-18,20,24,28-31,37-42 EFFECT ON EMISSIONS: RHC −37.2% NO_x −60.6% NH_3 +4.7%

[a] Control measures refer to the control measures numbered in Table I. Labels on columns and rows of this table are indicative of the maximum degree of NO_x control required.

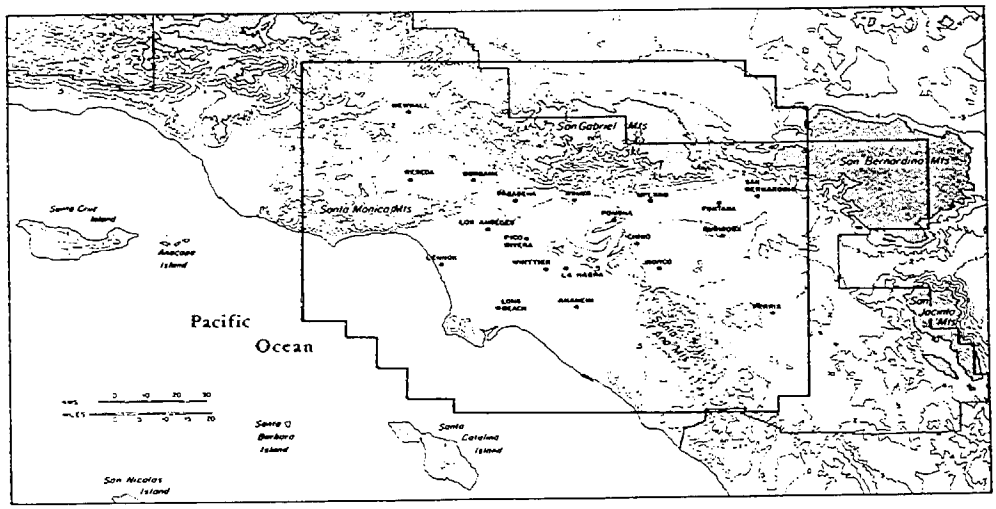

Figure 1. South Coast Air Basin showing 20 sites at which the effect of emission controls will be evaluated. Air quality modeling calculations are performed within the region bounded by the heavy solid line in the center of the map.

a reduction that is less than proportional to the degree of emission control achieved for either RHC or NO_x.

The effect of progressively more stringent NO_x controls on stationary sources alone is observed by moving down the left edge of Tables II–IV. Addition of noncatalytic ammonia injection technology at major stationary NO_x sources combined with AQMP hydrocarbon controls produces a net 10% reduction in basinwide NO_x emissions along with a +8.7% increase in basinwide NH_3 emissions, as seen in Table II. Most of these emissions changes occur in the heavily industrialized western portion of the air basin, which has very low ambient NH_3 levels at present (see Figures 2, 3, and 5 of ref 1). As a result of the NH_3 emissions from the ammonia injection systems, peak 1-h average ambient NH_3 levels near industrial areas at the coast (Long Beach and Lennox) rise by nearly 60%, while ambient NH_3 levels at central Los Angeles, La Habra, Anaheim, and Pico Rivera rise by 25% or more. HNO_3

Table III. Effect of Emission Controls on Basinwide Peak 1-h Average Pollutant Concentrations in the South Coast Air Basin, August 31, 1982[a]

	BASE CASE	MOBILE SOURCE CONTROLS: VEHICLE INSPECTION AND MAINTENANCE	MOBILE SOURCE CONTROLS: LIGHT DUTY FLEET 0.41 g/mi THC; 0.7 g/mi NO_x HEAVY DUTY FLEET 2.65 g/mi THC 10.7 g/bhp-hr NO_x	MOBILE SOURCE CONTROLS: LIGHT DUTY FLEET 0.41 g/mi THC; 0.4 g/mi NO_x HEAVY DUTY FLEET 2.65 g/mi THC 5.1 g/bhp-hr NO_x
STATIONARY SOURCE CONTROLS: AQMP EVAPORATIVE CONTROLS & COMBUSTION MODIFICATION		NO_2 0.150 ppm (−4.0%) TN 0.033 ppm (−6.8%) HNO_3 0.022 ppm (−9.2%) AN 85 μg m^{-3} (−5.5%) PAN 0.020 ppm (−2.2%) O_3 0.255 ppm (−1.6%)	NO_2 0.123 ppm (−21%) TN 0.021 ppm (−41%) HNO_3 0.013 ppm (−44%) AN 55 μg m^{-3} (−39%) PAN 0.018 ppm (−14%) O_3 0.230 ppm (−11%)	NO_2 0.089 ppm (−43%) TN 0.018 ppm (−48%) HNO_3 0.011 ppm (−55%) AN 49 μg m^{-3} (−47%) PAN 0.017 ppm (−19%) O_3 0.221 ppm (−15%)
STATIONARY SOURCE CONTROLS: AQMP + NON-CATALYTIC AMMONIA INJECTION	NO_2 0.156 ppm TN 0.036 ppm HNO_3 0.024 ppm AN 91 μg m^{-3} PAN 0.021 ppm O_3 0.26 ppm	NO_2 0.152 ppm (−2.6%) TN 0.033 ppm (−6.1%) HNO_3 0.021 ppm (−13%) AN 81 μg m^{-3} (−8.8%) PAN 0.020 ppm (−2.9%) O_3 0.254 ppm (−1.8%)	NO_2 0.118 ppm (−24%) TN 0.020 ppm (−42%) HNO_3 0.013 ppm (−45%) AN 52 μg m^{-3} (−41%) PAN 0.018 ppm (−15%) O_3 0.230 ppm (−11%)	NO_2 0.090 ppm (−42%) TN 0.017 ppm (−52%) HNO_3 0.010 ppm (−57%) AN 46 μg m^{-3} (−48%) PAN 0.016 ppm (−20%) O_3 0.219 ppm (−15%)
STATIONARY SOURCE CONTROLS: AQMP + SELECTIVE CATALYTIC REDUCTION		NO_2 0.155 ppm (−0.5%) TN 0.032 ppm (−9.2%) HNO_3 0.020 ppm (−13%) AN 78 μg m^{-3} (−14%) PAN 0.020 ppm (−4.6%) O_3 0.251 ppm (−3.1%)	NO_2 0.117 ppm (−25%) TN 0.019 ppm (−47%) HNO_3 0.012 ppm (−50%) AN 48 μg m^{-3} (−47%) PAN 0.017 ppm (−18%) O_3 0.224 ppm (−13%)	NO_2 0.073 ppm (−53%) TN 0.014 ppm (−59%) HNO_3 0.009 ppm (−59%) AN 39 μg m^{-3} (−57%) PAN 0.016 ppm (−22%) O_3 0.215 ppm (−17%)

[a] The combinations of emission control technologies considered in each cell of this matrix are defined in Tables I and II. Values shown are the peak 1-h average concentrations in the presence of the emission controls, followed by the percent of change relative to the base case (in parentheses). Aerosol nitrate concentrations shown are computed as if the aerosol is pure NH_4NO_3.

levels drop by as much as 25% at Lennox and by more than 13% at central Los Angeles, Anaheim, La Habra, and Pico Rivera, but this is largely due to the formation of additional aerosol nitrates by reaction of HNO_3 with the increased NH_3. Peak 1-h average aerosol nitrate levels rise by 14–21% at central Los Angeles, Long Beach, and Lennox in the presence of this NH_3 emission increase. Farther downward, in the vicinity of the Chino dairy area, the air is already loaded with very high NH_3 levels even in the base case (e.g., 0.67 ppm 1-h peak at Chino, see Table IV). As a result, NH_3 air quality at Chino is insensitive to small changes in upwind NH_3 emissions. The reduction in NO_x emissions that is achieved through a combination of controls that includes noncatalytic NH_3 injection at upwind sources does act to reduce TN and aerosol nitrate levels at Chino by 7–8%. In summary use of noncatalytic ammonia injection technology for NO_x emission reduction has the potential to degrade NH_3 and aerosol nitrate air quality in the industrialized western portion of the South Coast Air Basin, accompanied by aerosol nitrate concentration reductions in already NH_3-enriched agricultural areas downward.

Through addition of selective catalytic reduction (SCR) technology on stationary sources, combined with AQMP hydrocarbon controls, an 18% reduction in basinwide NO_x emissions is achieved relative to base case 1982 emissions accompanied by only a 0.7% increase in NH_3 emissions (lower left corner, Tables II–IV). These stationary source NO_x reductions are concentrated at a few major point source locations (e.g., power plants and petroleum refineries). As a result, the effect of these controls varies greatly between monitoring sites. When SCR is added to major point sources, NO_2 concentration reductions of 12–15% occur at Burbank, Long Beach, Azusa, and Anaheim. Typically, NO_2 levels in that case decline by 8.5% averaged over the 20 locations cited in Figure 1 and Table IV. At the location of the basinwide NO_2 concentration peak and at Upland and Fontana, NO_2 concentration reductions are small (2.6% or less). Total inorganic nitrate concentration improvements show less variability between monitoring sites: TN levels decline by 11–14% in the eastern portion of the air basin (from Pomona to Rubidoux) and by 5–10% in the western area of the basin. Reductions in basinwide 1-h peak HNO_3 and AN levels of 13 and 14%, respectively, also are computed. The basinwide peak O_3 and PAN concentrations decline slightly as stationary source NO_x controls are applied. At five of the sites shown in Figure 1 in the area from central Los Angeles and Pasadena to La Habra, addition of SCR on stationary sources alone causes peak 1-h O_3 levels to increase relative to the base case, but that increase is +3% or less. PAN air quality changes by amounts that are less than proportional to the NO_x reduction achieved, with 7 of the 20 sites studied experiencing a PAN increase. In short, with addition of SCR technology on stationary sources alone, improvements in many NO_x-related species concentrations are achieved. Those improvements are less than proportional to the NO_x emissions change and are accompanied by slight increases

Table IV. Effect of Emission Controls on Peak 1-h Average Pollutant Concentrations Observed at the 20 Sites Shown in Figure 1[a]

	BASE CASE	MOBILE SOURCE CONTROLS: VEHICLE INSPECTION AND MAINTENANCE	MOBILE SOURCE CONTROLS: LIGHT DUTY FLEET 0.41 g/mi THC; 0.7 g/mi NO_x HEAVY DUTY FLEET 2.65 g/mi THC 10.7 g/bhp-hr NO_x	MOBILE SOURCE CONTROLS: LIGHT DUTY FLEET 0.41 g/mi THC; 0.4 g/mi NO_x HEAVY DUTY FLEET 2.65 g/mi THC 5.1 g/bhp-hr NO_x
	NO_2 0.087 ppm (0.135-0.029 ppm) TN 0.022 ppm (0.031-0.009 ppm) HNO_3 0.012 ppm (0.021-0.006 ppm) NH_3 0.070 ppm (0.668-0.010 ppm) AN 42 $\mu g\ m^{-3}$ (85 $\mu g\ m^{-3}$-16 $\mu g\ m^{-3}$) PAN 0.011 ppm (0.018-0.006 ppm) O_3 0.170 ppm (0.233-0.110 ppm)			
STATIONARY SOURCE CONTROLS: AQMP EVAPORATIVE CONTROLS & COMBUSTION MODIFICATION		NO_2 -5.1% (-8.3% to -1.4%) TN -4.8% (-7.4% to -3.0%) HNO_3 -4.1% (-7.0% to -0.9%) NH_3 +1.0% (-3.5% to +10.1%) AN -3.4% (-6.7% to -1.1%) PAN -2.7% (-4.3% to -0.6%) O_3 -1.8% (-2.9% to -0.7%)	NO_2 -37.4% (-49.7% to -19.1%) TN -35.7% (-41.2% to -22.1%) HNO_3 -31.8% (-46.5% to -14.8%) NH_3 +10.6% (-4.1% to +29.8%) AN -22.7% (-40.1% to -4.4%) PAN -15.6% (-25.7% to -1.3%) O_3 -11.7% (-18.9% to -4.1%)	NO_2 -45.6% (-59.5% to -26.1%) TN -45.6% (-52.8% to -26.8%) HNO_3 -40.0% (-53.7% to -18.6%) NH_3 +9.0% (-5.9% to +27.4%) AN -34.0% (-52.8% to -17.1%) PAN -14.3% (-28.8% to +2.1%) O_3 -12.8% (-23.6% to -1.1%)
STATIONARY SOURCE CONTROLS: AQMP + NON-CATALYTIC AMMONIA INJECTION		NO_2 -5.9% (-9.1% to -0.04%) TN -5.5% (-8.4% to -3.2%) HNO_3 -9.3% (-25.0% to -3.6%) NH_3 +17.3% (-15.8% to +60.5%) AN +3.7% (-7.7% to +20.7%) PAN -2.0% (-4.2% to +2.2%) O_3 -1.7% (-3.1% to +0.6%)	NO_2 -38.4% (-50.9% to -19.0%) TN -36.7% (-41.8% to -22.4%) HNO_3 -34.4% (-49.0% to -21.0%) NH_3 +27.9% (-7.3% to +68.0%) AN -19.0% (-39.0% to +3.3%) PAN -15.3% (-25.1% to -0.1%) O_3 -11.7% (-19.0% to -1.6%)	NO_2 -46.9% (-59.8% to -27.2%) TN -46.8% (-54.5% to -28.2%) HNO_3 -42.5% (-55.7% to -24.9%) NH_3 +28.0% (-8.5% to +67.4%) AN -31.2% (-54.1% to -9.0%) PAN -14.3% (-30.0% to +3.1%) O_3 -13.4% (-24.4% to -1.2%)
STATIONARY SOURCE CONTROLS: AQMP + SELECTIVE CATALYTIC REDUCTION		NO_2 -8.5% (-14.9% to -1.8%) TN -8.9% (-14.3% to -5.0%) HNO_3 -9.9% (-13.3% to -6.0%) NH_3 +4.0% (-13.4% to +25.0%) AN -4.8% (-13.8% to +3.2%) PAN +0.4% (-7.1% to +7.7%) O_3 -1.4% (-4.9% to +3.0%)	NO_2 -42.4% (-55.3% to -21.4%) TN -41.3% (-46.9% to -25.5%) HNO_3 -37.7% (-51.0% to -21.2%) NH_3 +12.6% (-8.2% to +36.0%) AN -27.6% (-46.8% to -8.6%) PAN -14.3% (-27.6% to +1.0%) O_3 -12.6% (-22.2% to -2.8%)	NO_2 -51.9% (-67.4% to -27.8%) TN -52.3% (-60.0% to -33.1%) HNO_3 -47.3% (-60.7% to -27.1%) NH_3 -13.7% (-6.6% to +38.5%) AN -39.6% (-59.8% to -24.2%) PAN -14.8% (-36.0% to +7.2%) O_3 -15.0% (-28.2% to -0.7%)

[a] Values shown are averages over the 20 sites, followed by the range of the values observed among the 20 sites (in parentheses). Aerosol nitrate concentrations shown are computed as if the aerosol is pure NH_4NO_3.

in O_3 and PAN at a few locations.

The effect of progressively more stringent mobile source controls alone can be examined by moving from left to right across the upper row of Tables II–IV. As seen in Table II, complete conversion of the vehicle fleet to an intermediate level of mobile source control (light-duty fleet meets 0.41 g/mi THC; 0.7 g/mi NO_x along with additional heavy-duty vehicle controls plus AQMP stationary source controls) would result in a 37% reduction in basinwide NO_x emissions and a 37% reduction in RHC emissions relative to the base case. Tables III and IV show that major improvements in TN, HNO_3, and AN levels would result, with improvements almost directly proportional to the NO_x emission reduction achieved. Basinwide peak O_3 and PAN concentrations decline by 11 and 14%, respectively.

Further reduction in NO_x emissions from motor vehicles alone is examined in the upper right-hand corner of Tables II–IV. If a 0.4 g/mi NO_x emission rate from the light-duty fleet had been achieved in 1982 along with strict heavy truck NO_x controls, NO_x emissions would have been reduced by 48% relative to the base case, with similar major improvements in ambient NO_2, TN, HNO_3, and AN concentrations. Basinwide peak O_3 and PAN concentrations both decline by an additional 4% as additional NO_x controls are added to the vehicle fleet without further hydrocarbon controls beyond the 0.41 g/mi THC light-duty vehicle standard examined in the preceding square on the top row of Table II.

As seen in the lower right-hand corner of Table II, the simultaneous use of all mobile and stationary source control measures considered here would reduce NO_x emissions relative to the base case by 61% in the presence of a 37% decline in RHC emissions. This combination of controls is more effective than controls on either the mobile or stationary sources alone. Basinwide peak total inorganic nitrate, HNO_3, and aerosol nitrate concentrations are reduced by nearly 60%. Basinwide peak NO_2 concentrations are reduced by 53%. A 17% reduction in the basinwide peak O_3 concentration is achieved. The 1-h O_3 concentration peak is reduced relative to the base case at every site shown in Figure 1.

As is seen from Tables III and IV, the simultaneous use of all of the mobile and stationary source control measures considered produces major improvements compared to the base case in many air quality parameters at the time of the daily pollutant concentration peaks. The performance of that combination of control measures is explored in detail in Figures 2–7. Figure 2 gives the spatial distribution of pollutant concentrations in the presence of the maximum degree of NO_x control studied. By subtracting these pollutant levels from the spatial distribution of concentrations predicted by the base case simulation (see Figure 3 of ref 1), it is possible to define the spatial distribution of pollutant concentration changes experienced due to the emission controls, as seen in Figure 3. Figures 4–6 permit rapid visualization of changes in the diurnal pattern of pollutant levels at key monitoring sites characteristic of the western and eastern portions of the air basin. In Figure 7, the effect of this set of emissions

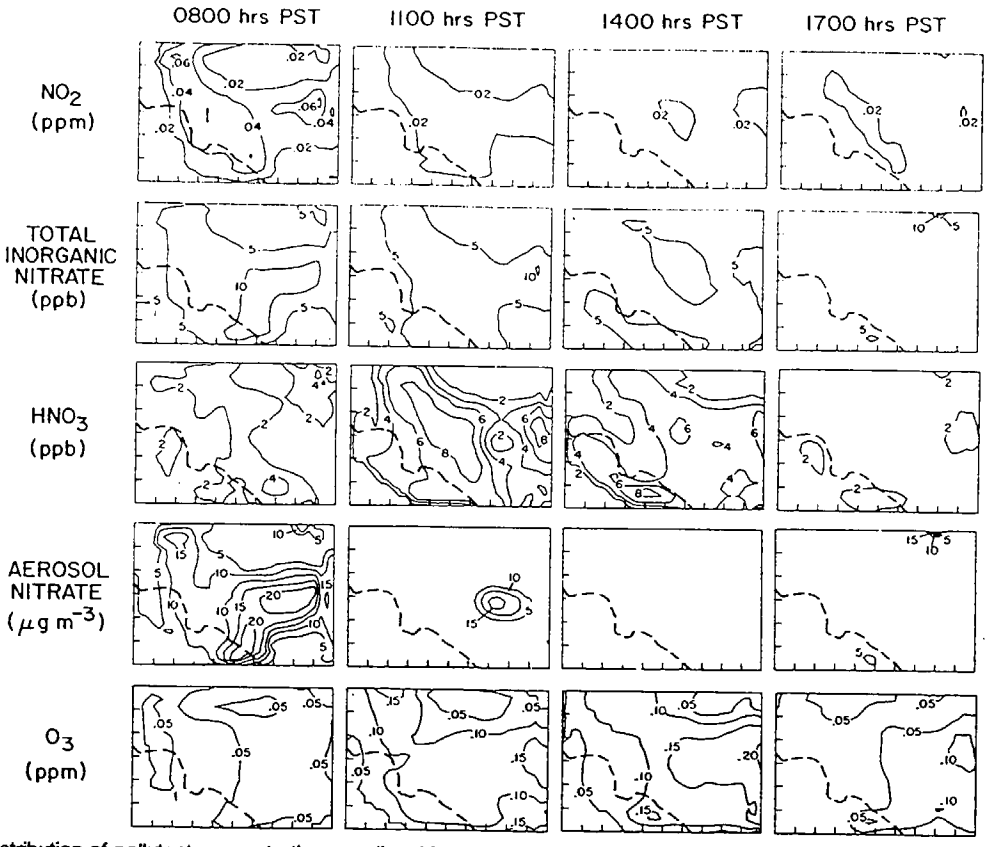

Figure 2. Spatial distribution of pollutant concentrations predicted in the presence of the maximum degree of NO_x and RHC control studied (case in lower right corner of Table II).

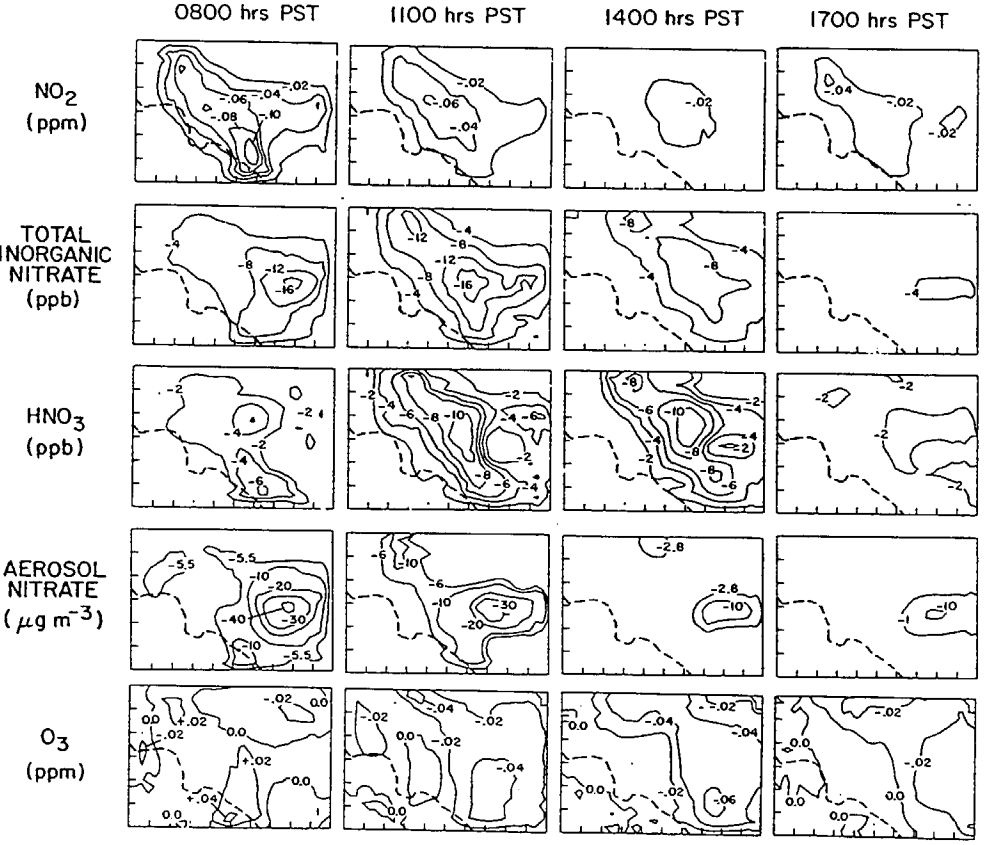

Figure 3. Spatial distribution of pollutant concentration changes predicted in the presence of the maximum degree of NO_x and RHC control studied (difference between the case in lower right corner of Table II vs the base case).

controls on 24-h average pollutant levels is explored.

One effect of the maximum degree of mobile and stationary source control considered in this study (case in lower right corner of Table II) is to preferentially reduce the NO_2 concentrations during the early morning peak hours of the day at sites in the western portion of the air

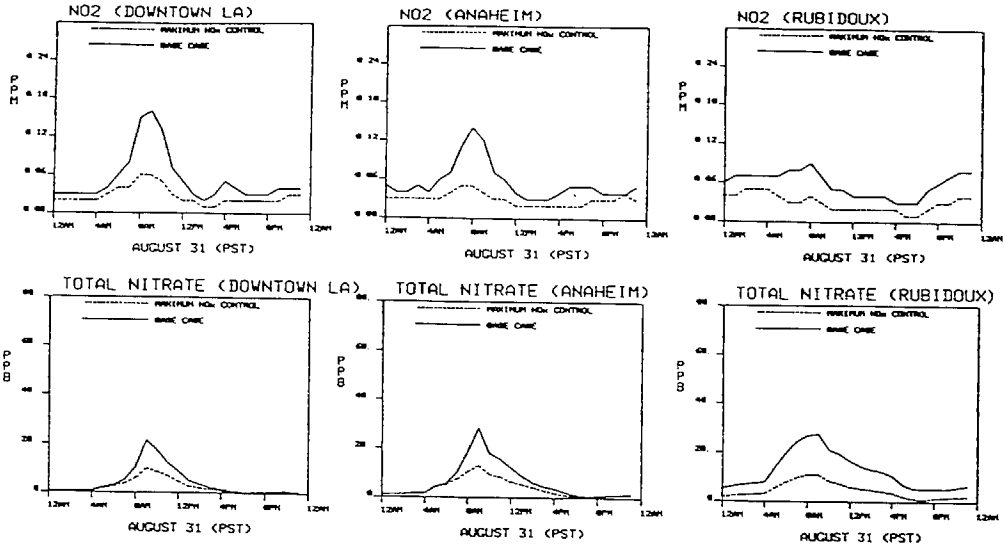

Figure 4. NO_2 and total inorganic nitrate (TN) concentrations at Los Angeles, Anaheim, and Rubidoux under base case conditions and in the presence of the maximum degree of NO_x and RHC control studied.

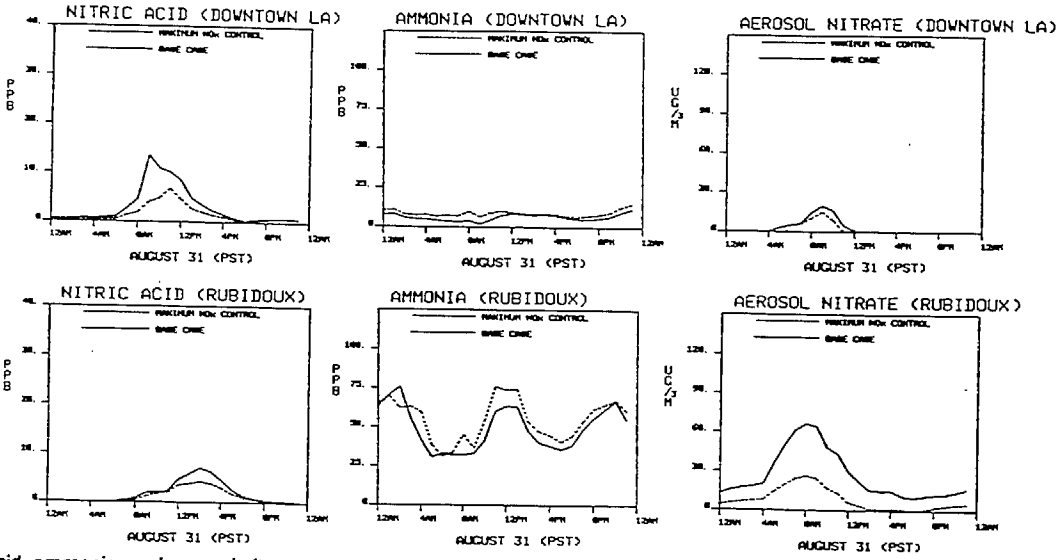

Figure 5. Nitric acid, ammonia, and aerosol nitrate concentrations at Los Angeles and at Rubidoux under base case conditions and in the presence of the maximum degree of NO_x and RHC control studied.

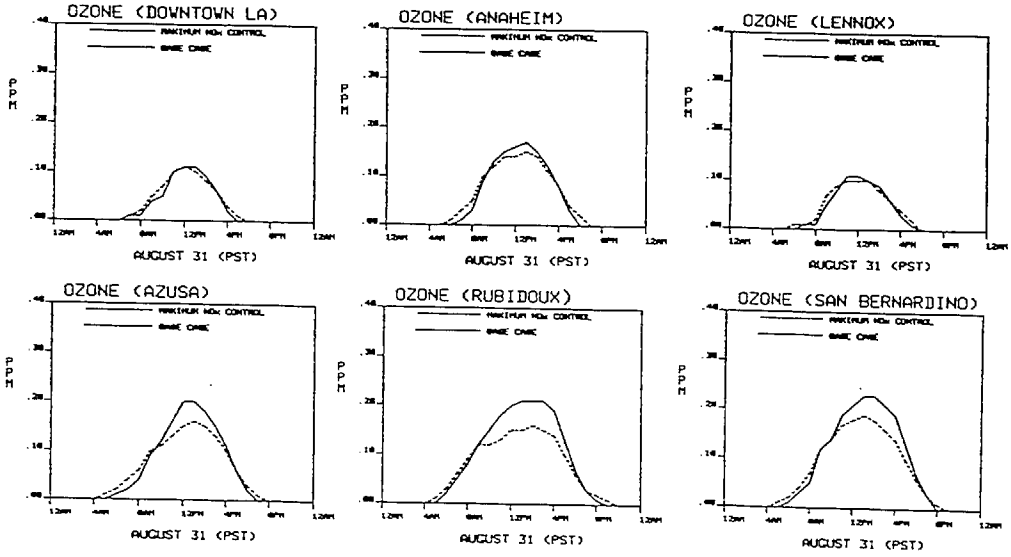

Figure 6. Ozone concentrations under base case conditions and in the presence of the maximum degree of NO_x and RHC control studied.

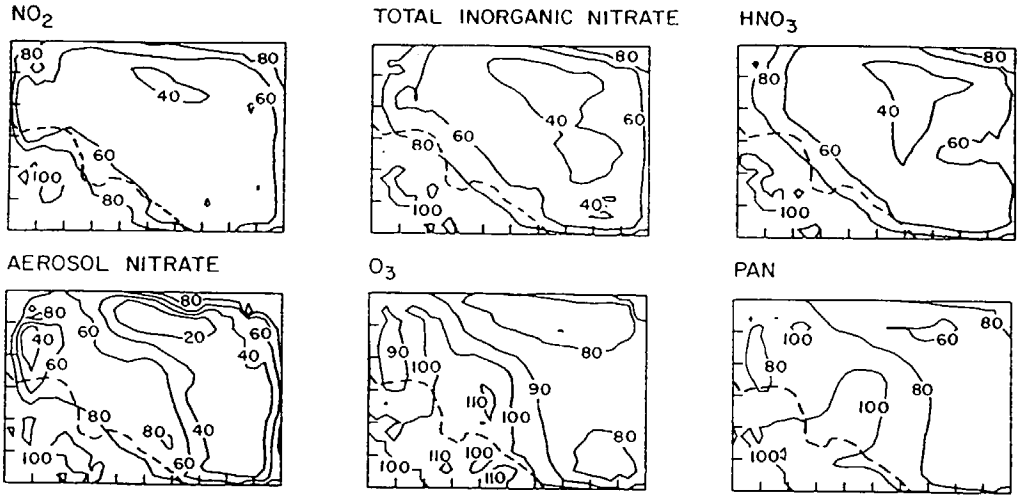

Figure 7. The 24-h average NO_2, inorganic nitrate, nitric acid, aerosol nitrate, O_3, and PAN concentrations in the presence of the maximum degree of NO_x and RHC control studied, expressed as a percentage of base case concentrations.

basin, like Los Angeles and Anaheim, as seen in Figures 3 and 4. NO_2 concentrations which exceeded 0.15 ppm during early morning hours under base case conditions have been reduced by more than 0.06 ppm at 0800 PST throughout much of the western area of the basin and by as much as 0.10 ppm in portions of coastal Orange County, as seen in Figure 3. At sites in the eastern area of the basin, at Upland, Rubidoux, and San Bernardino, NO_2 levels are reduced by large percentage amounts throughout the entire 24-h period studied (Figure 4). As a result, 24-h average NO_2 levels decline by between 40 and 60% throughout nearly the entire on-land portion of the air basin, as seen in Figure 7.

The effect of NO_x emission controls on total inorganic nitrate levels is felt to the greatest extent in the central and eastern portions of the air basin. As seen in Figure 3, TN concentration reductions in excess of 16 ppb occur in the inland areas throughout the morning hours in response to the maximum degree of NO_x control studied here.

The partition of this inorganic nitrate air quality improvement between reductions in gas-phase HNO_3 versus reductions in aerosol nitrate is determined by co-occurring NH_3 concentrations. In the western portion of the air basin, HNO_3 reductions, especially in the morning hours, are proportionally greater than aerosol nitrate reductions, as shown at Los Angeles in Figure 5. The use of selective catalytic reduction technology plus more effective reducing catalysts on mobile sources leads to a small increase in NH_3 emissions. While that NH_3 increase in very minor compared to basinwide NH_3 emissions, the NH_3 emissions increase by a significant *percentage* in the low NH_3 western urban area of the air basin (see the spatial distribution of base case NH_3 emissions in Figure 2 of ref 1). NH_3 concentrations at sites like downtown Los Angeles that are located in the immediate vicinity of stationary combustion sources and heavy traffic density experience a rough doubling of base case NH_3 levels during the morning traffic peak hours. The product of the NH_3 and HNO_3 concentrations is limited by the equilibrium dissociation constant for the NH_4NO_3–NH_3–HNO_3 system (*16*). The NH_3 concentration increase shifts the equilibrium HNO_3 concentration downward, while favoring aerosol nitrate formation. However, the same emission controls that produce the NH_3 emission increase also reduce NO_2 and TN concentrations by enough that a net increase in aerosol nitrate concentrations is not observed. Instead, both HNO_3 and AN decline in the western part of the air basin, but the HNO_3 reduction is more pronounced and begins in the morning as NH_3 levels rise, while the aerosol nitrate reduction relative to the base case occurs later in the day. In the central portion of the air basin, the combination of a major decrease in TN formation along with a small increase in NH_3 emissions is manifested by greater than a 10 ppb reduction in HNO_3 concentrations in the late morning and early afternoon (Figure 3).

In the eastern area of the air basin, base case NH_3 concentrations due to dairy farming and other agricultural sources are so high that a small change in upwind NH_3 emissions does not affect ambient NH_3 levels by more than a few percent. Again, the amount of gas-phase HNO_3 is limited by the co-occurring ammonia levels. In this case the postcontrol NH_3 levels are nearly unchanged as a percentage of the precontrol NH_3 levels, and as a result, HNO_3 concentrations do not change greatly. The large drop in TN levels at Rubidoux and San Bernardino that occurs when all available RHC and NO_x emission controls are applied thus is reflected in a major reduction in aerosol nitrate levels, and to a lesser degree by reduced HNO_3 concentrations as seen in Figure 5. At eastern basin sites, aerosol nitrate levels are reduced throughout the day, not just during peak hours.

The effect of RHC and NO_x controls on O_3 air quality has been a matter of considerable debate (*15–23*). The most recent studies (*15*, *22*) agree that large NO_x reductions (above 19%) in the Los Angeles area combined with RHC controls of comparable magnitude will produce lower O_3 levels in the downwind and eastern areas of the SoCAB near Rubidoux and San Bernardino where the highest O_3 levels often are observed. When a quantitative comparison is drawn between the O_3 control results of Tesche et al. (*22*) and the results of the present study, close agreement is found. Tesche et al. predict that the O_3 peak will decline by 17% in downwind areas in response to a combined RHC emission reduction of about 41.5% and a NO_x emission reduction of 45.5%. As seen in Tables II and III (top row, right-hand box), the present study predicts a decline of 15% in the basinwide peak O_3 level in response to a 37.2% reduction in RHC emissions and a 47.6% reduction in NO_x emissions. Concern has been voiced, however, that if NO_x emissions are controlled to the maximum extent possible, then O_3 levels will rise in the western portion of the air basin (*23*).

The results of this study indicate that the maximum degree of NO_x and RHC control studied here produces O_3 reductions in the eastern area of the South Coast Air Basin.

The peak measured and predicted O_3 levels on August 31, 1982, that occurred at Rubidoux and at San Bernardino would be reduced by the amount seen in Figure 6. Peak 1-h average O_3 levels in this case decline relative to the base case by 25% or more at Pomona, Chino, Norco, Upland, Fontana, and Rubidoux and by 21% at Azusa. The additional NO_x emission reductions achieved when moving from the group of control measures specified in the center column of Table II to the right-hand column of Table II leads to reduced O_3 levels in the high-O_3 concentration zone at the eastern end of the air basin without addition of further hydrocarbon emission controls, but the O_3 concentration improvement is much less than proportional to the degree of further NO_x control.

At all western urban sites, O_3 concentrations respond to this package of emission controls in a manner like that shown for central Los Angeles and Anaheim in Figure 6. In the presence of stringent NO_x controls, O_3 levels begin to rise at a slightly earlier hour in the morning due to less effective scavenging of O_3 by fresh NO emissions during the early morning traffic peak. Peak O_3 levels are decreased at all sites at midday, as mentioned previously. Then O_3 levels at western basin sites exceed 1982 base case concentrations for a short period in the afternoon in the presence of stringent NO_x controls, again due to less effective O_3 scavenging processes in the presence of the NO_x controls. If viewed on a 24-h average basis, O_3 concentrations do rise slightly in the western area of the air basin in response to this control program, as seen in Figure 7.

The final alteration in emissions studied involves removal of all agriculture-related NH_3 emissions from the base case 1982 emission inventory given in ref 15. NH_3 emissions from livestock waste decomposition in the Chino dairy area and elsewhere are suppressed, as are NH_3 emissions from chemical fertilizer application at farms. This type of change in emissions could occur as increasing urbanization displaces agricultural activities in the air basin. This alteration in NH_3 levels alone does not affect atmospheric NO_2, O_3, and PAN concentrations. Ammonia concentrations decline by 87–91% at Chino and Upland in the immediate vicinity of the dairy farms, and by about 70% at Rubidoux and San Bernardino downwind. Aerosol nitrate concentrations at San Bernardino, Fontana, Upland, and Pomona decline by more than 50% as the agricultural NH_3 emissions are suppressed. In response, HNO_3 levels increase in eastern basin locations by 43–45% at San Bernardino and Upland, and by 89–100% at Fontana and Rubidoux. Suppression of aerosol nitrate formation without a corresponding decrease in NO_x emissions acts to shift inorganic nitrate from the aerosol phase to gas-phase HNO_3. Total inorganic nitrate levels decline at Upland, Fontana, and Rubidoux by 7–13% as this shift from AN to HNO_3 formation occurs, probably because the deposition velocity for HNO_3 is higher than for fine aerosols.

Summary and Conclusions

Emission control measures that would reduce reactive hydrocarbon and NO_x emissions in the Los Angeles area by up to 37 and 61%, respectively, have been examined for their effects on air quality by using a photochemical airshed model applied over the 2-day period August 30–31, 1982. In most emission control cases studied, NO_2 and total inorganic nitrate concentrations decline by amounts only slightly less than proportional to the degree of precursor NO_x emission reduction. Peak 1-h average NO_2 and TN levels averaged over 20 monitoring sites would decline by more than 50% relative to 1982 base case conditions if the light-duty vehicle fleet in practice met the originally proposed federal exhaust emission standards (0.4 g/mi NO_x and 0.41 g/mi THC) in conjunction with heavy-duty vehicle control, evaporative hydrocarbon controls, plus installation of selective catalytic NO_x reduction systems on major stationary sources. This reduction in inorganic nitrate levels would be reflected in major improvements in HNO_3 and aerosol nitrate air quality.

The partition of inorganic nitrate air quality improvements between aerosol nitrate and HNO_3 can be affected by the choice of NO_x emission controls. In particular, widespread use of noncatalytic NH_3 injection technology for NO_x emission control at stationary sources alone has the potential to increase aerosol nitrate formation in near-source areas if significant co-occurring bleed-through of NH_3 to the atmosphere occurs. Selective catalytic reduction technology at stationary sources and advanced catalyst systems on vehicles also have the potential to increase NH_3 emissions, but in those cases the NH_3 increase is so slight that the NO_x emission decrease achieved through use of these devices will drive aerosol nitrate levels downward in spite of the added NH_3 emissions.

Installation of the most stringent set of NO_x and RHC emission controls studied here causes peak 1-h average O_3 concentrations to decline by 25% or more in the high O_3 concentration areas of eastern Los Angeles, Riverside, and San Bernardino counties. The final increment of NO_x control alone produces O_3 concentration improvements in the eastern portion of the air basin that, as shown in Tables III and IV, are less than proportional to the degree of NO_x control applied.

Registry No. PAN, 2278-22-0; NO_x, 11104-93-1; HNO_3, 7697-37-2; NH_3, 7664-41-7; O_3, 10028-15-6; NO_2, 10102-44-0.

Literature Cited

(1) Russell, A. G.; McCue, K. F.; Cass, G. R. *Environ. Sci. Technol.* **1988**, *22*, 263–271.

(2) Solomon, P. A.; Fall, T.; Salmon, L.; Lin, P.; Vasquez, F.; Cass, G. R. Acquisition of Acid Vapor and Aerosol Concentration Data for Use in Dry Deposition Studies in the South Coast Air Basin. Report 25; Environmental Quality Laboratory, California Institute of Technology: Pasadena, CA, 1988.

(3) South Coast Air Quality Management District *Final Air Quality Management Plan 1982 Revision*; South Coast Air Quality Management District: El Monte, CA, 1982; Final Appendix VII-A.

(4) California Air Resources Board *Public Meeting to Consider a Suggested Measure for the Control to Nitrogen from Boilers and Process Heaters in Refineries*; California Air Resources Board: Sacramento, CA, 1981; agenda item 81-23-2, Appendix L, p L-1.

(5) California Air Resources Board *Suggested Control Measure for the Control of Oxides of Nitrogen Emissions from Glass Melting Furnaces*; California Air Resources Board: Sacramento, CA, 1980.

(6) California Air Resources Board *Public Hearing to Consider Amendments to Section 2176, Title 13, California Administrative Code, to Implement and Adopt Standards for Loaded Mode Testing and Make Other Changes in Regard to Motor Vehicle Inspection Standards*; California Air Resources Board: Sacramento, CA, 1981; Table 5, p 16, option 3.

(7) California Air Resources Board *Report to the Legislature on the Feasibility of a 0.4 Gram per Mile Oxide of Nitrogen Exhaust Emission Standard for Passenger Cars and Light Trucks*; California Air Resources Board: Sacramento, CA.

(8) Cass, G. R.; Gharib, S. "Ammonia Emissions in the South Coast Air Basin 1982"; open file report 84-2; Environmental Quality Laboratory, California Institute of Technology, Pasadena, CA, 1984.

(9) Environmental Protection Agency. Control of Air Pollution from New Motor Vehicles and New Motor Vehicle Engines;

Gaseous Emission Regulations for 1987 and Later Model Year Light-Duty Vehicles, and for 1988 and Later Model Year Light-Duty Trucks and Heavy-Duty Engines; Particulate Emission Regulations for 1988 and Later Model Year Heavy-Duty Diesel Engines. U.S. Environmental Protection Agency: Washington, DC. *Federal Register* 40 CFR, Parts 86 and 600.

(10) Dziegiel, H. T.; Aure, T. B.; Anderson, D. W. The Thermal DeNO$_x$ Demonstration Project. Los Angeles Department of Water and Power: Los Angeles, CA, 1982. Presented at the Joint Symposium on Stationary Combustion NO$_x$ Control, Dallas, TX, Nov 1–4, 1982; Figures 11–13.

(11) California Air Resources Board *Suggested Control Measure for the Control of Emissions of Oxides of Nitrogen From Cement Kilns*; California Air Resources Board: Sacramento, CA, 1981; p 2.

(12) South Coast Air Quality Management District "Proposed Rule 1109—Petroleum Refinery Boilers and Process Heaters—Oxides of Nitrogen", staff report; South Coast Air Quality Management District: El Monte, CA, 1982.

(13) Kerry, H. A.; Weir, A., Jr. Operating Experiences on Southern California Edison's 107.5 MW Selective Catalytic Reduction DeNO$_x$ System. Southern California Edison Co.: Rosemead, CA, 1985. Presented at the Joint Symposium on Stationary Combustion NO$_x$ Control, Boston, MA, May 6–9, 1985; p 2.

(14) South Coast Air Quality Management District "Proposed Rule 1110.1—Emissions from Internal Stationary Combustion Engines"; staff report; South Coast Air Quality Management District: El Monte, CA, 1984; p 1.

(15) Russell, A. G.; Cass, G. R. *Atmos. Environ.* **1986**, *20*, 2011–2025.

(16) Russell, A. G.; McRae, G. J.; Cass, G. R. *Atmos. Environ.* **1983**, *17*, 949–964.

(17) Pitts, J. N.; Winer, A. M.; Atkinson, R.; Carter, W. P. L. *Environ. Sci. Technol.* **1983**, *17*, 54–57.

(18) Chock, D. P.; Dunker, A. M.; Kumar, S.; Sloane, C. S. *Environ. Sci. Technol.* **1981**, *15*, 933–939.

(19) Chock, D. P.; Dunker, A. M.; Kumar, S.; Sloane, C. S. *Environ. Sci. Technol.* **1983**, *17*, 58–62.

(20) Glasson, W. A. *J. Air Pollut. Control Assoc.* **1981**, *31*, 1169–1172.

(21) Glasson, W. A. *Environ. Sci. Technol.* **1983**, *17*, 62–63.

(22) Tesche, T. W.; Seigneur, C.; Oliver, W. R.; Haney, J. L. *J. Environ. Eng. (N.Y.)* **1984**, *110*, 208–225.

(23) Roth, P. M.; Reynolds, S. D.; Tesche, T. W.; Gutfreund, P. D.; Seigneur, C. *Environ. Int.* **1983**, *9*, 549–571.

Received for review May 26, 1987. Revised manuscript received March 14, 1988. Accepted April 14, 1988. This work was supported by the California Air Resources Board under Agreement A2-150-32 and by gifts to the Environmental Quality Laboratory.